

EXPLORATION OF CONDENSATION HEAT
TRANSFER COEFFICIENT AND PRESSURE
DROP ON SERRATED FIN SURFACES FOR
R134a

Thesis

Submitted in partial fulfillment of the requirements for the degree of

DOCTOR OF PHILOSOPHY

By

K. V. RAMANA MURTHY



DEPARTMENT OF MECHANICAL ENGINEERING
NATIONAL INSTITUTE OF TECHNOLOGY KARNATAKA
SURATHKAL, MANGALORE – 575025
October, 2018

**EXPLORATION OF CONDENSATION HEAT
TRANSFER COEFFICIENT AND PRESSURE
DROP ON SERRATED FIN SURFACES FOR
R134a**

Thesis

Submitted in partial fulfillment of the requirements for the degree of
DOCTOR OF PHILOSOPHY

By

K.V. RAMANA MURTHY
(Reg.No. ME09P08)

RESEARCH GUIDES

Dr. T.P. ASHOK BABU

&

Dr. C. RANGANAYAKULU



**DEPARTMENT OF MECHANICAL ENGINEERING
NATIONAL INSTITUTE OF TECHNOLOGY KARNATAKA
SURATHKAL, MANGALORE – 575025
October, 2018**

DECLARATION

by the Ph.D. Research Scholar

I hereby declare that the Research Thesis entitled “**Exploration of Condensation Heat Transfer Coefficient and Pressure Drop on Serrated Fin Surfaces for R134a**” which is being submitted to the **National Institute of Technology Karnataka, Surathkal** in partial fulfillment of the requirements for the award of the Degree of **Doctor of Philosophy in Mechanical Engineering** is a bonafide report of the research work carried out by me. The material contained in this Research Thesis report has not been submitted to any University or Institution for the award of any degree.

K.V. Ramana Murthy

Register Number: 092007ME09P08

Department of Mechanical Engineering

Place : NITK-Surathkal

Date :

CERTIFICATE

This is to *certify* that the Research Thesis entitled “**Exploration of Condensation Heat Transfer Coefficient And Pressure Drop On Serrated Fin Surfaces for R134a**” submitted by **K. V. Ramana Murthy** (Register Number: 092007ME09P08) as the record of the research work carried out by him is *accepted as the Research Thesis submission* in partial fulfilment of the requirements for the award of degree of **Doctor of Philosophy**.

Research Guides

(**Dr. C. Ranganayakulu**)

(**Dr. T. P. Ashok Babu**)

Chairman-DRPC
(Signature with Date and Seal)
Department of Mechanical Engineering

ACKNOWLEDGEMENTS

*I would like to express my deep sense of gratitude and respect to my supervisor **Dr. T. P. Ashok Babu**, Professor, Dean (FW) & former head of Mechanical Engineering Department, NITK, Surathkal, for his excellent guidance, suggestions and constructive criticism. I consider myself extremely lucky to be able to work under the guidance of such a dynamic personality. He has not only been a wonderful supervisor but also a sympathetic person, who stood by my side at difficult times during development and commissioning of test facility.*

*My sincere and heartfelt thanks to my internal research co-coordinator **Dr. C Ranganayakulu**, Scientist 'H', Outstanding Scientist, Aeronautical Development Agency (ADA), Bangalore for his enlightening discussions and guidance at every stage of my research programme. I thank him for sparing his invaluable time and motivating me to complete the dissertation work.*

*I express my sincere thanks to my RPAC members **Dr. A. V. Adhikari**, Professor, Department of Chemistry, NITK, Surathkal and **Dr. K.Rajendra Udupa**, Professor, Department of Metallurgy, NITK, Surathkal for their motivation and encouragement to achieve my goal. I would like to thank present and past HOD's of Mechanical department, present and past Deans of NITK, Surathkal for their encouragement.*

*I record my deepest gratitude to the Aeronautical Development Agency (ADA), Bangalore for allowing the project on development of condensation heat transfer and frictional pressure drop correlations. Grateful thanks are due to **PGD (CA) & Director-ADA and Sri R.Swaminathan, DS, APGD (CP) & TD (GS) of ADA**, Bangalore for permitting me to carryout research work. I am deeply indebted to **Mr. A.Panigrahi** of M/s BHEL-HPVP, Visakhapatnam, who has taken keen interest in development of brazed compact plate fin heat exchangers.*

*I record my appreciation for the continuous help extended to me by **Sri K.Nagaraja, Amaranatha Raju, Partha P Kemprai**, ADA during my entire thesis work. The invaluable experimental support extended by **B.Mahesh, J.N.Raghu, Atmanand, A.Goverdhan & M.Prakash Raju**, ADA is also gratefully acknowledged.*

*I record my special thanks to National Aerospace Laboratories (NAL), Bangalore for allowing to setup test facility to carry out the experimental work. I convey my sincere gratitude to **Dr. R Rajendran, Mr. Janakiram Reddy, Mr E.Rajesh, Mr. Pandyan, Mr Shasidhar** and other members of “Closed Circuit Centrifugal Compressor Test Rig, NAL for their support for successful completion of experiments. I enjoyed every moment working with them.*

*This work could have been a distant dream if I did not get the moral encouragement and help from my wife, **Lakshmi**. She equally shared my success and failures with me. I am indebted to my wife and my son, **Rahul Vamsi**, to fill my life with laughter.*

*I thank to **my mother, brothers and sister in-laws** for their support. Also, I would like to thank my **mother-in law and father-in law** for their encouragement. Without their cooperation and active support, I could not have tasted success. I take this opportunity to express my sincere gratitude to all of them.*

Last but not least, I thank those who helped me directly or indirectly during my research work.

*I thank **Lord Ganesha and Sri Saneeswaran** who gave me all the strength and energy to undergo the uphill task and complete the PhD thesis. Without these blessings I would not have completed this milestone.*

*Place: **NITK, Surathkal***

Date:

- K.V. Ramana Murthy

ABSTRACT

The compact plate fin heat exchanger (CPFHE) plays a major role in aerospace industry and various process plants because of their compactness, low weight and high effectiveness. The performance of a plate fin heat exchanger is determined, among other things, by the geometry and type of fins. The most popularly used fin surfaces in compact heat exchangers are the serrated (offset strip) fins, wavy fins, louvered fins and plain fins. Amongst these fin types the serrated fins assume lot of importance due to its enhanced thermo-hydraulic performance. Thermo-hydraulic design of CPFHEs is strongly dependent upon the predicted/measured dimensionless performance (Colburn j factor and Fanning friction f vs. Reynolds number) of heat transfer surfaces.

Two phase flow analysis for the condensation of refrigerants within the CPFHEs is an area of ongoing research. The condensation average refrigerant heat transfer coefficient (h_r) and two phase frictional pressure drop (ΔP_f) of the finned surface constitute the most important parameters for CPFHEs design. These parameters are functions of fin geometry, fluid properties (thermal conductivity and Prandtl number) and mass flow rate (Reynolds number). However, the complexity of the flow phenomena through the passages of a compact heat exchanger makes any theoretical analysis formidable. Experimental investigation becomes necessary for determining the thermo-hydraulic performance of such devices. In aircraft and automobiles, the demand on performance that is the volume and weight of the heat exchangers should be kept minimum.

An experimental apparatus, based on steady state method has been developed for conducting condensation experiments on four different serrated fin surfaces. Based on theoretical design, four test condensers are developed using vacuum brazing technology. The effects of saturation temperature (pressure), mass flux, heat flux, effect of fin surface characteristics and fluid properties are investigated inside a small brazed plate fin heat exchanger with serrated fin surface for R134a. The average condensation heat transfer coefficients and frictional pressure drops were determined experimentally for refrigerant R134a at different saturated temperatures (ranging from

32 °C to 44 °C). A transition point between gravity controlled and forced convection condensation has been found for a refrigerant mass flux around 20 kg/m²s. Correlations are provided for the measured heat transfer coefficients and frictional pressure drops separately for four different types of serrated fins.

CFD (Computational fluid dynamics) methodology has been used to develop the single phase water heat transfer coefficient and friction factor correlations for serrated fins using ANSYS Fluent 14.5. The results are compared with previous air-cooled models and experimental results of water. The water cooled CFD analysis results shows that the Prandtl number has a large effect on the Nusselt number of the serrated fin geometry. Finally, the generalized correlations are developed for serrated fins taking all geometrical parameters into account.

The influence of hydraulic diameter on experimental heat transfer coefficient and pressure drop measured during R134a saturated vapour condensation inside a brazed compact plate fin heat exchanger with serrated fins was studied. Test condensers are selected with four different hydraulic diameter (1.1894 mm , 1.345 mm, 1.7461 mm and 1.8667 mm) serrated fins to analyse the affect of heat transfer and frictional pressure drop characteristics.

The environmental control system (ECS) for a typical fighter aircraft is used for cabin cooling & pressurization, demisting operations and for avionics cooling. Most of the passenger and fighter aircrafts use bleed-air cycle for ECS. A new ECS called all electric environmental control system (AEECS) which works on vapour compression refrigeration system using ram air as medium. The AEECS is found to reduce the power requirement of the system to 80 kW compared to the bleed air cycle ECS which requires a power of 0.8 MW to run the system. In AEECS one of the components is condenser.

Keywords: Compact plate fin heat exchanger, serrated fin surface, R134a, average condensation heat transfer coefficient and frictional pressure drop.

CONTENTS

DECLARATION		
CERTIFICATE		
ACKNOWLEDGEMENTS		i
ABSTRACT		iii
CONTENTS		v
LIST OF FIGURES		viii
LIST OF TABLES		xii
NOMENCLATURE		xiv
CHAPTER	TITLE	PAGE No.
1	INTRODUCTION	1
	1.1 Background of the Research Topic	2
	1.2 Application Areas	5
	1.3 Compact Plate Fin Heat Exchangers	6
	1.4 Condensation Heat Transfer and Flow Friction	10
	1.5 Objectives of the Study	13
	1.6 Organization of Thesis	14
2	LITERATURE SURVEY	15
	2.1 Single Phase Heat Transfer and Pressure Drop Characteristics	15
	2.2 Two Phase Studies on Average Condensation Heat Transfer and Frictional Pressure Drop	26
	2.3 Reviews on Two-Phase Pressure Drop	36
	2.4 Summary from Review of Literature	37
3	COMPUTATIONAL STUDIES ON SERRATED FINS	39
	3.1 CFD Analysis	40
	3.2 CFD Approach	40
	3.3 Methodology	42
	3.4 Mathematical Model	42
	3.5 Assumptions	44
	3.6 Boundary Conditions	45

3.7	ANSYS CFD Package	45
3.8	Computation of j and f Factors	47
3.9	Problem Description	48
3.10	Serrated(Offset Strip) Fin Surface	49
3.11	Effect of Reynolds Number and Geometry Parameters	53
3.12	Generation of Flow Friction and Heat Transfer Correlations	60
3.13	Generation of Flow Friction and Heat Transfer Correlations for water Side Fin	61
4	DEVELOPMENT OF EXPERIMENTAL APPARATUS	63
4.1	Development of Brazed Compact Plate Fin Heat Exchangers	63
4.2	Experimental Test Rig Specification	76
4.3	Standards	78
4.4	Design and Development of Experimental Test Rig	78
4.5	Instrumentation and Data Acquisition System	94
4.6	Calibration of Sensors	100
4.7	Validation of Experimental Test Rig	100
5	EXPERIMENTAL PROCEDURE AND DATA REDUCTION	104
5.1	Measurement Principle	104
5.2	Experimental Procedure	105
5.3	Data Reduction	111
5.4	Preliminary Single –Phase Energy Balance Validation	118
5.5	Measurement of Lubricating Oil Concentration	118
5.6	Uncertainty Analysis	120
6	EXPERIMENTAL RESULTS AND DISCUSSION	126
6.1	Experimental Results and Analysis	127
6.2	Development of Correlations	141
6.3	Influence of Serrated Fin Geometries on Condensation Performance	148
6.4	Influence of Condensation Phenomena in the Presence of Lubricating Oil in R134a	152
6.5	Exploration of Condensation Correlations	153
7	CONCLUSIONS AND SCOPE FOR FUTURE WORK	156
7.1	Conclusions	156
7.2	Scope for Future Work	159
	REFERENCES	160
	APPENDIX-I: j & f Simulation Data	172

LIST OF FIGURES

Fig. No.	TITLE	PAGE No.
Chapter 1		
1.1	Bleed Air Cycle System	3
1.2	Bleed Less Vapour Compression Refrigeration System	4
1.3	Plate Fin Heat Exchanger Assembly	7
1.4	Types of Plate Fin Surfaces	8
1.5	Different Flow Configurations in Heat Exchanger	9
1.6	Different Types of Condensation	11
1.7	Typical Velocity & Temperature Profile of the Condensate	12
1.8	Dropwise Condensation Phenomenon	12
Chapter 3		
3.1	Computational Domain for Serrated Fin	41
3.2	Flow Chart of CFD Methodology	43
3.3	Schematics of Fin Geometry	49
3.4	Computational Fluid Domain in Mesh Form for Serrated Fin	50
3.5	Grid Independency Check for Serrated Fin Surface by CFD Analysis	51
3.6	Validation of CFD Results with Experimental Results	53
3.7	Colburn (j) and Friction (f) factor for Re: 1000-15000	53
3.8	Effect of s/h Ratio on Colburn j Factor of Serrated Fin Surface	54
3.9	Effect of t/s Ratio on Colburn j Factor of Serrated Fin Surface	55
3.10	Effect of t/l Ratio on Colburn j Factor of Serrated Fin Surface	56
3.11	Effect of s/h Ratio on f Factor of Serrated Fin Surface	56
3.12	Effect of t/s Ratio on f Factor of Serrated Fin Surface	57
3.13	Effect of t/l Ratio on f Factor of Serrated Fin Surface	58
3.14	Velocity (m/s) Vectors Plot of Serrated Fin at Re=500 for Water Medium	59
3.15	Velocity (m/s) Vectors Plot of Serrated Fin at Re=10000 for Water Medium	59
3.16	Pressure (Pa) Contour Plot of Serrated Fin at Re = 500 for Water Medium	59
3.17	Temperature (k) contour Plot of Serrated Fin at Re=500 for Water Medium	60
Chapter 4		
4.1	Serrated Fin	65
4.2	CAD Model of Test Condenser Core	65
4.3	Effect of Serrated Fin Heat Transfer Area on Heat Flux	69

4.4	Effect of Mass Flux through Serrated Fin on Heat Flux	69
4.5	Effect of Reynolds Number on Mass Flux	69
4.6	Brazing of Test Condenser	73
4.7	Thermocouples Arrangement in Test Condenser	73
4.8	Photograph Showing Thermocouples Fixing Arrangement in Test Condenser Core	74
4.9	Photograph of Test Condenser after Insulation	74
4.10	Helium Leak Test Setup	75
4.11	Photograph of Experimental Test Rig with Test Condenser	79
4.12	Schematic Diagram of the Vapour Compression Refrigeration System Experimental Test Rig with Instrumentation	80
4.13	Photograph of Experimental Test Rig with Test Condenser (Front View)	81
4.14	Photograph of Test Rig Data Acquisition System with Control Panel	81
4.15	Schematic Layout of Refrigerant Loop	84
4.16	Schematic Layout of Condenser Loop	86
4.17	Schematic Layout of De-Super Heater Loop	86
4.18	Schematic Layout of Evaporator Loop	88
4.19	Schematic Layout of Super Heater Loop	88
4.20	Photograph of Reciprocating Compressor	89
4.21	Photograph of Commercial Plate Heat Exchanger	89
4.22	Photograph of Electronic Expansion Valve	90
4.23	Photograph of Oil Separator	91
4.24	Photograph of Chiller Unit	92
4.25	Photograph of Solenoid Valve	93
4.26	Photograph of Test Rig Evacuation and Refrigerant Charging Unit	93
4.27	Photograph of Coriolis Flow Meter	94
4.28	Photograph of Turbine Flow Meter	95
4.29	Photograph of Pressure Transducer	96
4.30	Photograph of Differential Pressure Transducer	96
4.31	Block Diagram of Data Acquisition System	98
4.32	Validation of Experimental Results of Mass Flux with Two Phase Condensation Heat Transfer Coefficient	102
4.33	Validation of Experimental Results of Mass Flux with Two Phase Condensation Frictional Pressure Drop	103
 Chapter 5		
5.1	Schematic of Test Condenser	104
5.2	Chart Showing the Procedure to take Observations with Experimental Set Up	107
5.3	Typical Refrigerant Circuit with Sample Recorded Values	110
5.4	Pressure-Enthalpy and Schematic Diagrams of VCRS	111
5.5	Pictorial Presentation of Step by Step Procedure of Data Reduction	117
5.6	Measurement of Percentage of Lubricating Oil Mixing	119

Chapter 6

6.1	Effect of Refrigerant Mass Flux on Two Phase Condensation Heat Transfer Coefficient at Different Saturation Temperatures for Test Condenser 1 (TC1)	129
6.2	Effect of Refrigerant Mass Flux on Heat Flux at Different Saturation Temperatures for Test Condenser 1 (TC1)	130
6.3	Effect of Refrigerant Mass Flux on Condensation Frictional Pressure Drop at Different Saturation Temperatures for Test Condenser 1 (TC1)	130
6.4	Refrigerant KE/V vs. Effect of Kinetic Energy per Unit Volume (KE/V) on Condensation Frictional Pressure Drop at Different Saturation Temperatures for Test Condenser 1 (TC1)	131
6.5	Effect of Refrigerant Mass Flux on Two Phase Condensation Heat Transfer Coefficient at Different Saturation Temperatures for Test Condenser 2 (TC2)	133
6.6	Effect of Refrigerant Mass Flux on Heat Flux at Different Saturation Temperatures for Test Condenser 2 (TC2)	133
6.7	Effect of Refrigerant Mass Flux on Condensation Frictional Pressure Drop at Different Saturation Temperatures for Test Condenser 2 (TC2)	134
6.8	Refrigerant KE/V vs. Effect of Kinetic Energy per Unit Volume (KE/V) on Condensation Frictional Pressure Drop at Different Saturation Temperatures for Test Condenser 2 (TC2)	134
6.9	Effect of Refrigerant Mass Flux on Two Phase Condensation Heat Transfer Coefficient at Different Saturation Temperatures for Test Condenser 3 (TC3)	136
6.10	Effect of Refrigerant Mass Flux on Heat Flux at Different Saturation Temperatures for Test Condenser 3 (TC3)	137
6.11	Effect of Refrigerant Mass Flux on Condensation Frictional Pressure Drop at Different Saturation Temperatures for Test Condenser 3 (TC3)	137
6.12	Refrigerant KE/V vs. Effect of Kinetic Energy per Unit Volume (KE/V) on Condensation Frictional Pressure Drop at Different Saturation Temperatures for Test Condenser 3 (TC3)	138
6.13	Effect of Refrigerant Mass Flux on Two Phase Condensation Heat Transfer Coefficient at Different Saturation Temperatures for Test Condenser 4 (TC4)	140
6.14	Effect of Refrigerant Mass Flux on Heat Flux at Different Saturation Temperatures for Test Condenser 4 (TC4)	140
6.15	Effect of Refrigerant Mass Flux on Condensation Frictional Pressure Drop at Different Saturation Temperatures for Test Condenser 4 (TC4)	141
6.16	Refrigerant KE/V vs. Effect of Kinetic Energy per Unit Volume (KE/V) on Condensation Frictional Pressure Drop at Different Saturation Temperatures for Test Condenser 4 (TC4)	141

6.17	Comparison between Experimental and Predicted h_r in TC1	144
6.18	Comparison between Experimental and Predicted h_r in TC2	144
6.19	Comparison between Experimental and Predicted h_r in TC3	144
6.20	Comparison between Experimental and Predicted h_r in TC4	145
6.21	Comparison between Experimental and Predicted ΔP_f in TC1	147
6.22	Comparison between Experimental and Predicted ΔP_f in TC2	147
6.23	Comparison between Experimental and Predicted ΔP_f in TC3	147
6.24	Comparison between Experimental and Predicted ΔP_f in TC4	148
6.25	Effect of Refrigerant Mass Flux on Condensation Heat Transfer Coefficient at $T_{sat}=34$ °C for Different Hydraulic Diameters of Serrated Fin	150
6.26	Effect of Refrigerant Mass Flux on Condensation Heat Transfer Coefficient at $T_{sat}=40$ °C for Different Hydraulic Diameters of Serrated Fin	150
6.27	Effect of Refrigerant Mass Flux on Condensation Frictional Pressure Drop (ΔP_f) at $T_{sat}= 34$ °C for Different Hydraulic Diameters of Serrated Fin	151
6.28	Effect of Refrigerant Mass Flux on Condensation Frictional Pressure Drop (ΔP_f) at $T_{sat}= 40$ °C for Different Hydraulic Diameters of Serrated Fin	152
6.29	Comparison between Experimental h_r and Predicted h_r	154
6.30	Comparison between Experimental ΔP_f and Predicted ΔP_f	154

LIST OF TABLES

TABLE No.	TITLE	PAGE No.
Chapter 2		
2.1	Summary of Correlations for Single Phase Fluid	24
2.2	Summary of Correlations for Two Phase Heat Transfer in Tubes	31
2.3	Summary of Plate Heat Exchanger Correlations	37
Chapter 3		
3.1	Description of variables ϕ , Γ and S_ϕ for Conservation of Mass, Momentum and Energy	43
3.2	Test Condenser Water Side Serrated Fin Geometry Details	62
Chapter 4		
4.1	AA3003 Chemical Composition (%)	64
4.2	Serrated Fin Geometry Details	66
4.3	Calculation of Heat Flux, Mass Flux and Re For Different Serrated Fin Sizes	68
4.4	Calculation of Heat Flux and Mass Flux for Different Serrated Fin Geometry	71
4.5	Details of Operating Ranges of Compressors	83
4.6	Specification of Evaporator and Condenser Heat Exchangers	90
4.7	Specification of Expansion Valve	91
4.8	Specification of Chiller Unit	93
4.9	Specification of Coriolis Flow Meter	95
4.10	Specification of Turbine Flow Meter	95
4.11	Specification of Pressure Transducer	96
4.12	Specification of Differential Pressure Transducers	96
4.13	Specification of Temperature Transducers	97
4.14	Geometric Parameters of Plate Heat Exchanger	101
4.15	Tested Empirical Correlations	103
Chapter 5		
5.1	Measurement of Oil Mixing in Refrigerant	120
5.2	Accuracy Ranges of Measuring Devices	121
5.3	Parameters and Estimated Uncertainties	122
Chapter 6		
6.1	Geometrical Parameters of Serrated Fin Surfaces	126

6.2	Geometric Data of TC1 Fins	127
6.3	Operation Conditions during Experimental Tests on TC1	128
6.4	Geometric Data of TC2 Fins	131
6.5	Operation Conditions during Experimental Tests on TC2	132
6.6	Geometric Data of TC3 Fins	134
6.7	Operation Conditions during Experimental Tests on TC3	135
6.8	Geometric Data of TC4 Fins	138
6.9	Operation Conditions during Experimental Tests on TC4	139
6.10	Values of Coefficients for Condensation Heat Transfer Coefficient	142
6.11	Values of Coefficients for Refrigerant Two Phase Frictional Pressure Drop	145
6.12	Test Condenser Geometric Parameters	149

NOMENCLATURE

A	Heat transfer area	(m ²)
Al	Aluminium	
a	Ratio of fin area to total area	(dimensionless)
b	Plate spacing	(m)
C _p	specific heat at constant pressure	(kJ/kg.K)
Cr	Chromium	
Cu	Copper	
D _h	Hydraulic Diameter	(m)
<i>f</i>	Fanning friction factor	(dimensionless)
<i>f</i> _{tp}	Two phase friction factor	(dimensionless)
Fe	Ferrous	
G	mass flux	(kg/m ² s)
g	Acceleration due to gravity	(m/s ²)
H	Specific Enthalpy	(J/kg)
h	fin height	(m)
h _r	Refrigerant side heat transfer coefficient	(W/m ² °C)
h _w	Water side heat transfer coefficient	(W/m ² °C)
<i>j</i>	Colburn factor (StPr ^{2/3})	(dimensionless)
k	Turbulent kinetic energy	(m ² /s ²)
KE	Kinetic Energy	(J)
l	Offset strip fin length	(m)
L	Flow length	(m)
m	mass flow rate	(kg/s)
Mg	Magnesium	
Mn	Manganese	
Nu	Nusselt number (h D _h / λ)	(dimensionless)
P	Pressure	(Pa)
Pr	Prandtl number (μ C _p /k)	(dimensionless)
Q	Heat load	(kW)
q	Heat flux	(kW/ m ²)

Re	Reynolds number	(dimensionless)
Re*	Re at Point of transition	(dimensionless)
Re _D	Re at Transitional Range	(dimensionless)
r _h	hydraulic radius	(m)
s	fin spacing	(m)
S _φ	Conservation of energy	(J)
Si	Silicon	
St	Stanton number	(dimensionless)
T	Temperature	(⁰ C)
t	Fin thickness	(m)
Ti	Titanium	
U	overall heat transfer coefficient	(W/m ² ⁰ C)
V	Volume	(m ³)
u	velocity component in x direction	(m/s)
v	velocity component in y direction	(m/s)
w	velocity component in z direction	(m/s)
x	Refrigerant quality	(dimensionless)
L/D _h	length / hydraulic diameter	(dimensionless)

Greek Symbols

α	ratio of (s/h)	(dimensionless)
β	surface area per unit volume	(m ² /m ³)
δ	ratio of (t/l)	(dimensionless)
Δ	Increment	
ε	turbulence dissipation rate	(m ² /s ³)
η	Efficiency	(dimensionless)
γ	ratio of (t/s)	(dimensionless)
Γ	effective diffusivity	(m ² /s ²)
λ	Thermal conductivity	(W/ m. K)
μ	Dynamic viscosity	(Ns/m ²)
υ	specific volume	(m ³ /kg)
ρ	density	(kg/m ³)
φ	generalized transport variable	(dimensionless)

τ shear stress (N/m²)

Acronyms

AA	Aluminium Association
ACM	Air Cycle Machine
ASHRAE	American Society of Heating, Refrigeration and Air-conditioning Equipments
ASME	American Society of Mechanical Engineering
C	Cold
CAD	Computer Aided Design
CAU	Cold Air Unit
CFD	Computational fluid dynamics
CHE	Compact Heat Exchangers
COP	Coefficient of performance
CPTCV	Cooling Pack Temperature Control Valve
CPFHE	Compact Plate Fin Heat Exchangers
DM	Demineralised water
DNS	Direct Numerical Simulation
EADS	European Aeronautics Defence & Space Company
ECS	Environmental Control System
EEV	Electronic Expansion Valve
FPI	Fin density per inch
FTPBV	Fuel Tank pressurisation & bypass valve
FEM	Finite Element Method
FRV	Flow Regulating Valve
FT	Turbine Flow meter
H	Hot
HFC	Hydro Fluorocarbons
HPWS	High Pressure Water Separation
HVAC	Heating Ventilation and Air conditioning
LES	Large Eddy Simulation
LPM	Litres per minute

MCCB	Main Control Circuit Board
NAL	National Aerospace Laboratories
NRV	Non Return Valve
P	Pressure
PHE	Plate Heat Exchanger, Primary Heat Exchanger
PRSOV	Pressure Regulating & Shut off Valve
RTD	Resistance Temperature Detectors
SCADA	Supervisory Controller & Data Acquisition System
SHE	Secondary Heat Exchanger
SV	Solenoid Valve
T	Temperature
TC	Test Condenser Unit
TR	Tonne of refrigeration
UCAV	Unmanned combat aerial vehicle
VCRS	Vapour Compression Refrigeration System
VFD	Variable Frequency Drive

Subscripts

a	momentum
ave	average
c	manifold and ports
eq	equivalent
f	fin, frictional, liquid refrigerant
g	gravity, gas
i	Inlet
in	inlet
L	Liquid
l	flow length, liquid
m	mean
no oil	with out lubricating oil
o	overall
out	outlet

p	plate
r	refrigerant
sat	saturation
s	surface
sat	Saturation
t	fin thickness, total
tp	two phase
w	water, wall

CHAPTER 1

INTRODUCTION

Plate-fin compact heat exchangers are widely used in aerospace industry and various process plants. The compact heat exchanger (CHE) is characterized by a small volume and a high rate of energy exchange between two fluid streams. This high rate of heat exchange is made possible by employing intricate flow passages with large heat transfer areas. It is significant to know the heat transfer and flow friction characteristics (Colburn j and fanning f factors) of these enhanced surfaces for a proper selection and rating of the equipment. However, the complexity of the flow phenomena through the passages of a compact heat exchanger makes any theoretical analysis formidable. Experimental investigation becomes necessary for determining the thermo-hydraulic performance of such devices. But one thing has been universally recognized j and f data for complex plate-fin heat exchanger cores must be determined experimentally for each geometry. In spite of the great studies that computational fluid dynamics have done, j and f data of a plate fin surface, particularly of the serrated, louvered and wavy geometry's, cannot be determined with the required precision. In aircraft and automobiles, the requirement on performance that is the weight and volume of the heat exchangers should be kept in minimum. These necessities of modern devices have been the motivation for the development of compact plate fin heat exchangers.

Intensification of industrial thermal processes on one side as well as energy efficiency considerations on the other side has led to considerable interest in compact heat exchangers also for condensation, which call for a low temperature difference between the fluids and thus for high heat transfer coefficients. The hydraulic diameter of flow passages is usually less than 5 mm in compact heat exchangers. There are also other special applications in which compact plate fin heat exchanger passage geometry is needed to facilitate a highly resourceful heating or cooling process involving condensation or boiling. Instead of heat transfer between two streams, these applications may involve transport of heat to or from a condensing or evaporating

stream due to its proximity to a continuous source or sink of thermal energy. Applications of condensation in passages of spacecraft radiator panels, thermal control of avionics in high performance military aircraft or spacecraft payloads.

In condensation heat transfer of a compact heat exchanger the heat flux, mass flux and vapour quality are affecting the heat transfer coefficients in addition to fluid properties and geometrical parameters effects. An important obstacle to the application of compact condensers in the process industries is the lack of validated design correlations to predict the heat transfer coefficient. A few papers available in open literature on two-phase flow phenomena of compact heat exchangers concern with condensation on plate-fin surfaces. However, these correlations can't be used directly for the present fins, where fin geometry is different.

A great variety of geometries are now being offered by manufacturers of aluminum & aluminum alloys and stainless steel plate fin cores for aerospace applications. Many of them promise excellent performance j and f factors data which is not available in open literature. But quantitative data is required before design and construction of a compact heat exchanger, particularly for a demanding application like those in military aircraft. This data can be generated through a devoted experimental facility accompanied by some intelligent analysis or numerical analysis. Literature survey indicates that very limited research studies have been devoted to the condensation of R134a in compact plate fin heat exchangers and in particular serrated type fin surfaces. The proposed research project is a step in that direction.

1.1 Background of the Research Topic

Presently most of the fighter and passenger aircraft environmental control system (ECS) are having conventional air cycle machine (ACM) with high pressure water separation (HPWS) for which bleed air is drawn from aircraft engines. Very recent trend is for 'All Electric ECS', in which, no bleed air is extracted from the engines (Fabienne C, 2007). The aircraft ECS system has therefore now to find another source of air to perform the system functions.

The general aircraft bleed air cycle system schematic diagram is shown in Fig. 1.1. In conventional 'Bleed Air System', the air tapping from the compressor is too

much compressed and heated; the excess of energy is thrown away in the first heat exchanger. The amount of the wasted energy can reach about 30 %. The main disadvantages are that the compressed air is bled from the main engine leading to increased fuel consumption and lower engine efficiency. Also high temperature air needs to travel long distance from engines, make it necessary to use high temperature materials, seals and fire safety system. This leads to fire hazards in case of leakage or breakdown of insulation. This imposes additional inspection and maintenance, whereas in ‘All Electric ECS’, the right amount of power is extracted according to the flight phases system requirements. The implementation of electric compressors creates less pressure and then less energy waste.

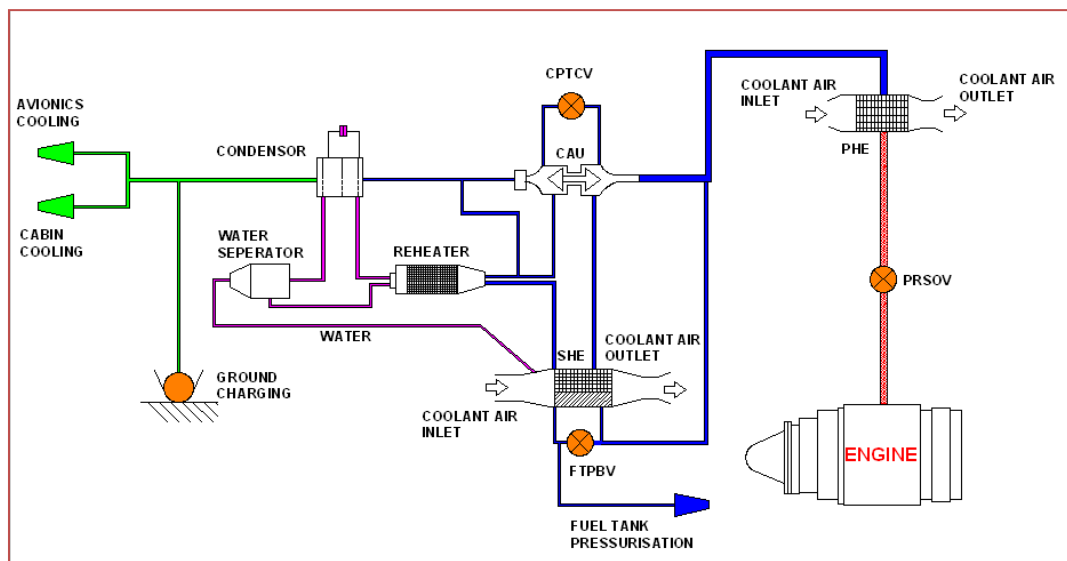


Fig. 1.1: Bleed Air Cycle System

All electric systems have the following advantages over the conventional systems.

- Electrical systems are designed to provide the right function at the right time.
- Electrical systems can be switched on & off as needed, thus conserving power.
- Electrical systems are designed to provide exactly the needed function.
- Losses in electrical cabling are lower than those in pneumatic piping.

The general schematic diagram of the ‘Bleed Less Vapour Compression Refrigeration System’ is shown in Fig. 1.2. In this system, the compressed air is generated from the cabin mounted centrifugal compressor and processed by suitable means of vapour cycle system. It uses vapour compression refrigeration system

(VCRS) to cool the hot exit air from compressors to the required temperature. The compressed air is produced by electrically driven compressors and the hot air is re-cooled by the ram air. This air is cooled to required temperature by vapour cycle refrigeration unit.

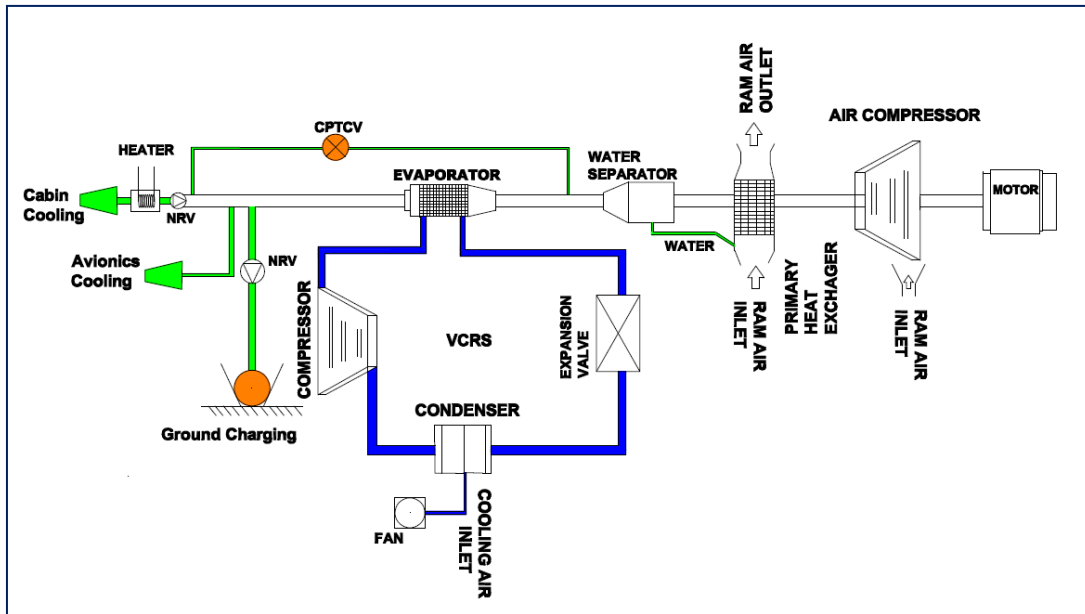


Fig. 1.2: Bleed Less Vapour Compression Refrigeration System

Vapour cycle system has got following advantages over bleed air cycle system:

- Gain of engine thrust
- Avoids high pressure and high temperature air from engine
- High coefficient of performance and high heat transfer rates
- Reduce the drag by minimizing the ram air intake ports

In vapour cycle system, compact heat exchangers will play vital role as condenser and evaporator. Until now compact plate fin heat exchangers are widely used in aerospace and process industries for sensible heat transfer applications. Use of compact plate fin heat exchangers as condenser and evaporator are explored in the last decade by industries. For the use of latent heat of vaporization and latent heat of condensation process of these heat exchangers in the VCRS, the design data (condensation heat transfer coefficients and two phase friction factor coefficients) for various ranges of serrated fin surfaces are not available in the open literature. Hence it is a step to develop the design data and development of two phase average

condensation refrigerant 134a heat transfer and two phase frictional pressure drop correlations for the serrated type fin surfaces.

1.2 Application Areas

World aircraft development industries are now switching over to age old VCRS system due to extensive developments in environmental control system and user friendly refrigerants. The VCRS system have high coefficient of performance (COP) and heat transfer rates compared to air. Hence, the size of components and space required for the system can drastically be reduced, which are the main constraints of any aircraft.

In bleed less vapour cycle ECS, the compressed air is generated from the cabin mounted centrifugal compressors and processed by suitable means of vapour cycle system. It uses vapour cycle refrigeration system to cool the hot exit air from compressors to the required temperature. The compressed air is produced by electrically driven compressors and the hot air is re-cooled by the ram air. This air is cooled to required temperature by vapour cycle refrigeration unit. The commonly used refrigerant is R134a. The conditioned air is now passed through the water separator and air manifold for distribution to cabin. The cabin air is re-circulated after filtering to the extent of 30% to 50%.

All the unmanned aircraft development programmes in the world have been switched over to VCRS and are in the process of testing in the aircraft. PC 12 (passenger Aircraft) and PC 21 (Swiss air force trainer) developed by PILATUS Aircraft Industries Switzerland has developed the VCRS system for aircraft and the systems are operational.

Basically, the aim of research is generation of design data of compact plate fin heat exchangers for condensation application. It is required to design the compact plate fin condenser for vapour compression refrigeration cycle system to use in an aircraft environmental control system and other areas are:

- Other defence applications
- All types air-conditioning systems
- Automobile/ locomotive air conditioning systems
- Process industries

1.3 Compact Plate Fin Heat Exchangers

Compact plate-fin heat exchangers are widely used in aerospace, automobile and cryogenic industries due to their high heat transfer area-to-volume ratio for any given thermal performance. It is resulting in reduced size, weight, support structure, energy requirement and cost. Depending on the application, various types of improved heat transfer surfaces, i.e., 'fins', such as Plain, Wavy, Serrated, Perforated and Louvered fins are used in compact heat exchangers. The higher rate of heat exchange within a small volume is accomplished by employing intricate flow passages offering large heat transfer areas. These requirements of modern devices have been the motivation for the development of a class of heat exchangers known as compact heat exchangers. If the surface area to volume is greater than $700 \text{ m}^2/\text{m}^3$ in either one or more channels of a two stream or a multi-stream heat exchanger (Shah et al., 1980) is called compact. Such compactness is achieved by providing a high density of fins in the flow passages. The brazed plate fin heat exchanger successfully incorporates all these positive features, has received wide acceptance in industry. Although these heat exchangers have been extensively used around the world for several decades, the technologies related to their design and manufacture remains confined to a few companies in the world.

A compact plate fin heat exchanger is essentially a stack of alternating layers of fins and flat plates bonded together to form a monolithic block with distinct passages for the fluid streams. A schematic view of such heat exchanger is given in Fig. 1.3. Heat transfer between the fluid streams takes place through the separating plates (primary surfaces) and the fins (secondary surfaces) connected to the primary surface. The fins apart from adding the heat transfer process provide rigidity to the structure against internal pressure. Side bars also bonded to the plates; prevent the fluid streams from spilling over or mixing among each other. An exploded view of two layers of a heat exchanger core assembly has been shown in Fig 1.3.

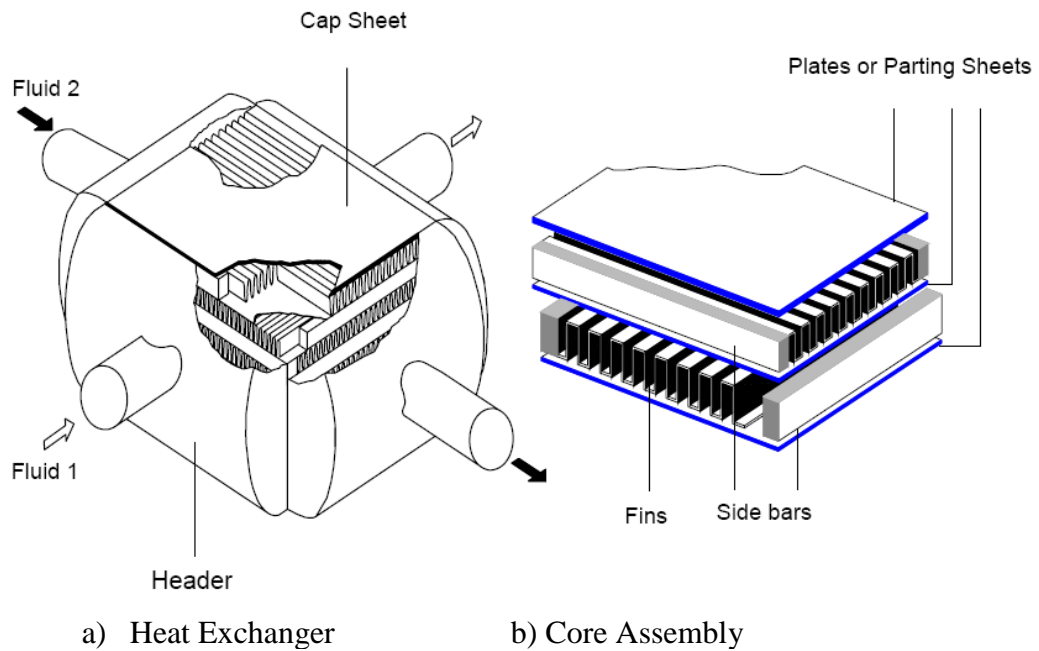


Fig. 1.3: Plate Fin Heat Exchanger Assembly

The design characteristics of heat exchanger surfaces are generally expressed in terms of two quantities called the heat transfer coefficient and friction factor. Due to their extensive practical applications, heat exchangers could attract the attention of a large number of researchers over years. The “Compact Heat Exchangers” by Kays and London (1984), provides an excellent introduction to the design of plate fin heat exchangers, and contains a valuable data base on the heat transfer and friction characteristics of several fin geometries for sensible heat applications.

The principle advantages of the plate fin geometry are:

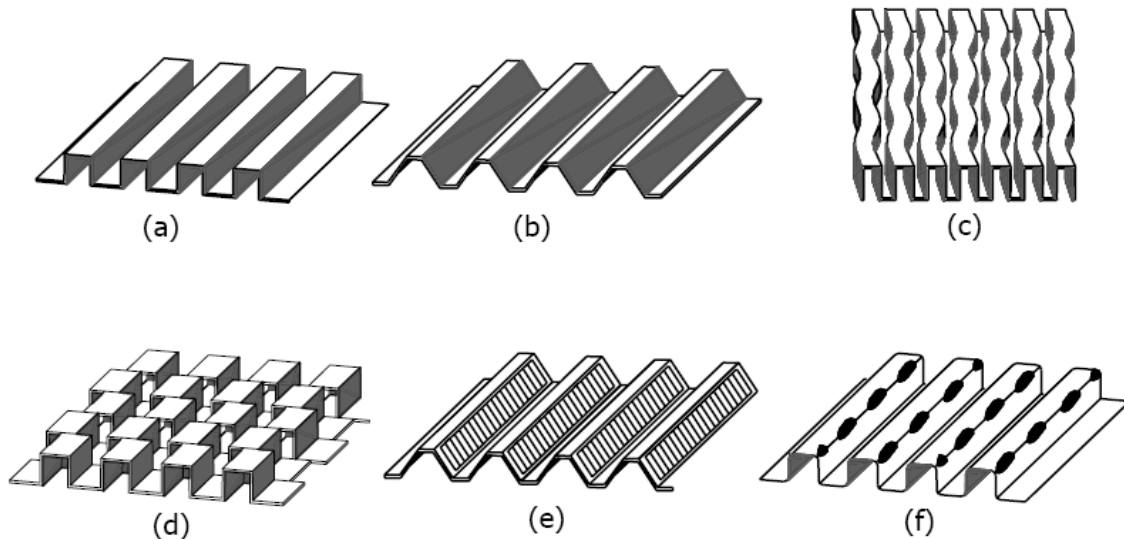
- a) High thermal effectiveness
- b) Large heat transfer surface area per unit volume
- c) Low weight

The principle disadvantages of the plate fin geometry are:

- a) Limited range of temperature and pressure,
- b) Difficulty in cleaning of passages, which limits its application to clean and relatively non-corrosive fluids
- c) Difficulty of repair in case of failure or leakage between passages.

1.3.1 Fin geometries

The plate fin heat exchanger performance is determined among other things, by the geometry of the fins. The most universal fin configurations are plain fins with rectangular, trapezoidal or triangular passages, uninterrupted wavy fins and interrupted fins such as offset strip, louvered and perforated fins. The schematics are of each fin type are shown in Fig. 1.4.



a) Plain Rectangular b) Plain Trapezoidal c) Wavy

d) Serrated e) Louvered f) Perforated

Fig. 1.4: Types of Plate Fin Surfaces

1.3.2 Flow arrangement

A compact plate fin heat exchanger accepts two or more streams, which may flow in directions parallel or perpendicular to one another. When the flow directions are parallel the stream may flow in the same or in opposite sense. The common three types of primary flow arrangements are parallel flow, counter flow and cross flow. Thermodynamically, the counter flow arrangement provides the highest heat (or cold) recovery and parallel flow geometry gives the lowest. The cross flow arrangement while providing intermediate thermodynamic performance, offers superior heat transfer properties and easier mechanical layout. Hybrid cross-counter flow geometry provides greater heat (or cold) recovery with superior heat transfer performance. The general three different flow arrangements are shown Fig. 1.5.

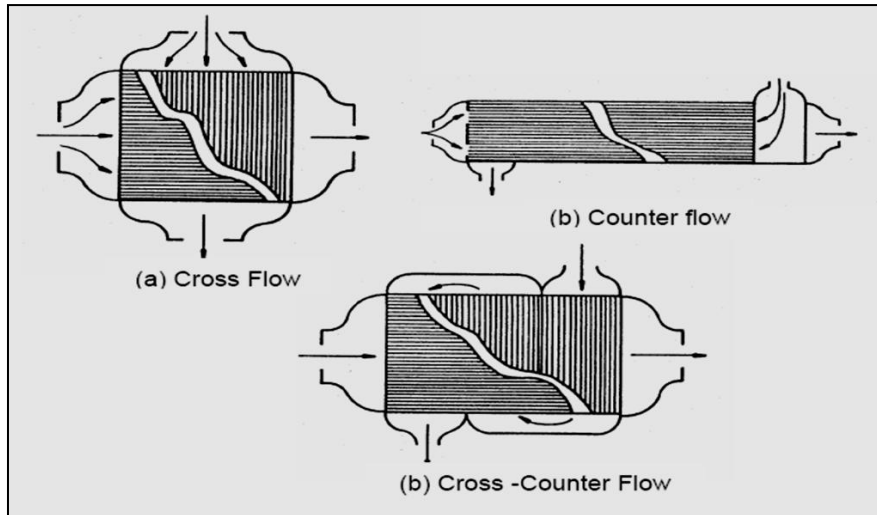


Fig.1.5: Different Flow Configurations in Heat Exchanger (Dipak Kumar Maiti, 2002)

1.3.3 Fabrication of compact plate fin heat exchangers

The basic approach to fabricate plate fin heat exchanger is to assemble the parting sheets (clad with brazing alloy), fins, sidebars and top plates together in a fixture. The entire assembly brazed to form the heat exchanger core. While the side bars and the parting sheets are cut to size by milling and shearing. The pre-formed thin walled fins are cut to required shape and size by employing electro discharge machining (EDM). Most plate-fin heat exchangers used for cryogenic applications are made of aluminum with a vacuum-brazed core. Corrosion-resistant and heat-resistant brazing alloys can be used for brazing of heat exchanger core.

Plate fin heat exchangers are made by the stacking of corrugated sheets (fins) separated by separation sheet that usually has a clad alloy on both sides that will melt at a lower temperature than the parent aluminum material during brazing and closed on the sides by lateral bars. A core is made of a great number of layers. The exchanger can be made of one or more cores. The number of plate and fin layers, the size of the plates and fin, the height of the fin and the type of fin are engineered for optimum performance. Manifold ducting and mounting brackets are then welded in place as required and any required paint or coating can be added.

The construction of materials selection is based on the maximum operating temperature of a plate-fin heat exchanger. Aluminum brazed plate-fin heat exchangers can be used from cryogenic temperatures (-180°C) up to 200°C depending on the

aluminum alloys. Stainless steel plate-fin heat exchangers are able to operate at up to 600°C, while titanium units can tolerate temperatures approaching 550°C. Aluminum brazed units can operate up to 4 MPa, depending on the physical size and the maximum operating temperature. Stainless steel plate-fin heat exchangers are limited to 5 MPa.

1.3.4 Applications

The compact heat exchangers are used in air separation plants (production of oxygen, helium and hydrogen liquefiers), oil and gas processing, automobile radiators and air conditioners, environment control and secondary power systems of aircraft. The applications such as:

1. Exchange of heat between gases, liquids or both,
2. Condensation
3. Boiling
4. Sublimation and
5. Heat or cold storage

1.4 Condensation Heat Transfer and Flow Friction

1.4.1 Condensation

If a vapour is exposed to a surface at a temperature below saturation temperature then condensation occurs on the surface in the form of a liquid film or individual droplets. It is usually done by bringing the vapour into contact with a solid surface whose temperature is below the saturation temperature of the vapor. This is considered to be form of convection heat transfer since they involve fluid motion such as the flow of condensate to the bottom. The temperature remains constant under equilibrium conditions during a phase-change process at a fixed pressure. In this process large amounts of heat (due to the large latent heat of vaporization released or absorbed) can be transferred during condensation particularly at constant temperature (Yunus A. Cengel, 2007). However, it is required to maintain some difference between the surface temperature and the saturation temperature for effective heat transfer mechanism. Heat transfer coefficients associated with condensation are

generally much higher than those in other forms of convection processes that involve a single phase.

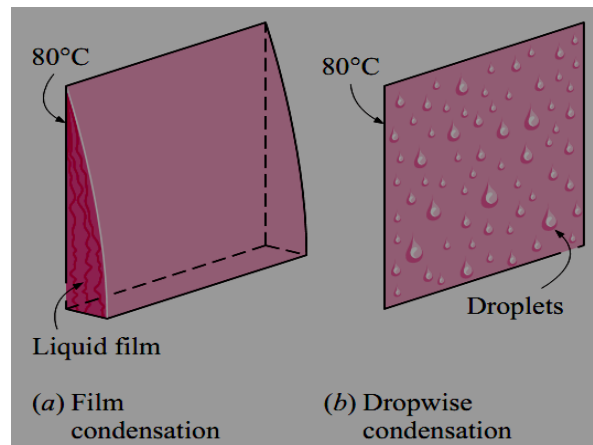


Fig. 1.6: Different Types of Condensation (Yunus A. Cengel, 2007)

Two distinct forms of condensation are shown in Fig. 1.6. They are film condensation and dropwise condensation. In film condensation, the condensate wets the surface and forms a liquid film on the surface that slides down under the influence of gravity. The liquid film thickness increases in the flow direction as more vapour condenses on the film. In dropwise condensation, the condensed vapour forms droplets on the surface instead of a continuous film, and the surface is covered by countless droplets of varying diameters.

1.4.2 Film condensation

In film condensation, the surface is covered by a liquid film of increasing thickness, and this “liquid wall” between solid surface and the vapour serves as a resistance to heat transfer. The velocity and temperature profiles of the condensate are also given in Fig. 1.7. Due to no-slip condition the velocity of the condensate at the wall is zero and it reaches a maximum at the liquid–vapour interface. At the interface the temperature of the condensate is saturation temperature and it decreases gradually to surface temperature at the wall. In forced convection involving a single phase, heat transfer in condensation also depends on whether the condensate flow is laminar or turbulent. Again the Reynolds number provides the criterion for the flow regime.

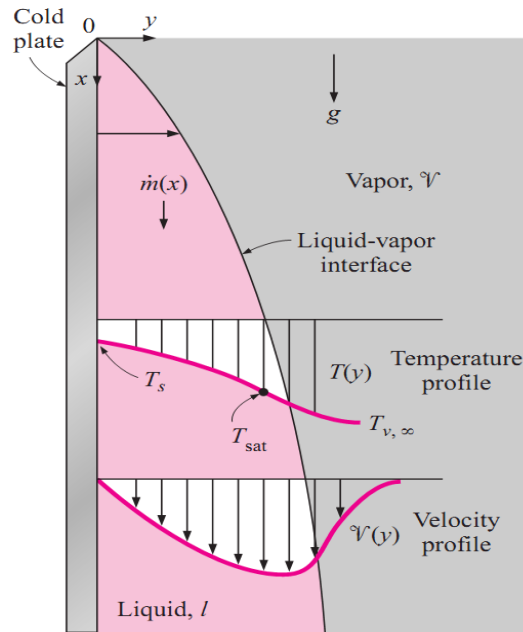


Fig. 1.7: Typical velocity & Temperature Profile of the Condensate
(Yunus A. Cengel, 2007)

1.4.3 Dropwise condensation

It is characterized by countless droplets of varying diameters on the condensing surface instead of a continuous liquid film. This is one of the most effective mechanisms of heat transfer, and tremendously large heat transfer coefficients can be achieved with this mechanism and is shown in Fig. 1.8.

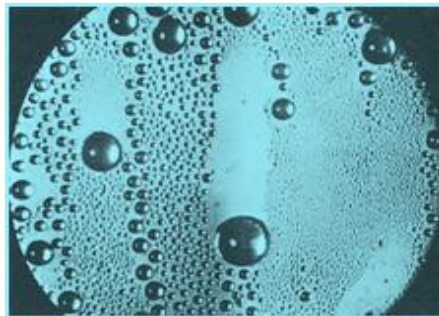


Fig.1.8: Dropwise Condensation Phenomenon (Yunus A. Cengel, 2007)

In this, the small droplets that form at the nucleation sites on the surface grow as a result of continued condensation, coalesce into large droplets and slide down when they reach a certain size. As a result, with dropwise condensation, heat transfer

coefficients can be achieved 10 times larger than those associated with film condensation. Therefore, dropwise condensation is the preferred mode of condensation in heat transfer applications and is achieved by adding a promoting chemical into the vapour or coating the surface with a polymer such as teflon or a noble metal such as gold, silver, rhodium, palladium, or platinum. Since the dropwise condensation achieved did not last long and converted to film condensation after some time. Therefore, it is common practice to be conservative and assume film condensation in the design of heat transfer equipment (Yunus A. Cengel, 2007).

1.5 Objectives of the Study

The proposed research shall be carryout to investigate the condensation heat transfer coefficient and pressure drops on selected geometries and develop the correlations for the each fin geometries. An experimental test facility had been set up for generation of condensation heat transfer coefficient and pressure drop data. The major objectives are listed below:

- 1) Generation of single phase heat transfer coefficient and friction factor correlations for serrated fin surface of a test condenser for water using CFD analysis.
- 2) To find the effect of refrigerant 134a mass flux and heat flux on average condensation heat transfer coefficient and frictional pressure drop on serrated fin geometry surfaces.
- 3) Development of serrated fin correlations for average condensation heat transfer coefficient and frictional pressure drop for R134a.
- 4) To study the influence of serrated fin surface hydraulic diameter on average condensation heat transfer coefficient and frictional pressure drop.
- 5) Development of generalized serrated fin correlations for average condensation heat transfer coefficient and frictional pressure drop for R134a.
- 6) Experimental study with different hydraulic diameter fins to identify the better serrated fin geometry which gives best performance.

1.6 Organization of Thesis

Thesis consists of total seven chapters starting with introduction and conclusions being last chapter. The chapter of introduction includes background of the problem, application of present work, brief explanation about the compact heat exchangers, condensation heat transfer techniques and brief explanation about the scope of present work. Review of the literature related to the research, single phase heat transfer and frictional coefficients, gaps in the two phase condensation research, and summary of the some of the authors correlations related to single phase as well as refrigerant two phase research work is presented in second chapter. The test facility was not having a provision to generate water side serrated fin surface heat transfer coefficient (j factor) and frictional pressure drop (f factor). To generate j and f data, Chapter 3 is included with computational approach to establish single phase heat transfer coefficient correlations for serrated fin surfaces with water using ANSYS Fluent. Explanation in the Chapter 4 consists of development of brazed plate fin heat exchangers includes, identification of fin surfaces, theoretical design of test units, brazing of test units, welding and leak testing of test condenser units. Also, Chapter 4 deals with details of experimental setup for exploration of average condensation heat transfer coefficient and frictional pressure drop of different serrated fin surfaces using R134a. Development of test facility and validation of the test facility are discussed in Chapter 4. Based on experimental observations, step by step procedure of data reduction to get results is explained in Fifth Chapter. Chapter 6 is included with the explanation of results, discussion on reasons of heat transfer coefficient & frictional pressure drop enhancement, and comparison of performance of different serrated fin surfaces. Method, process and performance of empirical correlation is explained in Chapter 6. Overall conclusions of the research along with future scope are presented in seventh chapter. Apart from chapters, list of tables, list of figures, list of appendix and references are also made as a part of the thesis.

CHAPTER 2

LITERATURE REVIEW

In this chapter extensive literature survey has been made through searching upto date available technical papers from internet and other sources. The literature survey reveals that no design data is available for condensation application in compact brazed plate fin heat exchangers. Extensive experimental data and empirical correlations have been obtained in inside tubes and herringbone fins for the average condensation heat transfer and pressure drop characteristics of an ozone-friendly refrigerant 134a and other refrigerants. Literature review has been done in the following aspects:

- Single phase heat transfer and pressure drop characteristics in serrated fin surfaces used in brazed compact plate fin heat exchangers.
- Two phase studies on average condensation heat transfer and flow friction pressure drop.

2.1 Single Phase Heat Transfer and Pressure Drop Characteristics

There is a rich literature on the subject of convective heat transfer, as well as on its application to heat exchanger design. More recently, there has been a lot of activity on numerical solution of heat transfer equations and generation of j and f data for a variety of surfaces.

2.1.1 Plate fin heat exchangers

Significant literature exists on the design data and performance of compact plate fin heat exchangers for sensible heat application. The works of Shah and Webb (1983), London (1983) and Shah (1981) provide a complete coverage of the analysis of these exchangers- rating, sizing and optimization. The performance of an enhanced surface is normally compared with that of the corresponding plain surface. Many authors have proposed performance comparison methods and have applied them to plate fin exchangers. Shah (1978) has surveyed more than thirty such methods in 1978 and more have been published [Soland et al. (1978), Webb (1981), Cowell (1990)]

since that date. A singular advantage of the plate fin heat exchanger is its capacity to accommodate many parallel streams. The design of multi stream exchanger, each stream divided into several parallel channels, however, poses special challenge.

The basic heat exchanger theory assumed that the fluid flow rate is distributed uniformly through the exchanger on each side of the heat transfer surface. However, in practice, flow maldistribution is more common and can reduce the idealized performance significantly (Warren et.al, 1998). Mueller and Chiou (1988) did extensive work and gave the different types of flow mal-distribution that can occur in compact heat exchangers. Many works were carried out on fluid flow non-uniformity.

Ranganayakulu et al. (1997 & 1999) studied the combined effects of two dimensional longitudinal heat conduction, flow and temperature non-uniformity in compact plate-fin heat exchangers using finite element method (FEM). They developed fluid flow and temperature mal-distribution models considering the possible deviations in fluid flow. The heat exchanger effectiveness and its deterioration due to the combined effects of longitudinal heat conduction, flow and temperature non-uniformity are calculated for various design and operating conditions of the exchanger using these models. They found that the performance variations are quite significant and cannot be neglected.

Ranganayakulu et al. (2005, 2006^a & 2006^b) studied the effects of flow mal-distribution using a CFD simulation tool 'Fluent' and found out that there was significant flow mal-distribution/flow non-uniformity in the heat exchangers that are concerned. The flow was visualized to confine to very few sections of the heat exchanger core while there was nearly zero flow or flow in reversed directions. When the same heat exchangers are optimized for thermo-hydraulic performance improvement, there was significant improvement in the performance of these heat exchangers.

The correlations of j' and f' presented by Pallavi and Ranganayakulu (2011), using CFD are compared with experimental results with air flow presented by Wieting (1975), Kays and London (1984), Mochizuki et al. (1987), Manglik and Bergles (1995) and Joshi and Webb (1987). Also, the colburn and friction factor correlations presented by Rao et al. (2013), using CFD are compared with Kays and London (1984), which were obtained from the experiments with air flow for the plain fins.

2.1.2 Offset strip fins

An extensive literature search revealed that empirical and analytical solutions for the performance of rectangular offset-strip plate-fin heat exchangers are virtually nonexistent for single phase till before 1950. In 1950, an empirical relationship for offset-fin surfaces was developed by Manson (1950). However, the correlation was based on limited data and several different types of offset fins.

Kays (1972) attempts the analytical modeling of the heat transfer and frictional drop in offset strip fins. His correlations are:

$$j = 0.665 \text{ Re}^{-0.5} \quad (2.1)$$

$$f = 0.44 \left(\frac{t}{l}\right) + 1.328 \text{ Re}^{-0.5} \quad (2.2)$$

However, his correlations don't consider the fin parameters that have significant role to play like the fin spacing and fin height.

Wieting (1975) presented experimental data with air as the working fluid for different fin geometries and developed correlations for heat transfer in the laminar and turbulent region by the multiple regression method. The fin parameter relationships indicate that the flow passage aspect ratio is significant only in the laminar flow regime and the fin thickness parameter is significant only in the turbulent regime. His correlations are

For $\text{Re} \leq 1000$

$$f = 7.661 \left(\frac{L}{D_h}\right)^{-0.384} \alpha^{-0.092} \text{Re}_D^{-0.712} \quad (2.3)$$

$$j = 0.483 \left(\frac{L}{D_h}\right)^{-0.162} \alpha^{-0.184} \text{Re}_D^{-0.536} \quad (2.4)$$

For $\text{Re} \geq 2000$

$$f = 1.136 \left(\frac{L}{D_h}\right)^{-0.781} \left(\frac{t}{D_h}\right)^{0.534} \text{Re}_D^{-0.198} \quad (2.5)$$

The applicability of the above correlations to fluids outside the gas Prandtl number range may not be suitable. The correlations are developed by considering the effect of fin length, height, thickness, spacing and hydraulic diameter on the performance. These relationships also indicated that the aspect ratio is significant only in the laminar region and that the fin thickness parameter (t/D_h) is significant only in the turbulent flow region.

Patankar et al. (1977) conducted numerical studies in channels whose walls are periodically interrupted along the stream wise direction on the heat transfer and fluid flow. The plates were unspecified to be of negligible thickness, smooth edged and isothermal. The results were employed to compare the heat transfer rates in heat exchangers composed either of interrupted-wall channels or of parallel plate channels. The heat transfer augmentation was markedly felt on relatively short heat exchanger channels and at high Reynolds numbers. The predictions lie about 20-35% above the heat transfer data, whereas the frictional loss predictions lay 10- 20% below the data.

Joshi and Webb (1987) have identified the transition region by conducting flow visualization experiments and modified the correlations of Wieting (1975). The authors developed elaborate analytical models based upon the predicted characteristics. They also came up with a separated definition for the Reynolds number (Re^*) in the transition region. Thus, the laminar, turbulent, and transition regions were identified. Further the hydraulic diameter defined as

$$D_h = \frac{2(s-t)h}{[(s+h)+\frac{th}{l}]} \quad (2.6)$$

and the laminar and turbulent flow limits given as $Re \leq Re^*$ and $Re \geq (Re^* + 1000)$ respectively, they gave the correlations as:

$$Re \leq Re^*$$

$$j = 0.53 Re_D^{-0.50} \left(\frac{1}{D_h}\right)^{-0.15} \alpha^{-0.14} \quad (2.7)$$

$$f = 8.12 Re_D^{-0.74} \left(\frac{1}{D_h}\right)^{-0.41} \alpha^{-0.02} \quad (2.8)$$

$$Re \geq (Re^*+1000)$$

$$j = 0.21 Re_D^{-0.40} \left(\frac{1}{D_h}\right)^{-0.24} \left(\frac{t}{D_h}\right)^{0.02} \quad (2.9)$$

$$f = 1.12 Re_D^{-0.56} \left(\frac{1}{D_h}\right)^{-0.65} \left(\frac{t}{D_h}\right)^{0.17} \quad (2.10)$$

where

$$Re^* = 257 \left(\frac{1}{s}\right)^{1.23} \left(\frac{t}{l}\right)^{0.58} D_h \left[t + 1.328 \left(\frac{Re}{l D_h}\right)^{-0.5} \right]^{-1} \quad (2.11)$$

Mochizuki et al. (1987) developed experimental correlations based on aluminium plate fin type heat exchangers with strip fins. Systematically the fin spacing and strip length are selected. Experiments were carried out using air as the

test fluid and condensing steam as the other medium. The correlations given by them are:

$Re < 2000$

$$j = 1.37 \left(\frac{1}{D_h} \right)^{-0.25} \alpha^{-0.184} Re^{-0.67} \quad (2.12)$$

$$f = 5.55 \left(\frac{1}{D_h} \right)^{-0.32} \alpha^{-0.184} Re^{-0.67} \quad (2.13)$$

$Re \geq 2000$

$$j = 1.17 \left(\frac{1}{D_h} + 3.75 \right)^{-1} \left(\frac{t}{D_h} \right)^{0.089} Re^{-0.36} \quad (2.14)$$

$$f = 0.83 \left(\frac{1}{D_h} + 0.33 \right)^{-0.5} \left(\frac{t}{D_h} \right)^{0.089} Re^{-0.20} \quad (2.15)$$

$$\text{where, } D_h = \frac{2sh}{(s+h)} \quad (2.16)$$

Manglik and Bergles (1995) studied the concepts of each correlation available in open literature and generated their own correlations. Various fin parameters from literature are taken into account while generating the correlations.

Sparrow et al. (1977) analysed the offset strip fins using numerical technique by solving the continuity equations numerically and getting the local heat transfer and pressure loss. They obtained the results for different Reynolds number and for several values of a dimensionless fin parameter characterizing of individual plate segments and at Prandtl number of 0.7 for air. They even compared their results with the experimental values. They found out that up to Reynolds number 900, the predictions of heat transfer lie above the data by 20-35% and friction factor lie below the data by 10-20% and gave explanation that this is due to the bent edges of the plates which have taken a toll in pressure drop while the heat transfer is reduced owing to the disturbance of the thin laminar boundary layers that are responsible for the augmentation. They gave their own correlations as:

$$j = 3.92 Re_D^{-0.792} \quad (2.17)$$

$$f = 9.60 Re_D^{-0.792} \quad (2.18)$$

Patankar and Prakash (1981) presented a numerical analysis for the flow and heat transfer in an interrupted plate passage, which is an idealization of an offset fin heat exchanger channel. The overall results are compared with available experimental data. Their calculation method was based on the periodically fully

developed flow through one periodic module and the fin thickness effect in the offset strip fins was studied. They also assumed stable laminar wake and used a constant heat flux boundary condition with the additional specification that each row of fins were at a fixed temperature. It was noticed that only when the plate is sufficiently thick, the recirculation zones extend to the next plate. They have concluded that a thick-plate situation leads to significantly higher pressure drop, while the heat transfer does not sufficiently improve, despite the increased surface area and increased mean velocity.

2.1.3 Wavy fins

Works carried out on wavy fins mainly focused on the corrugation inclination angle, inter wall spacing and other performance parameters.

Cur and Sparrow (1979) studied the heat transfer and pressure drop characteristics for wavy fins. They studied for both the developing flows and the fully developed flows. They found out that the thermal development is attained at or prior to the eight hydraulic diameters. The fully developed Nusselt number increases with plate thickness. At higher Reynolds numbers, the increase was about 40% over the range from $t/L = 0.04$ to 0.12 . Even larger increases were encountered at lower Reynolds numbers owing to the triggering to transition from laminar to turbulent. The presence of interruptions or the corrugations shown to bring about a significant increase in Nusselt number compared with that for continuous-walled duct. A comparison in the fully turbulent regime showed the augmentation to be about a factor of two.

Goldstein and Sparrow (1977) carried out the experiments on wavy channels using the naphthalene sublimation technique and determined the local and average transfer characteristics for flow. They covered the entire laminar, transition and turbulent regimes. They also visualized the secondary flows and associated span wise variations in mass transfer, suppression of the secondary flow by counteracting centrifugal forces and destruction of secondary flow by the onset of turbulence. The average transfer coefficients for the corrugated wall channel were moderately larger than those for a parallel-plate channel in the laminar range. On the other hand, in the turbulent regime, the wall corrugations were responsible for three times increase in the average coefficient compared with the smooth wall channel.

O'Brien and Sparrow (1982) experimentally studied the wavy channels/fins to determine the forced convection heat-transfer and friction factors characteristics. They took the 30° corrugation angle and the inter wall spacing was equal to the corrugation height. Nusselt numbers in the periodic fully developed regime, when correlated, resulted in a Reynolds-number dependence of $Re^{0.614}$ and a Prandtl number dependence of $Pr^{0.34}$. The correlation was given as:

$$Nu = 0.409 Re^{0.614} Pr^{0.34} \quad (2.19)$$

Sparrow and Comb (1983) performed experiments considering the effects of inter wall spacing, fluid flow inlet conditions and the role of non-corrugated side walls for the evaluation of heat transfer coefficient. They found out that the increase of the inter wall spacing substantial increase in heat transfer (30% increase), but the friction factor increased to more than a factor of two. Fluid inlet configurations were employed which created different degrees of turning of the flow. It was found that the greater the turning, the higher the entrance region heat transfer coefficients.

Focke et al. (1985) studied the effects of the corrugation inclination angle on the thermo-hydraulic performance and found that at angles up to about 80° maximum transfer rates takes place and angles greater than that, the flow pattern becomes less effective for transfer; in particular at 90° marked flow separations is observed. This is because up to angles of about 80° , the fluid flows mainly along the furrows of each plate and a secondary, swirling motion is imposed on the flow along it when its path is crossed by streams flowing along furrows on the opposite wall.

Amano (1985) used numerical technique to determine the hydrodynamic and performance characteristics in a periodically corrugated wall channel for both laminar and turbulent flows. Used the k- ϵ turbulence model with a refined near wall model with step ratios l/s ranging from two to four and Reynolds number ranging from 10 to 25,000 and the equations were solved using the modified hybrid scheme. The correlation for the Nusselt number as:

$$Nu = 0.307 Re^{0.642} \left(\frac{l}{s}\right)^{-0.592} \quad (2.20)$$

Amano et al. (1987) studied the turbulent heat transfer in corrugated wall channel with numerical technique using Reynolds stress model (RSM) and k- ϵ

turbulence models and found out that the RSM model gave more improved results by 30% as compared to k- ϵ model. They also found that inserting fins resulted in the flow passage resulted in considerable changes in flow pattern and skin friction but little effect on heat transfer rate.

Asako and Faghri (1987) used finite volume methodology to predict heat transfer coefficients, friction factors and streamlines. They used the algebraic coordinate transformation to map the complex flow geometry domain onto a rectangle. They observed the same flow patterns with highly complex recirculation zones. The significant work was the grid transformation.

Patel et al. (1991) used the boundary layer numerical concept to visualize the flow pattern in both the laminar and turbulent regions separately. For laminar region they found out that for deep enough cavities, the flow tends to become unsteady, presumable as a result of instability and transition to turbulence. For the turbulence analysis they highlighted the importance of turbulence two equations models developed by Chen and Patel and the breakdown of standard law of wall turbulence model in strong adverse and favourable pressure gradients.

Ciofalo et al. (1996) investigated the flow and heat transfer in corrugated passages using experiment and numerical simulation. Three-dimensional numerical predictions were obtained by a finite volume method using different turbulence models, which includes low-Reynolds number k- ϵ models, Direct Numeric Simulation (DNS) model and the Large Eddy Simulation (LES) model and the results are compared with the experimental data. It was found out that laminar and standard k- ϵ computations were unsatisfactory as they under-predict and over-predict f over most of the Reynolds number range. Laminar flow simulations over-predict the Reynolds number dependence of the friction coefficient. The trend is quite similar for Nusselt number also.

Wang and Vanka (1995) studied the rates of heat transfer using accurate numerical scheme and observed that the flow is steady until Re around 180 after which self-sustained oscillations dominated resulting in destabilization of laminar thermal boundary layers, replenishing the near-wall fluid with the fluid in the core region, and providing the natural mechanism of heat and mass transfer enhancement.

The heat transfer enhancement was found to be about a factor of 2.5 as compared to parallel-plate channel and friction factors were high about a factor of 2.

Rush et al. (1998) performed experiments and used visualization method to characterize the flow field as steady or unsteady. They found out that onset of mixing is depend on the Reynolds number and channel geometry and instabilities are manifest near the channel exit at low Reynolds numbers ($Re \sim 200$).

Manglik et al. (2005) studied the fin density effects on the performance of the wavy plate-fin heat exchangers. They considered air with Prandtl number of 0.7 as working fluid and the Reynolds number ranging from 10 to 1000. They found out that the fin waviness induced the steady and spatially periodic growth and disruption of symmetric pairs of counter-rotating helical vortices in the wall trough regions of the flow cross-section. The thermal boundary layers on the fin surface are thereby periodically interrupted, resulting in high local heat transfer near the recirculation zones. Increasing fin density tends to dampen the recirculation and confine it. The extent of swirl increases with flow rate, when multiple pairs of helical vortices are formed which significantly enhances the overall heat transfer coefficient as well as the pressure drop penalty, when compared with straight channel.

Hwang et al. (2006) used naphthalene sublimation technique to investigate the heat and mass transfer characteristics. They covered the Reynolds number range of 100 to 5000 and used “Fluent” CFD software. They found out that at low Reynolds number ($Re \leq 1000$), relatively high heat/mass transfer coefficients appear on both pressure and suction side walls due to the secondary vortex flows called Taylor-Goertler vortices perpendicular to the main flow direction and at high Reynolds numbers, these secondary flows disappear and boundary layer type flow develop on pressure-side wall.

Dipak Kumar Maiti (2002) carried out an in-depth numerical study on the heat transfer coefficients and flow friction factors in plate fin heat exchanger surfaces with plain, wavy and offset strip fins. A practical approach was evolved for determining the dependence of j and f factors on Re and dimensionless geometrical features. Sets of correlations were generated for use in the heat exchanger design.

Table 2.1: Summary of Correlations for Single Phase Fluid

Researcher	Correlation	Media	Remarks
Kays (1972)	$j = 0.665\text{Re}_1^{-0.5}$ $f = 0.44 \left(\frac{t}{l}\right) + 1.328\text{Re}_1^{-0.5}$	Air	Offset Strip fin,
Wieting (1975)	<p>For $\text{Re} \leq 1000$</p> $f = 7.661 \left(\frac{L}{D_h}\right)^{-0.384} \alpha^{-0.092} \text{Re}_D^{-0.712}$ $j = 0.483 \left(\frac{L}{D_h}\right)^{-0.162} \alpha^{-0.184} \text{Re}_D^{-0.536}$ <p>For $\text{Re} \geq 2000$</p> $f = 1.136 \left(\frac{L}{D_h}\right)^{-0.781} \left(\frac{t}{D_h}\right)^{0.534} \text{Re}_D^{-0.198}$	Air	22 heat exchanger geometries
Joshi and Webb (1987)	<p>$\text{Re} \leq \text{Re}^*$</p> $j = 0.53(\text{Re}_D)^{-0.50} \left(\frac{l}{D_h}\right)^{-0.15} \alpha^{-0.14}$ $f = 8.12(\text{Re}_D)^{-0.74} \left(\frac{l}{D_h}\right)^{-0.41} \alpha^{-0.02}$ <p>$\text{Re} \geq (\text{Re}^* + 1000)$</p> $j = 0.21(\text{Re}_D)^{-0.40} \left(\frac{l}{D_h}\right)^{-0.24} \left(\frac{t}{D_h}\right)^{0.02}$ $f = 1.12(\text{Re}_D)^{-0.36} \left(\frac{l}{D_h}\right)^{-0.65} \left(\frac{t}{D_h}\right)^{0.17}$	Air	Offset strip fin. laminar -turbulent transition

	$Re^* = 257 \left(\frac{l}{s}\right)^{1.23} \left(\frac{t}{l}\right)^{0.58} D_h \left[t + 1.328 \left(\frac{Re}{lD_h}\right)^{-0.5} \right]^{-1}$		
Mochizuki et al. (1987)	<p>Re < 2000</p> $j = 1.37 \left(\frac{l}{D_h}\right)^{-0.25} \alpha^{-0.184} Re^{-0.67}$ $f = 5.55 \left(\frac{l}{D_h}\right)^{-0.32} \alpha^{-0.184} Re^{-0.67}$ <p>Re ≥ 2000</p> $j = 1.17 \left(\frac{l}{D_h} + 3.75\right)^{-1} \left(\frac{t}{D_h}\right)^{0.089} Re^{-0.36}$ $f = 0.83 \left(\frac{l}{D_h} + 0.33\right)^{-0.5} \left(\frac{t}{D_h}\right)^{0.089} Re^{-0.20}$	Air	Compact heat exchangers with strip fins
Sparrow et al. (1977)	<p>Re < 900</p> $j = 3.92 Re_D^{-0.792}$ $f = 9.60 Re_D^{-0.792}$	Air	Offset strip fins using numerical technique
O'Brien and Sparrow (1982)	<p>Re = 1,500 to 25,000</p> $Nu = 0.409 Re^{0.614} Pr^{0.34}$	Air	experiments on Wavy channels/fins
Amano (1985)	<p>Re=10 to 25,000</p> $Nu = 0.307 Re^{0.642} \left(\frac{l}{s}\right)^{-0.592}$	Air	periodically corrugated wall channel

2.2 Two Phase Studies on Average Condensation Heat Transfer and Frictional Pressure Drop

Extensive experimental and empirical correlations are available in open literature for the condensation heat transfer and pressure drop characteristics of an ozone-friendly refrigerant R134a and other refrigerants in inside tubes, helicoidal pipes and herringbone fins. Yan et al. (1999) reported experimental data on condensation performance characteristics of refrigerant R134a in a vertical plate heat exchanger. The results indicated that the condensation heat transfer is slightly better for a higher average imposed heat flux and the associated frictional pressure drop (ΔP_f) rise was larger. Kang et al. (2000) and Han et al. (2005) experimented on condensation of R134a flowing inside helicoidal pipe. They carried out experiments for refrigerant flow mass fluxes from 100 to 400 kg/m²s. As the mass flux increases the overall condensing heat transfer coefficients of R134a also increased and associated pressure drops also increased. Longo et al. (2004) and Gstoehl et al. (2006) investigated the effects of enhanced surfaces during refrigerant condensation heat transfer coefficients. They presented the heat transfer coefficients for vaporization and condensation of refrigerant R22 in Plate heat exchangers (PHE) with a plate corrugation inclination angle of 65°. They also presented experimental data for both evaporation and condensation and reported that the surface enhancements in PHEs, compared to a smooth surface, cause an increase in heat transfer rate up to 40% for the vaporization, and to 60% for the condensation. Jokar et al. (2004) studied on condensation and evaporation of refrigerant R134a in PHEs with a plate corrugation inclination angle of 60°. Wang et al. (1999) obtained pressure drop characteristics of complete and partial condensation in a PHE. The Reynolds number of the condensate flow at exit ranged from 800 to 1800, where the flow was fully turbulent.

2.2.1 Tubes

Bassi and Bansal (2003) made a comparative study of the condensation heat transfer coefficients in a smooth tube with pure refrigerant R134a and its mixture with lubricant Castrol. The lubricant is synthetic polyol ester based oil commonly used in lubricating the compressors. Two concentrations of R134a-oil mixtures of 2% and 5%

oil (by mass) were analyzed for a range of saturation temperatures of refrigerant R134a between 35 °C and 45 °C. The effects of vapour quality, flow rate and saturation temperature on the heat transfer coefficient are investigated by analyzing the experimental data. Finally two new empirical models were developed to predict the two-phase condensation heat transfer coefficient for pure refrigerant R134a and a mixture of refrigerant R134a with castrol.

$$Nu = 0.0687 \times Re^{0.78} \times Pr^{\frac{1}{3}} - \text{For pure R134a} \quad (2.21)$$

$$\frac{h_{r \text{ oil}}}{h_{r \text{ no-oil}}} = e^{(-2.2\tau o)} - \text{For 134a oil mixture} \quad (2.22)$$

Where h_r - Condensation heat transfer coefficient (W/m²k)
 τo - Bulk oil mass in the mixture (%)

Contamination of R134a with synthetic polyol ester based oil resulted a decrease in condensation heat transfer coefficient in the in-tube. The coefficient decreased respectively by 5% and 10% when R134a was mixed with 2% and 5% oil.

Qian Su et al. (2009) attention is drawn, to the fact that, while four different correlations for condensation in micro channels are in fair agreement for the case of R134a and markedly they differ when applied to other fluids. It is of interest to note that the theoretical result is generally in fair agreement with the correlations for R134a. For ammonia its prediction relative to those of the correlations are depends on the vapour mass flux. Apart from suggesting that heat-transfer coefficient for ammonia might be around 10 times those for R134a under similar conditions, all that can be said from those comparisons is that it would be unsafe to use any of the correlations for fluids with properties widely different from those on which they were based. The general validity of the theory must await further and more accurate data for a range of fluids.

Cavallini et al. (2001) presented experimental measured data during condensation inside a smooth tube when operating with pure HFC refrigerants (R134a, R125, R236ea, R32, R410A). The effects of vapour quality, mass velocity, saturation temperature, driving temperature difference and reduced pressure are studied.

Park et al. (2011) presented the test facility for condensation experiments in vertically aligned multi-port minichannels. R134a, R236fa and R1234ze(E) were

tested over a wide range of test conditions with cooling water flowing in a 2 mm annulus gap around the multi-port tube in the condenser. The multi-port tube has rectangular channels with a hydraulic diameter of 1.45 mm. The effects of flow parameters were analyzed with the obtained database. The heat transfer coefficient decreased as condensation proceeded with decreasing vapour quality. The heat transfer coefficient increased with mass velocity but the increase was not significant at low mass velocities and low vapour qualities. They noted that the heat transfer coefficient was not affected by condensing heat flux and inlet vapour quality to the test section within the tested range.

Waldemar Kuczynski et al. (2012) presented the influence of hydrodynamic instabilities on heat transfer intensity during the condensation of R134a and R404A in pipe mini-channels. A decrease in the heat transfer coefficient results in decreased intensity of the heat removal process in the whole condenser. Disturbances of the condensation process were intentionally induced with a periodic stop and a repetition of the flow of the refrigerant. The reduction in the intensity of the heat transfer during the condensation process, which was induced with hydrodynamic instabilities, was presented in the form of the dependence of the heat transfer coefficient on the vapour quality and the frequencies of the disturbances.

Gstoehl et al. (2006) studied to determine the heat transfer coefficients for film condensation of R134a on tube arrays with plain and enhanced surfaces. New predictive methods were proposed based on the experimental results and visual observations of the liquid flow. The heat transfer coefficient of the finned tube has showed little variation with the inundation rate. The heat transfer coefficient was high at low film Reynolds numbers and decreases with increasing film Reynolds number.

Linlin Wang et al. (2012) presented on condensation performance characteristics of low GWP refrigerant HFO1234yf in a horizontal tube at a mass flux range of 100 to 400 kg/m²s and different saturation temperatures (40, 45, and 50⁰ C), and the results were compared with that of R134a and R32. Effects of mass flux, vapour quality, saturation temperature, and thermo physical properties on the heat transfer coefficient were analyzed. Mass flux and vapour quality were presented to primarily affect the heat transfer coefficient in shear-force dominated flow regimes,

whereas the thermal conductivity and density ratio are the primary parameters as thermo physical properties influencing the heat transfer coefficient.

Tadeusz Bohdal et al. (2011) presented on experimental investigations of characteristics during the condensation of the R134a and R404A refrigerants in pipe minichannels with internal diameter ranging from 0.31 mm to 3.30 mm. The results were compared with the correlations proposed by other authors. Within the range of the examined parameters of the condensation process in mini-channels produced from stainless steel, it was established that the values of the heat transfer coefficient may be described with Akers et al. (1958) and Shah (1979) correlations within a limited range of the mass flux density of the refrigerant and the mini-channel diameter. A pressure drop during the condensation of these refrigerants is described in a satisfactory manner with Friedel (1987) and Garimella (2001) correlations. On the basis of the experimental studies, the authors proposed the following correlation for the calculation of local heat transfer coefficient h_r .

$$Nu = 25.084 \cdot Re_1^{0.258} \cdot Pr_1^{-0.495} \cdot Pr^{-0.288} \cdot \left(\frac{x}{1-x}\right)^{0.266} \quad (2.23)$$

$$h_r = \frac{Nu_x \cdot \lambda_l}{d} \quad (2.24)$$

2.2.2 Helicoidal Pipes

Kang et al. (2000) studied condensation heat transfer of R134a in a helicoidal pipe. The refrigerant flows through the inner tube, and the cooling water flows in the passage (shell) formed by the inner and outer tubes. The heat transfer coefficient variations for R134a versus the coolant flow rate were analyzed and it has been found that the average heat flux of the refrigerant flow increases with the water flow rate. The helicoidal pipe heat transfer characteristic was expressed as

$$\frac{Nu}{Pr^{0.4}} = 2.3(Re^*)^{0.94} \quad (2.25)$$

where $1100 < Re^* < 2500$.

Han et al. (2005) have been investigated experimentally the condensation heat transfer coefficient and pressure loss characteristics of R134a in annular helical pipes which are significant importance to the effective design of the helical pipe heat exchangers. The tests were conducted for three different saturated temperatures with

varying mass flow rate from 100 kg/m²s to 420 kg/m²s. The average heat flux (q) and the mass flux (m_f) of R134a are respectively defined as:

$$q = \frac{Q}{\pi dl} \quad (2.26)$$

$$m_f = \frac{F_f \rho_f}{\left(\frac{\pi}{4}\right)(d_1^2 - d_2^2)} \quad (2.27)$$

Where, d, L, d₁ and d₂ denote the mean diameter, the length, the inner diameter of the outer tube, and the outer diameter of the inner tube of the test section respectively; F_f and ρ_f are respectively the volume flow rate and the density of refrigerant. The results show that the average condensation heat transfer coefficients and pressure drops of R134a increases with the increase of mass flux. The saturated temperatures have significant effect on condensation and also results were compared with straight pipes.

Table 2.2: Summary of Correlations for Two Phase Heat Transfer in Tubes

Researcher	Correlation	Media	Remarks
Bassi and Bansal (2003)	$Nu = 0.0687 \times Re^{0.78} \times Pr^{\frac{1}{3}}$ $\frac{h_{r \text{ oil}}}{h_{r \text{ no-oil}}} = e^{(-2.2\tau o)}$ <p>h_r - Condensation heat transfer coefficient (W/m²k) τo - Bulk oil mass in the mixture (%)</p>	R134a R134a Oil Mixture	Smooth tube with pure refrigerant R134a and its mixture with lubricant Castrol
Waldemar et al. (2012)	$h_i = \left[\frac{(T_{Wall} - T_{Water})}{q_i} - \frac{d_w}{2 \cdot \lambda} \cdot \ln \frac{d_e}{d_w} \right]^{-1}$	R134a R404A	In pipe mini-channels
Tadeusz et al. (2011)	$Nu = 25.084 \cdot Re_1^{0.258} \cdot Pr_1^{-0.495} \cdot Pr^{-0.288} \cdot \left(\frac{x}{1-x} \right)^{0.266}$ $h_r = \frac{Nu_x \cdot \lambda_l}{d}$	R134a, R404A	pipe channels with internal diameters of 0.31mm to 3.30 mm
Kang et al. (2000)	$1100 < Re^* < 2500 \quad \frac{Nu}{Pr^{0.4}} = 2.3(Re^*)^{0.94}$	R134a	helicoïdal pipe

2.2.3 Plate heat exchangers

Yan et al. (1999) studied experimentally the condensation characteristics for refrigerant R134a in a plate heat exchanger. The plate surfaces with corrugated sinusoidal shape of a chevron angle of 60° were used for experimentation. The convection heat transfer coefficient in the cold side was correlated by the least square method as:

$$Nu = 0.2121 \times Re^{0.78} \times Pr^{\frac{1}{3}} \quad (2.28)$$

Correlations to facilitate the use of the plate heat exchanger as a condenser have been developed for the dimensionless condensation heat transfer coefficient and friction factor. They are

$$Nu = \frac{h_r \times D_h}{\lambda_l} = 4.118 \times Re_{eq}^{0.4} Pr_l^{\frac{1}{3}} \quad (2.29)$$

$$f_{tp} \times Re^{0.4} \times Bo^{-0.5} \left(\frac{p_m}{P_c} \right)^{-0.8} = 94.75 \times Re_{eq}^{-0.0467} \quad (2.30)$$

The condensation heat transfer coefficient and pressure drop was higher at higher mean vapour quality. The results indicates, refrigerant mass flux only causes a mild increase in the refrigerant heat transfer coefficient in most of the cases and corresponding pressure drops are higher.

The application of the cross-grooved surface fins in to herringbone-type plate heat exchanger for R22 condensation has been investigated experimentally by Longo et al. (2004). Also, studied the effect of surface roughness in plate heat exchangers for the two phase heat transfer. The results compared with smooth surfaces and semi empirical correlations.

The micro-fin tubes show a better heat transfer with respect to the equivalent smooth tubes ranging from 80% to 180% and with a pressure loss increase from 20% to 80%. Cross-grooved tubes gives 25% to 30% higher heat transfer and 6% to 10% higher pressure drop than micro- fin tubes condensation. The surface roughness is increased by filling soldering material during the brazing process. Experimental vaporization data compared with Cooper correlations accounts for heat flux, surface roughness and pressure effect. It was found that the mean absolute percentage deviation compared with experimental data is around 9%.

$$h_r = 55P^{*(0.12-0.21\log_{10}R_p)}(\log_{10}P^*)^{-0.55}q^{0.67}M^{-0.5} \quad (2.31)$$

Where
$$P^* = \frac{P}{P_{cr}} \quad (2.32)$$

Amir Jokar et al. (2006) studied the parameters that affect the two-phase heat transfer within the mini-channel plate heat exchangers, and to utilize the dimensional analysis technique to develop appropriate correlations. Thermo-hydrodynamic performance of three mini-channel brazed-type plate heat exchangers was analyzed experimentally in this study. The results of this study showed that the two-phase theories and correlations that were established for conventional macro-channel heat exchangers may not hold for the mini-channel heat exchangers. Correlations for the single-phase and two-phase Fanning friction factors were also obtained based on a homogenous model. The condensation heat transfer coefficient correlation is given below:

$$Nu_{tp} = 3.371 Re_1^{0.55} Pr_1^{0.3} \left(\frac{G^2}{\rho_1^2 \Delta T C_{p,l}} \right)^{1.3} \left(\frac{\rho_1^2 i'_{fg}}{G^2} \right)^{1.05} \left(\frac{\rho_1 \sigma}{\mu G} \right)^{0.05} \left(\frac{\rho_l}{(\rho_l - \rho_v)} \right)^2 \quad (2.33)$$

Condensation heat transfer correlations in the modeling of plate heat exchangers have been investigated by Garcia-Cascalesa et al. (2007). The condensation heat transfer coefficient was correlated as a function of the Reynolds and the Prandtl numbers through an expression of the form:

$$Nu = A Re^b Pr^c \quad (2.34)$$

Where constants A, b and c are correlated with experimental data.

García-Cascalesa et al. (2007, 2010) studied on condensation modelling and evaluated with experimental data for the working fluids R134a and R410A and secondary fluid is air. Jongmin Shin et al. (2002) studied on the behavior of water hold-up by condensation on various shapes of fin-tube heat exchangers with different surface hydrophilicity. The results showed that the water hold-up of a heat exchanger could be reduced by the enhancement of the surface hydrophilicity and design of heat exchanger with a lower number of fins and with slant ends.

Chang Yong Park et al. (2009) studied the CO₂ flow condensation for 0.89 mm micro-channels at horizontal flow conditions. The results showed that the measured heat transfer coefficients increased with the increase of mass fluxes and

vapour qualities. CO₂ two-phase pressure drop, measured in adiabatic conditions, increased with the increase of mass flux and vapour quality and it decreased with the increase of saturation temperature.

Mohammed (2008) had carried out the review on the effect of oil in refrigeration as lubrication is necessary in all most all the refrigeration vapour compression systems. In many situations, oil is used for cooling compressor and at the same time there is a reduction in heat transfer coefficient in two phase heat exchanger (Condenser and evaporator). Further, indicated that the condenser is the least sensitive component to the presence of a lubricant. They noticed that the COP would be higher by 5% with miscible than with immiscible oils.

Giovanni (2008 & 2009) has been carried out experiments on small Brazed Plate Heat Exchanger (BPHE) using R134a and R410A. They measured the heat transfer coefficient and frictional pressure drop during R134a condensation inside a BPHE and investigated the effects of refrigerant in saturated and vapour super heating conditions. At low refrigerant mass flux (<20 kg/m²s), the heat transfer coefficients are not dependent on mass flux due to process was controlled by gravity. For higher mass fluxes, the heat transfer coefficients are depend on mass flux and forced convection condensation occurs. Also, found that the super heated vapour heat transfer coefficients are 8-10% higher than those of saturated vapour under the same refrigerant mass flux. Vapour super heating affects condensation kinetics reducing the condensate film thickness and increasing the heat transfer coefficient. The average heat transfer coefficient on refrigerant side was derived from the global heat transfer coefficient assuming no fouling resistance.

$$h_{r,ave} = \left(\frac{1}{U} - \frac{t}{\lambda_p} - \frac{1}{h_w} \right)^{-1} \quad (2.35)$$

$$h_w = 0.277 \left(\frac{\lambda_w}{D_h} \right) Re_w^{0.766} Pr_w^{0.333} \quad (2.36)$$

Where, λ_p is plate thermal conductivity (W/mk) and t is plate wall thickness (m).

A linear equation based on the kinetic energy (KE) per unit volume (V) of the refrigerant flow was proposed for the computation of the pressure drop.

$$\frac{KE}{V} = \frac{G^2}{2\rho_m} \quad (2.37)$$

$$\Delta P_f = 1.835 \left(\frac{KE}{V} \right) \quad (2.38)$$

A model for the analysis of compact heat exchangers as condensers has been investigated by **Garcia-Cascalesa et al.** (2010). The modeling strategy of a multiple-row, multiple-pass heat exchanger is described cell-by-cell discretization, carried out the energy and momentum balances for each cell of refrigerant path and the type of tube considered. Noticed that, the effect of gravity does not played any role on condensation for the type of tubes. A brief study on condensation heat transfer in micro and mini-channels was also carried out, and some correlations published in the literature are compared using conditions normally found in HVAC equipments. In micro and mini-channels gravity has practically no effect, instead, surface tension plays an important role. The experimental data of R134a in two row heat exchanger was compared with calculated data. As was mentioned, the correlations by Cavallini et al. (2005) and Bandhauer et al. (2006) have been implemented in the model and the results provided by each of them are compared as well.

Giovanni analysed that at low refrigerant mass flux (<20 kg/m²s) the saturated vapour condensation heat transfer coefficients are not dependent on mass flux and are well predicted by Nusselt analysis for vertical surface; the condensation process is gravity controlled. For higher refrigerant mass flux (>20 kg/m²s) the saturated vapour condensation heat transfer coefficients dependent on mass flux and are well predicted by Akers et al. (1959) equation [Giovanni, 2008]. The compactness of brazed plate fin heat exchangers results in a low refrigerant charge, which means lower environmental impact and higher safety level [Giovanni A. L, 2008]. These specific aspects are crucial with the advent of the ozone-depletion and global warming issues and the use of flammable refrigerants. In open literature, it is possible to find several works on traditional plate heat exchangers (PHE) in sensible heat transfer, whereas limited experimental data can be found on refrigerant condensation inside brazed PHE and data is not available for serrated fin surfaces.

Literature survey indicates that very limited work has been done to the condensation of R134a in plate-fin heat exchangers. While the thermo-hydraulic characteristics of R134a in fin surfaces are of significant importance to the effective design of compact plate-fin heat exchangers for cryogenic and aerospace applications.

There is no open literature has been presented on this subject. The primary objective is to investigate experimentally the condensation heat transfer coefficients and frictional pressure drops for R134a in serrated or offset strip fin surfaces.

2.3 Reviews on Two-Phase Pressure Drop

The total pressure drop for two-phase flow in heat exchangers consists of three components. These three components are due to friction, acceleration (change in momentum), and elevation (gravitation):

$$\left(\frac{dP}{dz}\right)_{\text{total}} = \left(\frac{dP}{dz}\right)_{\text{fric}} + \left(\frac{dP}{dz}\right)_{\text{acce}} + \left(\frac{dP}{dz}\right)_{\text{elev}} \quad (2.39)$$

The acceleration and gravitation pressure gradient components are due to vapour generation (or degeneration) and non-horizontal orientation of the flow channel. Traditionally, the two most important modelling methods of two-phase gas-liquid flow are the “homogeneous” model and the “separated flow” model. Both methods provide evaluations of the acceleration and gravitational pressure gradient components on a theoretical basis, while the frictional pressure gradient part is usually evaluated empirically.

2.3.1 The homogeneous flow model

The model considers the two phases to flow as a single phase possessing mean fluid properties. Those properties basically include the mean density and mean viscosity. The model has been in use in various forms in adiabatic two phase flow and refrigeration systems for a considerable time (Collier and Thome, 1994). This model has also found its application in two phase pressure drop calculation in PHE channels. Two important assumptions in a homogeneous model are:

- a) Equal vapour and liquid velocities
- b) Thermodynamic equilibrium between the phases.

The two phase friction factor f_{tp} can be calculated by any single phase friction factor equations with the Reynolds number determined using mean fluid properties or, alternatively, f_{tp} can be determined directly from measured two phase pressure drops, the latter usually has higher accuracy for the specified testing conditions. It assumes the two phase flow as single phase and there are three properties to be defined, namely the two phases mean velocity, density and viscosity. The model provides a

simple method for computing acceleration and gravitational components of pressure drop and are still a very common method of evaluating two phase frictional pressure gradients.

Table 2.3: Summary of Plate Heat Exchanger Correlations

Researcher	Correlation	Media	Remarks
Yan et al. (1999)	$Nu = \frac{h_r \times D_h}{\lambda} = 4.118 \times Re_{eq}^{0.4} Pr_1^{\frac{1}{3}}$ $f_{tp} \times Re^{0.4} \times Bo^{-0.5} \left(\frac{p_m}{P_C} \right)^{-0.8}$ $= 94.75 \times Re_{eq}^{-0.0467}$	R134a	Plate heat exchanger
Longo et al. (2004)	$h_r = 55 P^{*(0.12 - 0.21 \log_{10} R_p)} (\log_{10} P^*)^{-0.55} q^{0.67} M^{-0.5}$ $P^* = \frac{P}{P_{cr}}$	R22	cross-grooved surface fins in to herringbone - type PHE
Garcia-Cascalesa et al. (2007)	$Nu = A Re^b Pr^c$ <p>Where A, b and c are correlated with experimental data</p>	R410A	Plate heat exchanger
Nusselt (1916)	$h_{Nusselt} = 0.943 \left[\frac{\lambda_L^3 \rho_L^2 g \Delta T_{LG}}{\mu_L \Delta T L} \right]^{\frac{1}{4}}$		
Giovanni A.Longo (2008 & 2009)	$h_{r,ave} = \left(\frac{1}{U} - \frac{t}{\lambda_p} - \frac{1}{h_w} \right)^{-1}$ $h_w = 0.277 \left(\frac{\lambda_w}{D_h} \right) Re_w^{0.766} Pr_w^{0.333}$	R134a R410A	Brazed plate heat exchanger

2.4 Summary from Review of Literature

The literature survey indicates rich data is available for the sensible type of heat transfer for design of compact plate fin heat exchangers. More recently, there has been a lot of activity on numerical solution of heat transfer equations and generation of j and f data for a variety of compact plate fin surfaces.

A close inspection of literature relevant to the present study reveals that heat transfer characteristics for the in-tube, helicoidal pipes and plate heat exchanger condensation of the refrigerant R134a have been investigated. The two phase condensation heat transfer basically depends upon mass flux. The literature indicates the two phase condensation at lower mass flux is due to gravity controlled and at higher mass flux is due to forced convection condensation. Unfortunately, there are rather very limited open literature data available for the design of brazed compact plate fin heat exchangers for the condenser application.

Two-phase flow pressure drop depends on a large number of independent parameters including channel geometry, mass and volume fractions of the individual phases, fluid properties, pressure, mass flux, orientation of the channel (having an influence on the flow patterns), one or two components in the system, adiabatic or with phase-change, etc. Large numbers of correlations are reported in the literature, to cater for the needs of diverse applications. For improved accuracy, the parameter ranges need to be determined for the problem at hand, and correlations chosen accordingly. Due to the complexity of the problem, mean deviations of as much as 30% are common using these correlations; calculations for individual flow conditions can easily deviate 50% or more from experimental data (ASHRAE 2005 : Fundamentals Hand Book).

It is seen that a common strategy in both two-phase heat transfer and pressure drop modeling is to begin with a single-phase model and determine an appropriate two-phase multiplier to account for the two-phase effects. This “multiplier concept” approach goes back at least as far as the classic work of Lockhart and Martinelli (1949), and the majority of two-phase frictional pressure drop correlations are found to be falling into this category.

On gaining knowledge from literature, the present research study has taken to develop the condensation heat transfer coefficient and frictional pressure drop for different serrated fin surfaces of compact heat exchanger.

CHAPTER 3

COMPUTATIONAL STUDIES ON SERRATED FINS

Water side heat transfer coefficient can be calculated by using modified Wilson plot technique with specific set of experiments carried out on the test unit water circuit as per detailed procedure is reported in Longo and Gasparella (2007). Also, using CFD (Computational Fluid Dynamics) analysis these correlations are developed for different types of fins for different Reynolds numbers using air and water as reported in Ranganayakulu et al.(2007, 2008, 2011 and 2013). CFD analysis approach is used in accordance with Ranganayakulu et al. (2013) for development of single phase correlations for different geometries of serrated fins. Hence to find out single phase heat transfer coefficient h_f and frictional coefficient of fluid, numerical analysis using CFD has been carried out for serrated fin geometry using Water. This data is required to calculate the average condensation heat transfer coefficient for R134a. With objective of reducing the volume of expensive experiments, CFD method is being employed for calculating single phase heat transfer coefficient on water side using a serrated fin.

CFD analysis was carried out using ANSYS CFD 14.5 for an estimation of j and f factors for serrated fin geometry for water medium. A single layer of fin is modeled and meshed using CATIA and HYPERMESH respectively. The flow inside a serrated fin surface heat exchanger is characterized by a complex flow field, which is affected by blockage and recirculation zones enhanced by sharp rectangular edges and narrow gaps. The approach requires defining the mathematical equations that govern the physical process. Fluent, a computer program, based on a finite-volume method is among the more powerful packages of existing commercial software for solving fluid flow and heat transfer problems.

Giovanni et al. (2008, 2009 and 2010), Kang et al. (2000) and Han et al.(2005) proposed that the two phase condensation heat transfer coefficient of the fluid (h_r), as referred in Table 2.3. Hence to find out single phase heat transfer coefficient (h_f) and

frictional coefficient (f) of fluid numerical analysis using CFD has been carried out for fin geometry of serrated fins using water and developed a generalized correlation.

3.1 CFD Analysis

CFD is primarily used as a design aid for predicting the performance characteristics of equipment involving Fluid/Gas flow and heat transfer. The ability to simulate heat transfer and fluid flow problems numerically before a prototype is built cuts the cost and time of development by orders of magnitude. Of course, CFD must be continuously backed up by experimentation in order to ensure that the numerical predictions are reliable. Thus a cycle is formed involving theoretical predictions, CFD and experimentation. Validity of new mathematical models can be tested within the context of this relationship, with resulting improvements in the accuracy of CFD analysis.

All main three elements of formal computational software are pre-processor, solver and post processor. Pre-processing is the first step in CFD in which construction of geometry, the generation of the mesh on the surfaces or volumes shall be carried out. The solver is the heart of CFD software; it sets up the equation set according to the options chosen by the user and meshes points generated by the pre-processor, and solves them to compute the flow field. The post processor is the last part of CFD software. It helps to examine pressure contours and velocity contours of the results and extract useful data.

3.2 CFD Approach

The CFD analysis is carried out for an estimation of j and f factors for serrated fin geometry for water medium. A number of numerical experiments carried out to determine the thermo-hydraulic parameters with a view to arrive at the optimum parameters for a serrated fin. The three dimensional computational domain of serrated fin model shown in Fig.3.1. It is carried out for different geometric parameters and Reynolds numbers using Fluent in HP Z800 workstation with 20 GB RAM. In first phase of analysis, serrated fin is taken and characterized for f values over a range of Reynolds number. In second phase, the j value is determined for the same range by switching on the energy equation. In order to overcome the entrance effect, the concept of periodic fully developed flow as suggested by Patankar et al. (1977) is

implemented for flow analysis. After the analysis, the pressure drop for unit length is one of the outputs, and that is multiplied by the actual length to get the total pressure drop for corresponding fins. Friction factor is calculated from the pressure drop as per procedure given by Kays and London (1984). Similarly, the same procedure is repeated for the range of Reynolds numbers from 100 to 15,000 in order to draw the f vs. Reynolds number curves. The mesh finalization is done before analyzing for the ' j ' and ' f ' factors based on grid independency check. Then the mesh size is finalized based upon the curve where the slope is almost zero.

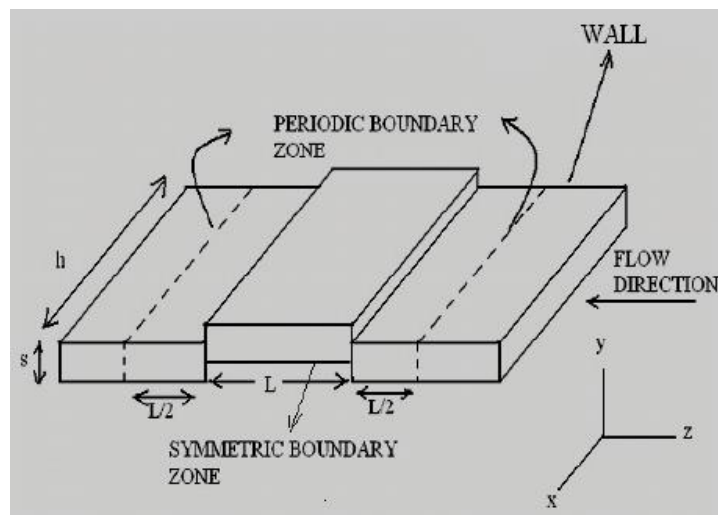


Fig.3.1: Computational Domain for Serrated Fin

The assumption of constant wall temperature boundary condition is employed for walls. After the thermal analysis, post processing is done for temperatures and pressures at the inlet and outlet using mass weighted average. The pressure, temperature and velocity profiles are taken at the various sections of the fins for corresponding Reynolds numbers. This temperature difference between inlet and outlet of the fin, in turn, is used for calculating j factor using Kays and London (1984) methodology. Similarly, the same procedure is repeated for the range of Reynolds numbers 1000 to 15,000 for turbulent flow and from 100 to 1000 for laminar flow in order to draw the j vs. Re characteristic curves. The actual mass flow rate is used as the boundary condition. No-slip boundary condition is used for walls. The ' j ' and ' f ' data is generated as stated above.

3.3 Methodology

The following steps are carried out in numerical analysis for generation of Colburn j factor and friction factor f for serrated fins using water. Fig. 3.2 shows the flow chart of CFD methodology.

- Modelling and numerical grid generation for the fin
- Applying the boundary conditions
- Analysis using ANSYS CFD software
- Computation of ' j ' and ' f ' factors
- Validation of results with standard values.
- Generation of j and f correlations

3.4 Mathematical Model

In CFD, the conservation equations of mass, momentum and energy are solved using the finite volume method. There are several turbulence models available in the code. The turbulent flow is calculated by the semi-implicit SIMPLER as mentioned in Versteeg and Malalasekera (1995) algorithm method in the velocity and pressure conjugated problem, and a second order upwind differential scheme is applied for the approximation of the convection terms. A standard κ - ϵ model as given in Versteeg and Malalasekera (1995) with enhanced wall treatment is used to predict turbulent flow in the plate-fin heat exchanger as well as in the fin geometry. The Reynolds transport equations can be written in a generalized form as given in Anderson (1995) and Patankar (1980).

$$\text{div}(\rho u \phi) = \text{div}(\Gamma \text{grad} \phi) + S_{\phi} \quad (3.1)$$

Where ϕ stands for a generalized transport variable, which is used for all conserved variables in a fluid flow problem, including, mass, momentum and the turbulence variables κ and ϵ . Γ represents the effective diffusivity (sum of the eddy diffusivity and the molecular diffusivity). S_{ϕ} is the source term for the respective dependent variable.

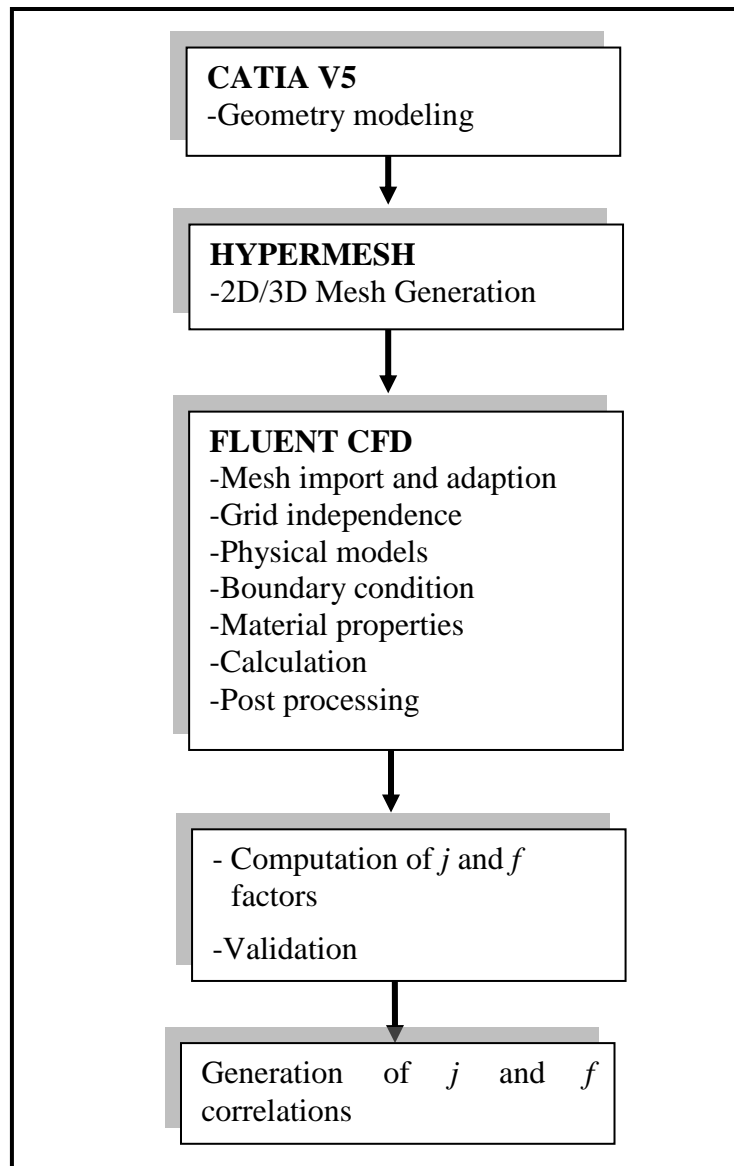


Fig. 3.2: Flow Chart of CFD Methodology

The solution of the above set of equations is applied to the prediction of velocity and turbulence levels throughout the domain. The convergent criteria are specified to absolute residuals ($\leq 1.0 \times 10^{-6}$). The meaning assigned to ϕ , Γ and S_ϕ for conservation of mass, momentum and energy are listed in Table 3.1.

Table 3.1: Description of Variables ϕ , Γ and S_ϕ for Conservation of Mass, Momentum and Energy

Conservation of law	ϕ	Γ	S_ϕ
Conservation of mass (Continuity equation)	1	0	0

Conservation of momentum in X-direction	u	μ	$-\frac{\partial \psi}{\partial x} + \rho g_x + \text{fluid friction} + S_u$
Conservation of momentum in Y-direction	v	μ	$-\frac{\partial \psi}{\partial y} + \rho g_y + \text{fluid friction} + S_v$
Conservation of momentum in Z-direction	w	μ	$-\frac{\partial \psi}{\partial z} + \rho g_z + \text{fluid friction} + S_w$
Conservation of Energy	θ	$\frac{k}{c_p}$	$-\frac{D\psi}{D\lambda} + \text{Viscous dissipation}$ + Other heat sources

Substitution of the variable in equation (3.1) by those defined in Table 3.1 leads to the general governing equations (3.2), (3.5) & (3.6) of fluid dynamics as follows.

Conservation of mass

$$\frac{D\rho}{D\lambda} = -\rho(\nabla \cdot \mathbf{u}) \quad (3.2)$$

$$\text{Where } \frac{D}{D\lambda} = \frac{\partial}{\partial \lambda} + u \frac{\partial}{\partial x} + v \frac{\partial}{\partial y} + w \frac{\partial}{\partial z} \quad (3.3)$$

$$\text{and } \nabla \cdot \mathbf{u} = \frac{\partial u}{\partial x} + \frac{\partial v}{\partial y} + \frac{\partial w}{\partial z} \quad (3.4)$$

Conservation of Momentum

$$\rho \frac{D\mathbf{u}}{D\lambda} = -\nabla \rho - [\nabla \cdot \boldsymbol{\tau}] + \rho \mathbf{g} \quad (3.5)$$

Conservation of energy

$$\rho \frac{DU}{D\lambda} = -(\nabla \cdot \mathbf{q}) - \psi(\nabla \cdot \mathbf{u}) - (\boldsymbol{\tau} \cdot \nabla \mathbf{u}) \quad (3.6)$$

3.5 Assumptions

- The flow is study and incompressible. The fluid density is constant throughout the computational domain.
- The effect of heat conduction through the fin and plate material is considered
- Water (liquid phase) used as working medium.
- The flow is periodically developed both hydro dynamically and thermally. Patankar et al. (1977) have shown that it is indeed the case in most practical situations.
- On the wall no slip boundary condition is considered.
- CAD model does not include the burrs, sharp edges etc.

3.6 Boundary Conditions

Proper boundary conditions are important for a successful computational work. Following Boundary conditions are used for analysing the models.

(a) No slip and isothermal condition

No-slip condition indicates that the fluid sticks to the wall and moves with the same velocity as the wall, it is moving.

(b) Periodicity condition

A periodic boundary condition is employed when the flow passage has features repeating at regular intervals. This situation occurs in offset strip and wavy fin passages. The concept of periodicity and periodic boundary conditions were given by Patankar et al. (1977).

(c) Total flow at the inlet

To estimate the fluid behaviour inside the control volume for different Reynolds number.

(d) Total temperature of fluid at inlet

To predict the fluid heat transfer behaviour for different Reynolds number.

(e) Symmetry boundary condition

These types of conditions are used when the physical geometry of interest, such as the outlined heat exchanger channel, and the expected pattern of the flow/thermal solution are symmetric. When using this type of boundary condition in such regions no additional boundary conditions are required. Fluent assumes zero flux of all quantities across a symmetric boundary.

3.7 ANSYS CFD Package

Commercially available software ANSYS Fluent 14.5 is used to solve the CFD equations along with appropriate boundary conditions. ANSYS CFD uses finite volume numerical procedures to solve the governing equations for fluid velocities, mass flow, pressure, temperature, species concentration and turbulence parameters and fluid properties. Numerical techniques involve the sub-division of the domain into a finite set of neighboring cells known as "control volumes" and applying the discretized governing partial differential equations over each cell. This yields a large

set of simultaneous algebraic equations, which are highly non-linear. These equations are in turn solved by iterative means until a converged solution is achieved.

Laminar modeling is quite easy and the standard NS equations and the other standard equations can be solved to determine the unknown parameters. But the case of turbulence is quite difficult as there are no straight equations to solve, as all the quantities are time dependent. Many models were developed but not even a single model predicts the most accurate results. The turbulence models are classified as follows [Launder and Spalding, 1972]:

1. Classification based on the number of differential equations.
2. Classification according to shear stress hypothesis.

The number of differential equations that must be solved in order to supply modeling parameters ranges from zero to twelve for the most complex of the Reynolds stress models. The purpose of introducing more number of equations is of course to enhance the realism of the model; that is, to widen the range of experimental conditions for which the model will make correct predictions, without the necessity for ad hoc adjustments to the empirical constants. It should be mentioned that all the turbulence models necessitate the obtaining from experiment of some of the constants or functions which appear in the equations; and, the greater the number of equations, the larger must this empirical input be. Turbulence models close to Reynolds equations can be divided into two categories [Versteeg and Malalasekera, 1995], according to whether or not the Boussinesq assumption is used. Models using this assumption will be referred to as category I, or turbulent viscosity models. These are also known as first-order models. Models that affect closure to the Reynolds equations without this assumption will be referred to as category II models and include those known as Reynolds stress or stress-equation models. The stress-equation models are also referred to as second-order or second-moment closures.

Category III models will be defined as those that are not based entirely on the Reynolds equations. Large-eddy simulations fall into this category, since it is a filtered set of conservation equations that is solved instead of the Reynolds equations. Some of the turbulence models that are used are:

1. Spalart Allmaras model (one equation model)

2. Standard k-ε model (two equation model)
3. Standard k-ω model (two equation model)
4. Large Eddy Simulation (LES model)
5. Direct Numeric Simulation (DNS model)
6. Reynolds Stress Model (RSM model)

In present study standard $\kappa - \varepsilon$ model is selected for these types of extended surfaces. The mathematical algorithm of standard $\kappa - \varepsilon$ model is presented. Standard $\kappa - \varepsilon$ model is considered the simplest ‘complete model’ of turbulence. This model is widely used in industrial flow simulation due to robustness, economy and reasonable accuracy for a wide range of turbulent flows.

The standard k-ε model is a two equation model based on model transport equations for the turbulence kinetic energy (k) and its dissipation rate (ε) . The model transport equation for k is derived from the exact equation, while the model transport equation for ε was obtained using physical reasoning and bears little resemblance to its mathematically exact counterpart.

In the derivation of the k-ε model, the assumption is that the flow is fully turbulent, and the effects of molecular viscosity are negligible. In this simulation work, molecular viscosity effects are assumed as negligible and only turbulence effects are considered, hence the standard k-ε model has been selected. This turbulence model results are more nearer to the experimental values compared to the other turbulence models for this type of application.

3.8 Computation of *j* and *f* Factors

The friction factor is computed from the area averaged mean pressure drop over the periodic length using the following relation

$$\Delta P = \frac{4f LG^2}{2\rho D_h} \quad (3.7)$$

Where G is mass velocity (kg/m²s), L= length of the passage (mm)

$$f = \frac{\Delta P D_h}{2 v_m^2 \rho l} \quad (3.8)$$

Where v_m is area averaged mean velocity at any cross section, D_h is hydraulic diameter

$$\Delta P = P_m(0) - P_m(L) \quad (3.9)$$

$P_m(y)$ being the mean pressure over the cross section at axial coordinate y .

The Colburn j factor is defined as

$$j = \frac{h_w}{G C_p} \text{Pr}^{\frac{2}{3}} \quad (3.10)$$

Equation (3.10) can be written in terms of the output variables of CFD simulation

$$j = \frac{D_h}{4\lambda} \text{Pr}^{\frac{2}{3}} \ln \left[\frac{T_m(0) - T_w}{T_m(L) - T_w} \right] \quad (3.11)$$

The mean variables $w_m(y)$, $p_m(y)$, and $T_m(y)$ are computed from the following expressions.

$$\text{Frontal area of section } y, A_F(y) = \iint dx. dz \quad (3.12)$$

$$\text{Mean velocity, } w_m(y) = \frac{1}{A_F(y)} \iint w(x, y, z) dx. dz \quad (3.13)$$

$$\text{Mean pressure, } P_m(y) = \frac{1}{A_F(y)} \iint P(x, y, z) dx. dz \quad (3.14)$$

$$\text{Mean temperature, } T_m(y) = \frac{1}{A_F(y)w_m(y)} \iint T(x, y, z)w(x, y, z) dx. dz \quad (3.15)$$

3.9 Problem Description

The geometrical parameters of the three dimensional serrated fin are described by the fin height (h), fin spacing (s), fin thickness (t) and offset strip length (l). The dimensionless representations of these variables are given by the flow cross-section aspect ratio (s/h), t/s and t/l . These dimensional notations are shown in Fig. 3.3. The performance of a plate fin surface determined by the geometric parameters such as fin height (h), fin spacing (s), fin thickness (t), and Offset strip fin length (l) and plays significant role as indicated by London and Shah (1968). It will be expensive and time consuming to fabricate and conduct experiments over reasonable ranges of all the geometric variables. On the other hand, it is relatively easy and cost effective to carry out parametric study through numerical simulation and derive acceptable correlations for use.

Several authors have contributed significantly in some or the other way to develop a correlation in order to determine j and f , but none of them had the same

conclusions. So, this work mainly focused to develop good correlations for serrated fins with water by taking all the necessary parametric effects.

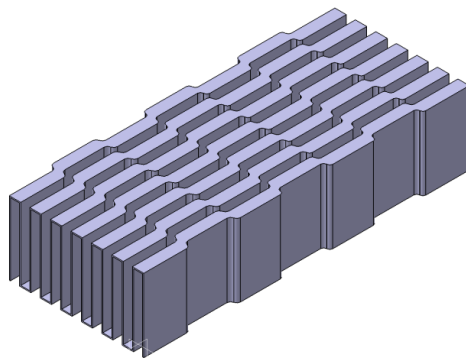
3.10 Serrated (Offset Strip) Fin Surface

The offset fins are widely used fins for high effectiveness. The flow is periodically interrupted, leading to creation of fresh boundary layers and consequent heat transfer enhancement. Interruption of flow also leads to greater viscous pressure drop.

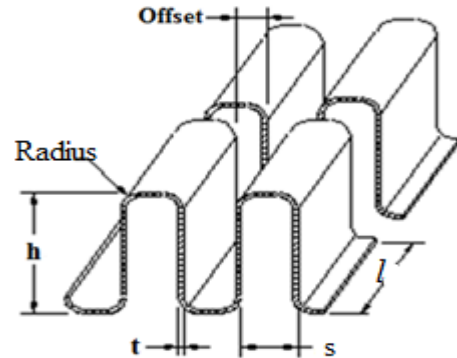
3.10.1 Numerical Model

The schematic of offset fin shown in the Fig.3.3 is defined by the following parameters.

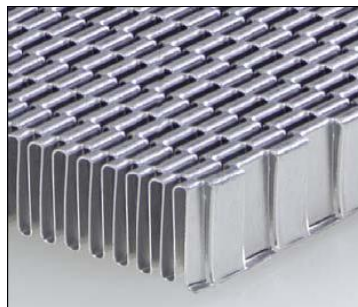
- fin thickness (t),
- fin height (h),
- lance length (l), and
- fin spacing (s).



a) Serrated Fin CAD Model



b) Serrated Fin Dimensional Notations



c) Photograph of Serrated Fin

Fig.3.3: Schematics of Fin Geometry

The serrated (offset) fin was modeled using CATIA software. Grid is generated using hyper mesh software. Initially 2D elements generated using quad elements. Hexa elements used for 3D domain for computation. The quality of the grid used in the computations directly influences the solution obtained. Lot of care has been taken in choosing the desirable features in the grid like orthogonality, control of spacing and skewness. Apart from these, very low aspect ratios of grid cells and highly stretched grids have been avoided to get better results.

3.10.2 Computational domain

Fig. 3.4 shows the computational domain taken for modeling fluid flow analysis over a serrated fin surface. Fin spacing (s) in the x-direction, lance length (l) in the y-direction and fin height (h) in the z-direction constitutes the computational domain.

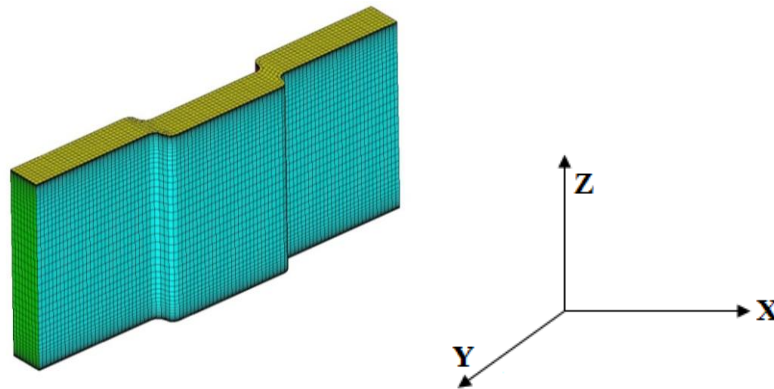


Fig 3.4: Computational Fluid Domain in Mesh Form for Serrated Fin

3.10.3 Dimensionless parameters

The optimum serrated fin surfaces are taken for parametric study. 108 fin surfaces of different geometries are modeled and CFD analysis is carried out for developing correlations. Using numerical methods, j and f factors for the offset fin surfaces with in the ranges of dimensionless parameters of offset fin surfaces are calculated. The ranges of dimensionless geometric parameters are taken as follows:

$$0.186 \leq \frac{s}{h} \leq 0.568 \quad (3.16)$$

$$0.0765 \leq \frac{t}{s} \leq 0.1675 \quad (3.17)$$

$$0.027 \leq \frac{t}{l} \leq 0.082 \quad (3.18)$$

The range of Reynolds number considered for analysis is given below:

$$100 \leq Re \leq 1000 \quad \text{for laminar region} \quad (3.19)$$

$$1000 \leq Re \leq 15000 \quad \text{for turbulent region} \quad (3.20)$$

The performance factors are evaluated for different types of serrated fins using ANSYS Fluent 14.5. The performance of serrated fins are presented for both laminar and turbulent regions of Re vs. ' j ' and ' f ' factors.

3.10.4 Grid independency check

Grid independency check was carried out as a first step in each and every analysis. Different mesh sizes ranging from very coarse to very fine mesh are taken first and solved with same boundary conditions. Pressure drop is taken as standard bench mark to determine the independency of the mesh and the graph between number of elements and the pressure drop is drawn in Fig. 3.5. Then the mesh size is finalized based upon the value where there is no change in the pressure drop.

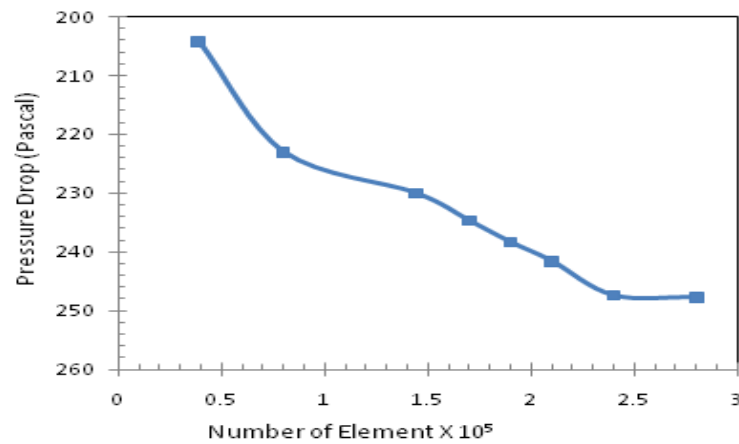


Fig.3.5: Grid Independency Check for Serrated Fin Surface by CFD Analysis

In second phase, the “velocity inlet” and “outflow” boundary conditions are used at the inlet and outlet of the fin geometry respectively. The two-dimensional fully developed velocity profile, which is taken from first phase analysis (pressure drop analysis), is used in the “velocity inlet” boundary condition.

3.10.5 CFD simulation studies

The CFD studies were carried out on the offset strip fin at different Reynolds number ranging from 100 to 15000 by applying the boundary conditions. The analysis was carried out in two phases. In first phase the fin characterized for friction factor ' f ' over above range of Reynolds number. In second phase the Colburn ' j ' factor is estimated for the same range of Reynolds number using energy equation.

3.10.6 Validation

Serrated fin has been analyzed with CFD and compared with experimental data. The results are further compared with open literature. Analysis has been carried out by considering uniform wall temperature boundary condition. A grid independence test is carried out for the same fin and graph is plotted as the number of elements versus pressure drop as shown in Fig. 3.5. This figure shows that after 280,000 cells there is no much variation in the pressure drop.

The results obtained from ANSYS Fluent in the form of Colburn j and Fanning friction factors are compared with the literature correlations for air and water medium in Fig. 3.6 and Fig. 3.7 for laminar region and turbulent region respectively. According to Sen Hu and Herold (1995), there will be a considerably large deviation in j values of air with water due to a large difference in Prandtl number and same was observed. The CFD results of serrated fins are compared with Wieting (1975), Sen Hu and Herold (1995) and Kim and Sohn (2006) as shown in Fig. 3.6. The numerical results are in good agreement with the analytical results given by Sen Hu and Herold, (1995) for the low Reynolds number region. The variations are found to be 5-14% in j values. Also, Fig. 3.6 shows the comparison of CFD results with the literature correlations [Sen Hu and Herold, (1995) and Kim and Sohn (2006)]. It is evident for f and j factors that Sen Hu and Herold (1995) correlations are close to CFD results. However, some variations with experimental results are due to the manufacturing aspects, testing conditions and fin geometries when compared with Fluent data.

It is found that the j of water is lower by about two times when compared with air, where as there is no significant deviation in f values as observed by Sen Hu and Herold, (1995). Even though j is lower for water, the heat transfer coefficient, h_w is much higher when compared to air. The f vs. Re and j vs. Re data for serrated fin surface shows significant nonlinearity over the Reynolds number range $100 \leq Re \leq 15000$. Therefore, two separate equations have been proposed for the low and the high Reynolds number regimes.

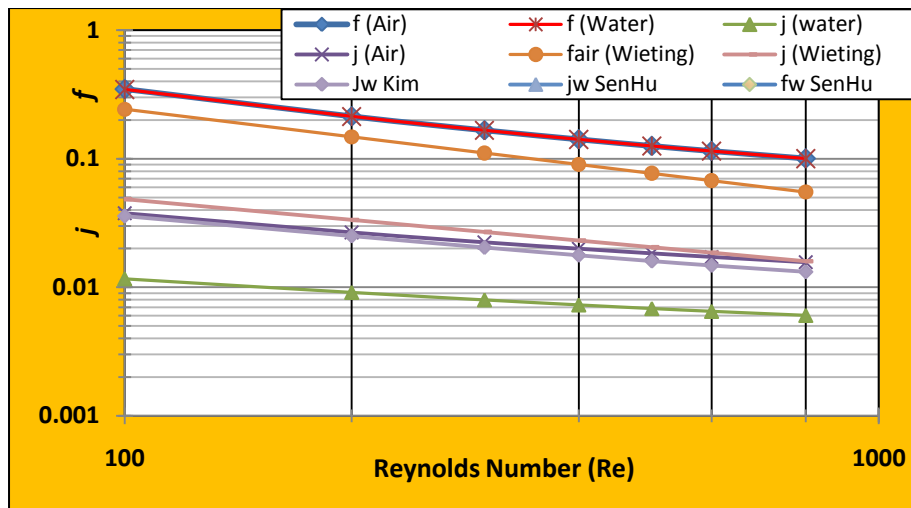


Fig.3.6: Validation of CFD Results with Experimental Results

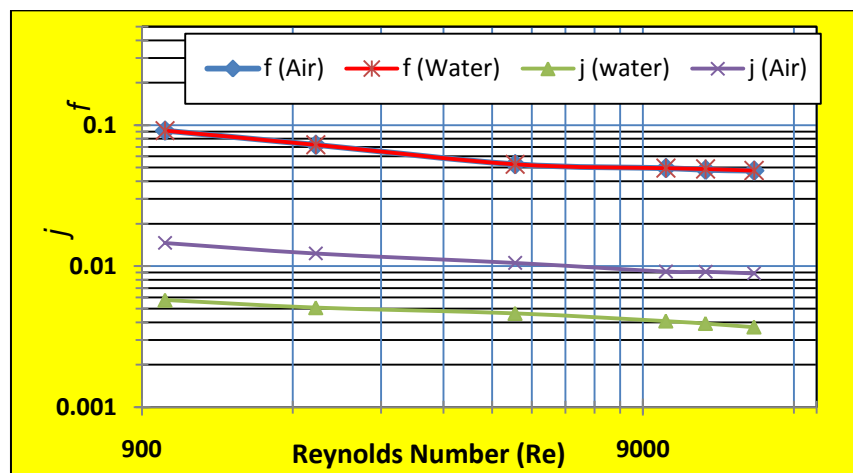


Fig. 3.7: Colburn (j) and Friction (f) Factor for Re: 1000-15000

3.10.7 Generation of f and j data

In Appendix-I the CFD results are provided in Table A1.1 and Table A1.2 gives consolidated simulation results of f and j factors of 45 offset strip fin surfaces. Based on these results correlations have been developed between f , j , Re and geometrical fin parameters.

3.11 Effect of Reynolds Number and Geometry Parameters

The numerical analysis for serrated fin surfaces is carried out using ANSYS Fluent with boundary conditions and respective mass flow rates for various Reynolds numbers. From these graphs (Fig. 3.6 and Fig. 3.7), it is observed that the j and f vs. Re curves of serrated fins follow the same trends as Sen Hu and Herold, (1995) and Kim and Sohn (2006) experimental results. The figures from 3.8 to 3.13 illustrates the

role of geometric parameters s/h , t/s , t/l vs. j and parameters s/h , t/s , t/l vs. f in determining the heat transfer and flow friction performance of a serrated fin surfaces. The individual effects of geometrical parameters are explained in the following paragraphs:

3.11.1 Effect of s/h ratio on j

The Colburn j factors are plotted against the fin spacing (s) to fin height (h) ratio for various Reynolds numbers as shown in Figure 5.8. The j factor decreases with Re number increases as expected. The rate of decrease is higher for low Reynolds numbers and lower for high Reynolds number. However, the ratio of increase is predominant for low Re (below 1000) and it is not significant for high Re (above 1000). The increase of this factor is mainly due to higher value of hydraulic diameter. As aspect ratio increases, the hydraulic diameter is also increased. At high Reynolds number (>2000), j values predominantly changing from 0.0109 to 0.00269 for a change in s/h value of 0.234 to 0.3155, there after j value is increasing. The change in j value is due to thermal boundary layer formation at particular s/h range.

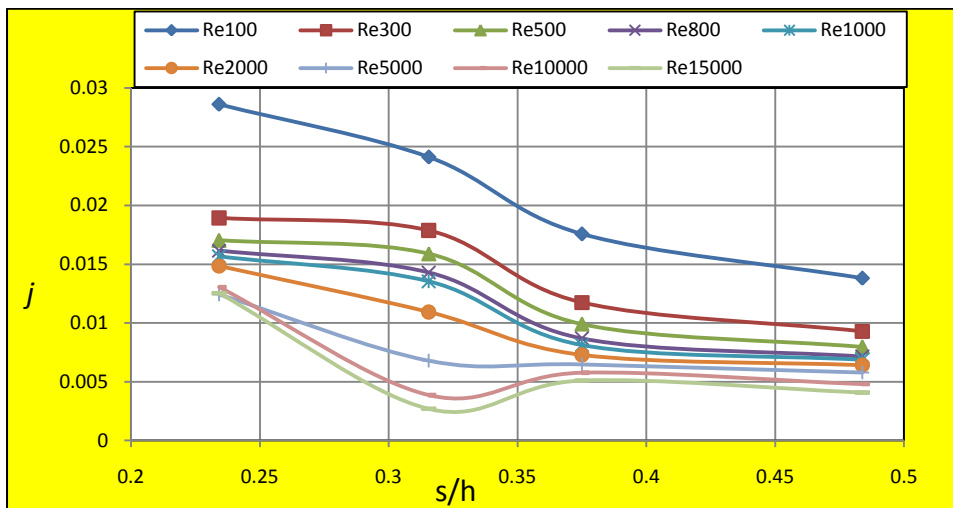


Fig. 3.8: Effect of s/h Ratio on Colburn j Factor of Serrated Fin Surface

3.11.2 Analysis of t/s ratio on j

The Colburn j factors are plotted against the fin thickness (t) to fin spacing (s) ratio (0.0765 to 0.1675) for various Reynolds numbers as shown in Fig. 3.9. It is observed that as Reynolds number increases, j factors are coming down. The rate of decrease is higher for low Reynolds numbers and lower for high Reynolds number. However, the ratio of increase is predominant for low Re (below 1000) and it is not

significant for high Re (above 1000). The increase of this factor is mainly due to higher value of hydraulic diameter. Also, it is noted that the j factor decrease with increase of t/s ratio (up to 0.15) for all Reynolds numbers. As t/s ratio increases, the recirculation zone tends to diminish due to higher flow velocity in the offset passages. This leads to decrease in heat transfer rate.

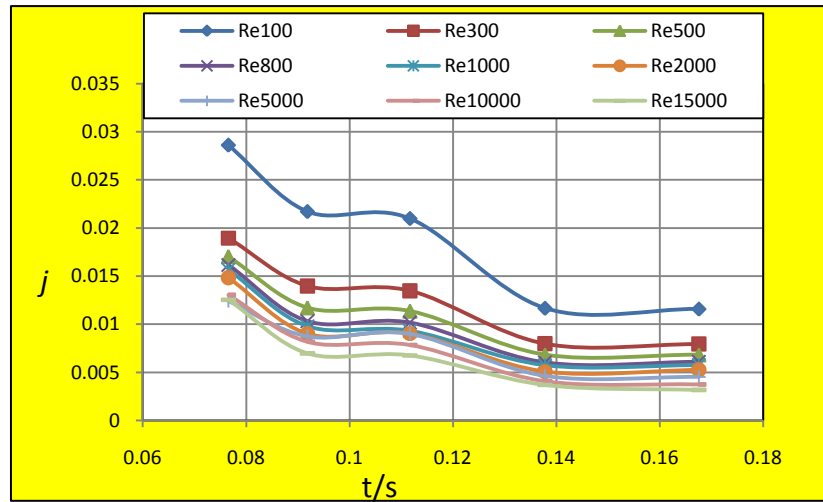


Fig. 3.9: Effect of t/s Ratio on Colburn j Factor of Serrated Fin Surface

3.11.3 Analysis of t/l ratio on j

The Colburn j factors are plotted against the fin-thickness (t) to fin length (l) ratio for various Reynolds numbers as shown in Fig. 3.10. It is observed that as Reynolds number increases, j factors are coming down. The rate of decrease is higher for low Reynolds numbers and lower for high Reynolds number. However, the ratio of increase is predominant for low Re (below 1000) and it is not significant for high Re (above 1000). The increase of this factor is mainly due to higher value of hydraulic diameter. The value of j decreases with increase of t/l for all Reynolds numbers. Also, it is noted that the j factor decreases with increase of t/l ratio (up to 0.05) for all Reynolds numbers. It is found that t/l ratio increases the recirculation zone at the interrupted layer increases. It is observed that as Reynolds number increases, j factors are coming down due to same reasons as mentioned in section 3.11.1.

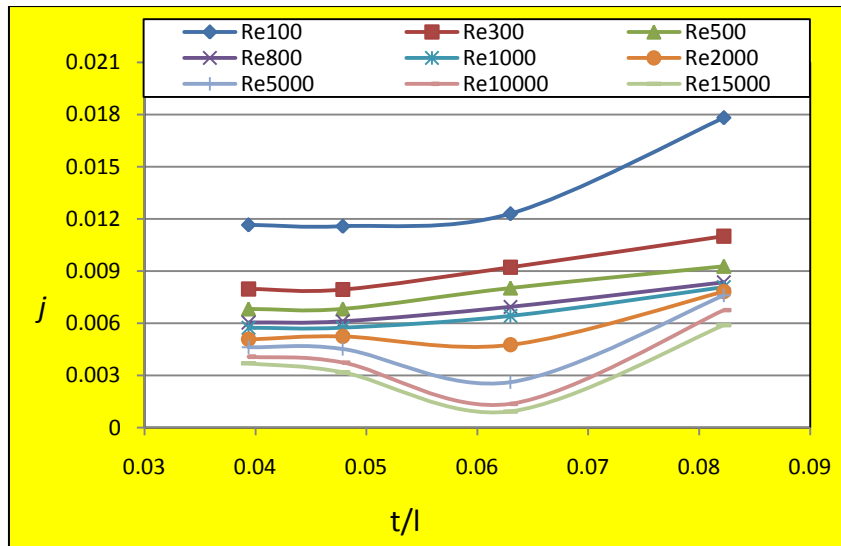


Fig.3.10: Effect of t/l Ratio on Colburn j Factor of Serrated Fin Surface

3.11.4 Analysis of s/h ratio on f

The friction factor f is plotted against the fin spacing (s) to fin height (h) ratio as shown in Fig 3.11. The f factor decreases with Re number increases as expected. As aspect ratio increases, the hydraulic diameter is also increased. The rate of decrease is higher for low Reynolds numbers and lower for high Reynolds number. However, the ratio of increase is predominant for low Re (below 1000) and it is not significant for high Re (above 1000). The increase of this factor is mainly due to higher hydraulic diameter.

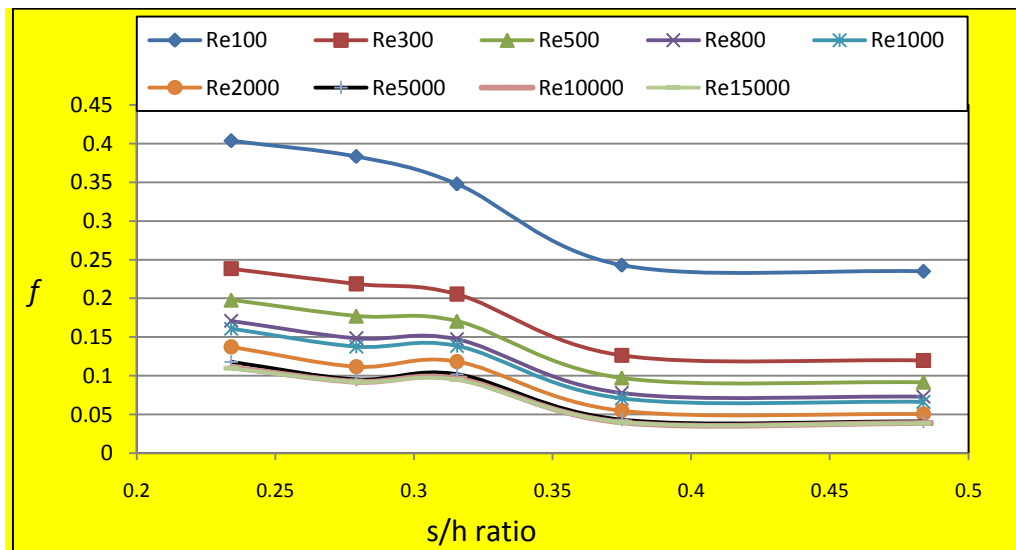


Fig.3.11: Effect of s/h Ratio on f Factor of Serrated Fin Surface

3.11.5 Analysis of t/s ratio on f

The friction factor f is plotted against the fin thickness (t) to fin spacing (s) ratio (0.0765 to 0.1675) for various Reynolds numbers as shown in Fig. 3.12. It is observed that as Reynolds number increases, f factors are coming down. The rate of decrease is higher for low Reynolds numbers and lower for high Reynolds number. However, the ratio of increase is predominant for low Re (below 1000) and it is not significant for high Re (above 1000). The increase of this factor is mainly due to higher value of hydraulic diameter.

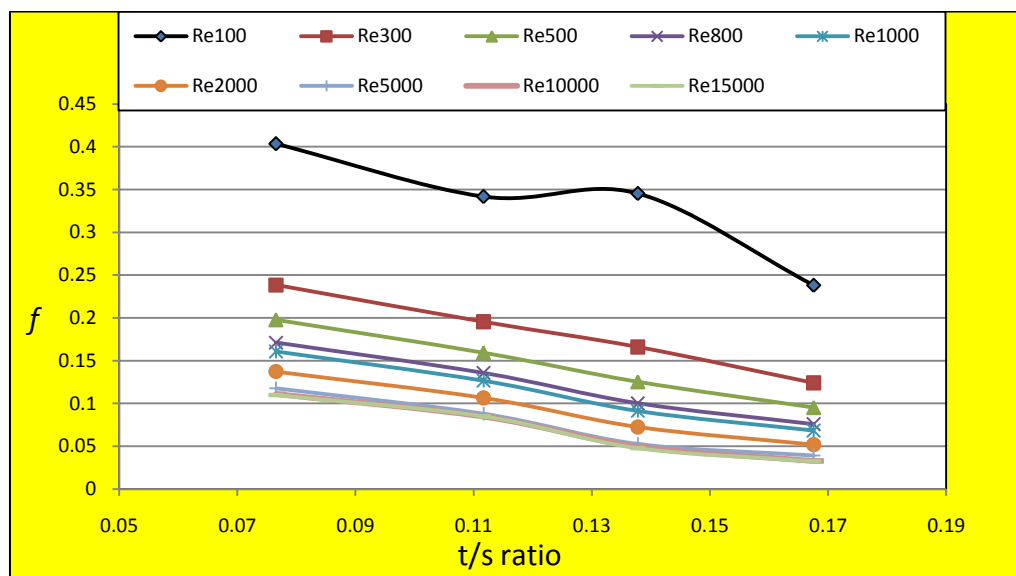


Fig.3.12: Effect of t/s Ratio on f Factor of Serrated Fin Surface

3.11.6 Analysis of t/l ratio on f

The friction factor f is plotted against the fin-thickness (t) to fin length (l) ratio (0.027 to 0.082) for various Reynolds numbers as shown in Fig. 3.13. It is observed that as Reynolds number increases f factors are coming down. The rate of decrease is higher for low Reynolds numbers and lower for high Reynolds number. However, the ratio of increase is predominant for low Re (below 1000) and it is not significant for high Re (above 1000).

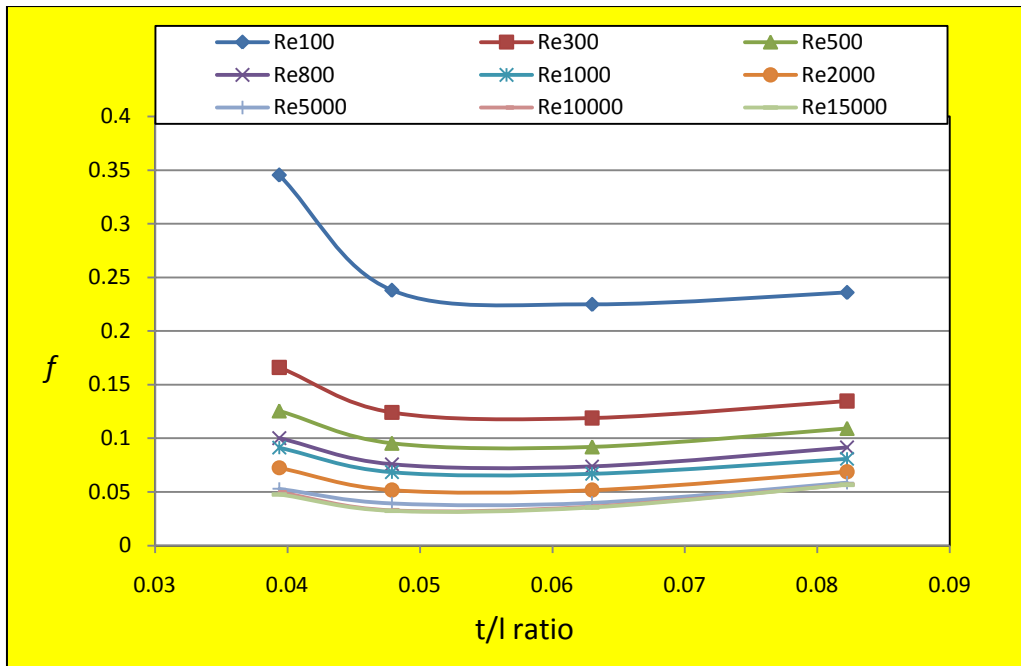


Fig. 3.13: Effect of t/l Ratio on f Factor of Serrated Fin Surface

3.11.7 Velocity, temperature and pressure contours

The velocity vector for the Reynolds numbers 500 and 10000 are shown in Fig. 3.14 and Fig. 3.15 for comparison of velocity magnitudes. From the velocity vectors it is quite clear that the flow is more laminar at Reynolds number 500 and is turbulent for the Reynolds number 10000. This is because the velocity profile is more parabolic in shape for the Reynolds number 500 and is more flat for the Reynolds number 10000. One more interesting feature is the shape of the vectors, which are pulled towards the interrupted part. This is basically because of the formation of the recirculation zone that is pulling the velocity contours towards it in order to compensate for the excess pressure drop due to the recirculation pocket.

The pressure and temperature contours are shown in Fig. 3.16 and Fig. 3.17 respectively for the same fin surface. It is clear that the boundary layer interrupts and fresh boundary layer starts from the interruption. This is more predominantly seen for the low Reynolds number case (Re 500). Moreover, high pressure drop occurs at the interruptions and the velocity reaches its maximum value at the same place.

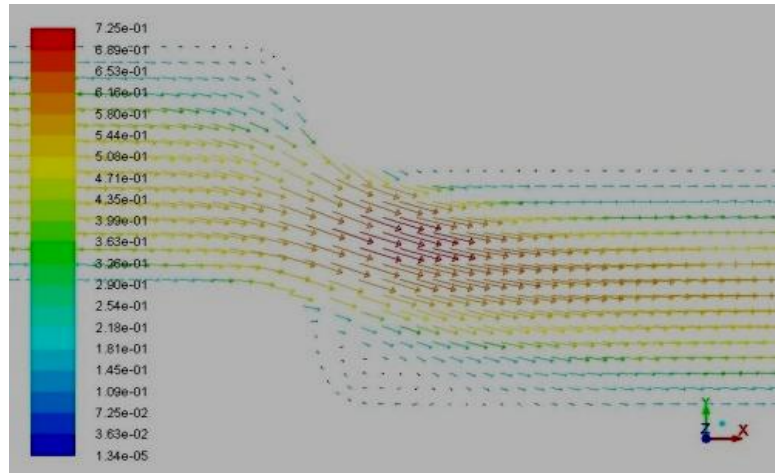


Fig.3.14: Velocity (m/s) Vectors Plot of Serrated Fin at Re=500 for Water Medium

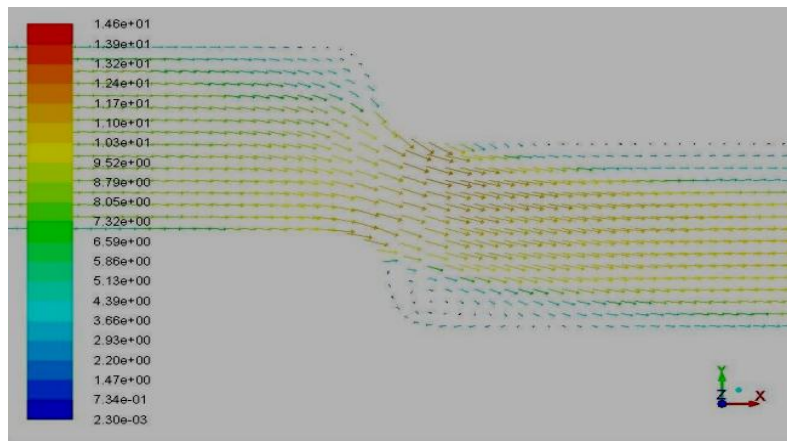


Fig.3.15: Velocity (m/s) Vectors Plot of Serrated Fin at Re=10000 for Water Medium

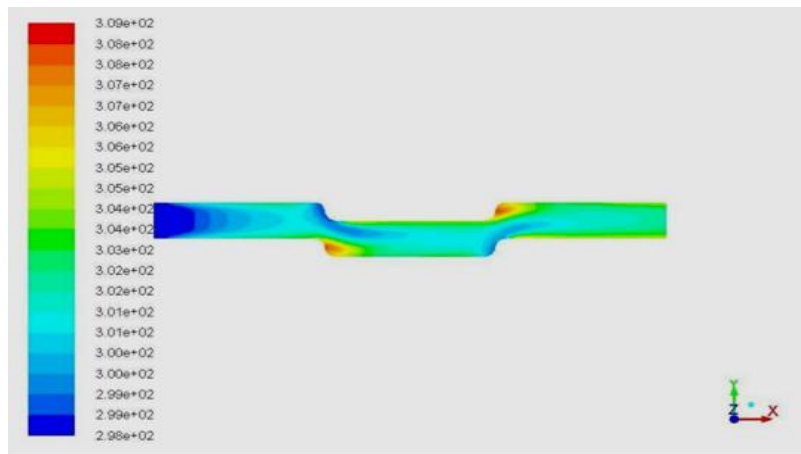


Fig.3.16: Pressure (Pa) Contour Plot of Serrated Fin at Re = 500 for Water Medium

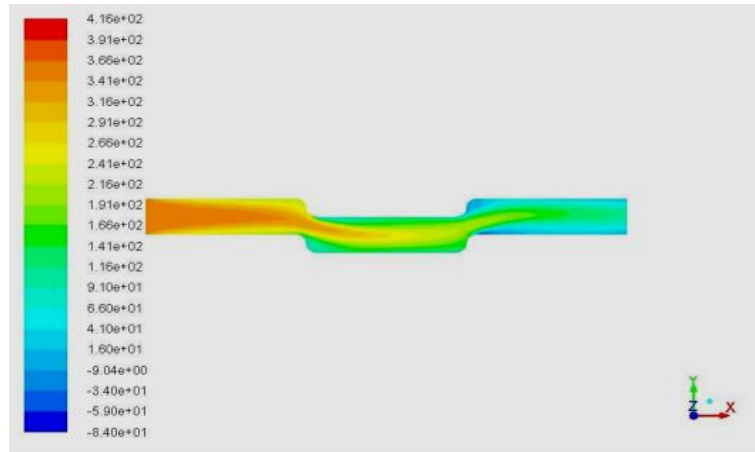


Fig. 3.17: Temperature (k) contour Plot of Serrated Fin at Re=500 for Water Medium

3.12 Generation of Flow Friction and Heat Transfer Correlations

An exhaustive CFD study has been carried out on the heat transfer phenomena in plate fin surfaces with serrated fins. The j vs. Re and f vs. Re curves shows significant non-linearity as shown in the above figures. The correlations have been expressed in terms of two separate equations over the low and high Re regions along with dimensionless geometric parameters. The power law expressions have been used for determining the Colburn factor j and friction factor f as a function of the Reynolds number and dimensionless fin parameters.

The colburn factor j are functionally related to Re , s/h , t/s and t/l and it can be represented as,

$$j = BRe^{a1} \left(\frac{s}{h}\right)^{a2} \left(\frac{t}{s}\right)^{a3} \left(\frac{t}{l}\right)^{a4} \quad (3.21)$$

where B , $a1$, $a2$, $a3$ and $a4$ are constants.

The use of these power law expressions is justified because variations in j with Re , s/h , t/s and t/l follow constant slope log-linear lines in both laminar and fully turbulent flow regions. The j vs. Re data for serrated fin surfaces shows significant nonlinearity over the Reynolds number range $100 \leq Re \leq 15000$. Therefore, two separate equations for the low and the high Re regions as follows:

for Laminar range ($100 \leq Re \leq 1000$)

$$j = 0.426Re^{-0.308} \left(\frac{s}{h}\right)^{0.585} \left(\frac{t}{s}\right)^{-0.929} \left(\frac{t}{l}\right)^{0.943} \quad (3.22)$$

for Turbulent range ($1000 \leq Re \leq 15000$)

$$j = 0.097Re^{-0.151} \left(\frac{s}{h}\right)^{0.526} \left(\frac{t}{s}\right)^{-1.238} \left(\frac{t}{l}\right)^{1.033} \quad (3.23)$$

The above correlations correctly predict 94% of the j data for laminar regime, and 93% of the j data for the turbulent regions lies within $\pm 10\%$ and root-mean-square error is 2.8%.

Similarly, the fanning friction factor f are functionally related to Re , s/h , t/s and t/l and it can be represented as

$$f = CRe^{b1} \left(\frac{s}{h}\right)^{b2} \left(\frac{t}{s}\right)^{b3} \left(\frac{t}{l}\right)^{b4} \quad (3.24)$$

where C , $b1$, $b2$, $b3$ and $b4$ are constants.

The use of these power law expressions is justified because variations in f with Re , s/h , t/s and t/l follow constant slope log-linear lines in both laminar and fully turbulent flow regions. The f vs. Re data for offset fin surfaces show significant nonlinearity over the Reynolds number range $100 \leq Re \leq 15000$. Therefore, two separate equations have been proposed for the low and the high Re regions as follows:

for Laminar range ($100 \leq Re \leq 1000$)

$$f = 3.152Re^{-0.481} \left(\frac{s}{h}\right)^{-0.272} \left(\frac{t}{s}\right)^{-1.237} \left(\frac{t}{l}\right)^{0.984} \quad (3.25)$$

for Turbulent Range ($1000 \leq Re \leq 15000$)

$$f = 0.421Re^{-0.205} \left(\frac{s}{h}\right)^{-0.135} \left(\frac{t}{s}\right)^{-1.673} \left(\frac{t}{l}\right)^{1.194} \quad (3.26)$$

The above correlations correctly predict 92% of the j data for laminar regime and turbulent regions lies within $\pm 12\%$ and root-mean-square error is 6.7%.

3.13 Generation of Flow Friction and Heat Transfer Correlations for Water Side Serrated Fin

In the entire test condenser units, water side same type of serrated fin surface is used and details of the fin are given below.

Table 3.2: Test Condenser Water Side Serrated Fin Geometry Details

Test Unit No.	Circuit Name	Fin density (FPI)	Lance Length (mm)	Hydraulic Diameter (mm)	Height (mm)	Fin Size (mm)	
						Flow Length	Thickness
TC1 to TC4	Water-side	28	3.175	1.3450	5	150	0.127

Hence, a detailed analysis has been carried out using fluent to estimate the 'j' and 'f' factors for serrated fins in accordance with Ranganayakulu et al. (2015). The correlation for water side heat transfer coefficient for the above selected serrated fin surface in laminar and turbulent range are as follows:

for Laminar Range ($100 \leq Re \leq 800$)

$$Nu_w = 0.049 Re_w^{0.69} Pr^{\frac{1}{3}}, \quad (3.27)$$

$$\text{Then, } h_w = 0.049 \left(\frac{\lambda_w}{D_h}\right) Re_w^{0.69} Pr^{\frac{1}{3}} \quad (3.28)$$

for Turbulent Range ($1000 \leq Re \leq 15000$)

$$Nu_w = 0.016 Re_w^{0.85} Pr^{\frac{1}{3}}, \quad (3.29)$$

$$\text{Then, } h_w = 0.016 \left(\frac{\lambda_w}{D_h}\right) Re_w^{0.85} Pr^{\frac{1}{3}} \quad (3.30)$$

The above correlations correctly predict 96% of the j data for laminar region and turbulent regions lies within $\pm 8\%$ and root-mean-square error is 3.2%.

CHAPTER 4

DEVELOPMENT OF EXPERIMENTAL APPARATUS

The literature survey signifies that very limited work has been done on the condensation of R134a in compact plate fin heat exchangers in specific to serrated fin surfaces. Due to compactness of these types of heat exchangers will led reduction in size and weight of the heat exchangers compared to shell & tube, plate heat exchangers and plate & tube heat exchangers. Apart from compactness, by using refrigerant R134a, which is user friendly and environmental friendly, having the high COP and heat transfer rates due to latent heat of condensation, the size and weight of heat exchangers shall be further reduced. While the condensation heat transfer and friction pressure drop characteristics of R134a in compact fin surfaces are of significant importance to the effective design of the compact plate-fin heat exchangers for aerospace applications. Open literature was not available on this subject. The primary objective was to investigate experimentally the condensation heat transfer coefficients and pressure drop for R134a in serrated fins. This chapter begins with a description of the development of small brazed compact heat exchangers with serrated fins for the required correlations to be developed. Also, highlighted the design and development of test rig in which the experiments were conducted. The construction and function of the test facility is discussed next, followed by an overview of the entire experimental system. This chapter ends with a validation of experimental test facility with empirical data.

4.1 Development of Brazed Compact Plate Fin Heat Exchangers

The theoretical design and development of compact plate fin heat exchangers (CPFHE) for generation of two phase condensation characteristics of serrated fin surfaces (Lance & offset) using R134a refrigerant are discussed in detail. The design of the experimental test rigs depends upon experimental unit size and thermal heat load. While designing experimental units, it is required to consider the effectiveness to weight ratio, availability of fins, cost, manufacturing capability and the application.

Until now, compact plate fin heat exchangers are widely used in aerospace and process industries for sensible heat transfer. Use of compact heat exchangers with fins for condenser and evaporator applications is explored in the last decade by industries. Minimum heat flux philosophy is followed for theoretical design of test units. Development feasibility of test cores using vacuum brazing process is followed. Thermocouples are placed inside the test units to continuous monitoring of refrigerant quality as well as the wall temperature of test units.

4.1.1 Selection of material

Compact plate fin heat exchangers can be made in a variety of materials based on design requirements. In cryogenic and aerospace applications, aluminium and its alloy is preferred because of its low density, high thermal conductivity and high strength at low temperature. The pure aluminum (1series) is having low strength mechanical properties compared to the other aluminum alloying materials. Aluminum-Manganese (3 series) material is having medium strength properties and very good brazeability and weldability properties (Shah R.K, 1990). Aluminum-Copper (2 series), Aluminum-Silicon (4 series), Aluminum-Magnesium (5series) and Aluminum-Zinc (7 series) are not suitable for vacuum brazing due to its low boiling point constituents. Aluminum-Manganese (3003) does not contain low boiling point constituents. Whereas, Aluminum-Magnesium-Silicon (6061) material is braze able with extra care (Shah, 1990). In general 6061 material is used for high operating temperature and pressure applications. An aluminum alloy of lower melting point with appropriate melting is used as brazing material in case of aluminum exchangers. Aluminum-Manganese alloy (AA3003) is selected for making fins due to high brazeability. The chemical composition of AA3003 is given in Table 4.1.

Table 4.1: AA3003 Chemical Composition (%)

Aluminium Alloy	Al	Mn	Si	Fe	Cu	Mg	Cr	Zn	Ti
AA 3003	97.94	1.1	0.2	0.6	0.1	0	0	0.02	0

4.1.2 Fin geometries

The selection of fin geometry plays a vital role while designing a plate fin heat exchanger among other things. The performance is more for high compactness fins and pressure drop is also more for the same fin. The selected fin configurations for

theoretical analysis are serrated fin type. In serrated fins, the offset of fins resulting in significant flow unsteadiness and highly turbulent even at low Reynolds number. The performance of serrated fins is high when compared with wavy fins due to offset of fins and frequent interruption of boundary layer. The photographic view of serrated fin and dimensional notations of fin are shown in Fig.4.1 below.

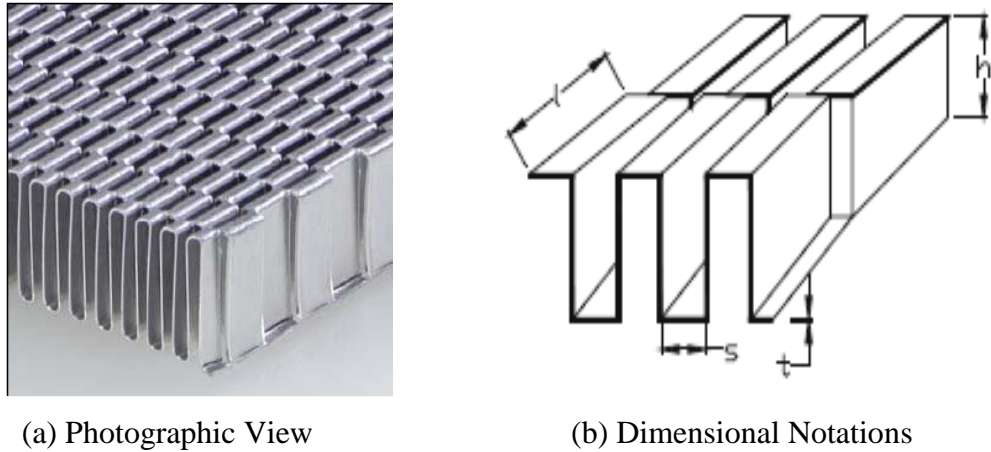


Fig. 4.1: Serrated Fin

4.1.3 Design methodology

The test unit is basically a cross flow arrangement with two passes on the water side and one pass on R134a side. The ease of manufacturing dictated to select cross flow arrangement. The CAD model of test condenser core is shown in Fig.4.2.

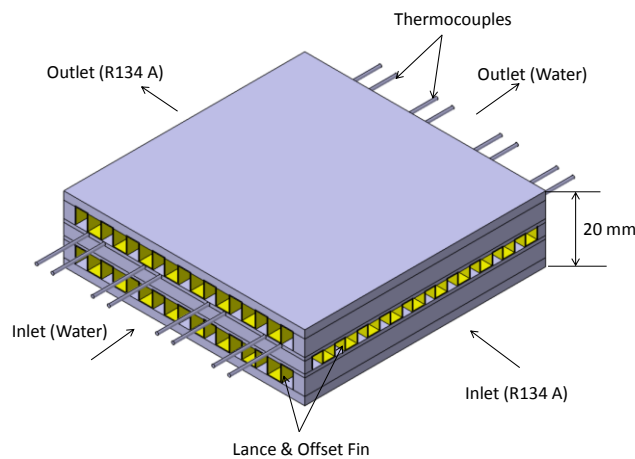


Fig.4.2: CAD Model of Test Condenser Core

4.1.3.1 Plate – fin type heat exchanger design

Test units are designed based on heat flux using ‘Compact Heat Exchangers’ by Kays and London (1984). Based on the availability of fins and its usage, 4 types of serrated fins are selected for characterisation. Test heat exchangers with different fin geometries have been identified for generation of average condensation refrigerant heat transfer coefficient and frictional pressure drop characteristics. The selected fin geometry details of the CPFHE test cores are given in Table 4.2. TC1, TC2, TC3 and TC4 are four brazed plate fin test condensers marked characterisation using R134a as working medium.

Table 4.2: Serrated Fin Geometry Details

Test Unit No.	Circuit Name	Fin Density (FPI)	Lance Length (mm)	Hydraulic Diameter (mm)	Height (mm)	Fin Size (mm)	
						Flow Length	Thickness
TC1	R134a-side	30	3.175	1.1894	3.05	150	0.1016
	Water-side	28	3.175	1.3450	5	150	0.127
TC2	R134a-side	28	3.175	1.3450	5	150	0.127
	Water-side	28	3.175	1.3450	5	150	0.127
TC3	R134a-side	18	1.588	1.7461	3.8	150	0.254
	Water-side	28	3.175	1.3450	5	150	0.127
TC4	R134a-side	18	3.175	1.8667	5	150	0.254
	Water-side	28	3.175	1.3450	5	150	0.127

Using Kays and London (1984) book of Compact Heat Exchangers, theoretical thermal design of test units were carried out for maximum heat flux of 25 kW/m² at a maximum heat load of 5 kW and mass flux of 60 kg/m²s at a mass flow rate of 0.04 kg/s. Serrated (L&O) type fin surfaces with different fin heights, fin density are selected for design data generation and analysis purpose. To measure the wall temperature, 16 numbers of thermocouples are inserted between the refrigerant circuit and water circuit. The theoretical thermal design of test units is carried out as per the procedure given by Kays and London (1984).

4.1.3.2 Design procedure for plate fin heat exchangers:

The detailed procedure is illustrated below step by step.

Step 1: Surface Characteristics:

- Based on the requirement, the core dimensions of the heat exchangers are fixed on the basis of heat flux. Selected the fin type that is to be characterised. Then, choose the surface characteristics of selected fin type such as,
 1. Plate spacing (b),
 2. Hydraulic radius (r_h),
 3. Fin thickness (δ),
 4. Separating sheet thickness (a)
 5. Transfer area / volume between plates (β),
- From heat exchanger core dimensions, calculate frontal area (A_{fr}) for both stream and volume of core (V).
- Choose the plate thickness between both streams (a) and assume a suitable material that should have higher thermal conductivity. Take 'k' for chosen plate.

Step 2: Heat transfer & Free flow areas:

- Calculate the value of ' α ' = $\frac{b_1\beta_1}{b_1+b_2+2a}$ (for plate-fin surface) for both streams.
- Then, calculate total heat transfer area on each side given by $A = \alpha V$ (i.e., A_c, A_h).
- Calculate the ratio of free flow area to frontal area, $\sigma = \alpha r_h$ and then calculate the values of free flow area ($A_{ff} = \sigma A_{fr}$) for both streams.

Step 3: Reynolds number & mass flux:

- Calculate the mass flux (G) = $\frac{m_r}{A_{ff}}$
- Calculate the Reynolds number (Re) = $\frac{4r_h G}{\mu}$

4.1.3.3 Analysis of theoretical design results

The theoretical analysis is carried out to optimize the heat exchanger core size. The serrated fin used on R134a side in test unit TC2 was taken for theoretical thermal

analysis due to its highest fin heat transfer area compared to all the four units. Heat load of 5 kW and the refrigerant mass flow rate of 0.04 kg/s are considered for the analysis with the fin flow length of 150mm and fin width of 75mm, 100mm, 125mm and 150mm are taken. Based on proposed test facility, the heat loads and refrigerant flow rates are selected. Theoretically calculated values of heat flux, mass flux and Reynolds number for serrated fin with four different fin widths by keeping the other fin parameters same are presented in Table 4.3.

Table 4.3: Calculation of Heat Flux, Mass Flux and Re for Different Serrated Fin Sizes

Refrigerant mass flow rate (kg/s)	Flow length (m)	Fin width (m)	Total heat transfer area (m ²)	Heat flux (kW/m ²)	Mass flux (kg/s m ²)	Re
0.04	0.15	0.075	0.120642987	41.444597	127.2635007	1047.5484
0.04	0.15	0.1	0.160857317	31.083448	95.4476255	785.6613
0.04	0.15	0.125	0.201071646	24.866758	76.3581004	628.5291
0.04	0.15	0.15	0.241285975	20.722298	63.63175033	523.7742

Fig.4.3 shows the effect of fin area on heat flux for different widths of serrated fin. As the fin area increases the heat flux shall decrease for the same heat load. The results indicated that, as the fin area increases the heat flux as well as mass flux is decreasing. The effect of mass flux on heat flux for serrated fin surfaces is shown in Fig.4.4. Fig.4.5 indicates the Reynolds number effect on heat flux for serrated fins. The Reynolds number decreases as free flow area increases. The Fig.4.3, Fig.4.4 and Fig.4.5 indicates the effects of total fin area on heat flux, mass flux and Reynolds number for three different sizes of serrated fin. The maximum heat flux and mass flux is considered for optimization of the fin size is 25 kW/m² and 60 kg/m²s respectively. These parameters are selected to cover the gravity controlled and forced convection condensation effects. The transition point in plate heat exchangers for R134a is around a mass flux of 15-25 kg/m²s (Longo, 2008). In compact plate fin heat exchangers are also assumed that the transition region shall fall between 15 kg/m²s to 25 kg/m²s. So, the selected mass flux range shall cover both the gravitational and forced convection effects on fin geometry.

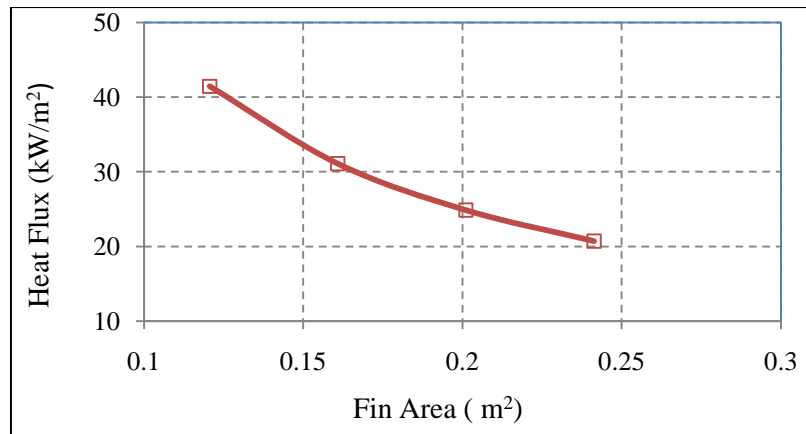


Fig. 4.3: Effect of Serrated Fin Heat Transfer Area on Heat Flux

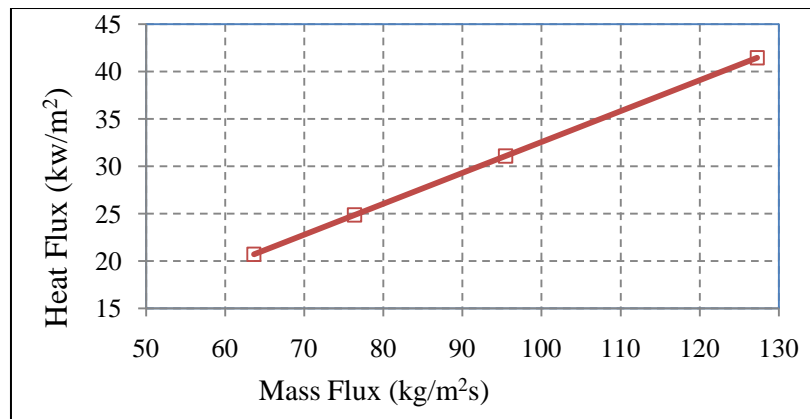


Fig. 4.4: Effect of Mass Flux through Serrated Fin on Heat Flux

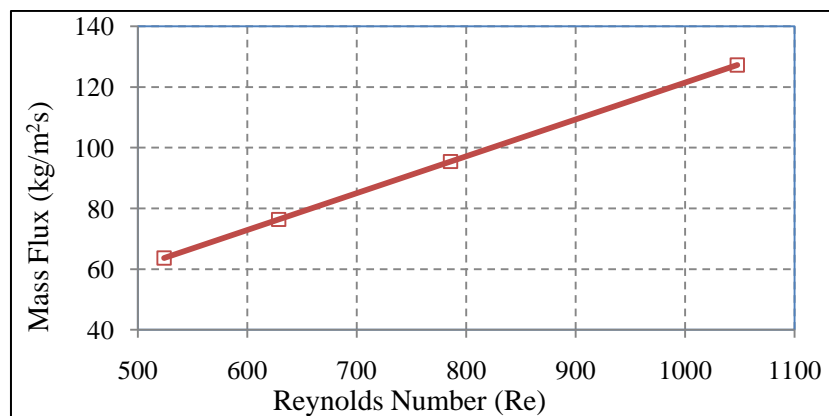


Fig.4.5: Effect of Reynolds Number on Mass Flux

The theoretically estimated heat flux and mass flux for a maximum heat load and mass flow rates for a heat exchanger core size of 150mm X 150mm meets the

requirements. The calculated heat flux and mass flux for core size of 150 mm X 150 mm are 20.7 kW/m^2 and $63.6 \text{ kg/m}^2\text{s}$. Based on theoretical calculations, the finalized compact plate fin heat exchanger core size was 150mm X 150mm and height of the unit varies based on selected fin height.

Based on the finalized heat exchanger core size, theoretically calculated the values of heat flux and mass flux for 4 types of serrated fin geometries. The calculated heat flux and mass flux for different serrated fins are presented in Table 4.4. The tabulated values are calculated for a refrigerant heat load of 5 kW and mass flow rate of 0.04 kg/s.

Table 4.4: Calculation of Heat Flux and Mass Flux for Different Serrated Fin Geometry

Name	Circuit Name	Fin Density (FPI)	Height (mm)	A_{fr}	D_h	β	α	σ	A_f	G	Re	A_h	Heat Flux
				mm ²	mm	m ² /m ³	1/m		mm ²	Kg/s.m ²		m ²	kw/m ²
TC1	R-134a	30	3.05	3379.6	1.1894	2860.892	724.1262	0.215314	368.4321	108.56	790.2158	0.1632	30.64
	Water	28	5	3379.6	1.3450	2492.724	1034.325	0.347783	1190.182	420.11	634.8853		
TC2	R-134a	28	5	3656.5	1.3450	2492.724	890.2586	0.299341	595.09	67.22	553.3103	0.2286	21.87
	Water	28	5	3656.5	1.3450	2492.724	890.2586	0.299341	1190.182	420.11	634.8853		
TC3	R-134a	18	3.8	3486.1	1.7461	1753.281	520.5053	0.227208	412.8962	96.88	1035.264	0.1296	38.58
	Water	28	5	3486.1	1.3450	2492.724	973.7203	0.327405	1190.182	420.11	634.8853		
TC4	R-134a	18	5	3656.5	1.8667	1669.291	596.1754	0.278214	552.6242	72.38	826.8773	0.1591	31.43
	Water	28	5	3656.5	1.3450	2492.724	890.2586	0.299341	1190.182	420.11	634.8853		

4.1.4 Brazing of Test Condenser

Vacuum brazing is one of the critical areas in the development of compact heat exchangers. The brazing cycle has an important effect on the joint strength. The test cores manufactured by stacking fins, side-bars, parting sheets and cover sheets are held together in a jig with predefined load. It is placed in a vacuum brazing furnace and brazed to form the plate fin heat exchanger core. The test core shall have stack of three fins, one fin on refrigerant side in which the condensation heat transfer and pressure drop shall be generated and two fins on water side. The assembled core in the brazing fixture was shown in Fig. 4.6(a). Before brazing the core 16 numbers of $\Phi 0.5\text{mm}$ stainless steel wires are inserted between the separating sheets. The test cores are brazed using vacuum brazing furnace which was shown in Fig. 4.6(b). The test core was brazed using pre-defined brazing cycle. The final brazed test condenser was shown in Fig. 4.6(c).

These wires are removed after the brazing and K-type thermocouples are inserted with conductive type adhesive. These thermocouples are required to measure the wall temperatures during condensation experimentation. The arrangement of thermocouples on circuit walls are shown in Fig.4.7.

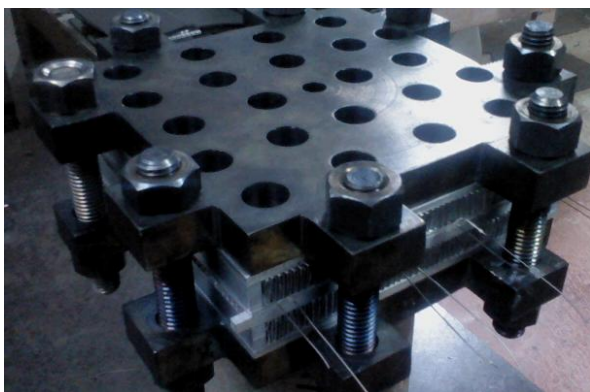


Fig. 4.6(a): Test Core Assembly

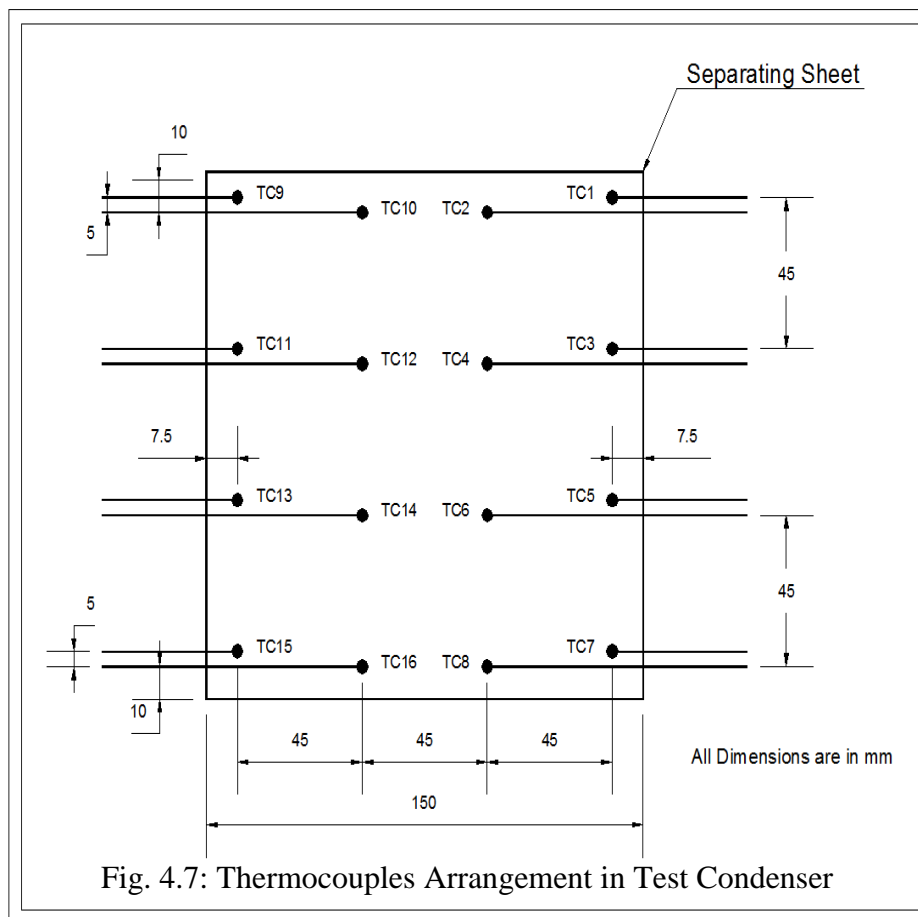


Fig. 4.6 (b): Brazing Furnace



Fig. 4.6 (c): Photograph of Brazed Test Core

Fig. 4.6: Brazing of Test Condenser Core



Thermocouples are inserted in the stainless steel wire removed location. K-type thermocouples with connector are inserted in place of Φ 0.5mm stainless steel wires through water side header. These thermocouples are fixed on water side circuit due to refrigerant circuit was required to use for high pressure. At pressure providing

leak tightness was difficult. Proper care has taken to insert these thermocouples inside the brazed core. The fixing arrangement of thermocouples with connector to the header was shown in Fig. 4.8.



Fig. 4.8: Photograph Showing Thermocouples Fixing Arrangement in Test Condenser Core

Headers and connectors are welded to the test core using TIG welding process. These headers and connectors are fabricated using high strength aluminum material of type AA5086. The test core has under gone pneumatic leak check on water side circuit as well as refrigerant side circuit. The size of the test core is 150mm X 150mm and core height varies based on the fin height. The overall size of test condenser was about 400 mm X 400 mm and unit height varies based on the fin height. The uniform length and width of core was maintained for easily removable and assembly of test condensers in the test rig. Vacuum test has been carried out on refrigerant circuit as it is required the vacuum tightness. The test condenser was insulated with 10 mm thick polyimide foam coated with hypalon to reduce heat loss to ambient. One of the final brazed test condensers with insulation and K-type thermocouples are shown in Fig.4.9.

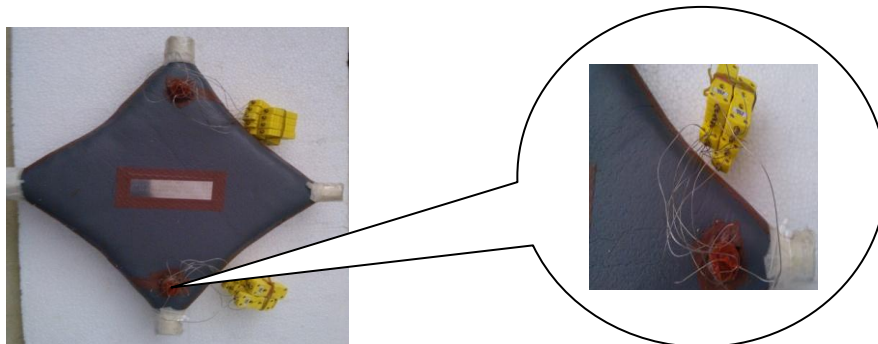


Fig. 4.9: Photograph of Test Condenser after Insulation

4.1.5 Procedure for helium leak test on test condenser

The test condensers before using in experimental test facility; it shall be checked with helium leak test for any internal and external leaks. The procedure followed for testing of units is as follows:

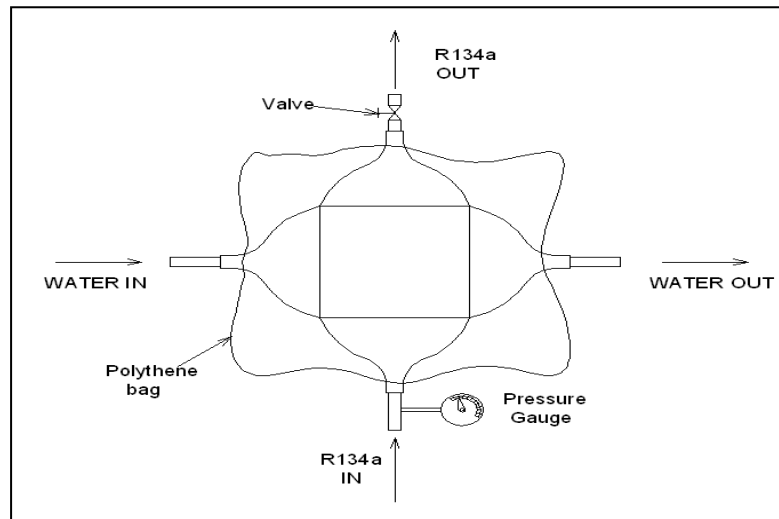


Fig. 4.10: Helium Leak Test Setup

4.1.5.1 Internal leak rate

- The test condenser was enclosed in a sealed polythene bag as per Fig. 4.10.
- The inlet port of R134a circuit of test condenser was fitted with a pressure gauge and outlet port of the R134a circuit was fitted with a needle valve. The valve was connected to 99.9% pure helium gas cylinder. The R134a circuit was then slowly charged with helium to a pressure of 0.2 MPa (g) and the valve was closed.
- The water circuit of the test condenser was then purged with argon gas for about 5 minutes to let out the air present in the water circuit. Then the inlet and outlet ports of water circuit were sealed with packing tape.
- The test condenser was kept under pressurised condition for 30 minutes and sniffer probe was inserted by puncturing a small hole in the sealing tape of one of the ports of the water circuit. The sniffer probe was also sealed to the port with packing tape.
- The probe was held in the same position for about 5 minutes to measure the inter pass leak rate.
- The inter-pass leak rate was recorded as 1×10^{-8} mbar lit/s at steady state.

4.2 Experimental Test Rig Specification

The condenser planned here is for combat aircraft radar cooling application. The radar will be operated in above ground (aircraft altitudes > 2 km) from flight. The experimental data generated using this test facility was used to design the condenser for aircraft application. It was intended to characterize/generation of design data (Two phase average condensation heat transfer coefficient and frictional pressure drop) for different types of serrated fin geometries using R134a as working fluid for wide range of operating conditions. In open literature most of the authors are conducted experiments for generation of average condensation heat transfer coefficient and frictional pressure drop for plate heat exchangers, In-tube and helical pipes using R134a was 30 °C to 45 °C. Based on literature data and test condenser mechanical design, the condensing saturation temperature (saturation pressure) varied between 32 °C to 44 °C. This range of saturated refrigerant condensation temperature (saturated pressures) is sufficient for proposed aircraft requirements. Accordingly the test rig specification was finalised.

The test rig specification arrived based on experimental test condenser interfaces and test requirements. Details of the experimental test rig of each circuit are given below. Also, the instrumentation and safety protection requirements of each circuit mentioned. The broad specifications of experimental test rig are:

- a) Test rig is designed for conducting performance tests on different types of test condensers as elaborated in further sections.
- b) Test rig consisted of refrigerant circuit and water cooling circuit.
- c) Variable refrigerant flow rate to be achieved by using variable frequency drive.
- d) Variable flow and temperature shall be achieved in condenser loop.
- e) Type of refrigerant : R134a
- f) Refrigerant flow rate : 0.01 kg/sec to 0.04 kg/s
- g) Refrigerant cooling capacity : 10 kW
- h) Cooling system : DM Water
- i) Type of control: Digital electronic control system.

- j) Type of measurement: Digital display for instruments and computer screen display.
- k) Computer based data acquisition and data processing.
- l) Control panel for digital display units with safety alarms & power isolator.
- m) Hardware: Data card, instrumentation, digital indication and sensors.
- n) Software: SCADA Base, functional on Microsoft windows operating systems.

4.2.1 Refrigerant circuit

- Flow rate : 0.01 kg/s to 0.04 kg/s
- Pressure range : 0-15 bar 'g'
- Working media : R134a
- Operating temperature range : 10 °C to 70°C
- Capacity : 10 kW
- Power supply : 440 V, 3Φ, 50 Hz
- This circuit can be used to test experimental compact heat exchangers as condenser.
- This circuit is fully instrumented to read pressure, flow and temperature etc. All the indicators are digital type and are connected to data acquisition system to log the data.
- Safety measures for the protection of the test rig included to cut off if the set pressure is exceeded and provision to detect the refrigerant leakage.

4.2.2 Condensation / Evaporation secondary circuit (water circuit)

- Flow rate : 5 to 60 lpm
- Pressure range : 0-2 bar 'g'
- Working media : DM Water
- Condensation loop (Operating temperature range) : 10 °C to 60 °C
- Evaporation loop (Operating temperature range) : 10 °C to 40 °C
- Power supply : 440 V, 3Φ, 50 Hz
- This circuit is fully instrumented to read pressure, flow and temperature etc. All the indicators are digital type and are connected to data acquisition system to log the data.

- Safety measures for the protection of the test rig included to cut off, if the set pressure is exceeded.

4.3 Standards

The following standards are used for various activities:

- 1) Thermodynamic property table for saturated R134a - ASHRAE Transaction 94, pp. 2095-118.
- 2) Thermodynamic property table for water (R718)
- 3) Compressor design as per sea-bird refrigeration Pvt. Ltd.
- 4) Evaporator and condenser design as per PHE B3-030, Technical brochure from Danfoss industries.
- 5) Chiller unit design as per Werner Finley Pvt.Ltd.
- 6) Pipe lines design as per ASME B- 88 and ASHRAE Guide and Data Book,
- 7) ASHRAE Handbook Refrigeration, Chapter 2, 2006.
- 8) Welding and Brazing qualifications as per ASME Section IX
- 9) Rules for construction of pressure vessels as per ASME Section VIII Div.1.

4.4 Design and Development of Experimental Test Rig

The test facility was established to study the condensation characteristics for R134a in different types of serrated fins used in small brazed compact plate fin heat exchangers. Test rig was designed based on the technical specification and experimental test units. The experimental test facility was shown in Fig. 4.12, has five main loops and SCADA system. The photograph of experimental test facility commissioned at NAL, Bangalore was shown in Fig. 4.11. Specifically, it consists of five loops. They are:

- i. Refrigerant Loop
- ii. Condenser Loop
- iii. Evaporator Loop
- iv. Super Heater Loop
- v. De-super heater Loop

Refrigerant R134a is circulated in the refrigerant loop to obtain different test conditions in the test heat exchanger. It is required to control the temperatures and

flow rates of the working fluids in the other loops. Super heater loop is introduced to ensure dry compression at the compressor inlet. De-super heater loop (cooling loop / heating) is provided before condenser to maintain the saturated conditions. The components and sub systems of the test facility are mounted on moveable platform and lifting screw jack assembly. The major components and sub systems of the test facility are variable speed reciprocating compressor, condenser, evaporator, cooling system, heating system, data acquisition & control system with instrumentation and digital display. Refrigerant R134a was used as refrigerant in this test facility.

Refrigerant R134a was circulated in one side of the test section. Water was used to heat liquid refrigerant in evaporator as well as to cool the refrigerant gas in the condenser. Water is circulated in the test core from the chillers units. Chillers will supply the water between 10 °C to 40 °C temperatures. Test facility consists of two separate chiller units for condenser and evaporator. Sampling ports are provided for easy charge/discharging of the refrigerant. Suitable evacuation and charging system is provided to charge and discharge the refrigerant. Seamless copper tubes are used as piping system in the test facility. The test facility is fully insulated to avoid heat loss to the environment. Leak detection sensor was installed in the test facility, which gives an alarm whenever there is a refrigerant leak noticed in the rig. Fig. 4.11 and Fig. 4.13 shows photograph the actual test facility designed and developed where as Fig. 4.14 shows the data acquisition system of the test facility.



Fig. 4.11: Photograph of Experimental Test Rig with Test Condenser

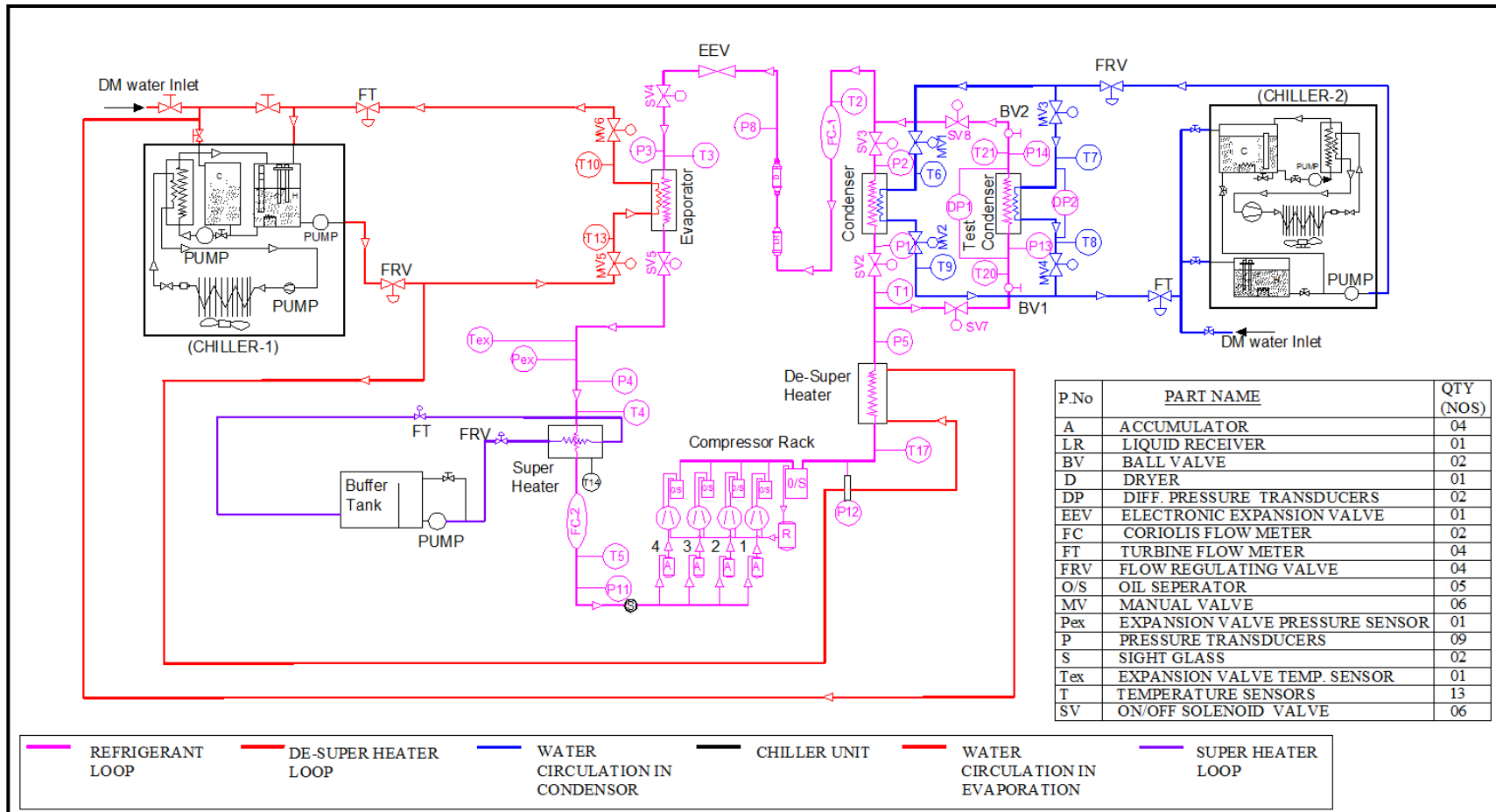


Fig. 4.12: Schematic Diagram of the Vapour Compression Refrigeration System Experimental Test Rig with Instrumentation

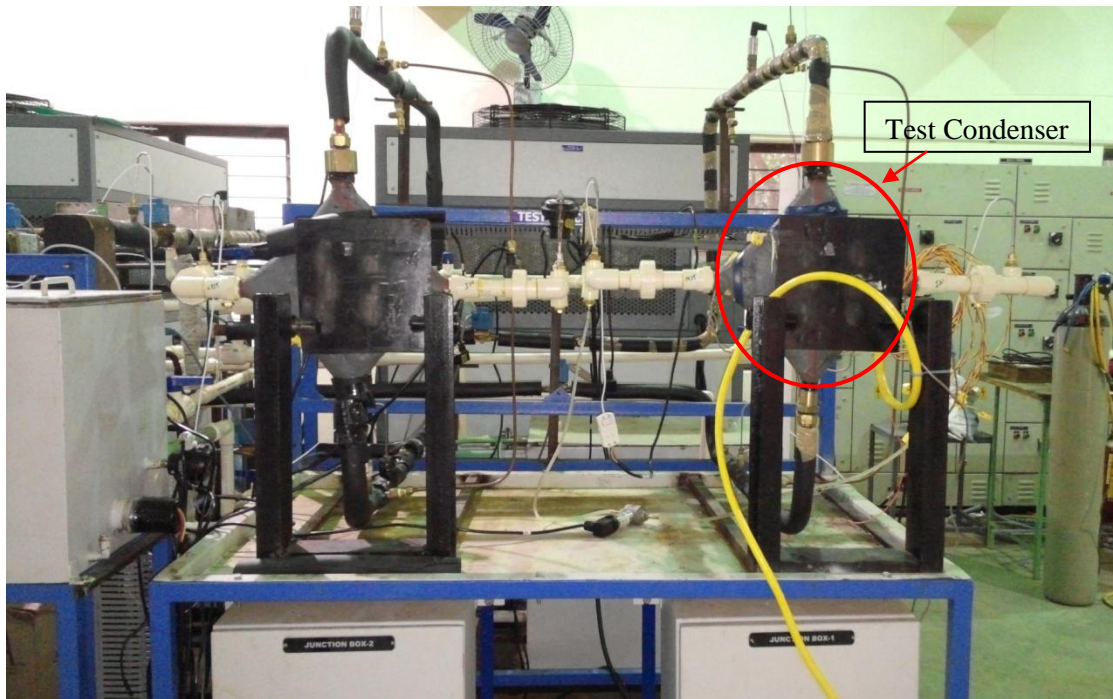


Fig. 4.13: Photograph of Experimental Test Rig with Test Condenser (Front View)



Fig. 4.14: Photograph of Test Rig-Data Acquisition System with Control Panel

4.4.1 Refrigerant loop

Refrigerant loop system employed in the test rig has been shown schematically in Fig. 4.15. The refrigerant loop contains compressors, accumulators, oil separators; de-super heater, test condenser (Brazed compact plate-fin heat exchanger), liquid receiver, filter drier, sight glasses, electronic expansion valve, evaporator, super heater and coriolis flow meter. It consists of semi hermitically sealed variable speed reciprocating compressor, condenser, expansion valve and evaporator. Based on the total flow requirement, four numbers of reciprocating compressors with variable frequency drive are connected in the refrigerant loop. The refrigerant used in the circuit is refrigerant R134a. These compressors with different capacity connected in a parallel to vary the flow rates and keeping pressure same at the delivery section. The oil separator provided in the refrigerant loop intercepts the oil mixed with compressed gas and returns it to the crankcase of the compressor thus assuring an efficient lubrication of its moving parts. Furthermore the oil separator maintains a high coefficient of condenser and evaporator performance by almost completely removing oil deposits from their exchange surfaces & limit accumulates of oil at sensitive system components. Separate oil separator for each compressor and a common oil separator are installed in the loop. Each compressor is provided with accumulators and gate valves or non return valves to avoid the backward flow. There are two sampling ports, one at the evaporator side and another at the condenser side. These ports are used to charge the system as well as discharge the system. Sampling port also used to collect the refrigerant for checking the purity of the refrigerant at stipulated periods. Solenoid valves are installed before and after condenser to bypass vapour refrigerant to the test heat exchanger mounted in the loop. Test bench is provided for easy mounting and removing of the test condenser in the test rig. Initially experiments were performed with condenser in the loop closing the solenoid valves in the test condenser side. Once the data stabilizes the solenoid valves in the condenser side closes and passes the refrigerant through test condenser.

The compressor rock was designed to control flow rate between 0.01 kg/s to 0.04 kg/s in steps of 0.005 kg/s using variable frequency drive. The refrigerant flow rates are controlled by using variable frequency drive. The flow rate was measured by a mass flow meter (Micro motion DN5) installed after the test condenser. Also,

refrigerant loop consists of lubricant oil management system. The details of selected compressor models and their operating ranges are shown in Table 4.5(a) and Table 4.5(b).

Table 4.5: Details of Operating Ranges of Compressors

a) At Condenser Temperature 20 °C and Evaporation Temperature -10 °C

S.No	Model No	Qty(No's)	Condenser Temperature 20 °C Evaporation Temperature -10 °C			
			Frequency(Hz) / Flow rate(kg/s)			
			30	35	50	65
1	2SB-34.07	1	0.0059	0.0069	0.009	0.012
2	2SB-38.2	1	0.008	0.009	0.0133	0.0174
3	2SB-55.4	2	0.0213	0.0248	0.0354	0.046

b) At Condenser Temperature 35.8 °C and Evaporation Temperature +20 °C

S.No	Model No	Qty(No's)	Condenser Temperature 35.8 °C Evaporation Temperature +20 °C			
			Frequency(Hz) / Flow rate(kg/s)			
			30	35	50	65
1	2SB-34.07	1	0.0194	0.0227	0.03242	0.0421
2	2SB-38.2	1	0.0249	0.0291	0.0415	0.054
3	2SB-55.4	2	0.0635	0.0741	0.105	0.1375

In compressor suction line accumulators are installed to prevent refrigerant liquid return to suction line to idled compressors. Oil separators are installed on the discharge line of an each compressor. The oil separator intercepts the oil mixed with compressed gas and returns it to the crankcase of the compressor thus assuring an efficient lubrication of its moving parts. The de-super heater installed in the downstream of compressor rock to control the inlet conditions of test condenser by water cooling system. After condensed, the liquid refrigerant flows back to the receiver.

The filter drier and collector tank is installed in the liquid line. The filter drier contains silica gel and absorbs traces of moisture present in the liquid refrigerant so that it does not enter the narrow cross-section of the expansion device causing moisture chocking by freezing. Further, it provides high water adsorption at low and high condensing temperatures, also at low and high degrees of humidity. The liquid line filter drier protect refrigeration system from moisture and solid particles.

Temperature and pressure sensors across the compressor, condenser, expansion valve and evaporator are provided for measurement temperature and pressure. The differential pressure sensors are provided across the condenser for measurement of differential pressure. Coriolis flow meter is installed in the circuit after evaporator and condenser to measure the vapour and liquid flow rates respectively. The system also fitted with sight glasses for physical verification of state of the refrigerant.

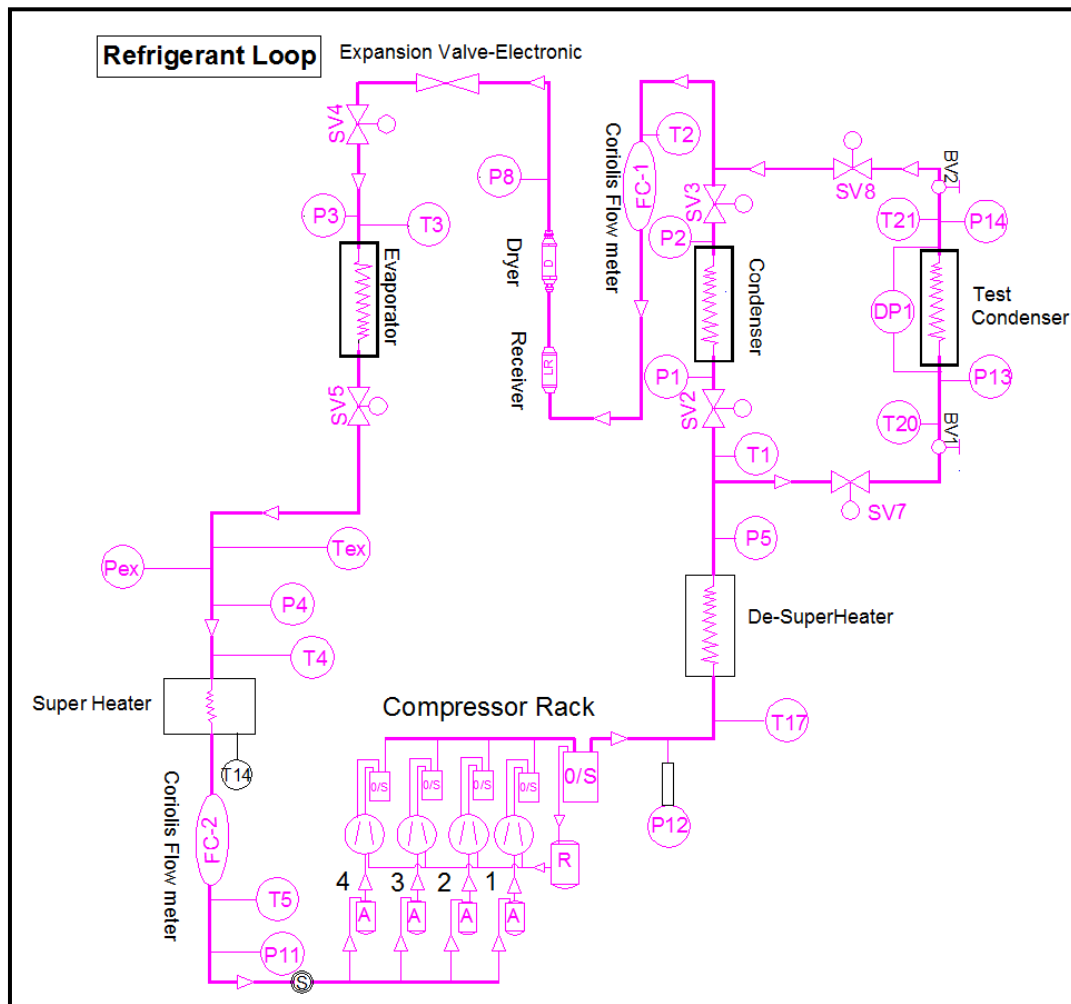


Fig. 4.15: Schematic Layout of Refrigerant Loop

4.4.2 Condenser loop

Condenser loop system employed in the test rig has been shown schematically in Fig. 4.16. The condenser cooling loop consists of Chiller unit (Tank with DM water, pump, flow control valve and shut off valves). Water is circulated to condense the refrigerant vapour in the condenser. The water mass flow rate can be varied from 0.1 to 0.8 kg/s in steps of 0.05 kg/s. The chiller unit and heater will control the inlet

water temperature to condenser from 10 °C to 40 °C. The Chiller unit consists of two tanks, cold water tank and hot water tank. Both the tanks are connected to the water pumps.

Cold water circuit consists of refrigeration system with compressor, condenser, expansion valve, and evaporator. R407 is used as a refrigerant in the chiller unit. Cold water pump sucks the water from cold water tank circulated through the chiller evaporator and gets cooled before supplied back to the tank. Temperature in cold water tank can be maintained up to 10 °C.

Hot water circuit consists of thermostat with heating system. The heaters heat the water in the tank to the desired temperatures and maintain the temperature. Temperature in hot water tank can be maintained up to 40 °C.

The water mass flow rate from the chiller unit to the condenser/test condenser can be varied from 0.1 to 0.8 kg/s in steps of 0.05kg/s. Both the tanks (cold water tank and hot water tank) are connected internally. The thermostat and heater will control the inlet water temperature to condenser/test condenser from 10 °C to 40 °C in steps 1 °C with an accuracy of ± 0.2 °C.

The cold water at desired temperature is circulated through water circuit of the condenser/test condenser. The water absorbs the heat from refrigerant R134a, which is circulating through refrigerant circuit of the condenser unit. The refrigerant becomes the liquid by rejecting heat to the cold water in the condenser and water gets heated by absorbing the heat from the refrigerant. Condenser circuit consists of solenoid valves to bypass the water flow to condenser/test condenser which is under test. It also consists of flow control valves and turbine flow meters to control water flow rate to the unit.

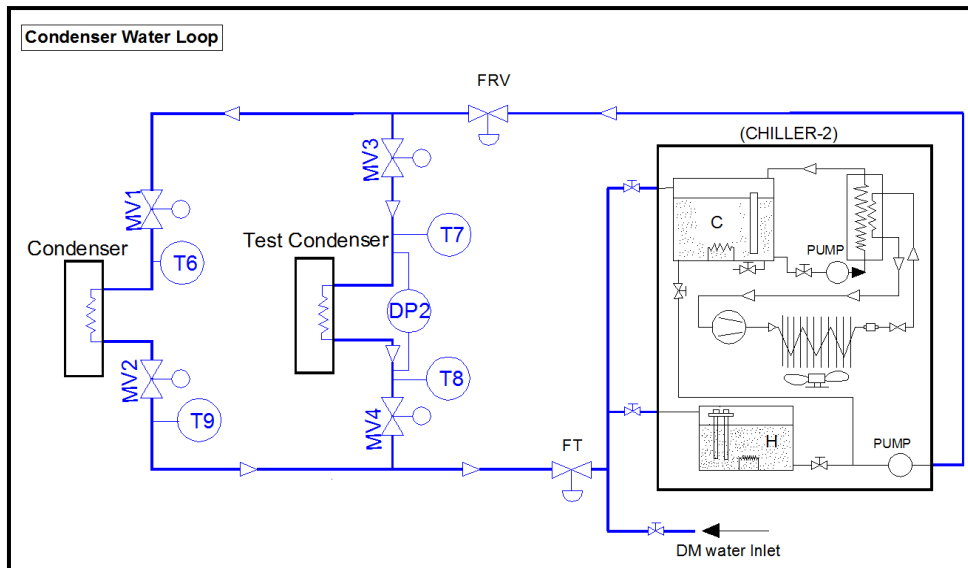


Fig. 4.16: Schematic Layout of Condenser Loop

4.4.3 De-super heater loop

In general the refrigerant vapour coming out of the compressor will be in super heated condition. To bring down the vapour to saturated a conditions at condenser inlet, de-super heater has been designed. De-super heater loop consists of plate heat exchanger, flow regulating valves, sight glass and instrumentation to measure temperature and flow rate. The schematic diagram of the de-super heater loop is shown in Fig. 4.17. Cold water is tapped from condenser chiller unit at a desired temperature and circulated through the water circuit of de-super heater plate heat exchanger. Water flow rate is regulated until the saturated conditions obtained at the inlet of the condenser. De-super heater loop consist of flow regulating valve and turbine flow meter to control the flow to tank.

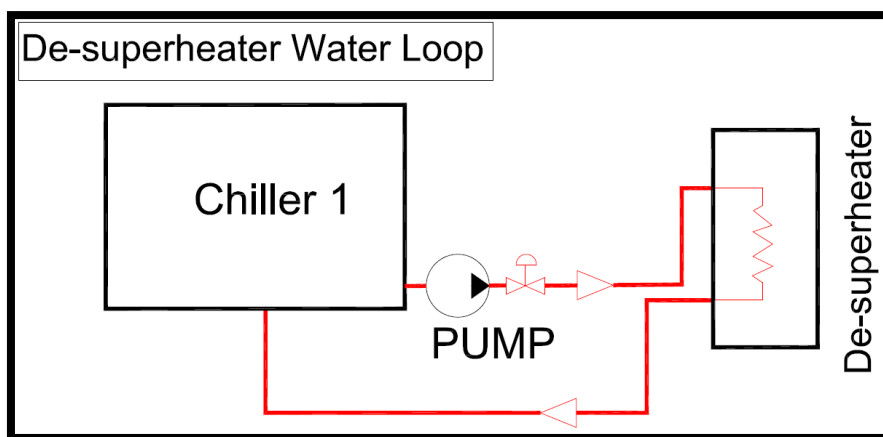


Fig. 4.17: Schematic Layout of De-Super Heater Loop

4.4.4 Evaporator loop

Evaporator loop system employed in the test rig is shown schematically in Fig. 4.18. The evaporation loop consists of chiller unit (Water tank with water thermostat with heater, pump, flow control valve and shut off valves). Hot water is circulated to evaporate the liquid refrigerant in the evaporator. The chiller unit consists of two tanks, cold water tank and hot water tank. Both the tanks are connected to the water pumps.

Cold water circuit consists of refrigeration system with compressor, condenser, expansion valve, and evaporator. R407 is used as a refrigerant in the chiller unit. Cold water pump sucks the water from cold water tank circulated through the chiller evaporator and gets cooled before supplied back to the tank. Temperature in cold water tank can be maintained up to 10 °C.

Hot water circuit consists of thermostat with heater system. The heaters heat the water in the tank to the desired temperatures and maintain the temperature. Temperature in hot water tank can be maintained up to 40 °C.

The water mass flow rate from the chiller unit to the evaporator/test evaporator can be varied from 0.1 to 0.8 kg/s in steps of 0.05 kg/s. Both the tanks (cold water tank and hot water tank) are inter connected. The thermostat & heater will control the inlet water temperature to evaporator from 5 °C to 40 °C in steps 1 °C with an accuracy of ± 0.2 °C.

The hot water at desired temperature is circulated through water circuit of the evaporator. The water rejects the heat to the refrigerant R134a, which is circulating through refrigerant circuit of the evaporator. The refrigerant becomes the vapour by absorbing heat from hot water in the evaporator and water gets cooled by rejecting the heat to refrigerant. The cooled water is supplied back to the water tank. Evaporator circuit also consists of flow control valves and turbine flow meters to control water flow rate to the unit.

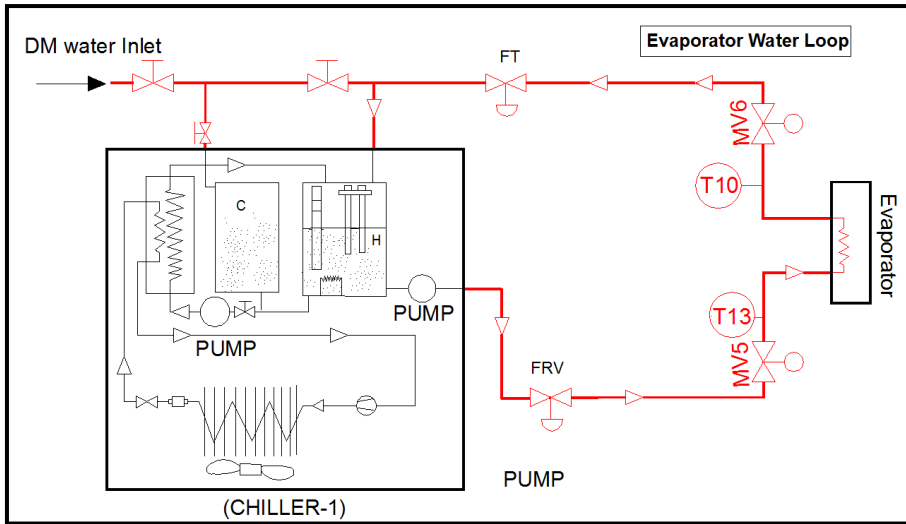


Fig. 4.18: Schematic Layout of Evaporator Loop

4.4.5 Super heater loop

The R134a coming out of the evaporator should be in fully vapour form to safeguard the compressor. In case the refrigerant is not in fully vapour form, it will be converted to fully vapour form in the super heater loop before entering into compressor. The super heater loop consists of 3kW heating system, buffer tank, pump, heat exchanger, shut off valves, pressure, flow and temperature sensors. The circuit diagram of the super heater loop is shown in Fig. 4.19. Water is heated up in the heaters to a desired temperature and circulated to super heater tank. Any traces of liquid refrigerant present in the vapour refrigerant coming out of the evaporator is converted to vapour before entering into the compressor system. Super heater loop consist of flow regulating valve and turbine flow meter to control the flow to tank.

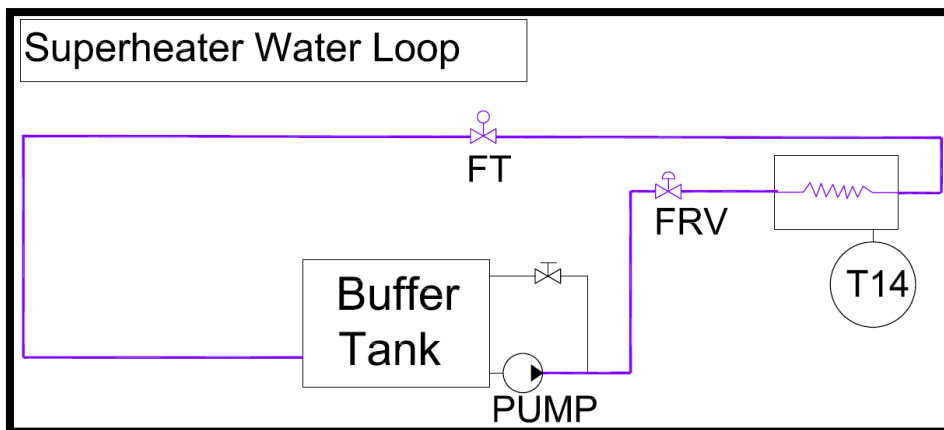


Fig. 4.19: Schematic Layout of Super Heater Loop

4.4.6 Details of major test rig components

The major components used in the VCRS test facility are explained below:

4.4.6.1 Compressor



Fig. 4.20: Photograph of Reciprocating Compressor

Compressor is one of the four essential parts of the vapour compression refrigeration system. The photograph of the reciprocating compressor is shown in Fig.4.20. The compressor operates in a cycle continuously, raising the refrigerant vapour pressure to the condenser pressure (corresponding to condensing temperature). Semi hermitically variable speed reciprocating compressor is used in the test facility. This type of compressor increases the vapour pressure by reducing the volume through the application of work. There is definite quantity of vapour delivered for each rotation of the crank shaft. Total four reciprocating compressors with different capacities are used in the test facility. The capacity of the compressor can vary by changing or controlling the speed of the each compressor.

4.4.6.2 Evaporator and condenser



Fig. 4.21: Photograph of Commercial Plate Heat Exchanger

Evaporator is one of the refrigeration unit in which the refrigerant absorbs heat from the space (object) by changing its phase from liquid to vapour. Condenser is also

component of refrigeration circuit in which it rejects the heat and condenses the refrigerant to become liquid state. The photograph of commercial plate heat exchanger is shown in Fig.4.21. Plate heat exchanger is a heat exchanger constructed using metal plates to transfer heat between two fluids. It consists of a series of thin, corrugated plates. These plates are welded or brazed together depending on the application of the heat exchanger. The plates are compressed together in a rigid frame to form an arrangement of parallel flow channels with alternating hot and cold fluids. The technical details of the evaporator and condenser are given in the Table 4.6.

Table 4.6: Specification of Evaporator and Condenser Heat Exchangers

	Evaporator	Condenser
Make	Danfoss	Danfoss
Model no.	PHE B3-052-60-3.0-HQ	PHE B3-030-70-3.0-HQ
Type	Plate heat exchanger	Plate heat exchanger
Capacity	30 kW	30 kW
Design Pressure	45 bar	45 bar

4.4.6.3 Electronic expansion valve



Fig. 4.22: Photograph of Electronic Expansion Valve

An expansion device is one of the main components of the VCRS test facility. It reduces the pressure of the liquid refrigerant and controls the flow of refrigerant from high pressure side to the low pressure side of the system. Electronic Expansion Valve (EEV) shown in Fig.4.22 has been used in the test facility to control the flow of refrigerant entering the evaporator. EEV has chosen to open and close automatically

without aid of an external device. It maintains constant refrigerant pressure in the evaporator. The specification of the EEV is given Table 4.7

Table 4.7: Specification of Expansion Valve

Make	CAREL
Model no.	E ² V-24
Capacity	20 kW
Flow rate	0.1 kg/s
Maximum working pressure	40 bar
Temperature range	-40°C to 65°C

4.4.6.4 Oil separators

The oil separator intercepts the oil mixed with compressed gas and returns it to the crankcase of the compressor thus assuring an efficient lubrication of its moving parts. The oil separator shown in Fig.4.23 maintains a high coefficient of condenser and evaporator performance by almost completely removing oil deposits from their exchange surfaces.



Fig. 4.23: Photograph of Oil Separator

They work by having the compressed mass flow enter into a larger separator chamber, which lowers the velocity. The atomized oil droplets collect on the impingement screen surface. As the oil droplets agglomerate, they fall to the bottom of the separator oil reservoir. Appropriate stainless steel metallic screens placed on the inlet and outlet, rapidly reduce gas speed and create the conditions required for the separation of the oil from the refrigerant. A float operated needle valve set on the bottom of the vessel to return the oil into the crankcase of compressor.

The oil separator is installed in the discharge line between the compressor and the condenser mounted securely in a vertical position as close to the compressor. Each compressor has a separate oil separator apart from common oil separator.

4.4.6.5 Chiller units

The test facility consists of chiller unit, which is assembly of water tank with water thermostat with heater, pump, flow control valve and shut off valves. The photograph of chiller unit is shown in Fig.4.24. The chiller unit consists of two tanks, cold water tank and hot water tank. Both the tanks are connected to the water pumps.

Cold water circuit consists of refrigeration system with compressor, condenser, expansion valve, and evaporator. R407 is used as a refrigerant in the chiller unit. Cold water pump sucks the water from cold water tank circulated through the chiller evaporator and gets cooled before supplied back to the tank. Temperature in cold water tank can be maintained up to 10°C.



Fig. 4.24: Photograph of Chiller Unit

Hot water circuit consists of thermostat with heater system. The heaters heat the water in the tank to the desired temperatures and maintain the temperature. Hot water pump sucks the water from hot water tank and supplies hot water to the evaporator. Temperature in hot water tank can be maintained up to 40°C. Both hot water tank and cold water tank interconnected through pipe line solenoid valve. The specification of chiller unit is given Table 4.8.

Table 4.8: Specification of Chiller Unit

Make	Werner-finley
Model no.	6TC10WC1X
Capacity	6 TR
Temperature range	10 °C - 40 °C
Flow rate	75 LPM

4.4.6.6 Solenoid valves



Fig. 4.25: Photograph of Solenoid Valve

Electromechanically operated solenoid valves are used in the test facility to bypass the refrigerant and water flow rates between condenser and test condenser unit which is under test is shown in Fig.4.25. The valve is controlled by an electric current through a solenoid. Two port type solenoid valves are used.

4.4.6.7 Piping

Seamless copper tubes are used in the test facility. Sizing of the pipe lines is done based on the ASTM B-88 standard. The equivalent lengths of suction line, discharge line and liquid line are calculated after considering the effect of reducing tee, straight tee, elbow, solenoid valve, flow meter, sight glass, pressure sensor etc. All the pipe lines are insulated to avoid the heat losses.

4.4.6.8 Evacuation and refrigerant charging system



Fig. 4.26: Photograph of Test Rig Evacuation and Refrigerant Charging Unit

A separate evacuation and gas charging unit procured to evacuate the refrigerant circuit of test rig and charge the refrigerant gas when ever is required. The photograph of evacuation and refrigerant charging unit is shown in Fig.4.26. It is a movable unit consists of vacuum pump mounted on a wheels. Charging can be done in two ways liquid charging or gas charging. The test facility have both charging ports. Generally before changing test condenser the gas is evacuated fully and stored in gas cylinder. After changing the test condenser the gas is charged using the same unit.

4.5 Instrumentation and Data Acquisition System

The instrumentation sub system comprises of instruments for measurement of flow rate, temperature and pressure and an electronic data acquisition system.

4.5.1 Instrumentation

The instrumentation is very important for any experimentation. The result of experiments depends on their accuracy and deviations of instrumentation. The detailed specification of instruments used in the experimental test rig is discussed in following paragraphs.

4.5.1.1 Coriolis flow meter



Fig. 4.27: Photograph of Coriolis Flow Meter

Refrigerant flow rate is probably the most important quantity to be measured. It is desirable to use a flow meter that measures the total flow rate rather than the velocity at a particular point. Coriolis flow found suitable for accurate measurement of flow rate and used in the test facility. The photograph of coriolis flow meter is shown in Fig.4.27. Two coriolis flow meters are installed in the test rig, one is at liquid line, after the condenser to measure liquid flow rate and another is at vapour

line, after the evaporator to measure the vapour flow rate. The details of the coriolis flow meter are given in Table 4.9.

Table 4.9: Specification of Coriolis Flow Meter

Make	Micro-Motion
Model no.	CMFS015
Electric supply	18 to 100 VDC and 85 to 265 VAC; self switching
Flow rate	0.003 to 0.09 kg/s
Accuracy	$\pm 0.05\%$ of rate for liquid, $\pm 0.35\%$ of rate for gas
Working pressure	40 bar
Working temperature	-15 to 70 °C

4.5.1.2 Turbine flow meter



Fig. 4.28: Photograph of Turbine Flow Meter

Turbine flow meters used in the test rig is shown in Fig.4.28. It is used to measure the water flow rate. Four turbine flow meters are installed in the test rig; they are at evaporator line, condenser line, super heater line and de-super heater line. The technical detail of the turbine flow meter is provided in Table 4.10.

Table 4.10: Specification of Turbine Flow Meter

Make	Rockwin
Model no.	TFM1015
Flow rate	6.6-66 LPM
Max temp	250 °C
Max Pressure	250 kg/ cm ²
Linearity	$\pm 0.23\%$

4.5.1.3 Pressure transducers

Pressure measurement in the refrigeration experiments very important parameter for maintaining accurate conditions at the inlet and outlet of the evaporator.

Pressure transducers have been employed to measure the pressure of refrigerant and water in the circuits at an entry and exits of test condenser, evaporator, condenser, expansion valve and compressor.



Fig. 4.29: Photograph of Pressure Transducer

The test facility has extensively instrumented with pressure sensors to measure the all data points. Differential pressure transducers are also installed in the test rig both in refrigerant circuit and water circuit to measure the pressure drops across the test condenser. The photograph of pressure transducer and differential pressure transducer is shown in Fig.4.29 and Fig.4.30 respectively.



Fig. 4.30: Photograph of Differential Pressure Transducer

The details of the pressure transducers and differential pressure transducers provided in the test facility are given in Table 4.11 and Table 4.12 respectively.

Table 4.11: Specification of Pressure Transducer

Make	Measurement specialties
Model no.	M5100
Pressure range	0-20bars
Accuracy	$\pm 0.25\%$
Stability	$\pm 1\%$ FS/year

Table 4.12: Specification of Differential Pressure Transducer

Make	Sesocon
Model no.	251-01

Capacity	0-5PSI
Electric supply	12-36 VDC
Accuracy	±0.25% F.S

4.5.1.4 Temperature sensors with digital indicator

The accuracy of any heat transfer study depends on that of the temperature measurement. Platinum resistance RTD's are employed to measure the temperatures of refrigerant and water at an inlet and exits of test condenser, evaporator, condenser, expansion valve, compressors, super heater side and de super heater side. The test facility has extensively instrumented with temperature sensors to measure the all data points. The details of the temperature sensors provided in the test facility are given in Table 4.13.

Table 4.13: Specification of Temperature Transducers

Make	RTD products, UK
Model no.	PT-100
Temperature range	-100 to +200°C
Accuracy	± 0.55 °C
Diameter	3 mm
Sheath length	3 mm
Power supply	230VAC±10%, 50Hz

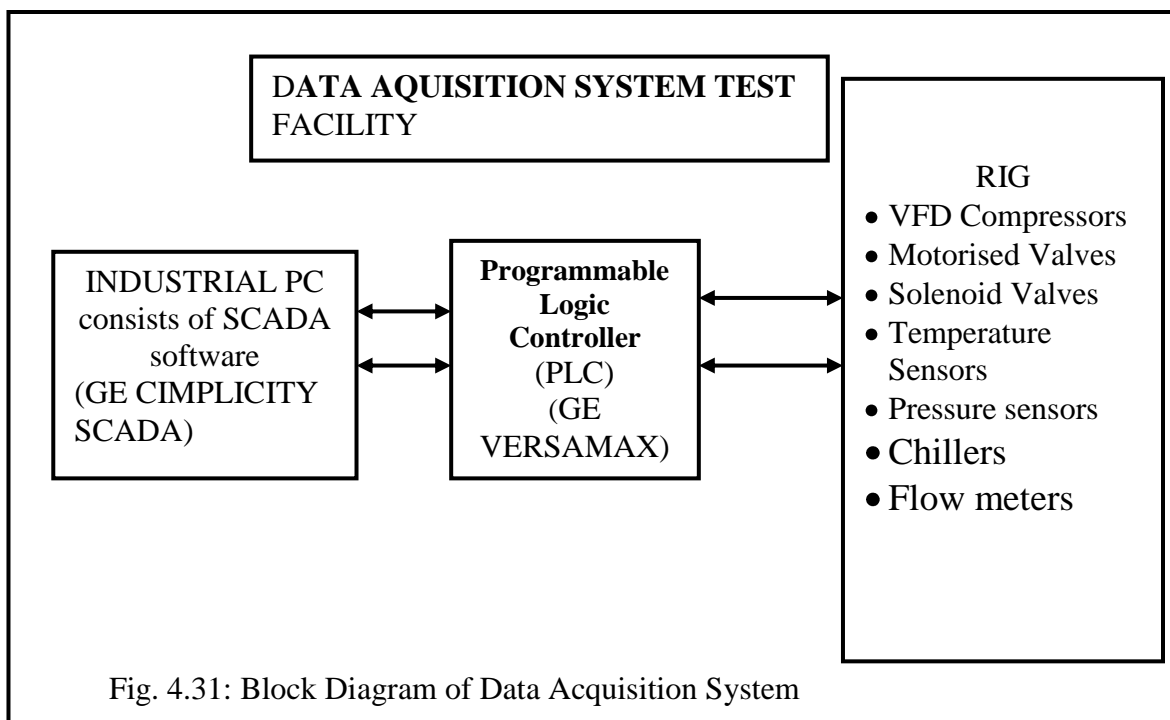
4.5.2 Data acquisition system

Pressure, differential pressure, temperature and flow sensors are connected to a PC through PLC and SCADA system. The vapour compression refrigeration test rig consists of various components like variable frequency drive (VFD) control compressors, motorized valves, solenoid valves, flow regulation valves and chillers which are controlled by SCADA and also temperature sensors, pressure sensors, thermocouples and flow meters that are monitored by SCADA for its smooth functionality and data gathering. These components need to be controlled in order to obtain the satisfying results which are carried out with the help of SCADA software. Block diagram of DAS of VCRS is shown in Fig.4.31. The data acquisition system consists of 64 analog, 32 digital input modules and 64 digital, 16 analog output modules of GE made. All this I/O modules are connected to a GE VERSAMAX PLC which contains 2 No's of RS484 & RS232 communication ports. The PLC is

connected to an industrial graded PC which is having GE CIMPLICITY SCADA software (Ver. 8.2) through RS 232 cable.

The variations occurring in different components of the test rig is controlled by the PLC that stores the values for further modifications, this information is sensed by the SCADA software that regulates the movement of the valves, all the pressure sensors (gauge and differential), temperature sensors, chillers temperature settings, test core thermocouples and motorised and solenoid flow regulation valves are connected to a PLC in respective modules through line resistance compensation cable. The sensor values / readings can be recorded / monitored with the help of SCADA. Pressure, temperature and flow rate of refrigerant and water in condenser and evaporator loop can be varied using SCADA that is, by varying the valve positions and by switching on/off the compressors.

The SCADA system is programmed in such a way as to control valves position, data monitor and logging, report generation, trend analysis, graphical analysis of data and process flow diagrams using ladder programming technique.



4.5.2.1 Display details

A) Display on main panel (digital meters)

Rack mounting type control with following displays.

- Pressure reading display, inlet pressure (bar) and diff. pressure (mbar)
- Flow rate display
- Temperature display
- Input voltmeter with selector switch
- Ammeter with selector switch
- 3-phase supply indications lamp

B) Facility on operator's panel

- Emergency (push button)
- Mains ON/OFF indications
- Alarm for gas leak detection

C) Electrical control details

- It have MCCB as incomer, separate MCB for motor, MCB for control, circuit etc. with twice the capacity of load.
- Provided double earthing interconnections with copper wire, earth-bus with all terminations and connections.
- A four core insulated copper cable for incoming power connection is provided.
- Water thermostats with heater are controlled by PID controller.

D) Electrical control panel

Control panel comprises of:

- Main power isolator, pumps & compressor on /off switches, mains indication, fuse units.
- Digital indication for pressures of upstream & downstream refrigerant line.
- Digital indication for temperatures of upstream & downstream refrigerant line.
- Digital indication for flow of upstream and downstream refrigerant line.

- Digital indication for pressures of upstream and downstream water line.
- Digital indication for temperatures of upstream and downstream water line.
- Digital indication for flow of upstream and downstream water line.

4.5.2.2 Electrical system

The MCC panel is intended to control the feeders listed below both in local and remote mode.

- Super heater feeder : 3 kW
- Water circulation pump : 0.37 kW
- Compressor 1 : 1.5 kW (VFD Control)
- Compressor 2 : 2.2 kW (VFD Control)
- Compressor 3 : 3.7 kW (VFD Control)
- DM water feeder 1 : 15 kW
- DM water feeder 2 : 15 kW

4.6 Calibration of Sensors

The following sensors are calibrated at National Aerospace Laboratory as per the applicable standards.

a) Temperature sensors

- Resistance temperature detectors (RTD's)
- Thermocouples

b) Pressure sensors

- Absolute and differential pressure sensors

c) Flow meters

- Coriolis and turbine flow meters

The details of sensors calibration and their certificates are provided in Appendix-II.

4.7 Validation of Experimental Test Rig

In order to assess the quality of results and to enhance the confidence on data, it was felt necessary to characterize with a known two phase condensation heat transfer coefficient and frictional pressure drop. However, a plate heat exchanger with specifications exactly matching those of the plates described in literature was not

available. The testing was carried out with industrial brazed PHE in condenser loop to validate the test facility. During operation, the vapour refrigerant R134a coming out from a compressor rack condenses in the condenser and the liquid refrigerant flows through coriolis flow meter, collector tank and filter dryer. The quality of R134a at the condenser inlet was kept at desired value by adjusting the temperature and flow rate of DM water in de-Super heater. The liquid refrigerant then passes through evaporator after expansion in the electronic expansion valve. Any change of the system variables will lead to fluctuations in the temperature, pressure and flow. The heat balance test is performed in the test condenser and evaporator after the system reaching steady state, a deviation to the extent of 5% was considered acceptable, and measured data within the range are considered for further calculation. The thermal properties of the R134a were taken from thermo-physical properties of refrigerants (ASHRAE Fundamental hand book). The experimental data obtained were validated with empirical correlations given by Giovanni (2008 & 2010) and Nusselt (1916) for plate heat exchangers. The results are found in good agreement in these comparisons.

4.7.1 Comparison with open literature

The two phase analytical heat transfer coefficients and frictional pressure drop for the plate heat exchangers are already well established. A commercial brazed plate heat exchanger has been analyzed for a saturation temperature of 36 °C. Most of the authors like Giovanni (2008 & 2010), Yan et al. (1999) and Amir Jokar et al. (2006) who did extensive experimental work on plate heat exchangers followed the same methodology. For the validation of the test rig, experiments were conducted on brazed plate fin heat exchanger at condensation saturated temperature 36 °C as per the methodology followed by the earlier authors [Giovanni (2008 & 2010), Yan et al. (1999) and Amir Jokar et al. (2006)]. The geometric parameters of plate heat exchanger are given in Table 4.14.

Table 4.14: Geometric Parameters of Plate Heat Exchanger

Geometrical characteristics of the condenser	Giovanni. A. Longo	Experimental Rig
Fluid flow plate length , (mm)	278.0	269.0
Plate width, (mm)	72.0	95.0

Area of the plate, A(m ²)	0.02	0.03
Enlargement factor, Φ	1.24	1.26
Corrugation type	Herringbone	Herringbone
Angle of the corrugation, ($^{\circ}$)	65	65
Corrugation amplitude, (mm)	2.0	2.0
Corrugation pitch, (mm)	8.0	8.0
Number of plates	10	70
Number of plates effective in heat transfer	8	68

The experimental results of plate heat exchanger are compared with Giovanni A Longo (2008) and Nusselt (1916) results as shown in Fig. 4.32 and Fig. 4.33 for heat transfer coefficient and frictional pressure drop respectively. Experimental results are in well accordance with the analytical results given by Giovanni A Longo (2008) for the low mass flux region and the variations are found to be about 8% in heat transfer coefficient and 11% in frictional pressure drop values. Giving exact reasons for variation of these factors may not be possible due to involvement of so many parameters such as manufacturing aspects, testing conditions and uncertainties in measurements. The empirical formulae used for calculation of two phase heat transfer and frictional pressure drop are provided in Table 4.15.

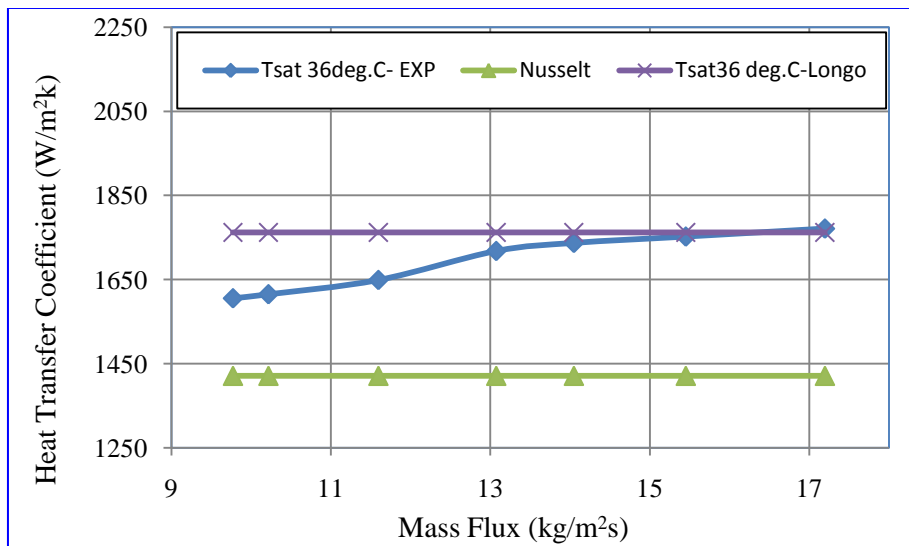


Fig. 4.32: Validation of Experimental Results of Mass Flux with Two Phase Condensation Heat Transfer Coefficient

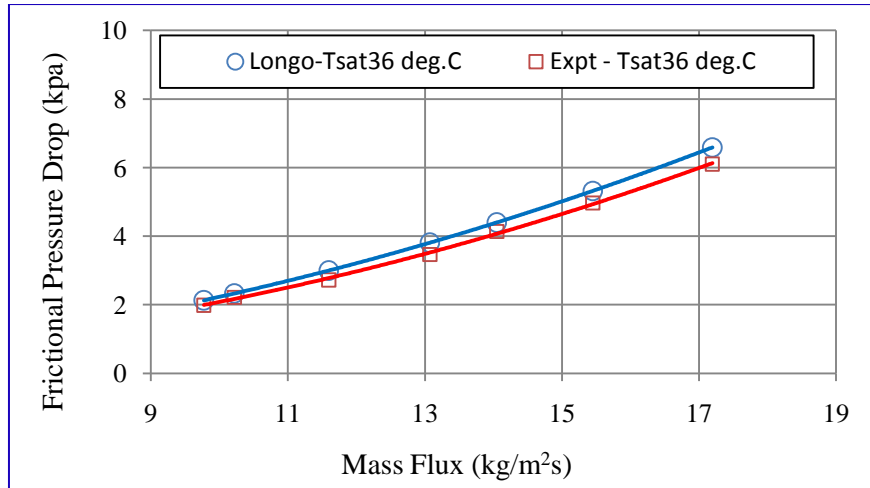


Fig. 4.33: Validation of Experimental Results of Mass Flux with Two Phase Condensation Frictional Pressure Drop

Table 4.15: Tested Empirical Correlations

Researcher	Correlation	Remarks
Nusselt	$h_{\text{Nusselt}} = 0.943 \left[\frac{\lambda_L^3 \rho_L^2 g \Delta J_{\text{LG}}}{\mu_L \Delta T L} \right]^{\frac{1}{4}}$	Valid for gravity controlled laminar film condensation inside tube
Akers	$h_{\text{Akers}} = 5.03 \left(\frac{\lambda_L}{D_h} \right) \text{Re}_{\text{eq}}^{\frac{1}{3}} \text{Pr}_L^{\frac{1}{3}}$	Valid for forced convection condensation inside tube
Giovanni A.Longo	$h_{r,\text{ave}} = \phi h_{\text{Nusselt}}$ $\phi = \frac{\text{Actual area of plates}}{\text{Projected area of plates}}$ $h_{r,\text{ave}} = \frac{1}{S} \int_0^S \phi h_{\text{akers}} \, dS$ <p>S= Nominal heat transfer area</p>	<p>Valid for gravity controlled laminar film condensation inside plate heat exchanger</p> <p>Valid for forced convection condensation inside Plate heat exchanger</p>

CHAPTER 5

EXPERIMENTAL PROCEDURE AND DATA REDUCTION

Commonly employed experimental techniques for measuring heat transfer and frictional pressure drop characteristics of heat transfer surfaces are the steady state and the transient methods. While the transient techniques are best suited for regenerative type heat exchangers, the steady state technique is ideal for recuperative heat exchangers (Shah and Zhou, 1997). Indranil Ghosh (2004) has used the steady state analysis for generation of colburn j factor and fanning friction factor for brazed compact plate fin heat exchangers using air medium by experimental method. The steady state test method given by Kays and London (1984) has been adopted to study characteristics of serrated fin heat transfer surfaces.

5.1 Measurement Principle

In the steady state method, a cross flow heat exchanger is employed as test heat exchanger. The schematic of a heat exchanger test set up shown in Fig.5.1.

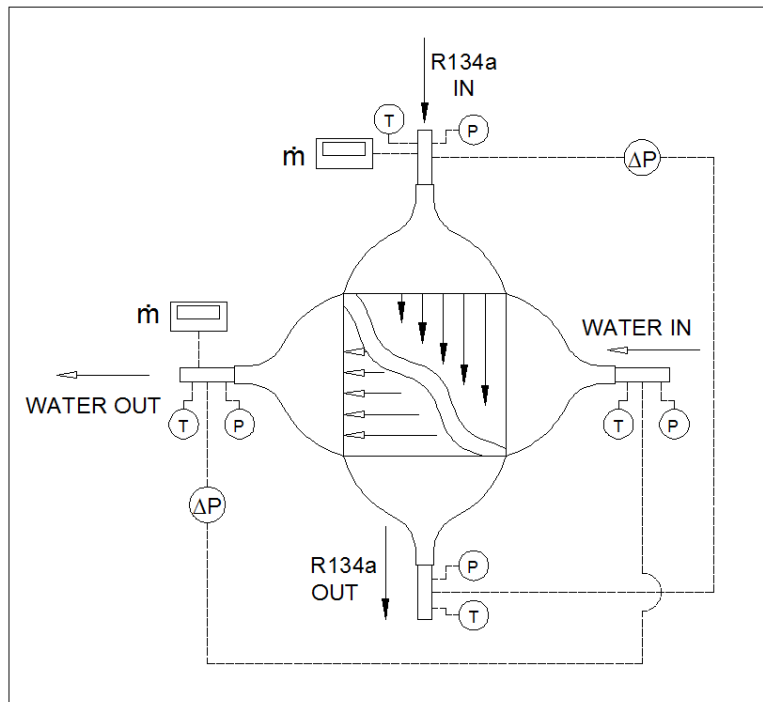


Fig. 5.1: Schematic of Test Condenser

One layer of the cross flow test condenser is made of the fin surface to be characterized. The fluid flowing over this surface should be one which is likely to be used in service. The two phase condensation experimental results can be used for any other serrated fin surfaces. For the second side of the cross flow heat exchanger, the choice of heat transfer surface is not stringent. In a steady state experiment, measurement of temperature, pressure, differential pressure and mass flow rates in the two sides provides the required information to develop the required correlations.

5.2 Experimental Procedure

The experimental test facility is established, to study the condensation of R134a in different types of serrated fins used in compact plate fin heat exchangers. The condenser and evaporator loops are capable of supplying DM water flow at a constant temperature in the range of 5 °C to 60 °C with stability within ± 0.5 k. In order to obtain different conditions of R134a in the test heat exchanger, it is required to control the temperature and flow rate of the working fluids in the other loops.

Refrigerant loop is a basic vapour compression refrigeration system, consisting of four parallel semi hermitically sealed variable speed reciprocating compressors having different capacity, test condenser, condenser, electronic expansion valve and evaporator. The variable speed reciprocating compressor rack is designed to control the flow rate between 0.005 kg/s to 0.06 kg/s in steps of 0.005 kg/s using variable frequency drive. The flow rate was measured by a mass flow meter (Micro motion DN4) installed after the test condenser.

The de-super heater installed in the downstream of compressor rack, controls the inlet conditions to test condenser by water cooling system. After condenser, the liquid refrigerant flows back to the receiver. The filter drier provides high water adsorption at low and high condensing temperatures, as well as at low and high degrees of humidity. The liquid line filter drier protects refrigeration system from moisture and solid particles. Coriolis flow meter is installed in the circuit after evaporator and after condenser to measure the refrigerant flow rate. The system also has sight glasses for physical verification of state of the refrigerant R134a. The standard brazed plate heat exchanger is installed in the main circuit for calibration of

test rig. After attaining the required conditions the condenser is bypassed by the test heat exchanger which is installed as a separate test section. This test condenser provides a water circuit to supply the cooling fluid, where the water flow rate can be varied between 0.08 kg/s to 0.7 kg/s. The pressure transducers and temperature sensors are located at the entry and exit of the Test Condenser.

In each test the system pressure is maintained at a specified level by adjusting expansion valve and also by adjusting the DM water temperature and its flow rate. The vapour quality of R134a at the entry of the test section was kept at near to one by controlling the temperature and water flow rates for the de-super heater. Finally the heat transfer rate between the test sections can be varied by changing the temperature and flow rate in the water loop for the test condenser. Any change of the system variables will lead to fluctuations in the temperature and pressure of the flow. It takes about 30 to 120 minutes to reach a statistically steady state at which variations of the time-average inlet and outlet temperatures are less than 0.1 °C and variations of the pressure and heat flux are within 2% and 5%, respectively. Observations are noted at steady state condition for inlet temperature range of 32 °C to 44 °C and refrigerant mass flow rate range of 0.005 kg/s to 0.04 kg/s. Procedure to take observations with experimental set up is pictorially presented in the Fig.5.2. Then the data acquisition is initiated to scan all data channels 20 samples per second and logged data for 30 seconds. The mean values of the data for each channel are obtained to calculate the two phase condensation heat transfer coefficient and frictional pressure drop. Additionally, the flow rate of water in the test condenser maintained high enough to have turbulent flow in the water side so that the associated single phase heat transfer in it high enough for balancing the condensation heat transfer in the refrigerant side.

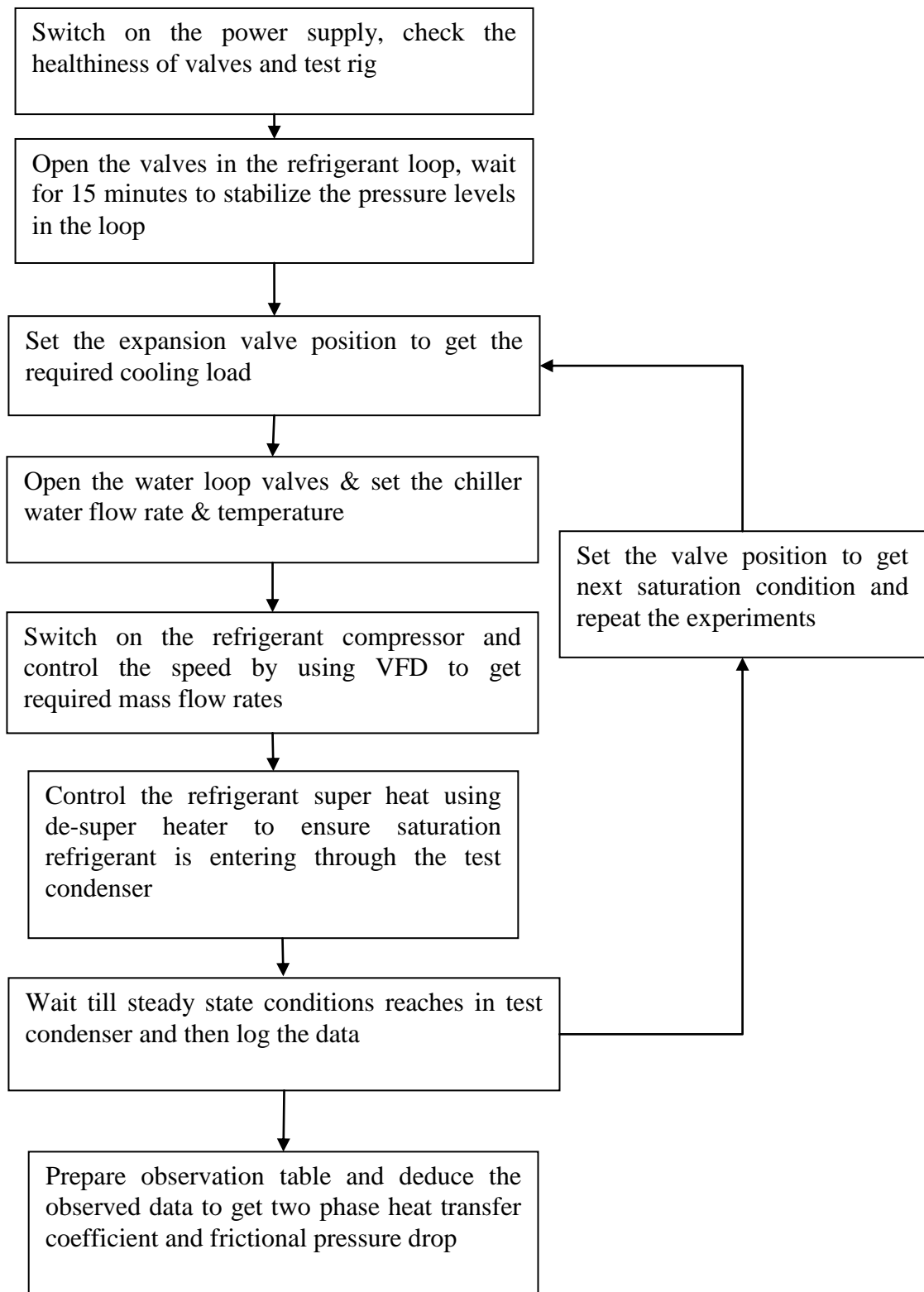


Fig.5.2: Chart Showing the Procedure to take Observations with Experimental Set Up

Developed experimental setup is first tested with industrial plate heat exchanger and the results are compared with available empirical correlation such as Akers (1959) and Longo (2008) equations. Testing with R134a is done to validate the developed experimental set up using plate heat exchanger. Then four different brazed plate fin heat exchangers with serrated fins are tested one after the other for different saturation temperatures. Observations are noted at steady state condition for R134a refrigerant saturated inlet temperature range of 32 °C to 44 °C in steps of 2 °C. For each R134a refrigerant saturated condition the refrigerant mass flow rates are changed from 0.01 kg/s to 0.04 kg/s in steps of 0.005 kg/s. The refrigerant flow rates are achieved by controlling the reciprocating compressors using variable frequency drive. Also, observations are noted for super heated refrigerant vapour for different mass flow rates.

The test condenser was installed in the test rig as per the circuit, which is shown in the Fig. 5.3. The shut off valves before and after the refrigerant circuit condenser are closed to avoid refrigerant flow to the refrigerant circuit condenser. The refrigerant flow was bypassed before refrigerant loop condenser to the test condenser, which is under test. The operating procedure to log the required data with experimental set up is shown in Fig.5.1. Observations are noted and the data is used for further calculation and analysis.

The refrigerant R134a coming out of the evaporator shall be fully vapour form, in case the fluid is not in fully vapour form, the same should be converted to fully vapour form in the super heater. Then the vapour refrigerant R134a, coming out from super heater is compressed in the compressor of the refrigerant. Then the refrigerant R134a in vapour form at high pressure will enter in to the condenser at different heat flux and mass flux. The R134a fluid will reject heat (latent heat) to the condenser loop (water circuit) and comes out as liquid with high pressure. The flow rate on refrigerant circuit was monitored by a coriolis mass flow meter. Sight glasses are provided in refrigerant circuit to ensure the fluid condition at each stage.

The test section loop consists of a water pump, a thermostat for heating, chiller unit for cooling, turbine flow meter and a sight glass. Temperature sensors one each at inlet and outlet of R134a circuit and the water stream of test section and one at inlet of the expansion valve, condenser, and one in super heater outlet side are installed for

measurement. Pressure drops of both circuits are measured using differential pressure transducers for the test unit. All the sensors are connected through a Siemens based data converter to the computer for data acquisition. The operation of the compressors and the electronic expansion valve also carried out through the SCADA program.

5.2.1 Thermodynamic analysis

Refrigerant R134a is compressed from pressure P_{11} (1.76 bar), Temperature T_5 (34.5 °C) to pressure P_{12} (9.65 bar), Temperature T_{17} (66.5 °C) with the mass flow rate m_r (0.0203889 kg/s). The compressors have the provision for changing the mass flow rates from 0.01 to 0.04 kg/s in steps of 0.005 kg/s. The refrigerant coming-out from compressor is in the form of super-heated vapour. To ensure the saturated conditions entry to the test condenser, super-heated load from temperature T_{17} to T_1 is rejected to the water media in the de-super heater as shown in Fig. 5.3.

Then the saturated refrigerant R134a in vapour form will pass into the condenser at T_1 and P_1 and at different mass flow rates (from 0.01 to 0.04 kg/s in steps of 0.005kg/s). The working fluid will reject heat (latent heat) of to the Condenser water loop and comes out as liquid with T_2 and P_2 (38.02 °C and 9.647 bar). The outlet pressure and temperature of test condenser, mass flow rate and differential pressures are measured for analysis.

The condenser loop has capability to change mass flow from 0.1 to 0.8 kg/s in steps of 0.05 kg/s. The condensation loop have a provision to control inlet temperature to condenser unit from 10 °C to 50 °C in steps 1 °C. The experimental measured values for one typical refrigeration cycle are shown in Fig.5.3.

The refrigerant coming out of condenser will enter into expansion valve with high pressure and high temperature (T_2 and P_2) and will come out with low pressure and low temperature (T_3 and P_3) as liquid.

The refrigerant R134a coming out of expansion valve will enter into the evaporator with T_3 and P_3 (-7 °C, 2.17 bar) and at a mass flow rates of m_r (0.01906 kg/s) in liquid form. The working fluid will absorb heat (latent heat) from the evaporation water loop and comes out as full vapour with almost T_4 and P_4 (24.79 °C and 1.78 bar). The evaporation loop has capability to change mass flow rate from 0.1 to 0.8 kg/s in steps of 0.05 kg/s. The evaporation loop has a provision to control inlet

temperature to evaporator unit from 20 °C to 30 °C in steps 1 °C. The inlet temperature to evaporator unit for various test points should be maintained constant within ± 0.2 °C.

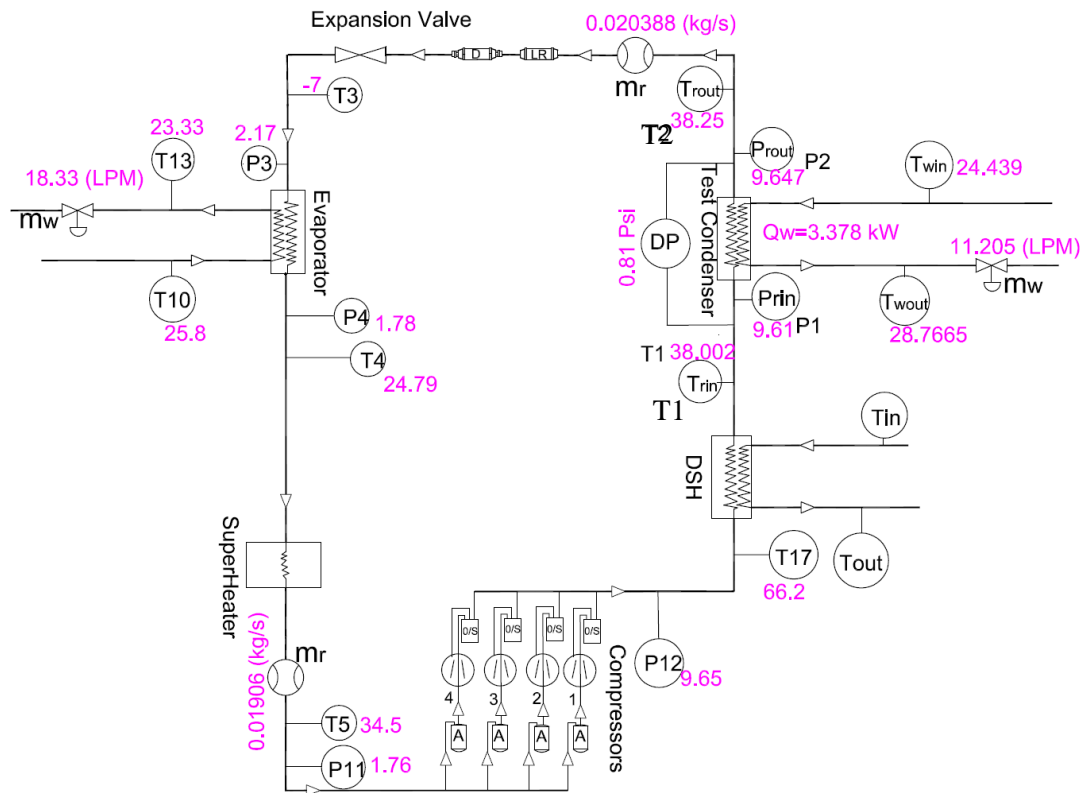
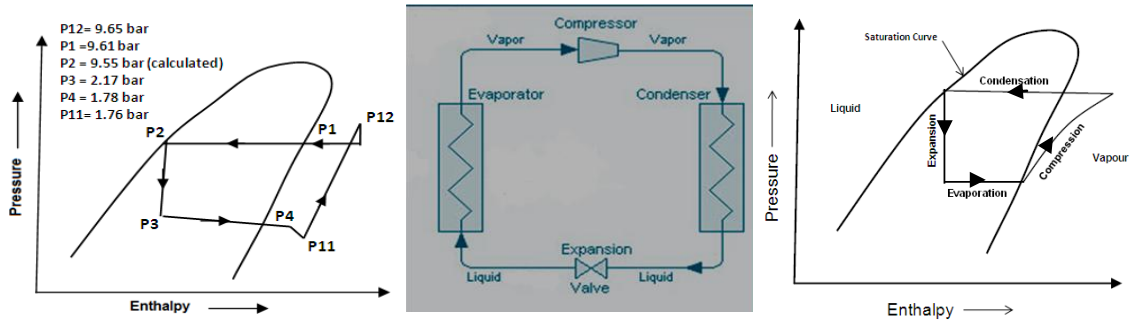


Fig. 5.3: Typical Refrigerant Circuit with Sample Recorded Values

The R134a coming out of the evaporator will be in the form of full vapor, in case the fluid is not in full vapour, the same should be converted to full vapour in the super heater. It is required to ensure that the refrigerant is fully converted to vapour form before entering into compressor. This loop is designed for 3 kW heating capacity with variation of heat load. The actual and simple VCERS on p-h diagram and schematic diagram of simple VCERS are shown in Fig.5.4.



a) p-h diagram for actual VCRES

b) Schematic diagram of simple VCRES

c) p-h diagram for simple VCRES

Fig. 5.4: Pressure-Enthalpy and Schematic Diagrams of VCRES

5.3 Data Reduction

The data reduction and analysis is carried out in the present investigation to deduce the heat transfer rate from the refrigerant flow to the water flow in the test condenser.

5.3.1 Two phase condensation heat transfer coefficient

The amount of heat transfer from the refrigerant to the water can be determined from the energy conservation principle. Therefore, the heat transfer from the refrigerant to the water can be calculated from the following equations:

$$Q_w = m_w C_{pw} (T_{wo} - T_{wi}) \quad (5.1)$$

Based on Newton's law of cooling, the overall heat transfer coefficient can be determined by

$$Q_w = UA_w \Delta T_{ln} \quad (5.2)$$

Where ΔT_{ln} , is the logarithm mean temperature difference defined as

$$\Delta T_{ln} = \frac{(T_{rsat} - T_{wi}) - (T_{rsat} - T_{wo})}{\ln \frac{T_{rsat} - T_{wi}}{T_{rsat} - T_{wo}}} \quad (5.3)$$

Where T_{rsat} is the average saturation temperature of the refrigerant derived from the average pressure measured on refrigerant side and T_{wi} , T_{wo} are the water temperatures at the inlet and outlet of the test unit. The average condensation heat transfer coefficient (h_r) on refrigerant side of the test unit is derived from the global heat transfer coefficient (U) assuming no fouling resistance.

$$\frac{1}{U} = \frac{1}{\eta_{or}h_r} + \frac{t}{\lambda\left(\frac{A_p}{A_r}\right)} + \frac{1}{\eta_{ow}h_w\left(\frac{A_w}{A_r}\right)} \quad (5.4)$$

where A_w is the water side area, h_r and h_w are the refrigerant side and water side heat transfer coefficients respectively and η_0 is the overall fin surface efficiency, which is defined as;

$$\eta_o = 1 - a(1 - \eta_f) \quad (5.5)$$

in which 'a' is the ratio of the fin area to the total area,

$$\eta_f = \frac{\tanh(ml)}{ml} \quad (5.6)$$

$$\text{Where } m = \sqrt{\frac{2h_w(1+\frac{t}{l})}{\lambda*t}} \quad \text{and} \quad l = \frac{h}{2} \quad (5.7)$$

Equation (5.4) shows that, if the heat transfer coefficient at the water side is known, the average condensation heat transfer coefficient h_r can be directly calculated from the experimental data. For general cases the Wilson plot technique could be used for finding both heat transfer coefficients as explained in Kumar et al. (2001) and Styrylska et al. (2003). This method has been widely applied for separating individual resistances from an overall resistance. Unfortunately, due to lack of data, it is not possible to apply this method in the present investigation using the test rig. Hence, the water side heat transfer coefficient h_w is estimated separately as explained in the following sections.

5.3.2 Single phase Water heat transfer coefficient:

Generally, the single-phase heat transfer coefficient can be expressed with the Colburn j factor,

$$j_w = \frac{h_w}{G C_p} Pr^{\frac{2}{3}} \quad (5.8)$$

For the present fin geometry, the Reynolds number for water flow is defined as

$$Re_w = \frac{\rho V D_h}{\mu} = \frac{G D_{hw}}{\mu} \quad (5.9)$$

Where

$$G = \frac{\dot{m}}{A_f} \quad (5.10)$$

$$\text{And, } D_{hw} = \frac{2(s-t)h}{[(s+h)+\frac{th}{l}]}$$

The correlation for water side heat transfer coefficient for the above selected serrated fin surface in laminar range and turbulent range are as follows:

$$\text{Nu}_w = 0.049 \text{Re}_w^{0.69} \text{Pr}^{\frac{1}{3}}, \quad \text{for Laminar Range } (100 \leq \text{Re} \leq 800) \quad (5.12)$$

$$\text{Then, } h_w = 0.049 \left(\frac{\lambda_w}{D_h}\right) \text{Re}_w^{0.69} \text{Pr}^{\frac{1}{3}} \quad (5.13)$$

$$\text{Nu}_w = 0.016 \text{Re}_w^{0.85} \text{Pr}^{\frac{1}{3}}, \quad \text{for Turbulent Range } (1000 \leq \text{Re} \leq 15000) \quad (5.14)$$

$$\text{Then, } h_w = 0.016 \left(\frac{\lambda_w}{D_h}\right) \text{Re}_w^{0.85} \text{Pr}^{\frac{1}{3}} \quad (5.15)$$

The steady state conditions for the test condenser are determined by checking the heat balance between the released heat from R134a and the heat absorbed by the cooling water. The amount of heat released from R134a can be calculated by the following equation:

$$Q_r = m_r \Delta H \quad (5.16)$$

Where Q_r , m_r and ΔH are the heat load, mass flow rate and enthalpy drop of R134a across the test condenser respectively. The criterion used for the steady state condition during the test is given below:

$$\frac{|Q_r - Q_w|}{Q_{ave}} \leq 5\% \quad (5.17)$$

Where Q_{ave} , is the average value of heat exchanged between R134a and the cooling water and is determined by the following relation:

$$Q_{ave} = \frac{1}{2} (Q_r + Q_w) \quad (5.18)$$

5.3.3 Two phase frictional pressure drop

To measure the frictional pressure drop on the refrigerant side is computed in accordance with Yan et al. (1999) by subtracting the pressure losses at the test condenser inlet and exit manifolds and ports (ΔP_c) then adding the momentum pressure rise (deceleration, ΔP_a) and the gravity pressure rise (elevation, ΔP_g) to the total pressure drop measured (ΔP_t).

$$\Delta P_f = \Delta P_t - \Delta P_c + \Delta P_a + \Delta P_g \quad (5.19)$$

The momentum and gravity pressure drops are estimated by the homogeneous model for two phase gas-liquid flow as per Collier (1982) as follows:

$$\Delta P_a = G^2 (v_g - v_l) |\Delta x| \quad (5.20)$$

$$\Delta P_g = g \rho_m L \quad (5.21)$$

Where v_g and v_l are the specific volume of liquid and vapour phase, $|\Delta x|$ is the absolute value of the vapour quality change between inlet and outlet and

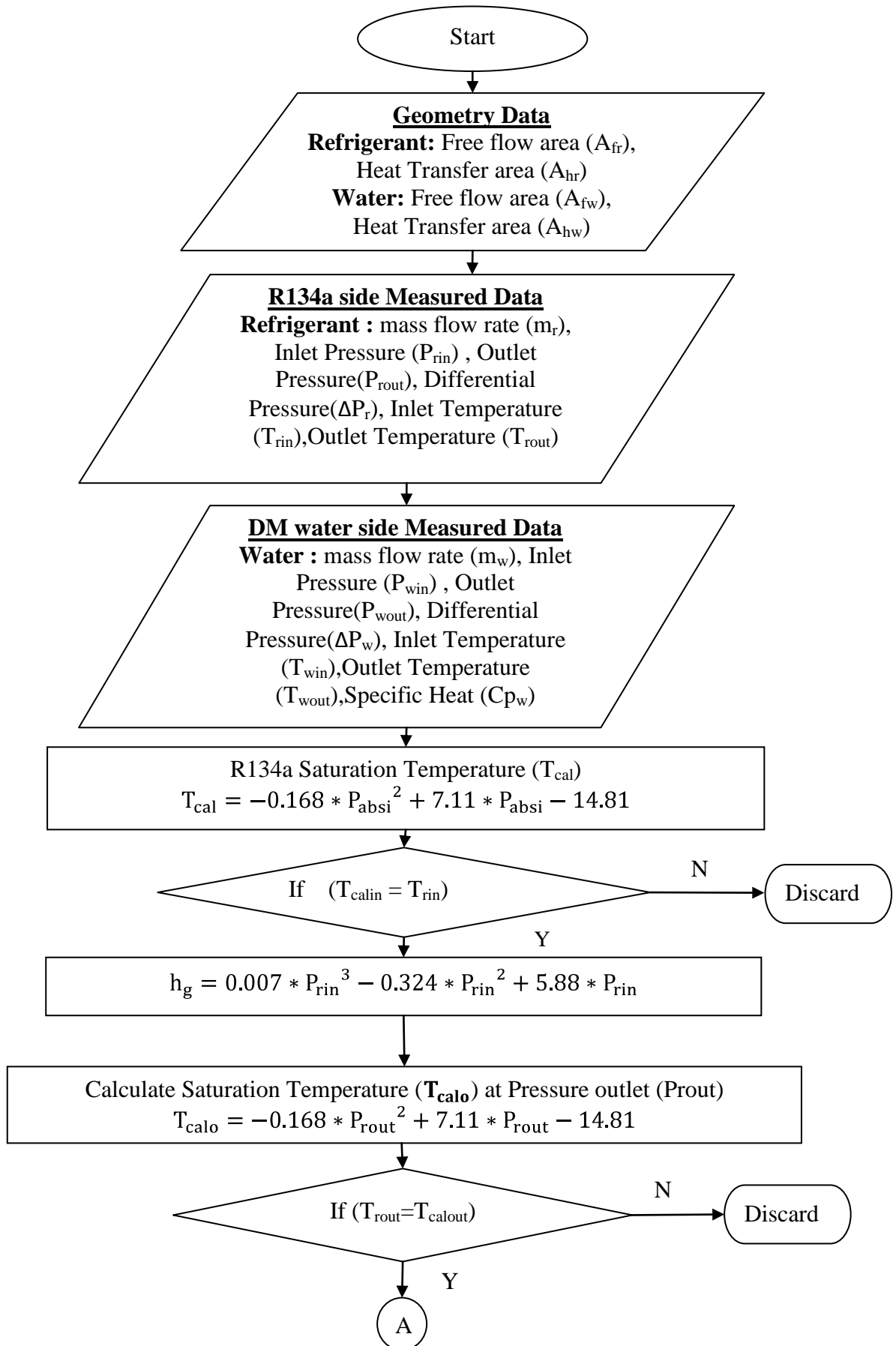
$$\rho_m = \left[\frac{x_m}{\rho_g} + \frac{(1-x_m)}{\rho_l} \right]^{-1} \quad (5.22)$$

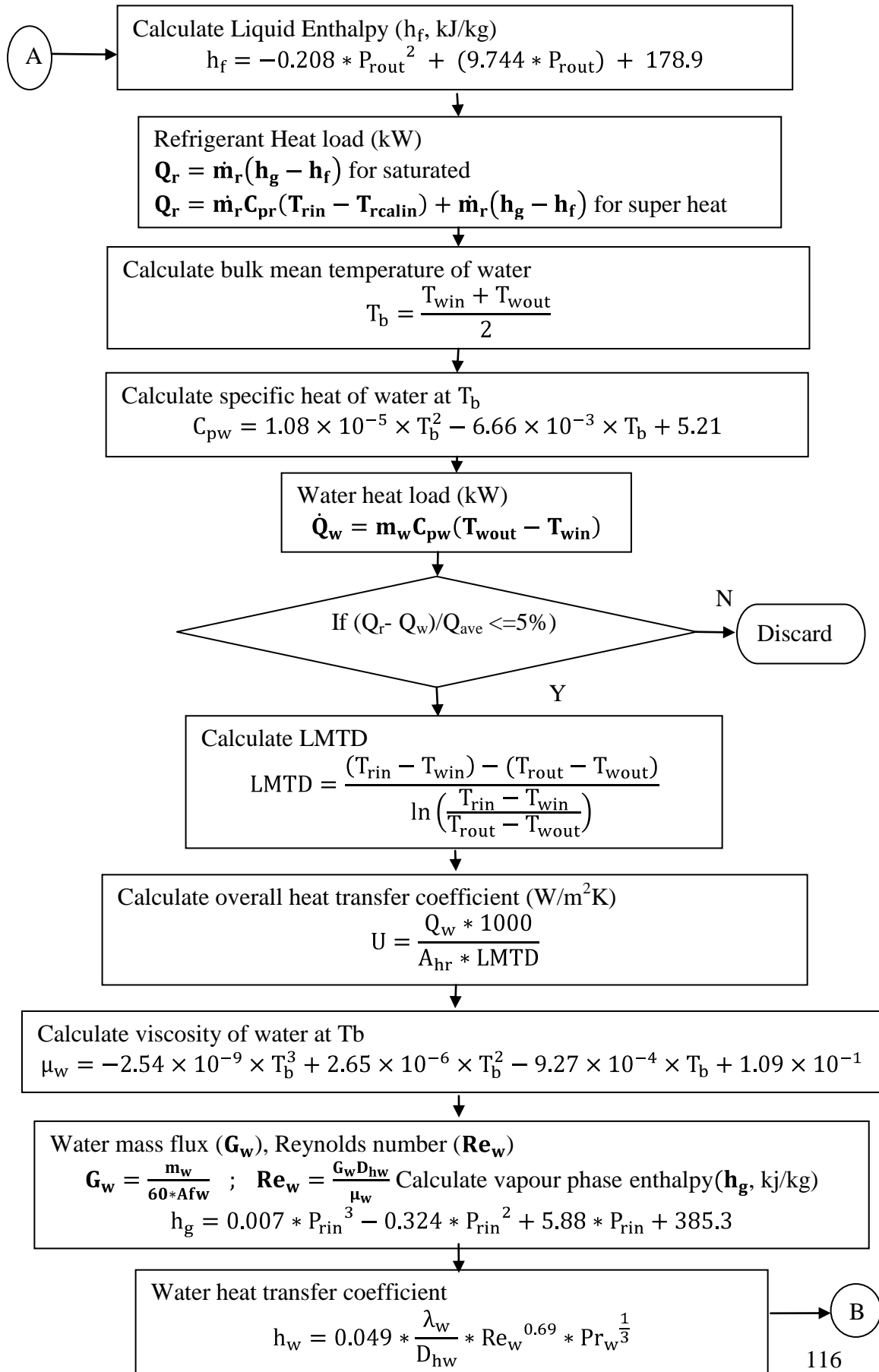
ρ_m is the average two-phase density between inlet and outlet calculated by the homogeneous model at the average vapour quality x_m between inlet and outlet. The pressure drop in the inlet and outlet manifolds and ports are empirically estimated, in accordance with Shah and Focke (1988) as follows:

$$\Delta P_c = 1.5 \frac{G^2}{2\rho_m} \quad (5.23)$$

A data reduction analysis is needed in the present measurement to deduce the heat transfer rate from the refrigeration flow to the water flow in the test heat condenser. The calculation of the condensation heat transfer coefficients and frictional pressure drops on the refrigerant side by using temperature, pressure, flow rate and differential pressure on both the circuits. The properties of pure R134a are used for the calculation and oil content is neglected as compressor rock contains the oil management system including oil separators. With the above procedure, the observed data is reduced to get the results. Pictorial representation of step by step procedure of data reduction to get results is shown in Fig. 5.5.

The step by step procedure to determine saturated heat transfer coefficient (h_r) and two phase frictional pressure drop (ΔP_f) are provided in Appendix-III. Also, sample calculations to determine two phase condensation heat transfer coefficient and frictional pressure drop for R134a using serrated fins are presented in Appendix-I. Experimental observations are reduced to get average two phase heat transfer coefficient (h_r) and frictional pressure drop (ΔP_f) across test condenser. All thermo physical properties required for calculations are taken at bulk mean temperature.





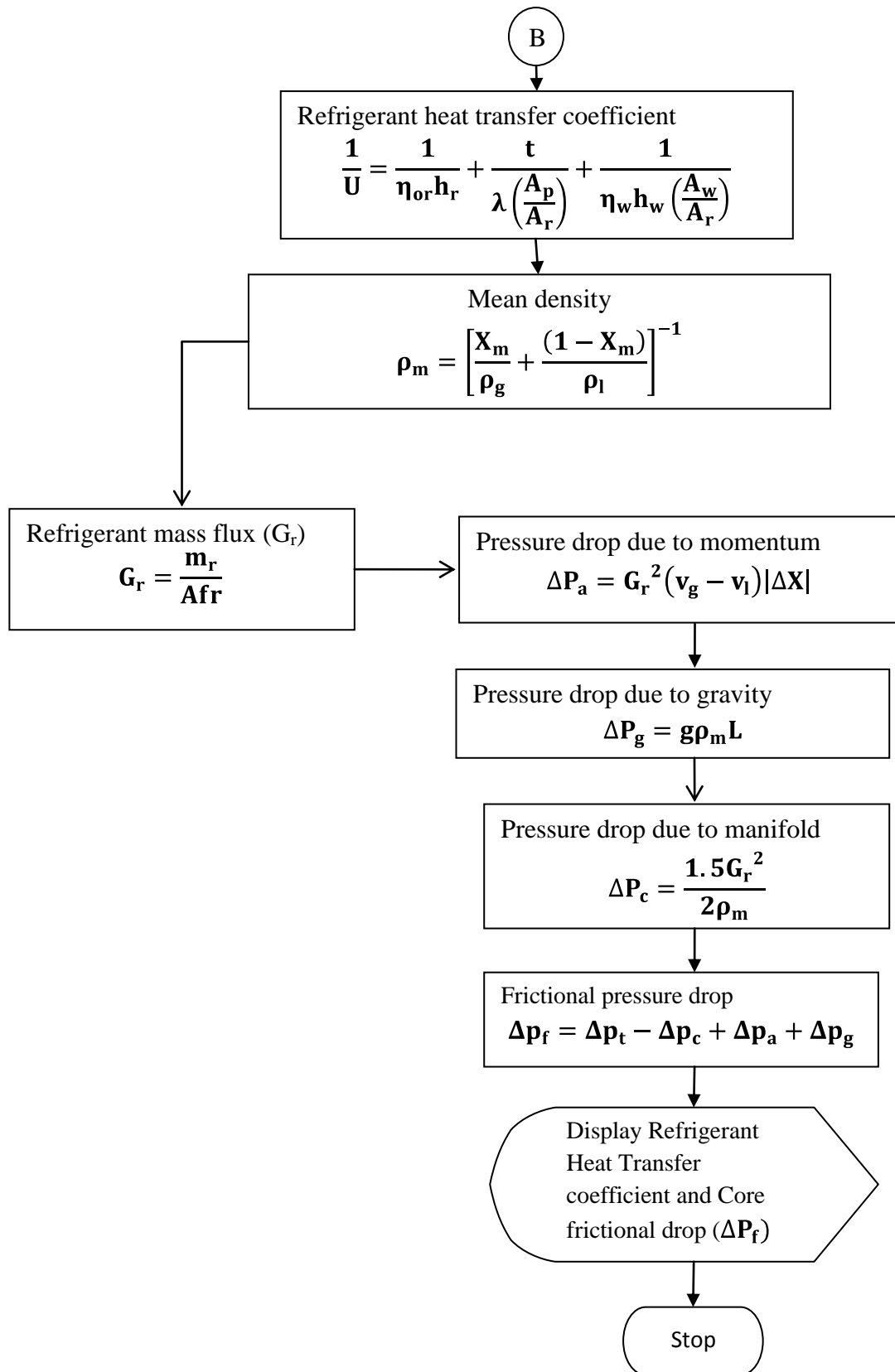


Fig.5.5: Pictorial Presentation of Step By Step Procedure of Data Reduction

5.4 Preliminary Single –Phase Energy Balance Validation

An energy balance between the super heated refrigerant flow and the cold water was verified before starting condensation experiments. Basically, most of the heat from vapour refrigerant is delivered to the cold water flow. Part of the energy is inevitably dissipated to the ambient by external surface of the water jacket. To reduce these losses the test condenser is insulated with 10 mm thick polyimide foam coated with hypalon, which is an aerospace grade insulation material. Also, the test condenser size is small (Approx.150X150X25 mm³) and corresponding outer surface heat transfer area also less. In test condenser, the refrigerant is passing through middle layer and water is passing through top and bottom layers (As shown in Fig.4.2). Therefore, the single phase tests with different flow condition were carried out to estimate the heat losses to the ambient as a function of surface temperature of the water jacket. The estimated values are around 0.06-0.1% of the heat duty. The estimated values are very small due to high quality of aerospace grade insulation material. The heat leakage during testing of the condenser was very less (0.06 to 0.1% of the heat duty) while obtaining energy balance between two streams due to small temperature gradient between ambient and test condenser water jacket temperature. The heat leakage values found from literature (Farahani et al., (2013)) are around 2 % of the heat duty. Hence, the heat leakage values are found to be very small enough to neglect while evaluating experimental heat transfer coefficient. The heat leakage values are neglected and not considered in the data reduction for evaluating experimental heat transfer coefficient. It is observed that the heat leakage loss is around 0.1% of the heat duty and by neglecting the heat leakage is not affecting the heat transfer coefficient.

5.5 Measurement of Lubricating Oil Concentration

Synthetic polyol ester oil is used in the vapour compression cycle system to provide lubrication for compressors. The lubrication oil mixes with refrigerant during condensation experiments even though system is equipped with two levels of oil separating system. Bassi and Bansal (2002) conducted in-tube condensation experiments with a mixture of R134a and polyol ester oil resulted in a decrease in the

in-tube condensation heat transfer compared with pure R134a. So, it is required to measure the percentage of oil mixing in the R134a during condensation experimentation. To estimate the concentration of oil mixed in the refrigerant R134a the following method was followed.

The VCRS test rig was charged with pure refrigerant was ensured. The percentage of oil mixed in the refrigerant circuit during condensation experiments are measured as per the procedure given below.

1. Taken the empty cylinder and evacuated using vacuum pump. Measured the weight of the empty cylinder using digital weight balance and noted.
2. Collected the refrigerant from the sampling port to the cylinder after the each test condenser condensation experiment.
3. Measured the weight of cylinder with refrigerant as shown in the Fig 5.6 and noted the reading.



Fig 5.6: Measurement of Percentage of Lubricating Oil Mixing

4. Opened the cylinder cap and vented the refrigerant from the cylinder at very slow phase.
5. The refrigerant was vented out as it was in vapour form and lubricating oil was settled at bottom of the cylinder due to high density.

6. At the vented location filter paper was used to check the oil droplets coming out from the cylinder. No oil content was noticed on the filter paper.
7. After venting, the weight of the cylinder was measured. The measurements are provided in the Table 5.1

Table 5.1: Measurement of Oil Mixing in Refrigerant

SI. No	Empty cylinder weight (kg)	Cylinder weight with refrigerant (kg)	Net weight of refrigerant (kg)	Weight of the cylinder after venting (kg)	% of oil mixed
1	0.775	1.243	0.468	0.7789	0.83
2	0.775	1.240	0.465	0.7786	0.77
3	0.775	1.255	0.480	0.7791	0.85

The procedure was repeated for all the test sections and estimated percentage of oil mixed in the refrigerant circuit during condensation experiments. The results indicated that the oil mixed in the refrigerant was found less than 1% in all the cases.

5.6 Uncertainty Analysis

Measurement uncertainty is the doubt that exists about a measurement results. Evaluating the uncertainty in the measurement process determines the “goodness” of a measurement. Uncertainty is calculated to support decisions based on measurements. Again, measurement is a process where by the value of a quantity is estimated. All measurements are accompanied by error. The first step in any uncertainty analysis is to identify the physical quantity whose value is estimated through measurement.

Errors and uncertainties are generated from disturbances, instrument selection, calibration and environmental conditions. But, it is important to find out accuracy level of the measuring instruments and method. It needs to find out propagated error in result due to error in measurement. The parameters which are measured for the present study are pressure, temperature and mass flow rate on both the refrigerant side and water side circuits. The accuracy range of measuring devices are listed in Table 5.2.

Table 5.2: Accuracy Ranges of Measuring Devices

	Device	Type	Range	Accuracy
1	Resistance thermometers	RTD	-40 to 100 °C	±0.15°C
2	Thermocouples	Type K	-40 to 1200 °C	±0.5°C
3	Refrigerant flow meter	Coriolis effect	0 to 0.09 kg/s	±0.05% for liquid and ±0.035% for gas
4	Water flow meter	Turbine	0 to 60 LPM	0.25%
5	Pressure transducers	Stain gage type	0 to 20 bar (abs)	0.25% full scale
6	Differential pressure transducers	Stain gage type	0 to 5 PSI	0.025% full scale

In many experiments, an important quantity is not directly measured but is rather calculated as a function of one or more variables that are directly measured,

$$Y = f(X1, X2 \dots) \quad (5.24)$$

The measured variables, X1, X2, etc. have a random variability which is referred to as its uncertainty. The method for determining the uncertainty is described in NIST Technical Note 1297 (Taylor B.N. and Kuyatt, C.E., Guidelines for Evaluating and Expressing the Uncertainty of NIST Measurement Results, National Institute of Standards and Technology Technical Note 1297, 1994). Assuming the individual measurements are uncorrelated and random, the uncertainty in the calculated quantity can be estimated as

$$U_y = \sqrt{\sum_i \left(\frac{\partial Y}{\partial X_i}\right)^2 U_{x_i}^2} \quad (5.25)$$

All the parameters like mass flow rates, inlet and outlet pressures, temperatures and pressure drops across the test condenser for both refrigerant and water sides were recorded. The equations of state of R134a are taken from EES. Using these data, uncertainty analysis has been carried out for estimation of uncertainties in saturated condensation heat transfer coefficient and two phase frictional pressure drop parameters using the Engineering Equation Solver (EES) program developed for such purpose. The programme written in EES for estimation of uncertainties of different parameters is presented in Appendix-IV. The analysis indicates the overall uncertainty within ±16.7% for the refrigerant condensation heat transfer coefficient measurement

and within $\pm 4.5\%$ for the refrigerant measured frictional pressure drop. The detailed results of the different parameters and their estimated uncertainties are tabulated in Table 5.3.

Table 5.3: Parameters and Estimated Uncertainties

Parameter	Uncertainty
Plate length, Width(m)	± 0.0005
Plate area (m ²)	± 0.00007
Fin frequency (Fins per meter)	± 5
Fin height (mm)	± 0.01
Fin thickness (mm)	± 0.002
Serration length (mm)	± 0.005
Total heat transfer area (m ²)	± 0.00007
Hydraulic Diameter (mm)	± 0.002
Water inlet temperature, T_{wi} (°C)	± 0.15
Water outlet temperature, T_{wo} (°C)	± 0.15
Refrigerant inlet temperature, T_{ri} (°C)	± 0.15
Refrigerant outlet temperature, T_{ro} (°C)	± 0.15
Refrigerant inlet pressure, P (%)	± 0.25
Differential Pressure, ΔP (%)	± 0.025
Heat flow rate, Q (%)	± 6.8
Refrigerant mass flux, G_r (%)	± 1.2
Refrigerant heat flux, q_r (%)	± 2
Overall heat transfer coefficient, U (%)	± 7.2
Water heat Transfer coefficient, h_w (%)	± 5.3
Refrigerant average heat transfer coefficient, h_r (%)	± 16.7
Refrigerant Frictional pressure drop, ΔP_f (%)	± 4.5

5.5.1 Sample calculation of uncertainty in h_r and ΔP_f

Uncertainties of the following parameters are estimated using EES programme. As an example, the measurement of uncertainties in saturated condensation heat transfer coefficient and two phase frictional pressure drop parameters are given below:

Uncertainties in temperature difference

$$\Delta T_w = T_o - T_i \quad (5.26)$$

$$\Delta T_w = f(T_i, T_o) \quad (5.27)$$

$$W_{\Delta T_w} = \sqrt{\left(\frac{\partial \Delta T_w}{\partial T_i}\right)^2 W_{T_i}^2 + \left(\frac{\partial \Delta T_w}{\partial T_o}\right)^2 W_{T_o}^2} \quad (5.28)$$

$$W_{\Delta T_w} = 3.847 \pm 0.2121$$

$$W_{\Delta T_w} = 5.52 \%$$

Uncertainty in heat absorbed by the fluid

$$Q_w = \dot{m}_w C_{pw} \Delta T \quad (5.29)$$

$$Q_w = f(\dot{m}_w, \Delta T) \quad (5.30)$$

$$W_{Q_w} = \sqrt{\left(\frac{\partial Q_w}{\partial \dot{m}_w}\right)^2 W_{\dot{m}_w}^2 + \left(\frac{\partial Q_w}{\partial \Delta T}\right)^2 W_{\Delta T}^2} \quad (5.31)$$

$$W_{Q_w} = 3.35 \pm 0.1849$$

$$W_{Q_w} = 5.52 \%$$

Uncertainty in refrigerant mass flux

$$G_r = \frac{\dot{m}_r}{A_{fr}} \quad (5.32)$$

$$G_r = f(\dot{m}_r, A_{fr}) \quad (5.33)$$

$$W_{G_r} = \sqrt{\left(\frac{\partial G_r}{\partial \dot{m}_r}\right)^2 W_{\dot{m}_r}^2 + \left(\frac{\partial G_r}{\partial A_{fr}}\right)^2 W_{A_{fr}}^2} \quad (5.34)$$

$$W_{G_r} = \sqrt{\left(\frac{\partial G_r}{\partial \dot{m}_r}\right)^2 W_{\dot{m}_r}^2 + \left(\frac{\partial G_r}{\partial A_{fr}}\right)^2 W_{A_{fr}}^2} \quad (5.35)$$

$$W_{G_r} = 36.13 \pm 0.0236$$

$$W_{G_r} = 36.13 \pm 0.4336$$

$$W_{G_r} = 1.2 \%$$

Uncertainty in water mass flux

$$G_w = \frac{\dot{m}_w}{A_{fw}} \quad (5.36)$$

$$G_w = f(\dot{m}_w, A_{fw}) \quad (5.37)$$

$$W_{G_w} = \sqrt{\left(\frac{\partial G_w}{\partial \dot{m}_w}\right)^2 W_{\dot{m}_w}^2 + \left(\frac{\partial G_w}{\partial A_{fw}}\right)^2 W_{A_{fw}}^2} \quad (5.38)$$

$$W_{G_w} = 175 \pm 0.438$$

$$W_{G_w} = 0.25 \%$$

Uncertainty in overall heat transfer coefficient

$$Q_w = UA_{hr} \left(\frac{(T_{ri}-T_{wi})-(T_{ro}-T_{wo})}{\ln\left(\frac{(T_{ri}-T_{wi})}{(T_{ro}-T_{wo})}\right)} \right) \quad (5.39)$$

$$U = f(T_{ri}, T_{ro}, T_{wi}, T_{wo}, Q_w) \quad (5.40)$$

$$W_u = \sqrt{\left(\frac{\partial U}{\partial Q_w}\right)^2 W_{Q_w}^2 + \left(\frac{\partial U}{\partial T_{ri}}\right)^2 W_{T_{ri}}^2 + \left(\frac{\partial U}{\partial T_{ro}}\right)^2 W_{T_{ro}}^2 + \left(\frac{\partial U}{\partial T_{wi}}\right)^2 W_{T_{wi}}^2 + \left(\frac{\partial U}{\partial T_{wo}}\right)^2 W_{T_{wo}}^2} \quad (5.41)$$

$$W_u = 1646 \pm 86.54$$

$$W_u = 5.25 \%$$

Uncertainty analysis of heat transfer coefficient

$$\frac{1}{U} = \frac{1}{\eta_{or} h_r} + \frac{t}{\lambda \left(\frac{A_p}{A_r}\right)} + \frac{1}{\eta_{ow} h_w \left(\frac{A_w}{A_r}\right)} \quad (5.42)$$

$$h_r = f(m_w, T_{ri}, T_{ro}, T_{wi}, T_{wo}) \quad (5.43)$$

$$W_{hr} = \sqrt{\left(\frac{\partial h_r}{\partial m_w}\right)^2 W_{m_w}^2 + \left(\frac{\partial h_r}{\partial T_{ri}}\right)^2 W_{T_{ri}}^2 + \left(\frac{\partial h_r}{\partial T_{ro}}\right)^2 W_{T_{ro}}^2 + \left(\frac{\partial h_r}{\partial T_{wi}}\right)^2 W_{T_{wi}}^2 + \left(\frac{\partial h_r}{\partial T_{wo}}\right)^2 W_{T_{wo}}^2} \quad (5.44)$$

$$W_{hr} = 4709 \pm 630.2$$

$$W_{hr} = 13.4 \%$$

Uncertainty analysis of frictional pressure

$$\Delta p_f = ((6.895 * \Delta p_t) - \Delta p_c + \Delta p_a + \Delta p_g) \quad (5.45)$$

$$\text{Where, } \Delta P_a = 0.001 * G_r^2 (v_g - v_l) |\Delta X| \quad (5.46)$$

$$\Delta P_g = 0.001 * g \rho_m L \quad (5.47)$$

$$\rho_m = \left(\frac{x}{\rho_g} + \frac{1-x}{\rho_l} \right)^{-1} \quad (5.48)$$

$$\Delta P_c = \frac{0.001 * 1.5 * G_r^2}{2 \rho_m} \quad (5.49)$$

$$\Delta p_f = f(m_r, \Delta p_t) \quad (5.50)$$

$$W_{\Delta p_f} = \sqrt{\left(\frac{\partial \Delta p_f}{\partial m_r}\right)^2 W_{m_r}^2 + \left(\frac{\partial \Delta p_f}{\partial \Delta p_t}\right)^2 W_{\Delta p_t}^2} \quad (5.51)$$

$$W_{\Delta p_f} = 5.47 \pm 0.1332$$

$$W_{\Delta p_f} = 2.42\%$$

Summary: Experimental set up to determine average two phase condensation heat transfer coefficient and frictional pressure drop is developed. Testing of the set up has been done with different serrated fins and then observations are noted for all the considered saturated conditions at different refrigerant mass flow rates. The matrix of experiments has been carried out and the experimental data is reduced to calculate two phase saturated condensation heat transfer coefficient and two phase frictional pressure drop. The results related to two phase condensation heat transfer coefficient and frictional pressure drop characteristics are discussed in detail in Chapter 6.

CHAPTER 6

EXPERIMENTAL RESULTS AND DISCUSSION

The average condensation heat transfer coefficient and frictional pressure drop variations are found to be 8% and 11% respectively between the experimental results of plate heat exchanger reported in Chapter 4, Section 4.7 and data reported by Giovanni (2008, 2010) and Nusselt (1916), confirms the accuracy and reliability of the measurements and paves the way for study of thermo-hydraulic performance of plate fin surfaces. The experimental set up described in Chapter 4, section 4.4 is used to study four types of serrated fin surfaces, on which no experimental data was previously available. The geometrical parameters describing the four serrated fin surfaces are listed in Table 6.1.

Table 6.1: Geometrical Parameters of Serrated Fin Surfaces

Test Unit No.	Circuit Name	Fin Density (FPI)	Lance Length (mm)	Hydraulic Diameter (mm)	Height (mm)	Fin Thickness (mm)
TC1	R134a side	30	3.175	1.1894	3.05	0.1016
	Water side	28	3.175	1.3450	5	0.127
TC2	R134a side	28	3.175	1.3450	5	0.127
	Water side	28	3.175	1.3450	5	0.127
TC3	R134a side	18	1.588	1.7461	3.8	0.254
	Water side	28	3.175	1.3450	5	0.127
TC4	R134a side	18	3.175	1.8667	5	0.254
	Water side	28	3.175	1.3450	5	0.127

The results related to serrated fin geometric parameters effect on condensation heat transfer and frictional pressure drop characteristics are discussed in this chapter. The effect of mass flux and heat flux on heat transfer coefficient and frictional pressure drop at different saturation temperatures are also highlighted in this chapter. The results obtained through experimental observations are considered for the

discussion. Analyzing the experimental results and reaching the conclusion about condensation heat transfer and frictional pressure drop correlations for different types of serrated fins individually are the prime objectives in this chapter. Also, analyzed the combined effect of fin geometries on condensation heat transfer coefficient and frictional pressure drop is the main focus of the discussion. Following is sequential order of the topics considered for the discussion of test condenser.

- Experimental results and analysis of test condensers with refrigerant R134a at saturated conditions.
- Development of condensation correlations.
- Influence of serrated fin geometries on condensation performance.
- Exploration of condensation heat transfer coefficient and frictional pressure drop correlations.

6.1 Experimental Results and Analysis

The identified 4 types of test condensers namely TC1, TC2, TC3 and TC4 are tested using test rig described in Chapter 5. The experiments are carried out for different saturated temperatures at different refrigerant mass fluxes. The experimental details, results and their analysis are discussed in subsequent paras.

6.1.1 Test Condenser1 (TC1)

The brazed plate fin heat exchanger fin details are given in Table 6.2.

Table 6.2: Geometric Data of TC1 Fins

Parameter	Unit	Value	
		DM Water side	Refrigerant side
Type		Serrated (Lanced & Offset)	
Material		Aluminium	
Fin frequency	Fins per meter (FPI)	1102.4 ±5 (28)	1181±5 (30)
Fin height	mm	5±0.01	3.05±0.01
Fin thickness	mm	0.127±0.002	0.1016±0.002
Serration length	mm	3.175±0.005	
No of layers		2	1
Total heat transfer area	m ²	0.4616±0.00007	0.1642±0.00007
Hydraulic diameter	mm	1.3450±0.002	1.1894±0.002

The condensation tests were carried out with R134a down-flow and water horizontal-flow at six different saturated temperatures (32 °C, 34 °C, 36 °C, 38 °C, 40 °C and 42 °C) to determine the effect of saturated temperature on the two phase condensation heat transfer and frictional pressure drop of R134a inside a brazed plate fin heat exchanger. Table 6.3 indicates the operating conditions in the condenser under experimental tests on TC1.

Table 6.3: Operation Conditions during Experimental Tests on TC1

Set	P_{sat} (MPa)	T_{sat} (°C)	Runs (Nos)	Quality		G_r (kg/m ² s)	q_r (kW/m ²)
				X_{in}	X_{out}		
1 st	0.814±0.01	32±0.2	20	0.95-1	0-0.07	20-42	15-32.3
2 nd	0.863±0.01	34±0.2	45	0.97-1	0-0.03	18-41	14-31
3 rd	0.912±0.01	36±0.3	25	0.94-1	0-0.06	20-44	15-33
4 th	0.961±0.01	38±0.3	20	0.93-1	0-0.07	19-40	14-30
5 th	0.101±0.01	40±0.3	30	0.94-1	0-0.06	16-42	11-33
6 th	0.107±0.01	42±0.2	30	0.94-1	0-0.06	19-41	14-29

The mass flow rate and heat flux of R134a were varied from 16 kg/m²s to 44 kg/m²s and 11 kW/m² to 33 kW/m² respectively in the first test condenser. Fig.6.1 and Fig.6.2 shows the effect of refrigerant mass flux on refrigerant heat transfer coefficient and heat flux respectively for saturated vapour condensation at different saturation temperatures. Results are indicating that the effect of saturation temperature not much significant on heat transfer coefficient when the mass flux is less than 22 kg/m²s and probably condensation is controlled by gravity, which is shown in the Fig.6.1. At low refrigerant mass flux (<22 kg/m²s) the condensation heat transfer coefficients are not depend on mass flux and are predicted by Giovanni (2008). For higher refrigerant mass flux (>22 kg/m²s), the heat transfer coefficient increased as mass flux increased due to forced convection condensation, shown in the Fig.6.1. For higher refrigerant mass flux (>22 kg/m²s) the heat transfer coefficients depend on mass flux and are well predicted by Akers et al. (1959). Fig.6.1 indicates the effect of mass flux vs. refrigerant heat flux, as the mass flux increases the refrigerant heat flux also increased. The average refrigerant heat transfer coefficient increased by 47% for 40.7% higher frictional pressure drop and the corresponding mass flux increased by 34.7%. The physical phenomenon of two phase refrigerant heat transfer coefficient in

serrated fins is the fins boundary layer is periodically interrupted and the thickness of the condensate film reduces. Fig.6.2 indicates, as the refrigerant saturation temperature increases the heat flux reduced at same mass flux due to reduction in enthalpy change. The refrigerant density and specific heat are comes down as the refrigerant saturation temperature increased. Fig.6.3 and Fig.6.4 indicates the effect of refrigerant mass flux and refrigerant kinetic energy per unit volume on refrigerant frictional pressure drop. Results show that, the frictional pressure drop increases as the mass flux increased. Also, further observed that the average refrigerant heat transfer coefficient increased by 7.4 % for 11.7 % higher frictional pressure drop and the corresponding absolute saturation temperature (absolute Pressure) reduced by 3.2 % at constant mass flux. The reduction of frictional pressure drop on refrigerant as the saturation temperature increased due to reduction in density of R134a. The frictional pressure drop varies from 88% to 96% of the refrigerant side total pressure drop.

All the parameters like flow rates, inlet and outlet pressures and temperatures and pressure drops across the test condenser for both refrigerant and water sides were recorded. The equations of state of R134a are taken from EES. The analysis indicates the overall uncertainty within $\pm 16.7\%$ for the refrigerant condensation heat transfer coefficient measurement and within $\pm 4.5\%$ for the refrigerant measured frictional pressure drop.

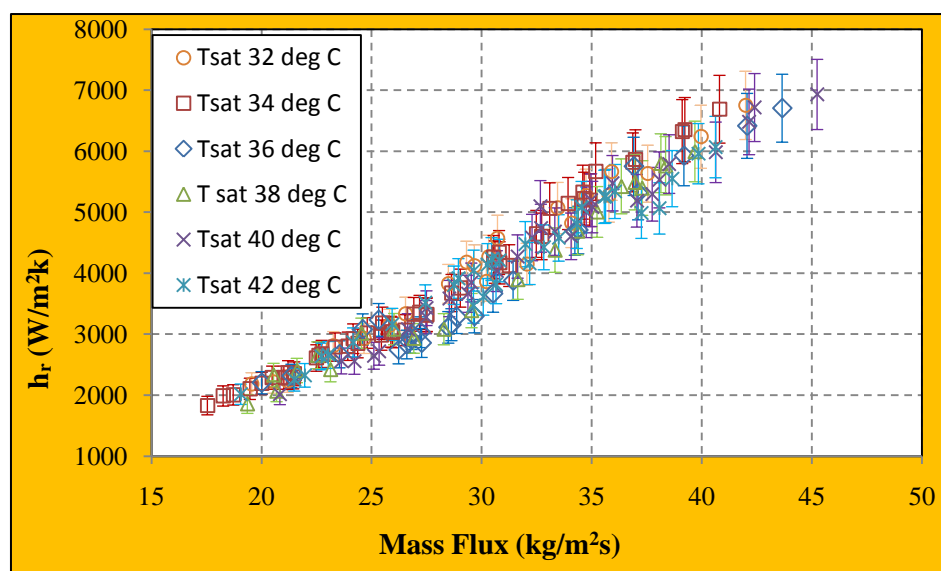


Fig. 6.1: Effect of Refrigerant Mass Flux on Two Phase Condensation Heat Transfer Coefficient at Different Saturation Temperatures for Test Condenser 1 (TC1)

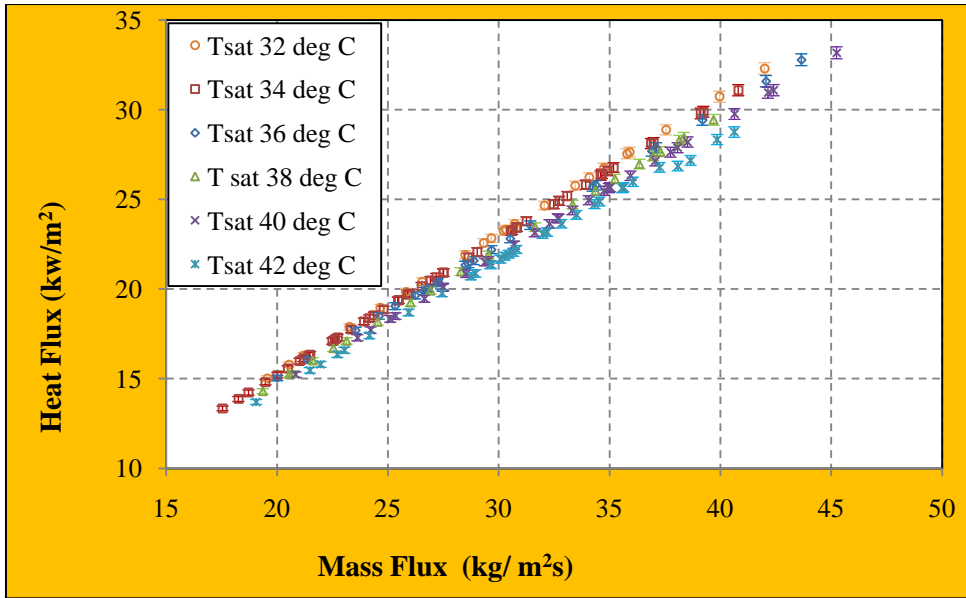


Fig. 6.2: Effect of Refrigerant Mass Flux on Heat Flux at Different Saturation Temperatures for Test Condenser 1 (TC1)

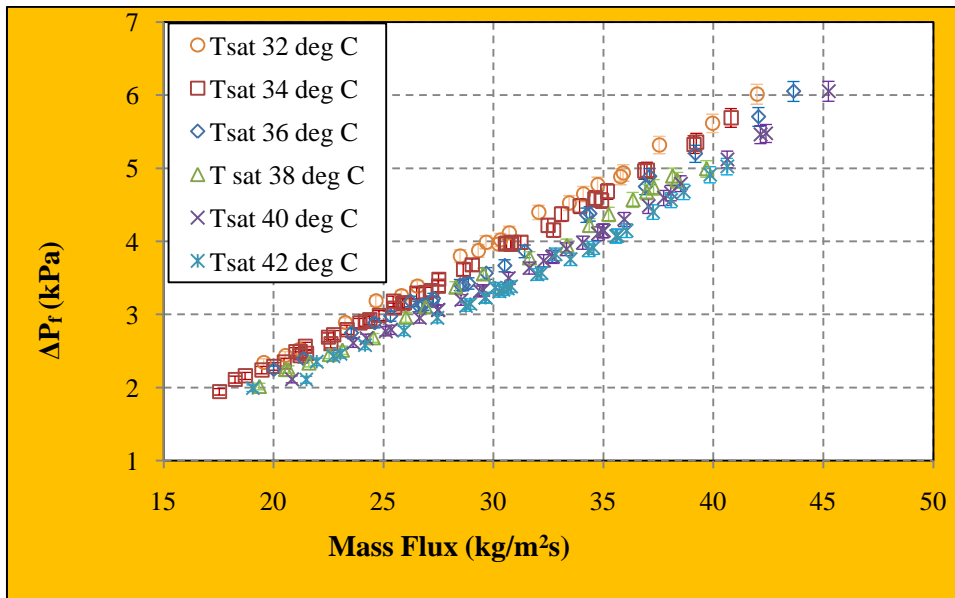


Fig.6.3: Effect of Refrigerant Mass Flux on Condensation Frictional Pressure Drop at Different Saturation Temperatures for Test Condenser 1 (TC1)

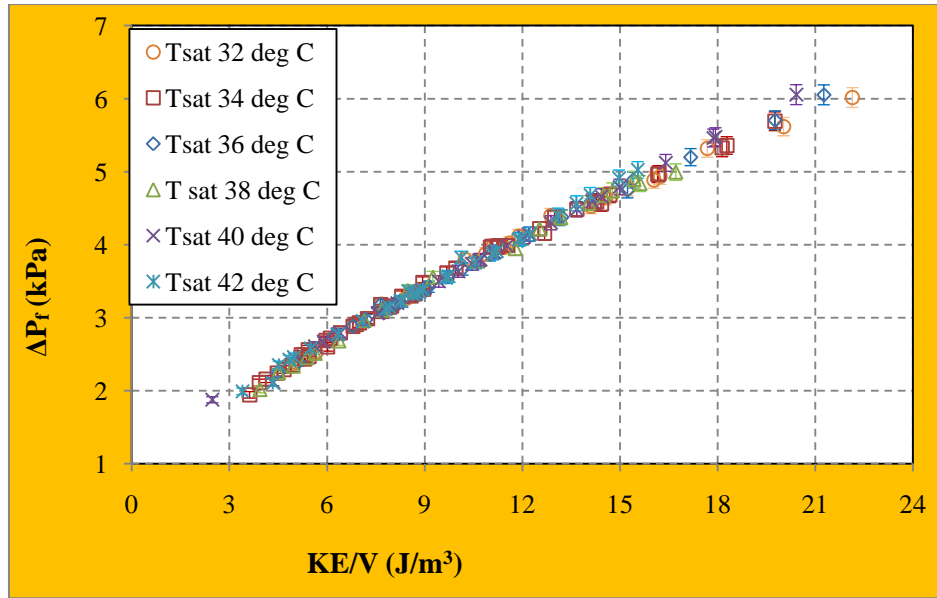


Fig.6.4: Effect of Kinetic Energy per Unit Volume (KE/V) on Condensation Frictional Pressure Drop at Different Saturation Temperatures for Test Condenser 1 (TC1)

6.1.2 Test Condenser 2 (TC2)

The brazed plate fin heat exchanger fin details are given in Table 6.4.

Table 6.4: Geometric Data of TC2 Fins

Parameter	Unit	Value	
		DM Water side	Refrigerant side
Type		Serrated (Lanced & Offset)	
Material		Aluminium	
Fin frequency	Fins per meter (FPI)	1102.4 ±5(28)	
Fin height	mm	5±0.01	
Fin thickness	mm	0.127±0.002	
Serration length	mm	3.175±0.005	
No of layers		2	1
Total heat transfer area	m ²	0.4616±0.00007	0.2286±0.00007
Hydraulic diameter	mm	1.3450±0.002	

The condensation tests were carried out with R134a down-flow and water horizontal-flow at five different saturated temperatures (34 °C, 38 °C, 40 °C, 42 °C and 44 °C) to determine the effect of saturated temperature on the two phase condensation heat transfer and frictional pressure drop of R134a inside a brazed plate

fin heat exchanger. Table 6.5 indicates the operating conditions in the condenser under experimental tests.

Table 6.5: Operation Conditions during Experimental Tests on TC2

Set	P_{sat} (MPa)	T_{sat} (°C)	Runs (Nos)	Quality		G_r (kg/m ² s)	q_r (kW/m ²)
				X_{in}	X_{out}		
1 st	0.866±0.02	34±0.5	30	0.95-1	0-0.07	16-40	7-17
2 nd	0.96±0.02	38±0.5	20	0.97-1	0-0.03	29-42	12-17.5
3 rd	0.101±0.02	40±0.5	20	0.94-1	0-0.06	19-46	8-9.5
4 th	0.107±0.01	42±0.5	30	0.93-1	0-0.07	23-37	10-15
5 th	0.113±0.01	44±0.5	20	0.94-1	0-0.06	18-40	7.5-16

The mass flow rate and heat flux of R134a was varied from 16 kg/m²s to 46 kg/m²s and 7 kW/m² to 18 kW/m² respectively in the second test condenser. Fig.6.5 and Fig.6.6 shows the effect of refrigerant mass flux on refrigerant heat transfer coefficient and heat flux respectively for saturated vapour condensation at different saturation temperatures. Results are indicating that the effect of saturation temperature not much significant on heat transfer coefficient when the mass flux is less than 22 kg/m²s and probably condensation is controlled by gravity, which is shown in the Fig.6.5. It indicates as the mass flux increases the refrigerant heat flux also increased. The average refrigerant heat transfer coefficient increased by 57.7 % for 37.3 % higher frictional pressure drop and the corresponding mass flux increased by 32.9 %.

Fig.6.6 indicates, as the refrigerant saturation temperature increases the heat flux reduced at same mass flux due to reduction in enthalpy change. The refrigerant density and specific heat are comes down as the refrigerant saturation temperature increased. Fig.6.7 and Fig.6.8 indicates the effect of refrigerant mass flux and refrigerant kinetic energy per unit volume on refrigerant frictional pressure drop. Results show that, the frictional pressure drop increases as the mass flux increased. Also, further observed that the average refrigerant heat transfer coefficient increased by 6 % for 7.5 % higher frictional pressure drop and the corresponding absolute saturation temperature (absolute Pressure) reduced by 3.2 % at constant mass flux. The reduction of pressure drop on refrigerant as the saturation temperature increased due to reduction in density of R134a. The frictional pressure drop varies from 89% to 95% of the refrigerant side total pressure drop.

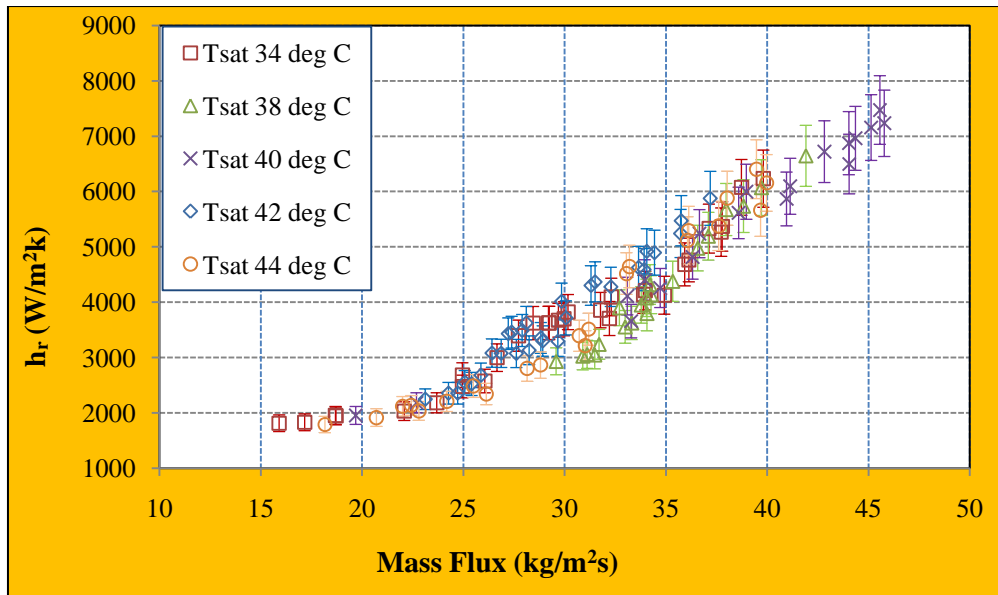


Fig. 6.5: Effect of Refrigerant Mass Flux on Two Phase Condensation Heat Transfer Coefficient at Different Saturation Temperatures for Test Condenser 2 (TC2)

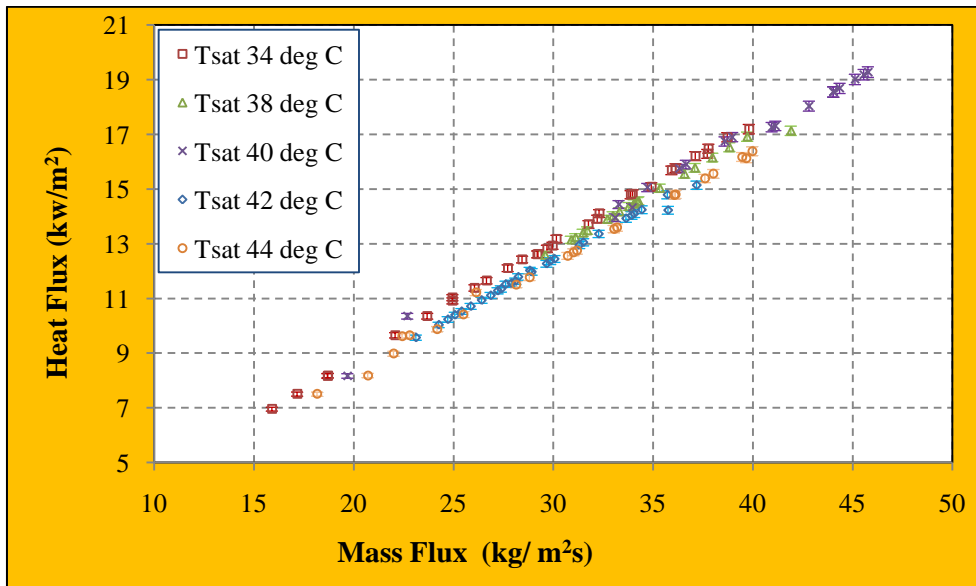


Fig.6.6: Effect of Refrigerant Mass Flux on Heat Flux at Different Saturation Temperatures for Test Condenser 2 (TC2)

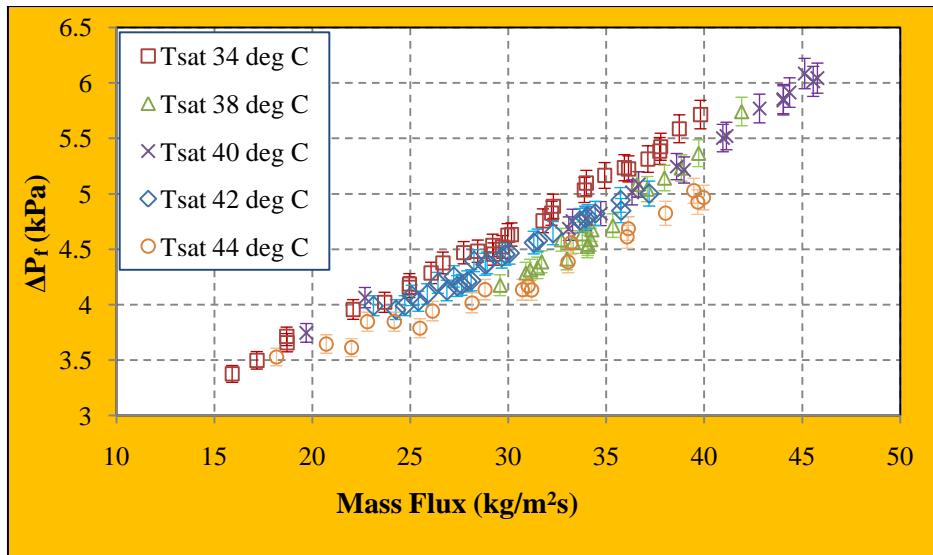


Fig.6.7: Effect of Refrigerant Mass Flux on Condensation Frictional Pressure Drop at Different Saturation Temperatures for Test Condenser 2 (TC2)

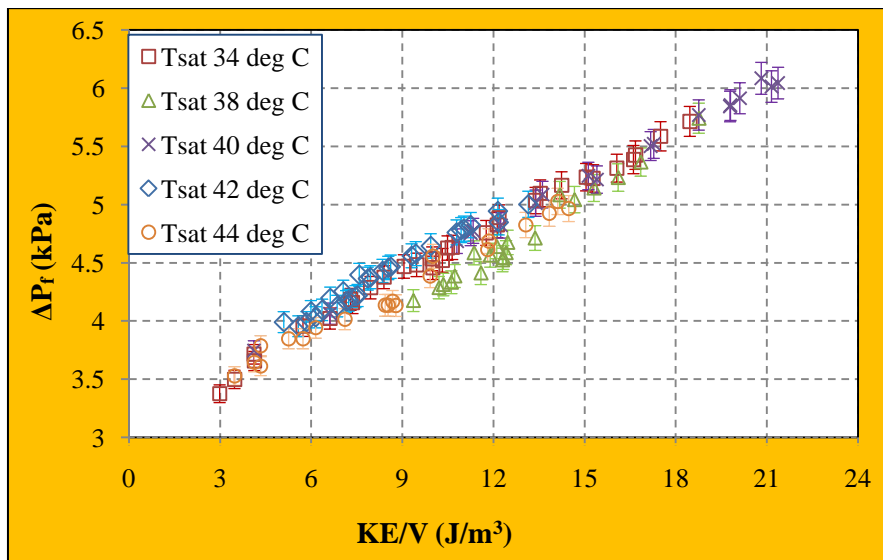


Fig.6.8: Effect of Kinetic Energy per Unit Volume (KE/V) on Condensation Frictional pressure drop at Different Saturation Temperatures for Test Condenser 2 (TC2)

6.1.3 Test Condenser 3 (TC3)

The brazed plate fin heat exchanger fin details are given in Table 6.6.

Table 6.6: Geometric Data of TC3 Fins

Parameter	Unit	Value	
		DM Water side	Refrigerant side
Type		Serrated (Lanced & Offset)	

Material		Aluminium	
Fin frequency	Fins per meter (FPI)	1102.4 ±5 (28)	
Fin height	mm	5±0.01	3.8±0.01
Fin thickness	mm	0.127±0.002	
Serration length	mm	3.175±0.005	1.588±0.005
No of layers		2	1
Total heat transfer area	m ²	0.4616±0.00007	0.1296±0.00007
Hydraulic diameter	mm	1.3450±0.002	1.7461±0.002

The condensation tests were carried out with R134a down-flow and water horizontal-flow at five different saturated temperatures (34 °C, 36 °C, 38 °C, 40 °C, 42 °C and 44 °C) to determine the effect of saturated temperature on the two phase condensation heat transfer and frictional pressure drop of R134a inside a brazed plate fin heat exchanger. The operating conditions in the condenser under experimental tests are indicated in Table 6.7.

Table 6.7: Operation Conditions during Experimental Tests on TC3

Set	P _{sat} (MPa)	T _{sat} (°C)	Runs (Nos)	Quality		G _r (kg/m ² s)	q _r (kW/m ²)
				X _{in}	X _{out}		
1 st	0.865±0.01	34±0.2	25	0.95-1	0-0.07	16-42	9-21.5
2 nd	0.912±0.01	36±0.2	30	0.97-1	0-0.03	15-36	9-20
3 rd	0.974±0.01	38±0.5	15	0.94-1	0-0.06	25-37	14-21
4 th	0.102±0.02	40±0.5	20	0.93-1	0-0.07	20-40	9-23
5 th	0.107±0.01	42±0.5	20	0.94-1	0-0.06	21-40	11-22
6 th	0.113±0.02	44±0.3	20	0.96-1	0-0.04	18-37	10-21

The mass flow rate and heat flux of R134a was varied from 16 kg/m²s to 40 kg/m²s and 9 kW/m² to 23 kW/m² respectively in the third test condenser. Fig.6.9 and Fig.6.10 shows the effect of refrigerant mass flux on refrigerant heat transfer coefficient and heat flux respectively for saturated vapour condensation at different saturation temperatures. Results are indicating that the effect of saturation temperature not much significant on heat transfer coefficient when the mass flux is less than 22 kg/m²s and probably condensation is controlled by gravity, which is shown in the Fig.6.9. It indicates the effect of mass flux vs. refrigerant heat flux, as the mass flux increases the refrigerant heat flux also increased. The average refrigerant heat transfer

coefficient increased by 60.7 % for 46.9 % higher frictional pressure drop and the corresponding mass flux increased by 36.1 %.

Fig.6.10 indicates, as the refrigerant saturation temperature increases the heat flux reduced at same mass flux due to reduction in enthalpy change. The refrigerant density and specific heat are comes down as the refrigerant saturation temperature increased. Fig.6.11 and Fig.6.12 indicates the effect of refrigerant mass flux and kinetic energy per unit volume on frictional pressure drop. Results show that, the frictional pressure drop increases as the mass flux increased. Also, further observed that the average refrigerant heat transfer coefficient increased by 4.6 % for 2.6 % higher frictional pressure drop and the corresponding absolute saturation temperature (absolute Pressure) reduced by 3.2 % at constant mass flux. The reduction of pressure drop on refrigerant as the saturation temperature increased due to reduction in density of R134a. The frictional pressure drop varies from 90% to 95 % of the refrigerant side total pressure drop.

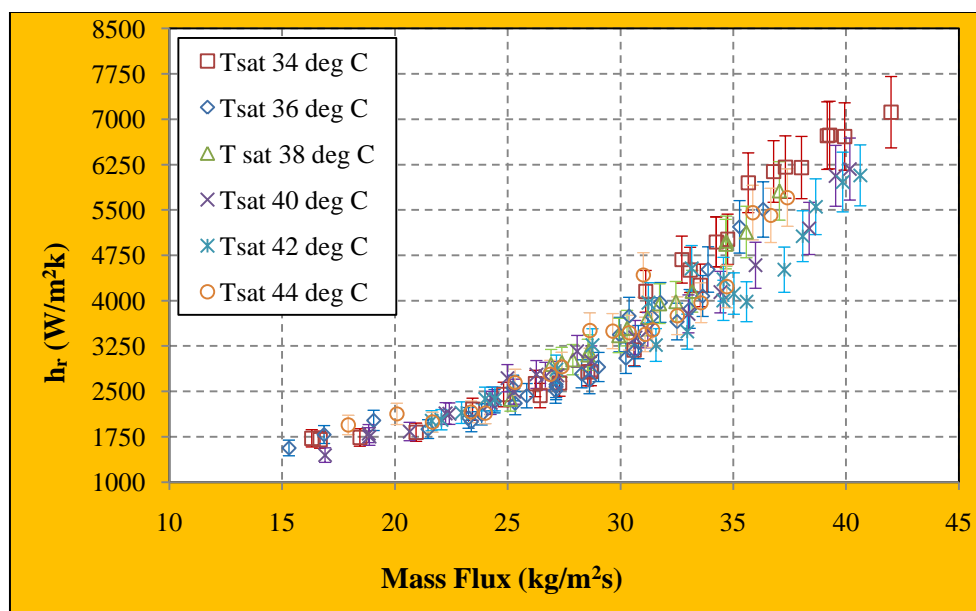


Fig.6.9: Effect of Refrigerant Mass Flux on Two Phase Condensation Heat Transfer Coefficient at Different Saturation Temperatures for Test Condenser 3 (TC3)

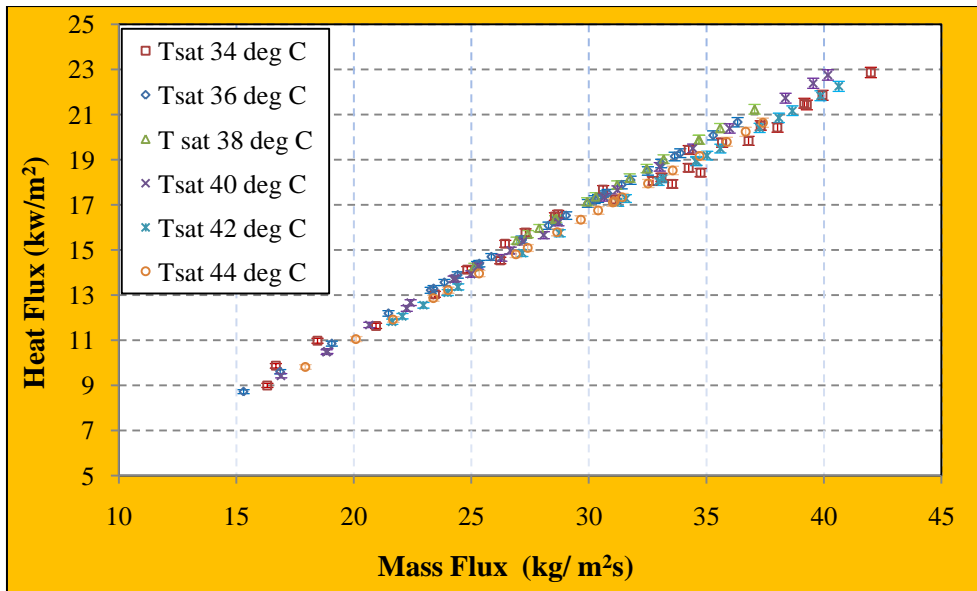


Fig. 6.10: Effect of Refrigerant Mass Flux on Heat Flux at Different Saturation Temperatures for Test Condenser 3 (TC3)

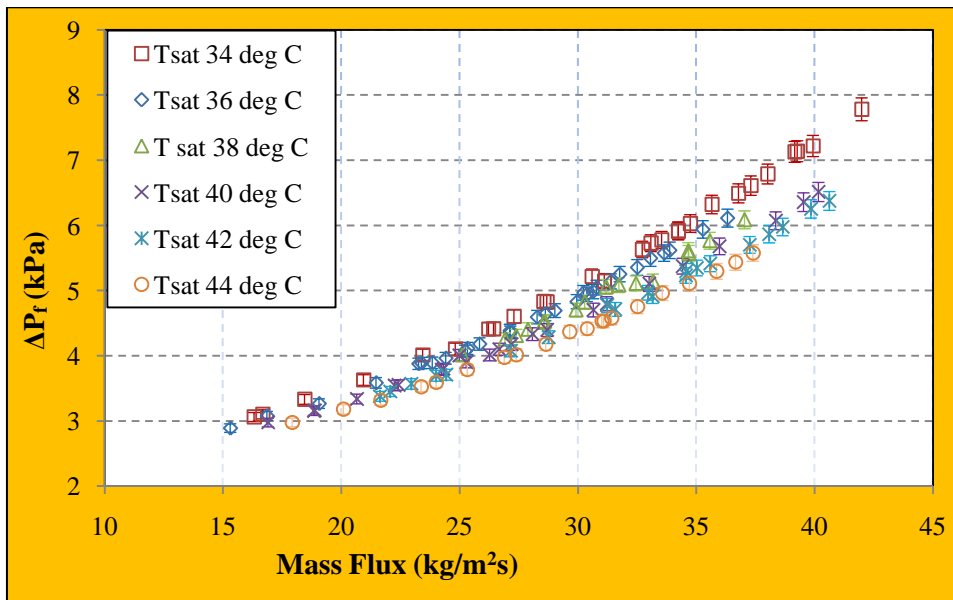


Fig. 6.11: Effect of Refrigerant Mass Flux on Condensation Frictional Pressure Drop at Different Saturation Temperatures for Test Condenser 3 (TC3)

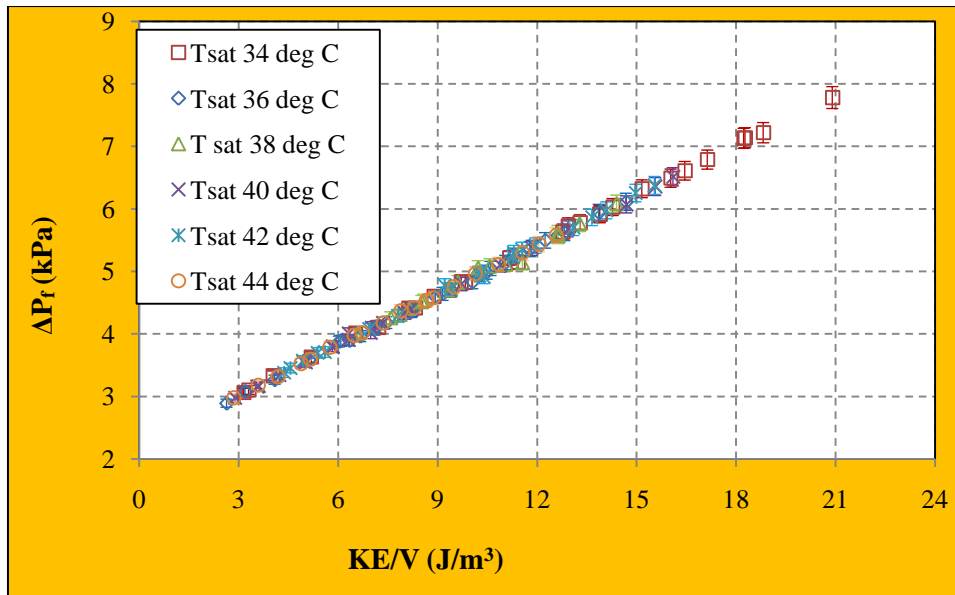


Fig. 6.12: Effect of Kinetic Energy per Unit Volume (KE/V) on Condensation Frictional Pressure Drop at Different Saturation Temperatures for Test Condenser 3 (TC3)

6.1.4 Test Condenser 4 (TC4)

The brazed plate fin heat exchanger fin details are given in Table 6.8.

Table 6.8: Geometric Data of TC4 Fins

Parameter	Unit	Value	
		DM Water side	Refrigerant side
Type		Serrated (Lanced & Offset)	
Material		Aluminium	
Fin frequency	Fins per meter (FPI)	1102.4±5 (28)	708.7±5 (18)
Fin height	mm	5±0.01	5±0.01
Fin thickness	mm	0.127±0.002	0.254±0.002
Serration length	mm	3.175±0.005	
No of layers		2	1
Total heat transfer area	m ²	0.4616±0.00007	0.159±0.00007
Hydraulic diameter	mm	1.3450±0.002	1.8667±0.002

The condensation tests were carried out with R134a down-flow and water horizontal-flow at five different saturated temperatures (32 °C, 34 °C, 36 °C, 42 °C and 44 °C) to determine the effect of saturated temperature on the two phase

condensation heat transfer and frictional pressure drop of R134a inside a brazed plate fin heat exchanger. Table 6.9 indicates the operating conditions in the condenser under experimental tests.

Table 6.9: Operation Conditions during Experimental Tests on TC4

Set	P_{sat} MPa (abs)	T_{sat} (°C)	Runs (Nos)	Quality		G_r (kg/m ² s)	q_r (kW/m ²)
				X_{in}	X_{out}		
1 st	0.813±0.01	32±0.2	20	0.95-1	0-0.07	18-30.5	12-22
2 nd	0.863±0.01	34±0.3	15	0.97-1	0-0.03	22-41	14-28
3 rd	0.912±0.01	36±0.2	10	0.94-1	0-0.06	20-40	13-26
4 th	0.107±0.01	42±0.5	20	0.93-1	0-0.07	21-51	13.5-35
5 th	0.113±0.02	44±0.5	20	0.94-1	0-0.06	21-38	13.5-24.5

The mass flow rate and heat flux of R134a was varied from 18 kg/m²s to 51 kg/m²s and 12 kW/m² to 35 kW/m² respectively in the final test condenser. Fig.6.13 and Fig.6.14 shows the effect of refrigerant mass flux on heat transfer coefficient and heat flux respectively for saturated vapour condensation at different saturation temperatures. Results are indicating that the effect of saturation temperature not much significant on heat transfer coefficient when the mass flux is less than 23 kg/m²s and probably condensation is controlled by gravity, which is shown in the Fig.6.13. For higher refrigerant mass flux (>23 kg/m²s) the heat transfer coefficients depend on mass flux and are well predicted by Akers et al. (1959). It indicates, as the mass flux increases the refrigerant heat flux also increased. The average refrigerant heat transfer coefficient increased by 55.8 % for 45.8 % higher frictional pressure drop and the corresponding mass flux increased by 39.1 %.

Fig.6.14 indicates, as the refrigerant saturation temperature increases the heat flux reduced at same mass flux due to reduction in enthalpy change. The refrigerant density and specific heat are comes down as the refrigerant saturation temperature increased. Fig.6.15 and Fig.6.16 indicates the effect of refrigerant mass flux and kinetic energy per unit volume on frictional pressure drop. Results show that, the frictional pressure drop increases as the mass flux increased. Also, further observed that the average refrigerant heat transfer coefficient increased by 4 % for 9.1 % higher frictional pressure drop and the corresponding absolute saturation temperature (absolute Pressure) reduced by 3.8 % at constant mass flux. The reduction of pressure

drop on refrigerant as the saturation temperature increased due to reduction in density of R134a. The frictional pressure drop varies from 93 % to 97 % of the refrigerant side total pressure drop.

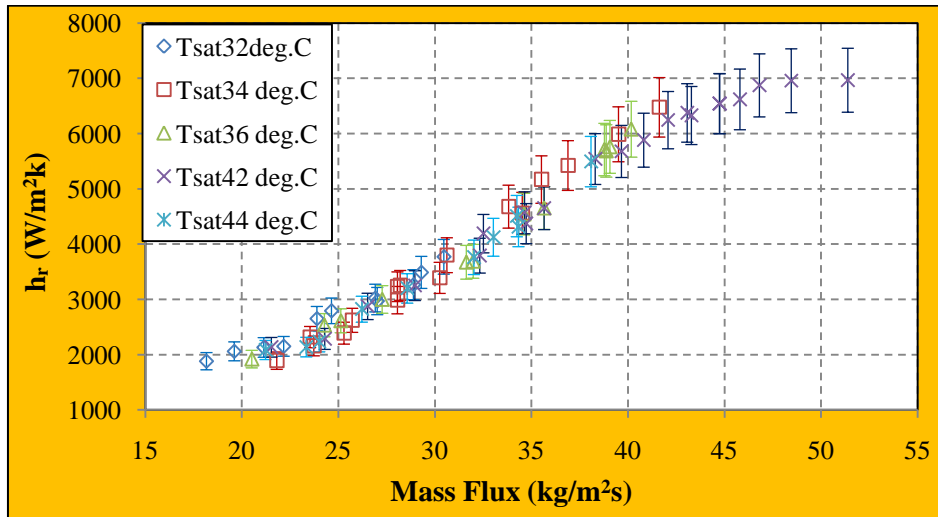


Fig. 6.13: Effect of Refrigerant Mass Flux on Two Phase Condensation Heat Transfer Coefficient at Different Saturation Temperatures for Test Condenser 4 (TC4)

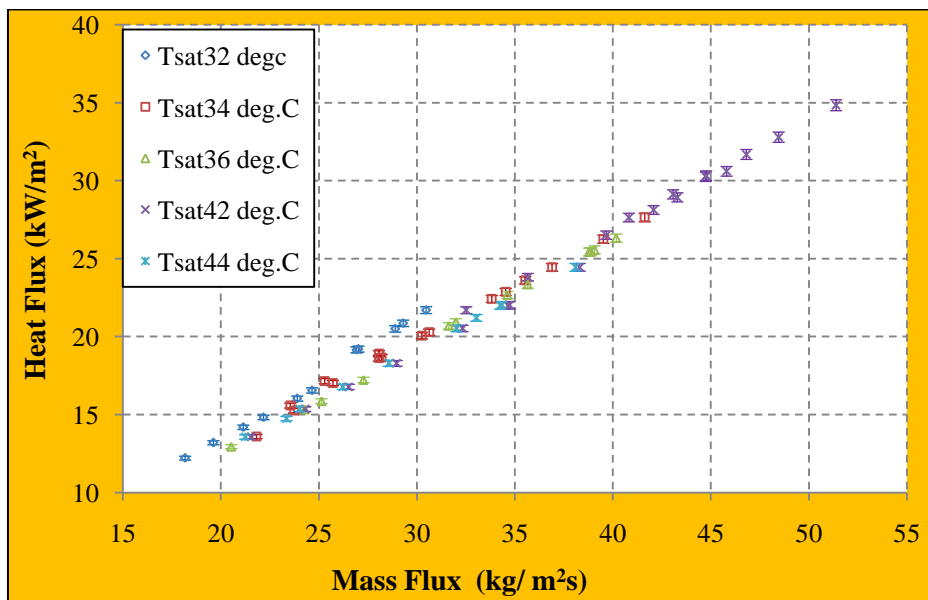


Fig. 6.14: Effect of Refrigerant Mass Flux on Heat Flux at Different Saturation Temperatures for Test Condenser 4 (TC4)

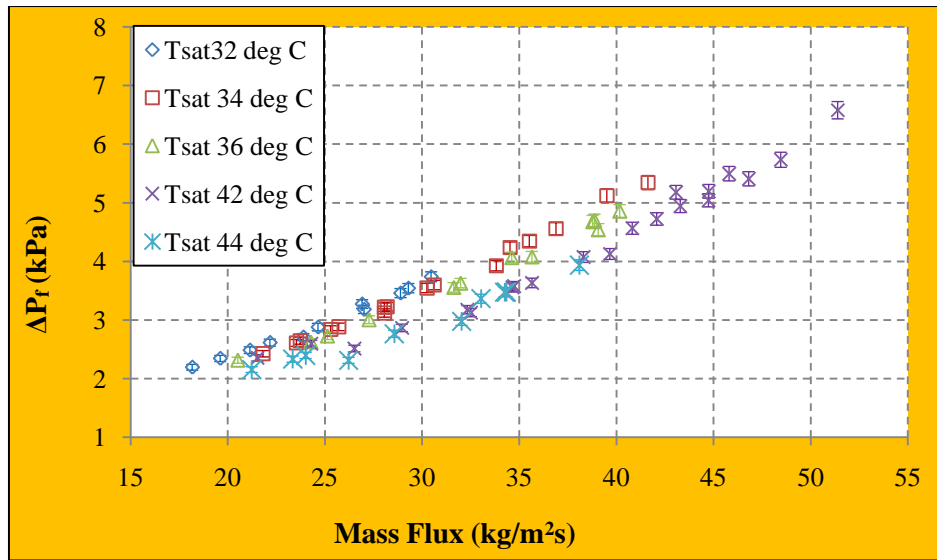


Fig. 6.15: Effect of Refrigerant Mass Flux on Condensation Frictional Pressure Drop at Different Saturation Temperatures for Test Condenser 4 (TC4)

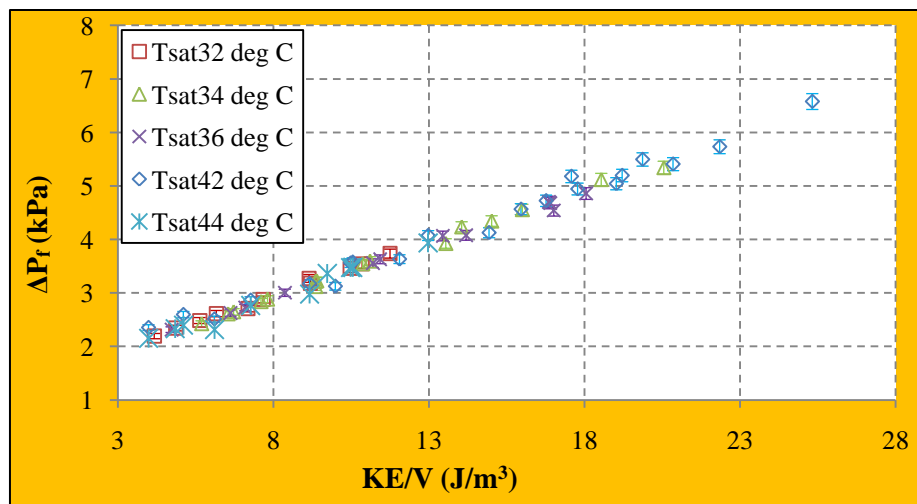


Fig. 6.16: Effect of Kinetic Energy per Unit Volume (KE/V) on Condensation Frictional Pressure Drop at Different Saturation Temperatures for Test Condenser 4 (TC4)

6.2 Development of Correlations

Using experimental results of the selected four types of serrated fin surfaces, empirical correlations are proposed. The development of empirical correlations is discussed below.

6.2.1 Condensation heat transfer coefficient correlations

An exhaustive experimental study has been carried out on the heat transfer phenomena in plate fin surfaces with serrated fins. The refrigerant mass flux versus condensation heat transfer coefficient curves shows significant non-linearity. The correlations have been expressed in terms of equivalent Reynolds number, liquid Prandtl number, liquid thermal conductivity and fin hydraulic diameter. The power law expressions have been used for determining the two phase refrigerant heat transfer coefficient. The two phase refrigerant condensation heat transfer coefficient (h_r) is functionally related to (λ_L/D_h) , Re_{eq} , Pr_L and it can be represented as:

$$h_r = B \left(\frac{\lambda_L}{D_h} \right)^{a_1} Re_{eq}^{a_2} Pr_L^{a_3} \quad (6.1)$$

$$\text{and } Re_{eq} = G[(1 - x) + x \left(\frac{\rho_L}{\rho_g} \right)^{1/2}] D_h / \mu_L$$

Where B, a1, a2 and a3 are arbitrary constants to be estimated from experimental data by multiple regression analysis. The values of coefficients B, a1, a2 and a3 are determined by multiple regression analysis of experimental data. The data analysis tool of MS-EXCEL is used for regression analysis. The estimated values of coefficients for calculating condensation heat transfer coefficient are presented in Table 6.10.

Table 6.10: Values of Coefficients for Condensation Heat Transfer Coefficient

Unit No.	B	a1	a2	a3	R ²	Standard Error	No. of Observations
TC1	6.5139X10 ⁻⁴	0.08826	1.5747	3.7787	0.966	0.0282	170
TC2	6.909X10 ⁻²⁸	12.174	1.594	8.024	0.919	0.046	120
TC3	2.2284X10 ⁻⁴	0.1465	1.6917	3.7301	0.910	0.051	130
TC4	3.0172X10 ⁻²²	9.99534	1.6491	7.2095	0.976	0.027	85

With the values of estimated coefficients as per Table 6.10, the, Eq. 6.1 can be written as Eq.6.2, Eq. 6.3, Eq. 6.4 and Eq.6.5 for TC1, TC2, TC3 and TC4 respectively. The reduced equations given in Eq.6.2 to Eq.6.5 are proposed as empirical correlation for determination of two phase average refrigerant R134a condensation heat transfer coefficient (h_r) for the selected four types of serrated fin

surfaces. The given correlations correctly predict 93% of the h_r data for equivalent Reynolds number range of 600 to 1800, and standard maximum error is 5.1%.

Therefore, the proposed empirical correlation for TC1, TC2, TC3 and TC4 refrigerant side serrated fin surface saturated average R134a refrigerant heat transfer coefficient are given in Eq.6.2, Eq. 6.3, Eq. 6.4 and Eq.6.5 respectively. These are as follows:

$$h_r = 6.5139 \times 10^{-4} \left(\frac{\lambda_L}{D_h}\right)^{0.08826} (Re_{eq})^{1.5747} (Pr_L)^{3.7787} \quad \text{for TC1} \quad (6.2)$$

$$h_r = 6.909 \times 10^{-28} \left(\frac{\lambda_L}{D_h}\right)^{12.174} (Re_{eq})^{1.594} (Pr_L)^{8.024} \quad \text{for TC2} \quad (6.3)$$

$$h_r = 2.2284 \times 10^{-4} \left(\frac{\lambda_L}{D_h}\right)^{0.1465} (Re_{eq})^{1.6917} (Pr_L)^{3.7301} \quad \text{for TC3} \quad (6.4)$$

$$h_r = 3.01722 \times 10^{-22} \left(\frac{\lambda_L}{D_h}\right)^{9.99534} (Re_{eq})^{1.6491} (Pr_L)^{7.2095} \quad \text{for TC4} \quad (6.5)$$

The value of h_r obtained from proposed correlation (Eq. 6.2 to Eq 6.5) are to be compared with actual value from experimental results to verify the correctness of proposed correlation. The graph of predicted value of h_r as a function of experimental value is plotted and the plot is shown in Fig. 6.17 for an experimental data of TC1. The figure indicates that all the values of experimental h_r lies within the band of ± 20 % of the predicted value. The comparison indicates that experimental value lies within the band of ± 20 % of predicted value. From Fig. 6.17, it can be concluded that the developed correlation is giving the value of heat transfer coefficient for serrated fins within ± 20 % accuracy. Similarly for the remaining three test condensers (TC2, TC3 and TC4) the value of h_r obtained from proposed correlation (Eq 6.3 to Eq 6.5) are compared with actual value from experimental results to verify the correctness of proposed correlation. They are given in Fig. 6.18 to Fig.6.20 for the test condensers of TC2 to TC4.

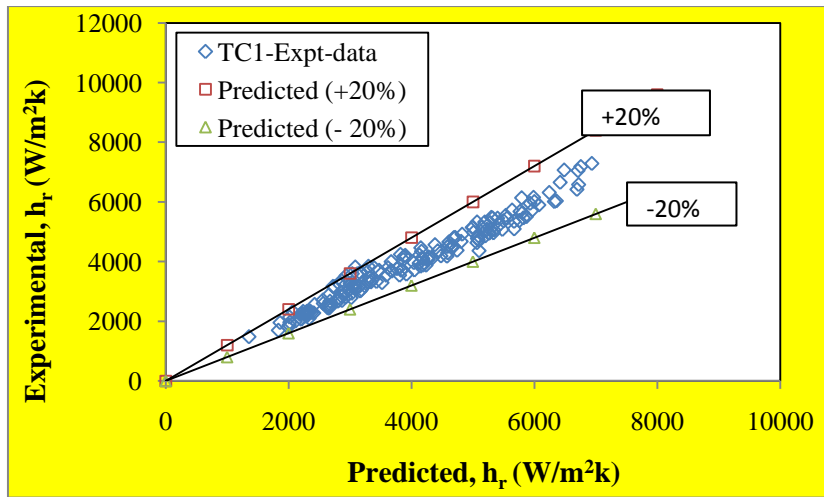


Fig. 6.17: Comparison between Experimental and Predicted h_r in TC1

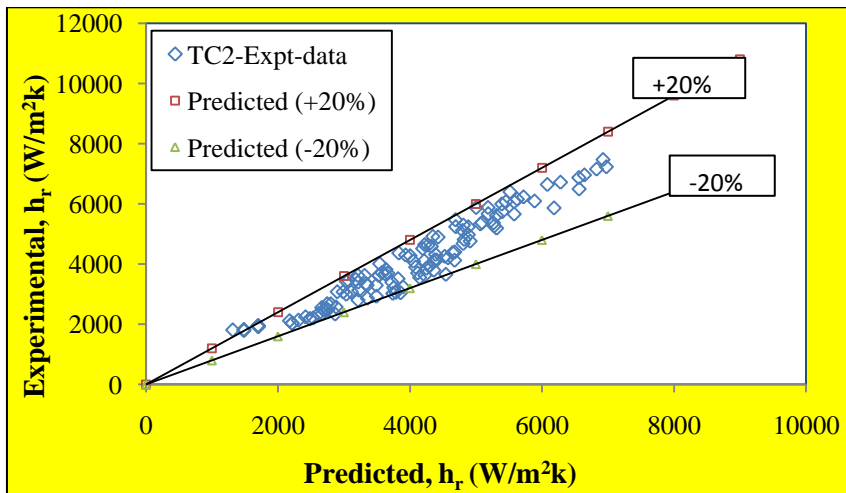


Fig. 6.18: Comparison between Experimental and Predicted h_r in TC2

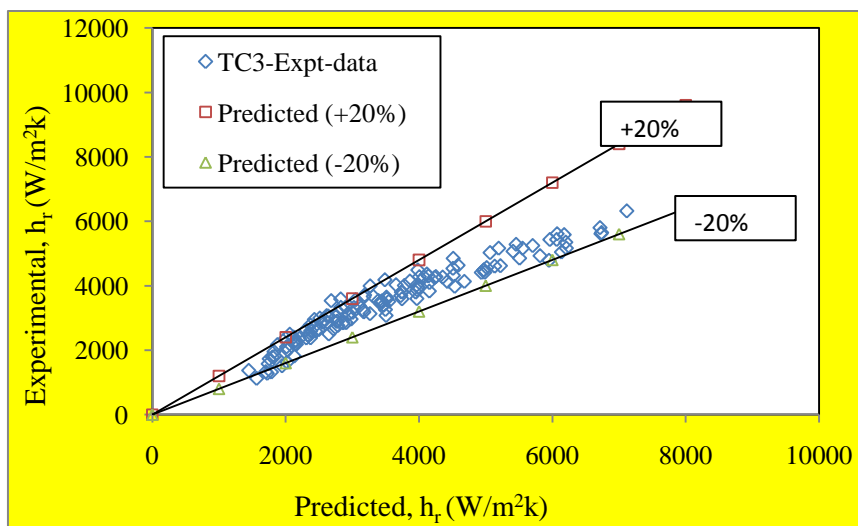


Fig.6.19: Comparison between Experimental and Predicted h_r in TC3

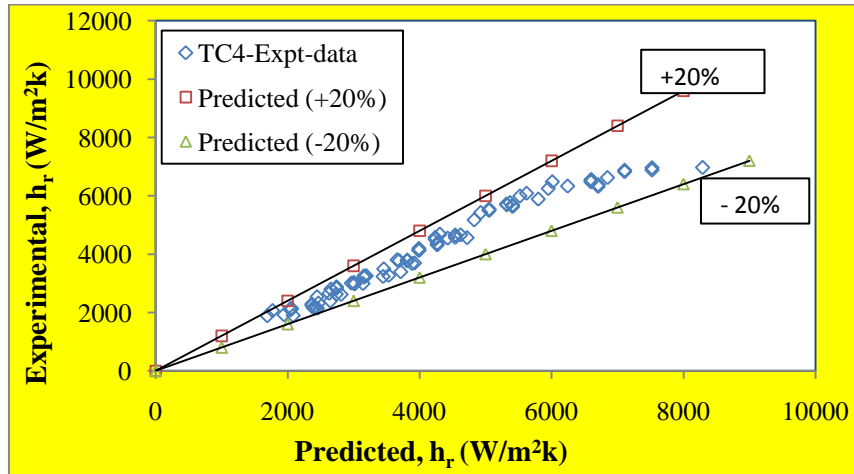


Fig.6.20: Comparison between Experimental and Predicted h_r in TC4

6.2.2 Two phase frictional pressure drop correlations

The refrigerant mass flux versus frictional pressure drop curves shows slight non-linearity. The correlations have been expressed in terms of kinetic energy per unit volume. The power law expressions have been used for determining the two phase refrigerant frictional pressure drop as a function of kinetic energy per unit volume. The two phase serrated fin surface frictional pressure drops are functionally related to kinetic energy per unit volume (KE/V) and it can be represented as:

$$\Delta P_f = C \left(\frac{KE}{V} \right)^{b1} \quad (6.6)$$

where C and b1 are arbitrary constants to be estimated from experimental data by multiple regression analysis.

The values of coefficients C and b1 are determined by multiple regression analysis of experimental data. The data analysis tool of MS-EXCEL is used for regression analysis. The estimated values of coefficients for calculating condensation heat transfer coefficient are presented in Table 6.11.

Table 6.11: Values of Coefficients for Refrigerant Two Phase Frictional Pressure Drop

Unit No.	C	b1	R ²	Standard Error	No. of Observations
TC1	0.88288	0.62	0.993	0.009	170
TC2	2.389	0.283	0.930	0.015	120
TC3	1.654	0.478	0.981	0.0132	130
TC4	0.8875	0.5867	0.974	0.0198	85

With the values of estimated coefficients, the Eq. 6.6 can be written as Eq. 6.7, Eq. 6.8, Eq.6.9 and Eq.6.10. The reduced equations given in Eq.6.7 to Eq.6.10 are proposed as empirical correlation for determination of two phase average refrigerant R134a frictional pressure drop (ΔP_f) for the selected four types of serrated fin surfaces. The given correlations correctly predict 95% of the ΔP_f data for (KE/V) range of 2 to 24 j/m^3 , and standard maximum error is 1.9 %.

Therefore, the proposed empirical correlation for TC1, TC2, TC3 and TC4 refrigerant side serrated fin surface saturated average R134a refrigerant two phase frictional pressure drop are given in Eq.6.7, Eq. 6.8, Eq. 6.9 and Eq.6.10 respectively. These are as follows:

$$\Delta P_f = 0.8828 \left(\frac{KE}{V} \right)^{0.62} \quad \text{for TC1} \quad (6.7)$$

$$\Delta P_f = 2.389 \left(\frac{KE}{V} \right)^{0.283} \quad \text{for TC2} \quad (6.8)$$

$$\Delta P_f = 1.654 \left(\frac{KE}{V} \right)^{0.478} \quad \text{for TC3} \quad (6.9)$$

$$\Delta P_f = 0.8875 \left(\frac{KE}{V} \right)^{0.5867} \quad \text{for TC4} \quad (6.10)$$

The value of ΔP_f obtained from proposed correlations (Eq. 6.7 to Eq. 6.10) are to be compared with actual value from experimental results to verify the correctness of proposed correlation. The graph of predicted value of ΔP_f as a function of experimental value is plotted and the plot is shown in Fig. 6.21 for an experimental data of TC1. The figure indicates that all the values of experimental ΔP_f lies within the band of $\pm 15\%$ of the predicted value. The comparison indicates that experimental value lies within the band of $\pm 15\%$ of predicted value. From Fig. 6.21, it can be concluded that the developed correlation is giving the value of two phase frictional pressure drop for serrated fin within $\pm 15\%$ accuracy. Similarly for the remaining three test condensers (TC2, TC3 and TC4) the value of ΔP_f obtained from proposed correlation (Eq. 6.8 to Eq. 6.10) are compared with actual value from experimental results to verify the correctness of proposed correlation. The comparisons are given in Fig. 6.18 to Fig.6.20 for the test condensers of TC2 to TC4.

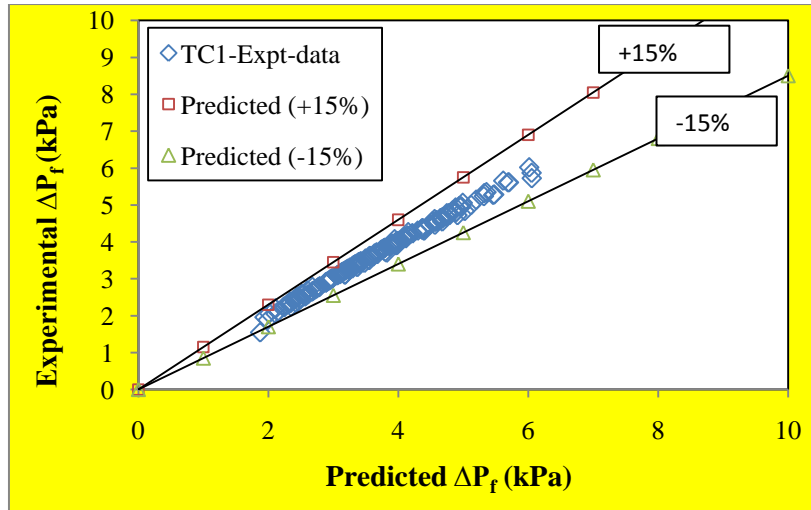


Fig.6.21: Comparison between Experimental and Predicted ΔP_f in TC1

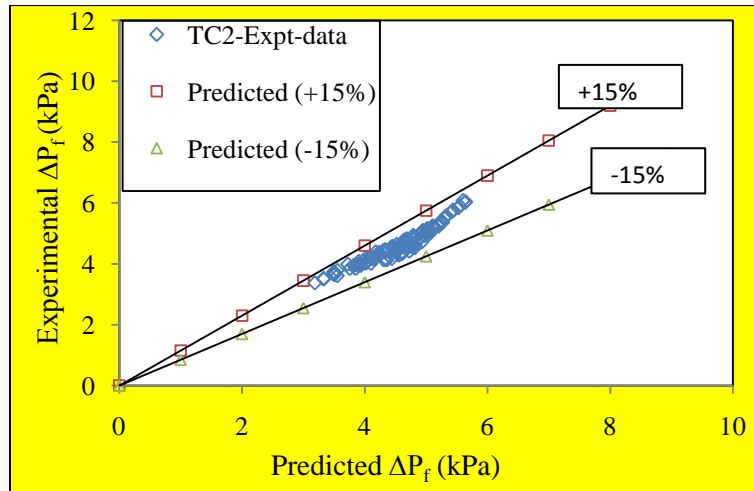


Fig.6.22. Comparison between Experimental and Predicted ΔP_f in TC2

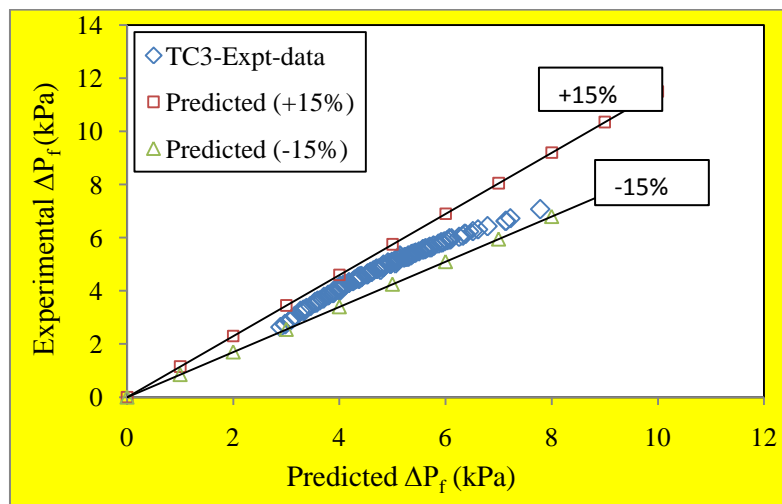


Fig.6.23. Comparison between Experimental and Predicted ΔP_f in TC3

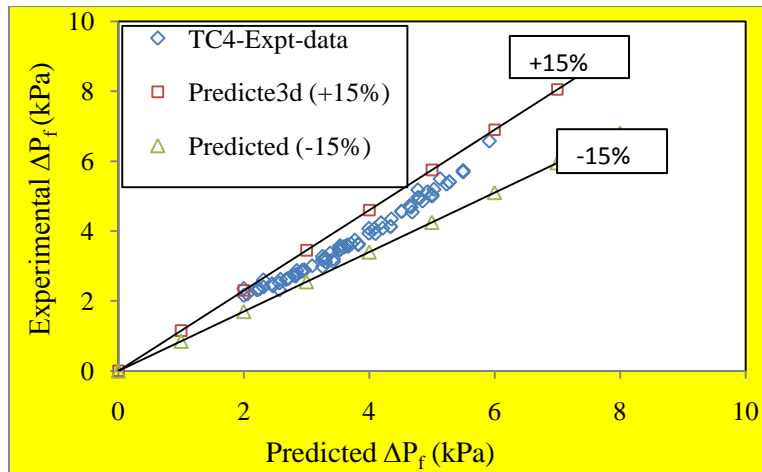


Fig.6.24 Comparison between Experimental and Predicted ΔP_f in TC4

6.3 Influence of Serrated Fin Geometries on Condensation Performance

The influence of hydraulic diameter and fin density on experimental heat transfer coefficient and pressure drop with offset fins for R134a at saturated conditions was discussed. The effects of saturation temperature (pressure), refrigerant mass flux, refrigerant heat flux, effect of fin surface characteristics and fluid properties are investigated. The average condensation heat transfer coefficients and frictional pressure drops were determined experimentally for refrigerant R134a at different saturated temperatures (ranging from 32 °C to 44 °C). The heat transfer coefficients show weak sensitivity to saturation temperature (Pressure) and great sensitivity to refrigerant mass flux and fluid properties. The test condensers are selected with four different hydraulic diameters (1.1894 mm, 1.345 mm, 1.7461 mm and 1.8667 mm) to analyze the affect of heat transfer and pressure drop characteristics. The details of the selected fin geometries are provided in Table 6.12. The influence of fin geometries and condensation performance are discussed below.

6.3.1 Influence of fin geometries on condensation heat transfer coefficient

The condensation experiments and their results are discussed in detail of each test condenser in para 6.1. In refrigerant circuit the selected serrated fins of different fin heights and fin densities. The experiments were carried out with R134a down-flow and water horizontal-flow at four different saturated temperatures (34 °C, 38 °C, 40 °C and 42 °C) on all the selected test condensers to determine the effect of saturated

temperature on the condensation heat transfer of R134a inside a brazed plate fin heat exchangers.

The mass flow rate and heat flux of R134a was varied from 16 to 46 kg/m²s and 7 to 33 kW/m² respectively in the test condenser. The first three test condensers are considered for comparison purpose as the TC4 test unit hydraulic diameter is very near to TC3. Fig. 6.25 and Fig. 6.26 shows the effect of refrigerant mass flux on refrigerant heat transfer coefficient for refrigerant saturated temperatures 34 °C and 40 °C respectively at three different hydraulic diameters of serrated fin geometries.

Table 6.12: Test Condenser Geometric Parameters

Parameter	Unit	Common	TC1	TC2	TC3	TC4
		DM Water side	Refrigerant side			
Type		Serrated (Lanced & Offset)				
Material		Aluminium				
Fin frequency	FPI	1102.4±5 (28)	1181±5 (30)	1102.4±5 (28)	708.7±5 (18)	708.7±5 (18)
Fin height	mm	5±0.01	3.05±0.01	5±0.01	3.8±0.01	5±0.01
Fin thickness	mm	0.127 ± 0.002	0.1016 ± 0.002	0.127 ± 0.002	0.254 ± 0.002	0.254 ± 0.002
Serration length	mm	3.175 ± 0.005	3.175 ± 0.005	3.175 ± 0.005	1.588 ± 0.005	3.175 ± 0.005
No of layers	No.	2	1	1	1	1
Hydraulic diameter	mm	1.3450 ± 0.002	1.1894 ±0.002	1.345 ±0.002	1.7461 ±0.002	1.8667 ±0.002
Heat Transfer Area	m ²	0.4572 ±0.00007	0.1632 ±0.00007	0.2286 ±0.00007	0.1296 ±0.00007	0.1591 ±0.00007
Free flow area	mm ²	1190±5	368±5	595±5	413±5	552±5

Results are indicating that the effect of hydraulic diameter much significant on heat transfer coefficient. When the hydraulic diameter decreases for the same mass flux and heat flux the heat transfer coefficient increased due to increased heat transfer

area. Also, due to capillarity in brazed plate fin surface, the thickness of condensate film reduces and increases the heat transfer coefficient. The effect of refrigerant mass flux on heat transfer coefficients were constant when the mass flux is less than 20 kg/m²s, probably the condensation is controlled by gravity, which is shown in the Fig. 6.25 and Fig. 6.26. The average refrigerant heat transfer coefficient increased by 21% for a 32% reduction of hydraulic diameter and the fin density increased by 40%. The physical phenomenon of two phase refrigerant heat transfer coefficient in serrated fins is the fins boundary layer is periodically interrupted and the thickness of the condensate film reduces. As the hydraulic diameter decreases the vapour shear reduces the thickness of the condensate film and increases the heat transfer coefficient.

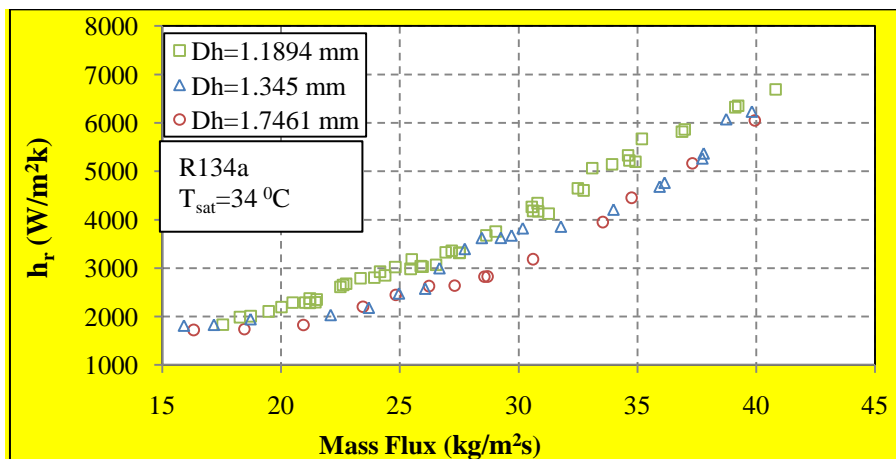


Fig. 6.25: Effect of Refrigerant Mass Flux on Condensation Heat Transfer Coefficient at $T_{sat} = 34$ °C for Different Hydraulic Diameters of Serrated Fin

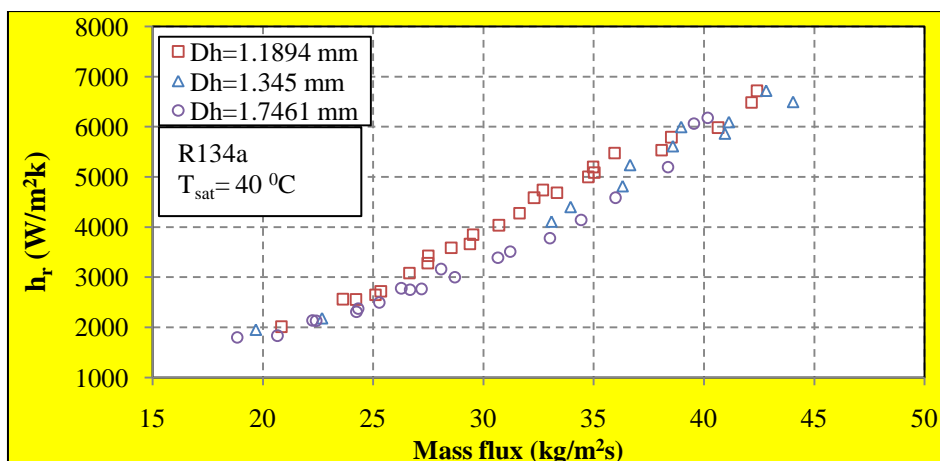


Fig. 6.26: Effect of Refrigerant Mass Flux on Condensation Heat Transfer Coefficient at $T_{sat} = 40$ °C for Different Hydraulic Diameters of Serrated Fin

6.3.1 Influence of fin geometries on two phase frictional pressure drop

The condensation experiments and their results are discussed in detail of each test condenser in para 6.1. In refrigerant circuit the selected serrated fins of different fin heights and fin densities. The experiments were carried out with R134a at four different saturated temperatures (34 °C, 38 °C, 40 °C and 42 °C) on all the selected test condensers to determine the effect of saturated temperature.

In this analysis also, first three test condensers are considered for comparison purpose as the TC4 test unit hydraulic diameter is very near to TC3. Fig. 6.27 and Fig. 6.28 shows the effect of refrigerant mass flux on frictional pressure drop for saturated temperatures of 34 °C and 40 °C respectively at three different hydraulic diameters of serrated fin geometries.

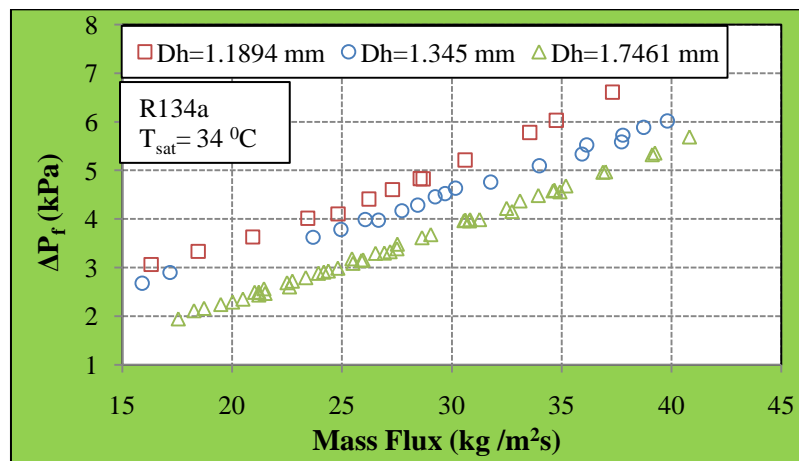


Fig. 6.27: Effect of Refrigerant Mass Flux on Condensation Frictional Pressure Drop (ΔP_f) at $T_{sat}=34\text{ }^{\circ}\text{C}$ for Different Hydraulic Diameters of Serrated Fin

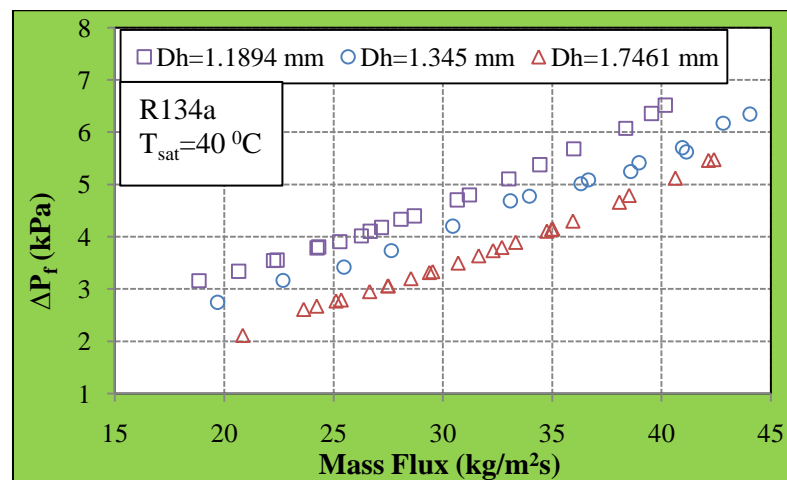


Fig. 6.28: Effect of Refrigerant Mass Flux on Condensation Frictional Pressure Drop (ΔP_f) at $T_{sat}=40\text{ }^{\circ}\text{C}$ for Different Hydraulic Diameters of Serrated Fin

Results are indicating that the effect of hydraulic diameter much significant on frictional pressure drop. The frictional pressure drop varies from 84% to 96% of the refrigerant side total pressure drop. The average refrigerant frictional pressure drop increased by 29% for a 32% reduction of hydraulic diameter and the fin density increased by 40%. The physical phenomenon of two phase frictional pressure drop increase in serrated fins is the fins boundary layer is periodically interrupted and also due to reduction in free flow area. As the hydraulic diameter increases the refrigerant free flow area increases and corresponding fin frictional pressure drop decreases.

At the constant refrigerant mass flux, the average increase in two phase frictional pressure drop is 29% and corresponding rise in refrigerant saturated heat transfer coefficient is 21%.

6.4 Influence of Condensation Phenomena in the Presence of Lubricating Oil in R134a

The lubricating oil mixing has an affect on average condensation heat transfer coefficient and frictional pressure drop. Lubricating oil mixing will decrease the condensation heat transfer coefficient and increase the frictional pressure drop. Maximum precautions are taken to minimize the oil mixing in the refrigerant circuit of test rig. In the refrigerant circuit, two levels of lubrication oil separators are provided. Each individual compressor has oil separator and also a common oil separator in the refrigerant circuit. The oil mass fraction was measured before and after experimentation and it was found that the maximum percentage of lubricating oil mass fraction present in the mixture was 0.85%. In practical cases compressors has to run with lubrication oil. It may be unavoidable. In experimental set up, the experiments were not conducted with pure R134a, since compressors requires lubrication. Further, Mohammed and Jocelyn (2008) admitted that the condenser is the least sensitive component to the presence of a lubricant.

In-tube condensation of mixture of R134a and ester oil was well explained by Bassi and Bansal (2002) and Fukushima and Kudou (1990). The experimental results are indicated that 10 % oil mass fraction will decrease the heat transfer coefficient by 20% and pressure drop increases by 1.4 times than that of pure refrigerant R134a. In experimentation the maximum oil mass fraction was 0.85%. Hence, by co-relating

above results decrease in condensation heat transfer coefficient was only 1.7 % and increase in frictional pressure drop by 0.034 times than the Pure R134a. The condensation heat transfer coefficient decreases and pressure drop increases gradually with an increase in the oil mass fraction with pure R134a. The experimental results are provided with 0.85% oil mass fraction. The average condensation heat transfer coefficient decreased about 1.7% and frictional pressure drop increased about 0.034 times at 0.85% oil mass fraction to that of pure refrigerant.

6.5 Exploration of Condensation Correlations

Fig.6.29 indicates the comparison between experimental and predicted (proposed) condensation average refrigerant heat transfer coefficient correlation to the present data. It shows that most of the experimental values are within $\pm 20\%$. Fig.6.30 shows the comparison between experimental and predicted (proposed) condensation frictional pressure drop correlation to the present data. It is found that the average deviation is about $\pm 20\%$ between the frictional pressure drop correlation and the measured data.

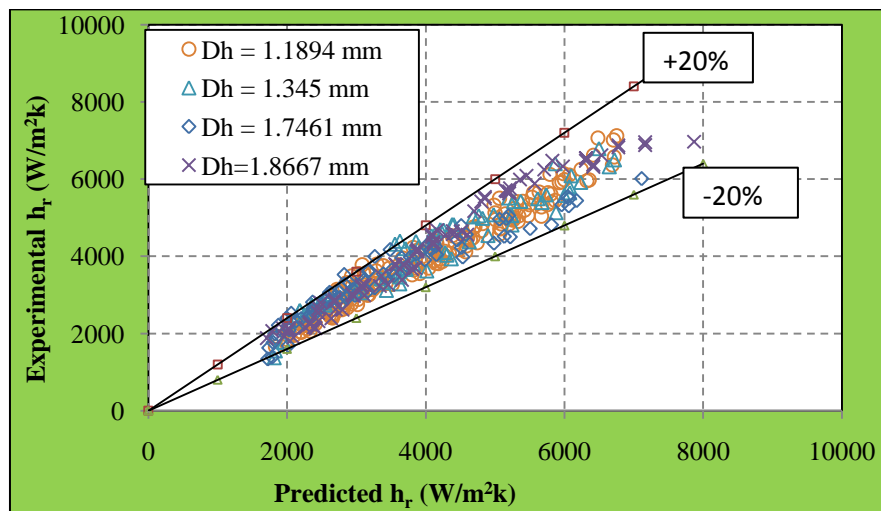


Fig.6.29: Comparison between Experimental h_r and Predicted h_r

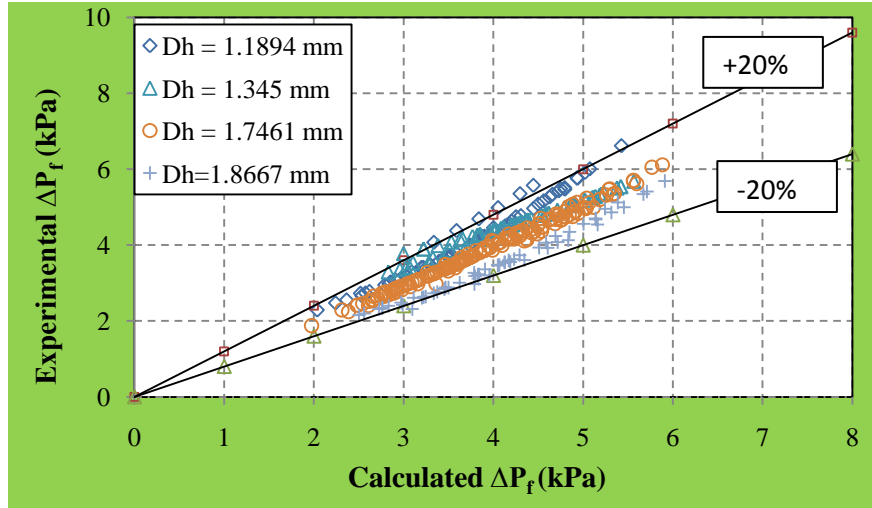


Fig.6.30: Comparison between Experimental ΔP_f and Predicted ΔP_f

The two phase refrigerant condensation heat transfer coefficient (h_r) is functionally related to (λ_L/D_h) , Re_{eq} and Pr_L , it can be represented as:

$$h_r = B \left(\frac{\lambda_L}{D_h} \right)^{a1} Re_{eq}^{a2} Pr_L^{a3} \quad (6.11)$$

Where B, a1, a2 and a3 are constants.

Therefore, the proposed equation for the selected serrated fin surfaces as follows:

$$h_r = 1.786 \times 10^{-4} \left(\frac{\lambda_L}{D_h} \right)^{0.271} Re_{eq}^{1.5947} Pr_L^{4.105} \quad (6.12)$$

The above correlations correctly predict 94% of the h_r data for equivalent Reynolds number range of 600 to 1800, and root-mean-square error is 3.8%.

Similarly, the two phase serrated fin surface frictional pressure drops are functionally related to KE/V and it can be expressed as:

$$\Delta P_f = C \left(\frac{KE}{V} \right)^{b1} \quad (6.13)$$

where C and b1 are constants.

Therefore, the proposed equation for this particular serrated fin surface as follows:

$$\Delta P_f = 1.2556 \left(\frac{KE}{V} \right)^{0.4987} \quad (6.14)$$

The above correlations correctly predict 87% of the ΔP_f data for equivalent Reynolds number range of 600 to 1800, and root-mean-square error is 4.3 %. The correlations are explored for the serrated fin surfaces of hydraulic diameter ranging from 1.11894 mm to 1.8667 mm and serrated fin density ranging from 18 FPI to 30 FPI with lubricating oil mass fraction of 0.85%. The experimental results follow the same trend as presented by different authors [Kang et al.(2000), Han et al.(2005), Longo et al.(2004), Jokar et al.(2004), Wang et al.(1999), Longo(2008,2009 & 2010), Jokar et al.(2006) and Longo & Gasparella (2007)]. An empirical correlation was proposed on the basis of the experimental results for the calculation of the average condensation heat transfer coefficient and frictional pressure drop.

CHAPTER 7

CONCLUSIONS AND SCOPE FOR FUTURE WORK

7.1 Conclusions

Condensation saturated refrigerant heat transfer and frictional pressure drop data for serrated fin surfaces are not readily available in open literature. Most available data remain proprietary information of the concerned institutions. Compact plate fin heat exchangers with four different types of serrated fins are successfully designed and developed in M/s BHEL, Heavy Plate and Vessels Plant, Visakhapatnam in India. An experimental test rig has been setup at NAL, Bangalore in India and calibrated successfully with known plate heat exchanger. It has been tested plate fin heat exchangers with serrated fin surfaces of different geometrical parameters.

The Condensation heat transfer and frictional pressure drop study is made at steady state saturated conditions. The contamination of oil in the refrigerant during experiments was estimated as 0.85% maximum. The findings of the study are presented here.

- ❖ The generalized correlation for water side heat transfer coefficient for the selected serrated fin surface are developed using CFD tool ANSYS Fluent in laminar and turbulent range are as follows:

for Laminar Range ($100 \leq Re \leq 800$)

$$Nu_w = 0.049 Re_w^{0.69} Pr^{\frac{1}{3}},$$

$$\text{Then } h_w = 0.049 \left(\frac{\lambda_w}{D_h}\right) Re_w^{0.69} Pr^{\frac{1}{3}}$$

for Turbulent Range ($1000 \leq Re \leq 15000$)

$$Nu_w = 0.016 Re_w^{0.85} Pr^{\frac{1}{3}},$$

$$\text{Then, } h_w = 0.016 \left(\frac{\lambda_w}{D_h}\right) Re_w^{0.85} Pr^{\frac{1}{3}}$$

The above correlations correctly predict 96% of the j data for laminar and turbulent regions lies within $\pm 8\%$ and root-mean-square error is 3.2%.

- ❖ In TC1, h_r value increased by 47% for 40.7% higher ΔP_f and the corresponding mass flux increased by 34.7%. In TC2, h_r value increased by 57.7 % for 37.3 % higher ΔP_f and the corresponding mass flux increased by 32.9 %. In TC3, h_r value increased by 60.7 % for 46.9 % higher ΔP_f and the corresponding mass flux increased by 36.1 %. In TC4, h_r value increased by 55.8 % for 45.8 % higher ΔP_f and the corresponding mass flux increased by 39.1 %.
- ❖ Empirical correlations are developed by using power law equation and regression analysis for four types of fins separately. The proposed empirical correlations for saturated average R134a refrigerant heat transfer coefficient (h_r) and frictional pressure drop (ΔP_f) for a serrated fin surface hydraulic diameters of ranged from 1.1894 mm, 1.345 mm, 1.7461 mm and 1.8667 mm are given below.

Unit No.	h_r (w/m ² k) Correlations	ΔP_f (kPa) Correlations
TC1	$h_r = 6.5139 \times 10^{-4} * \left(\frac{\lambda_L}{D_h}\right)^{0.08826} (Re_{eq})^{1.5747} (Pr_L)^{3.7787}$	$\Delta P_f = 0.8828 \left(\frac{KE}{V}\right)^{0.62}$
TC2	$h_r = 6.909 \times 10^{-28} * \left(\frac{\lambda_L}{D_h}\right)^{12.174} (Re_{eq})^{1.594} (Pr_L)^{8.024}$	$\Delta P_f = 2.389 \left(\frac{KE}{V}\right)^{0.283}$
TC3	$h_r = 2.2284 \times 10^{-4} * \left(\frac{\lambda_L}{D_h}\right)^{0.1465} (Re_{eq})^{1.6917} (Pr_L)^{3.7301}$	$\Delta P_f = 1.654 \left(\frac{KE}{V}\right)^{0.478}$
TC4	$h_r = 3.1072 \times 10^{-22} * \left(\frac{\lambda_L}{D_h}\right)^{9.9534} (Re_{eq})^{1.6491} (Pr_L)^{7.2095}$	$\Delta P_f = 0.8875 \left(\frac{KE}{V}\right)^{0.5867}$

The correlations are applicable for equivalent Reynolds number range of 600 to 1800 for refrigerant saturated conditions of serrated fins used for experiments. The correlations of condensation refrigerant heat transfer coefficients are accurate within a variation band of $\pm 20\%$ while correlations of frictional pressure drop are accurate within a variation band of $\pm 15\%$. The correlations are established with oil contamination of 0.85% in refrigerant R134a.

- ❖ Studied the influence of hydraulic diameter on condensation heat transfer coefficient and frictional pressure drop. The results indicated that the average refrigerant heat transfer coefficient increased by 21% for a 32% reduction of

hydraulic diameter and the fin density increased by 40%. The average refrigerant frictional pressure drop increased by 29% for a 32% reduction of hydraulic diameter and the fin density increased by 40%.

- ❖ The average h_r and ΔP_f experimentally determined have uncertainty with $\pm 16.7\%$ and $\pm 4.5\%$ respectively.
- ❖ The correlations are explored for serrated fin surface hydraulic diameter ranges from 1.1894 mm to 1.8667 mm and fin density ranges from 10 FPI (393.7 fins per meter) to 30 FPI (1181 fins per meter) with lubricating oil mass fraction of 0.85% as:

Unit No	h_r (w/m ² k) Correlations	ΔP_f (kPa) correlation
TC1, TC2 TC3 & TC4	$h_r = 1.786 \cdot 10^{-4} * \left(\frac{\lambda_L}{D_h}\right)^{0.271} * (Re_{eq})^{1.5947} * (Pr_L)^{4.105}$	$\Delta P_f = 1.2556 * \left(\frac{KE}{V}\right)^{0.4987}$

The above h_r correlations correctly predict 94% of the h_r data for equivalent Reynolds number range of 600 to 1800, and root-mean-square error is 3.8%. The above ΔP_f correlations correctly predict 87% of the ΔP_f data for equivalent Reynolds number range of 600 to 1800, and root-mean-square error is 4.3 %.

- ❖ The condensation heat transfer coefficient decreases and pressure drop increases gradually with an increase in the lubricating oil mass fraction with pure R134a. The experimental results are provided with 0.85% oil mass fraction. The average condensation heat transfer coefficient decreased about 1.7% and frictional pressure drop increased about 0.034 times at a 0.85% oil mass fraction to that of pure refrigerant.
- ❖ Based on the open literature, the correlations are explored for serrated fin surface hydraulic diameter ranges from 1.1894 mm to 1.8667 mm and fin density ranges from 10 FPI (393.7 fins per meter) to 30 FPI (1181 fins per meter) using pure R134a as working fluid were developed to predict the average condensation heat transfer coefficient and frictional pressure drop as:

Unit No	$h_{r-no\ oil}$ (w/m ² k) Correlation	$\Delta P_{f-no\ oil}$ (kPa) correlation
TC1,TC2 TC3& TC4	$h_{r-no\ oil} = 1.7556 * 10^{-4} * \left(\frac{\lambda_L}{D_h}\right)^{0.271} * (Re_{eq})^{1.5947} * (Pr_L)^{4.105}$	$\Delta P_{f-no\ oil} = 1.2983 * \left(\frac{KE}{V}\right)^{0.4987}$

- ❖ Studied the four types serrated fin geometry surfaces on condensation heat transfer coefficient and frictional pressure drop. The results of serrated fin geometry used in TC2 on refrigerant circuit indicated that the average refrigerant heat transfer coefficient increased by 57.7% and for the average refrigerant frictional pressure drop increased by 37.25% for a 32.9% rise of refrigerant mass flux. Compared to other serrated fin geometry surfaces TC2 gives the best results with respect to average heat transfer coefficient and frictional pressure drop.

7.2 Scope for Future Work

- ❖ Effect of different fin surfaces like wavy, plain, perforated fins etc. on the condensation heat transfer coefficient and frictional pressure drop can be assessed.
- ❖ Condensation heat transfer coefficient and frictional pressure drop can be assessed with different environmental friendly refrigerants with zero global warming potential and ozone depletion like HFO1234ze.
- ❖ The present study can be extended to numerical study as the cost of experiments is very expensive.

REFERENCES

Journal References:

Akers, W., Deans, O.K., Crosser, O.K. (1958). "Condensation heat transfer within horizontal tubes." *Chem. Eng. Prog.*, 54, 89–90.

Akers, W., Deans, O.K., Crosser, O.K. (1959). "Condensation heat transfer within horizontal tubes." *Chem. Eng. Prog. Symp.*, 55, 171–176.

Amano, R.S. (1985). "A Numerical Study of Laminar and Turbulent Heat Transfer in a Periodically Corrugated Wall Channel." *Transactions of ASME, J.Heat Transfer*, 107, 564-569.

Amano, R.S., Bagherlee, A., Smith, R.J., Niess, T.G. (1987). "Turbulent Heat Transfer in Corrugated-Wall Channels With and Without Fins." *Transactions of ASME, J. Heat Transfer.*, 109, 62-67.

Amir Jokar, Mohammad, H.H., Steven, J.E. (2006). "Dimensional analysis on the evaporation and condensation of refrigerant R-134a in minichannel plate heat exchangers." *Appl. Therm. Eng.*, 26, 2287–2300.

Asako, Y., Faghri, M. (1987). "Finite-Volume Solutions for Laminar Flow and Heat Transfer in a Corrugated Duct." *Transactions of ASME, J.Heat Transfer.*, 109, 627-634.

Bandhauer, T.M., Agarwal, A., Garimella, S. (2006). "Measurement and modeling of condensation heat transfer coefficients in circular microchannels." *J. Heat Transfer.*, 128, 1050–1059.

Bassi, R., Bansal, P.K. (2003). "In-tube condensation of mixture of R134a and ester oil: empirical correlations." *Int. J. Refrig.*, 26, 402–409.

- Bhowmik, H., Kwan, S.L. (2009). "Analysis of Heat Transfer and Pressure Drop Characteristics in an Offset strip fin Heat Exchanger." *Int. Commun. Heat Mass Transfer.*, 36, 259-263.
- Cavallini, A., Censi, G., Del, C.D., Doretti, L., Longo, G.A., Rossetto, L. (2001). "Experimental investigation on Condensation heat transfer and Pressure drop of new HFC refrigerants (R134a, R125, R32, R410A, R236ea) in a horizontal smooth tube." *Int. J. Refrig.*, 24, 73-87.
- Cavallini, A., Del, C.D., Doretti, L., Matkovic, M., Rossetto, L., Zilio, C. (2005). "Two-phase frictional pressure gradient of R236ea, R134a and R410A inside multi-port mini-channels." *Exp. Therm. Fluid Sci.*, 29, 861–870.
- Chang, Y.P., Pega, H. (2009). "CO₂ flow condensation heat transfer and pressure drop in multi-port microchannels at low temperatures." *Int. J. Refrig.*, 32, 1129–1139.
- Ciofalo, M., Stasiek, J., Collins, M.W. (1996). "Investigation of Flow and Heat Transfer in Corrugated Passages-II. Numerical Simulations". *Int. J. Heat Mass Transfer.*, 39, 165-192.
- Cowell, T.A. (1990). "A General method for the comparison of compact heat transfer surfaces." *ASME J. Heat Transfer.*, 112, 288-294.
- Cur, N., Sparrow, E.M. (1979). "Measurements of Developing and Fully Developed Heat Transfer Coefficients along a Periodically Interrupted Surface." *Transactions of ASME, J. Heat Transfer.*, 101, (1979) 211-216.
- Farahani, F.V., Agostini, B., Thome, J.R. (2013). "Experimental study on flow boiling heat transfer of multiport tubes with R245fa and R1234ze(E)." *Int. J. Refrig.*, 36, 335-352.
- Focke, W.W., Zachariades, J., Olivier, I. (1985). "The Effect of the Corrugation Inclination Angle on the Thermo-hydraulic Performance of Plate Heat Exchangers." *Int. J. Heat Mass Transfer.*, 28, 1469-1479.

Friedel, L. (1987). "Improved friction pressure drop correlation for horizontal and vertical two-phase pipe flow." *European Two-Phase Flow*, Ispra, Italy, 2.

García-Cascalesa, J.R., Vera-García, F. (2007). "Assessment of boiling and condensation heat transfer correlations in the modelling of plate heat exchangers." *Int. J. Refrig.*, 30, 1029-1041.

García-Cascalesa, J.R., Vera-García, F. (2010). "Compact heat exchangers modelling: Condensation." *Int. J. Refrig.*, 33, 135 –147.

Garimella, S. (2004). "Condensation flow mechanism in micro-channel: basis for pressure drop and heat transfer model." *Heat Trans. Eng.*, 25 (3), 104–116.

Giovanni, A.L. (2008). "Refrigerant R134a condensation heat transfer and pressure drop inside a small brazed plate heat exchanger." *Int. J. Refrig.*, 31, 780-789.

Giovanni, A.L. (2009). "R410A condensation inside a commercial brazed plate heat exchanger." *Exp. Therm. Fluid sci.*, 33, 284-291.

Giovanni, A.L., Claudio, Z. (2013). "Condensation of the low GWP refrigerant HFC1234yf inside a brazed plate heat exchanger." *Int. J. Refrig.*, 36, 612-621.

Giovanni, A.L. (2010). "Heat Transfer and pressure drop during hydrocarbon refrigerant condensation inside a brazed plate heat exchanger." *Int. J. Refrig.*, 33, 944-953.

Goldstein, L.J., Sparrow, E.M. (1977). "Heat and Mass Transfer Characteristics for Flow in a Corrugated Wall Channel." *Transactions of ASME, J. Heat Transfer.*, 99, 187-195.

Gstoehl, D., Thome, J.R. (2006^a). "Film Condensation of R-134a on Tube Arrays With Plain and Enhanced Surfaces: Part I Experimental Heat Transfer Coefficients." *Int. J. Heat Transfer.*, 128, 21-32.

- Gstoehl, D., Thome, J.R. (2006^b). "Film Condensation of R-134a on Tube Arrays With Plain and Enhanced Surfaces:Part II—Experimental Heat Transfer Coefficients." *Int. J. Heat Transfer.*, 128, 33-43.
- Han, J.T., Lin, C.X., Ebadian, M.A. (2005). "Condensation heat transfer and pressure drop characteristics of R-134a in an annular helical pipe." *Int. Commun. Heat Mass Transfer.*, 32, 1307-1316.
- Hwang, S.D., Jang, I.H., Cho, H.H. (2006). "Experimental Study on Flow and Local Heat and Mass Transfer Characteristics Inside Corrugated Duct." *Int. J. Heat Fluid Flow.*, 27, 21-32.
- Jokar, A., Eckels S.J., Hosni, M.H., Giolda, T.P. (2004). "Condensation heat transfer and pressure drop of the brazed plate heat exchangers using R-134a." *J. Enhanced Heat Transfer.*, 11 (2), 161–182.
- Jokar, A., Hosni, M.H., Eckels, S.J. (2006). "Dimensional Analysis on the evaporation and condensation of refrigerant R-134a in minichannels plate heat exchanger." *Appl. Therm. Eng.*, 26, 2287-2300.
- Jongmin, S., Samchul, H. (2002). "The effect of hydrophilicity on condensation over various types of fin-and-tube heat exchangers." *Int. J. Refrig.*, 25, 688–694.
- Joshi, H.M., Webb, R.L. (1987). "Heat Transfer and Friction in the Offset Strip-Fin Heat Exchanger." *Int. J. Heat Mass Transfer.*, 30, 69-84.
- Kang, H.J., Lin, C.X., Ebadian, M.A. (2000). "Condensation of R134a flowing inside helicoidal pipe." *Int. J. Heat Mass Transfer.*, 43, 2553-2564.
- Kim, B., Sohn, B. (2006). "An experimental study of flow boiling in a rectangular channel with offset strip fins." *Int. J. Heat Fluid Flow.*, 27, 514-521.
- Kumar, R., Varma, H.K., Agrawal, K.N., Mohanty, B.A. (2001). "Comprehensive study of modified Wilson plot technique to determine the heat transfer coefficient during condensation of steam and R-134a over single horizontal plain and finned tubes." *Heat Transfer Eng.*, 22, 3-12.

Lauder, B.E., Spalding, D.B. (1972). "Turbulent Models and Their Application to the Prediction of Internal Flows." *Heat Fluid Flow.*, 2, 43-54.

Linlin, W., Chaobin, D., Eiji, H. (2012). "Experimental study on condensation heat transfer and pressure drop of low GWP refrigerant FO1234yf in a horizontal tube." *Int. J. Refrig.*, 35, 1418 – 1429.

Lockhart, R.W., Martinelli, R.C. (1949). "Proposed correlation of data for isothermal two-phase two-component flow in pipes." *Chem. Eng. Prog.*, 45, 39–48.

Longo, G.A., Gasparella, A., Sartori, R. (2004). "Experimental heat transfer coefficients during refrigerant vaporisation and condensation inside herringbone-type plate heat exchangers with enhanced surfaces." *Int. J. Heat Mass Transfer.*, 47, 4125-4136.

Longo, G.A., Gasparella, A. (2007). "Refrigerant R134a vaporisation heat transfer and pressure drop inside a small brazed plate heat exchanger." *Int. J. Refrig.*, 30, 821-830.

Longo, G.A., Gasparella, A., Sartori, R. (2004). "Experimental heat transfer coefficients during refrigerant vaporisation and condensation inside herringbone-type plate heat exchangers with enhanced surfaces." *Int. J. Heat Mass Transfer.*, 47, 4125-4136.

Manglik, R.M., Bergles, E. (1995). "Heat Transfer and Pressure Drop Correlations for the Rectangular Offset Strip Fin Compact Heat Exchanger." *Exp. Therm. Fluid Sci.*, 10, 171-180.

Manglik, R.M., Zhang, J., Arun Muley. (2005). "Low Reynolds Number Forced Convection in Three-Dimensional Wavy Plate Fin Compact Channels: Fin Density Effects." *Int. J. Heat Mass Transfer.*, 48, 1439-1449.

Mohammed, Y., Jocelyn, B. (2008). "The effect of oil in refrigeration: Current research issues and critical review of thermodynamic aspects." *Int. J. Refrig.*, 31, 165-179.

- Mochizuki, S., Yagi, Y., Yang, W.J. (1987). "Transport Phenomena in Stacks of Interrupted Parallel-Plate Surfaces." *Exp. Heat Transfer.*, 1, 127-140.
- Mueller, A.C., Chiou, J.P. (1988). "Review of Various Types of Flow Maldistribution in Heat Exchangers." *Heat Transfer Eng.*, 9, 36-50.
- Nusselt, W. (1916). "Die oberflächenkondensation des wasserdampfes." *Z.Ver. Dt Ing.*, 60 (541-546), 569-575.
- O'Brien, J.E., Sparrow, E.M. (1982). "Corrugated-Duct Heat Transfer, Pressure Drop, and Flow Visualization." *Transactions of ASME, J. Heat Transfer.*, 104, 410-416.
- Park, J.E., Vakili-Farahani, F., Consolini, L., Thome, J.R. (2011). "Experimental study on condensation heat transfer in vertical minichannels for new refrigerant R1234ze(E) versus R134a and R236fa." *Exp. Therm. Fluid Sci.*, 35, 442-454.
- Patankar, S.V., Liu, C.H., Sparrow, E.M. (1977). "Fully Developed Flow and Heat Transfer in Ducts Having Streamwise-Periodic Variations of Cross-Sectional Area." *Transactions of ASME, J. Heat Transfer.*, 99, 180-186.
- Patankar, S.V., Prakash, C. (1981). "An Analysis of the Effect of Plate Thickness on Laminar Flow and Heat Transfer in Interrupted-Plate Passages." *Int. J. Heat Mass Transfer.*, 24, 1801-1810.
- Patel, V.C., Tyndall, C.J., Yoon, J.Y. (1991^a). "Laminar Flow Over Wavy Walls." *Transactions of ASME, J. Fluids Eng.*, 113, 574-577.
- Patel, V.C., Tyndall, C.J., Yoon, J.Y. (1991^b). "Turbulent Flow in a Channel With a Wavy Walls." *Transactions of ASME, J. Fluids Eng.*, 113, 579-586.
- Pallavi, P., Ranganayakulu, C. (2011). "Development of Heat transfer coefficient and friction factor correlations for offset fins using CFD." *Heat Fluid Flow.*, 21(8), 935-951.
- Qian Su., Guang Xu Yu., Hua, S.W., John, W.R. (2009). "Microchannel condensation Correlations and theory." *Int. J. Refrig.*, 32, 1149-1152.

Ranganayakulu, C., Stephan Kabelac. (2015). “Boiling of R134a in a Compact Plate-Fin Heat Exchanger having Offset strip fins.” *ASME J. Heat Transfer*, No. HT-14-1235.

Ranganayakulu, C., Seetharamu, K.N., Sreevatsan, K.V. (1997). “The Effects of Inlet Fluid Flow Non-uniformity on Thermal Performance and Pressure Drops in Cross-Flow Plate-Fin Compact Heat Exchangers.” *Int. J. Heat Mass Transfer.*, 40, 27-38.

Ranganayakulu, C., Seetharamu, K.N. (1999). “The Combined Effects of Longitudinal Heat Conduction, Flow Non uniformity and Temperature Non-uniformity in Cross-Flow Plate-Fin Heat Exchangers.” *Int. Commun. Heat Mass Transfer.*, 26, 669-678.

Rao, R.B.S., Ranganath, G., Ranganaykulu, C. (2013). “Development of colburn ‘j’ factor and fanning friction factor ‘f’ correlations for compact heat exchangers plains fins by using CFD.” *Int. J. Heat Mass Transfer.*, 49(4).

Rush, T.A., Newell, T.A., Jacobi, A.M. (1998). “An experimental study of flow and heat transfer in sinusoidal wavy passages.” *Int. J. Heat Mass Transfer.*, 42, 669-678.

Sen Hu, S., Herold, K.E. (1995^a). “Prandtl number effect on offset fin heat exchanger performance: predictive model for heat transfer and pressure drop.” *Int. J. Heat Mass Transfer.*, 38, 1043-1051.

Sen Hu, S., Herold K.E. (1995^b). “Prandtl number effect on offset fin heat exchanger performance: experimental results.” *Int. J. Heat Mass Transfer.*, 38, 1053-1061.

Shah, M.M. (1979). “A general correlation for heat transfer during film condensation inside pipes.” *Int. J. Heat Mass Transfer.*, 22, 547–556.

Soland, J.G., Mack, W.N., Rohsemnow, W.B. (1978). “Performance ranking of plate fin heat exchanger surface.” *ASME J. Heat Transfer.*, 100, 514-519.

Sparrow, E.M., Baliga, B.R., Patankar, S.V. (1977). “Heat Transfer and Fluid Flow Analysis of Interrupted-Wall Channels, With Application to Heat Exchangers.” *Transactions of ASME, J. Heat Transfer.*, 99, 4-11.

- Sparrow, E.M., Comb, J.W. (1983). "Effect of Interwall Spacing and Fluid Flow Inlet Conditions on a Corrugated-Wall Heat Exchanger." *Int. J. Heat Mass Transfer.*, 26, 993-1005.
- Styrylska, T.B., Lechowska, A.A. (2003). "Unified Wilson Plot Method for Determining Heat Transfer Correlations for Heat Exchangers." *Transactions of ASME.*, 125:752.
- Tadeusz, B., Henryk, C., Magorzata, S. (2011). "Comparative investigations of the condensation of R134a and R404A refrigerants in pipe minichannels." *Int. J. Heat Mass Transfer.*, 54, 1963-1974.
- Waldemar, K., Henryk, C., Tadeusz, B. (2012). "Influence of hydrodynamic instability on the heat transfer coefficient during condensation of R134a and R404A refrigerants in pipe mini-channels." *Int. J. Heat Mass Transfer.*, 55, 1083-1094.
- Wang, G., Vanka, S.P. (1995). "Convective Heat Transfer in Periodic Wavy Passages." *Int. J. Heat Mass Transfer.*, 38, 3219-3230.
- Wang, L.K., Sunde'n, B., Yang, Q.S. (1999). "Pressure drop analysis of steam condensation in a plate heat exchanger." *Heat Transfer Eng.*, 20(1), 71-77.
- Webb, R.L. (1981). "Performance evaluation criteria for use of enhanced heat transfer surfaces in heat exchanger design." *Int. J. Heat Mass Transfer.*, 24, 715-726.
- Wieting, A.R. (1975). "Empirical Correlations for Heat Transfer and Flow Friction Characteristics of Rectangular Offset-Fin Plate-Fin Heat Exchangers." *Translations of ASME, J. Heat Transfer.*, 97, 488-490.
- Yan, Y., Hsiang-Chao, L., Tsing-Fa, L. (1999). "Condensation Heat transfer and Pressure drop of refrigerant R-134a in a plate heat exchanger." *Int. J. Heat Mass Transfer.*, 42, 993-1006.

Books:

ALPEMA, *The standards to the Brazed Aluminium Plate Fin Heat Exchanger Manufactures Association* (<http://www.alpema.org/>).

Anderson, J.D. (1995). “*Computational Fluid Dynamics-The Basic with Applications.*” McGraw-Hill Companies, Inc, New York.

ASHRAE. (2005). “*Fundamental hand book, Thermophysical properties of refrigerants.*”

Collier, J.G. (1982). “*Convective Boiling and Condensation.*” 2nd ed., McGraw Hill.

Collier, J.G., Thome, J.R. (1996). “*Convective Boiling and Condensation.*” 3rd ed., Oxford University Press, New York, USA.

Dipak Kumar Maiti. (2002). “*Heat transfer and flow friction characteristics of plate fin heat exchanger surfaces – A numerical study.*” Ph.D. Thesis, IIT Kharagpur, India.

Engineering Equation Solver (EES). F-chart Software, Madison, WI 53744, USA.

Fabienne, C., Lawson, C. (2007). “*Environmental Control System for the All Electric Aircraft*” MSc Thesis, School of Engineering, Cranfield University.

Hesselgreaves, J.E. (2001). “*Compact heat exchangers: Selection, design and operation.*” 1st Edition, Pergamon.

Indranil Ghosh. (2004), “*Experimental and Computational Studies on Plate Fin Heat Exchangers.*” PhD Thesis, IIT-Kharagpur, India.

Kays, W.M., London, A.L. (1984). “*Compact Heat Exchangers.*” 3rd Edition, McGraw-Hill, New York.

Kays, W.M. (1972). “*Compact Heat Exchangers, AGARD Lecture Ser. No. 57 on Heat-Exchanger, AGARD-LS-57-72.*” NATO, Paris.

London, A.L. (1983). “*Compact heat exchangers- Design Methodology in S. Kakac , R.K. Shah and A.E. Bergles (Eds), Low Reynolds number flow heat exchangers.*” Hemisphere Publishing Corp. Washington DC , pp.21-27.

Manson, S.V. (1950). “*Correlations of Heat Transfer Data and of Friction Data for Interrupted Plate Fins Staggered in Successive Rows, NACA Tech. Note 2237.*” National Advisory Committee for Aeronautics, Washington, DC.

Patankar, S.V. (1980). “*Numerical heat transfer and fluid flow.*” Hemisphere publications.

Shah R.K. (1980). “Classification of heat exchangers, Heat Exchangers, Thermal - Hydraulic Fundamentals and Design by S.Kakac, A.E.Bergles, F.Mayinget, Hemisphere Publishing Corp., Washington DC, 9-46.

Shah, R.K., Focke, W.W. (1988). “Plate Heat Exchangers and their design theory, Heat Transfer Equipment Design.” Hemisphere, Washington, 227-254.

Shah, R.K. (1981). “Compact heat exchangers , in S. Kakac , R. K. Shah and F. Mayinget (Eds), Heat exchangers – Thermal hydraulic fundamentals and design.” Hemisphere Publishing Corp., Washington DC, 495-536.

Shah, R.K., Kakac, S., Bergles, A.E., Mayinger, F. (1980). “*Heat exchangers – Thermal hydraulic fundamentals and design.*” Hemisphere Publishing Corp., Washington DC, 9-46.

Shah, R.K., Webb, R.L. (1983). “*Compact and enhanced heat exchangers, in J. Taborek, G.F.Hewitt and N. Afgan (Eds), Heat Exchangers-Theory and Practice.*” McGraw Hill, New York, 425-468.

Taylor, M.A. (1987). “*Plate-Fin Heat Exchangers – Guide to their specification and use.*” 1st edition, HTFS, Harwell Laboratory, OX110RA, UK.

Versteeg, H.K., Malalasekera, W. (1995). “*An Introduction to Computational Fluid Dynamics – The Finite Volume Method*”, Prentice Hall Publications, England.

Warren, M., Rohsenow, J.P., Hartnett., Young, I.C. (1998). “Handbook of Heat Transfer.” 3rd Edition, MacGraw Hill, New York.

Yunus A.C. (2007). “Heat and Mass Transfer.’ 3rd ed.” Tata McGraw-Hill Publications, New York.

Conference proceedings:

Fukushima, T., Kudou, M., (1990). “Heat transfer coefficients and pressure drop for forced convection boiling and condensation of HFC 134a.” International Refrigeration and Air Conditioning Conference, Purdue University, USA, pp.196-201.

Ismail, L.S., Ranganayakulu, C., Shah, R.K. (2007). “Numerical study of flow patterns of compact platefin heat exchangers and generation of design data for offset and wavy fins.” Proceedings of 6th International conference on Enhanced, Compact and Ultra-compact Heat Exchangers: Science, Engineering and Technology, CHE2007-0016, Potsdam, Germany, pp. 113-122.

Ranganayakulu, C., Ismail, L.S., Vengudupathi, C. (2006^c). “Uncertainties in Estimation of Colburn (j) Factor and Fanning Friction (f) factor for Offset Strip Fin and Wavy Fin Compact Heat Exchanger Surfaces.” XVIII National Heat and Mass Transfer, VII ISHMT-ASME Heat and Mass Transfer Conference, IIT Guwahati, 1096-1103,.

Ranganayakulu, C., Ismail, L.S., VasudevaRao, V., Rajeshwar, S., Ramu, M. (2005). “Optimization of Compact Plate-Fin Heat Exchanger – a CFD Approach” 184-191, National Conference TAME, SIST, Hyderabad.

Ranganayakulu, C., Ismail L.S., Vasudeva Rao V., Rajeshwar S., Ramu M. (2006^a). “Effects of Flow Maldistribution in a Compact Plate-Fin Heat Exchanger for Aerospace Applications – a CFD Approach.” ISTP17, Toyama, Japan.

Ranganayakulu, C., Ismail, L.S., VasudevaRao, V., Rajeshwar, S., Ramu, M. (2006^b). “Investigation of Waviness of Wavy Fins and Maldistribution Effects on the

Performance of Compact Plate Fin Heat Exchanger, PLMSS-2006.” 159-168, Indian Institute of Science, Bangalore.

Ranganayakulu, C., Ismail, L.S., VasudevaRao, V., Rajeshwar, S. (2008). “*Optimization of Wavy Fin Parameters in Compact Heat Exchangers.*” Proceedings of XIX National Heat and Mass Transfer & VIII ISHMT-ASME Heat and Mass Transfer Conference, held at JNTU, Hyderabad, India.

Ranganayakulu, C., Iris, M., Stephan, K. (2013). “Boiling of R134a in a Plate-Fin Heat Exchanger Having Offset Fins.” Proceedings of the 22nd National and 11th International, ISHMT-ASME HMT Conference December 28-31, IIT Kharagpur, India.

Shah, R.K. (1978). “Compact heat exchanger surface selection methods in heat transfer” Proceedings of the 5th international heat transfer conference, Hemisphere Publishing Co., New York.193-199.

Shah, R.K., Zhou, S.Q. (1997). “*Experimental Techniques for obtaining Design Data of compact heat exchanger surfaces.*” proceedings of the Int. Conference on compact heat exchangers in the process industries, 365-379.

APPENDIX – I

j & *f* SIMULATION DATA

Table A1.1: Simulation Frictional Factor (*f*) Data of Water

Sl. No	s	t	h	l	D _h	Re	s/h	t/s	t/l	<i>f</i>
1	1.3611	0.125	4.875	3.175	1.961703	100	0.2792	0.091837484	0.039370079	0.383293355
2	0.947696	0.105833	2.527364	3.175	1.249372	100	0.374974	0.111674381	0.033333333	0.242935506
3	0.907142	0.125	1.875	3.175	1.081099	100	0.483809	0.137795406	0.039370079	0.234978
4	1.633008	0.125	2.875014	1.52	1.947873	100	0.568	0.076546	0.082237	0.403685955
5	1.361104	0.152	3.848014	3.175	1.822124	100	0.353716	0.111674	0.047874	0.341872772
6	0.907143	0.125	4.875015	3.175	1.343126	100	0.18608	0.137795	0.03937	0.34546023
7	0.907143	0.152	2.848002	3.175	1.179821	100	0.318519	0.167559	0.047874	0.238060914
8	0.907143	0.125	4.875015	3.175	1.343126	100	0.18608	0.137795	0.03937	0.34546023
9	1.103088	0.152	2.280006	3.175	1.314621	100	0.483809	0.137795	0.047874	0.238060914
10	0.907141	0.2	4.79999	3.175	1.225837	100	0.188988	0.220473	0.062992126	0.224894539
11	1.3611	0.125	4.875	3.175	1.961703	300	0.2792	0.091837484	0.039370079	0.218873412
12	0.907142	0.125	2.874997	1.52	1.217896	300	0.315528	0.137795406	0.082236842	0.205554614
13	0.947696	0.105833	2.527364	3.175	1.249372	300	0.374974	0.111674381	0.033333333	0.126438349
14	0.907142	0.125	1.875	3.175	1.081099	300	0.483809	0.137795406	0.039370079	0.119851185
15	1.633008	0.125	2.875014	1.52	1.947873	300	0.568	0.076546	0.082237	0.238422979
16	1.361104	0.152	3.848014	3.175	1.822124	300	0.353716	0.111674	0.047874	0.195442374
17	0.907143	0.125	4.875015	3.175	1.343126	300	0.18608	0.137795	0.03937	0.166063501
18	0.907143	0.152	2.848002	3.175	1.179821	300	0.318519	0.167559	0.047874	0.1241596
19	0.907143	0.125	4.875015	3.175	1.343126	300	0.18608	0.137795	0.03937	0.166063501

20	0.907141	0.2	4.79999	3.175	1.225837	300	0.188988	0.220473	0.062992126	0.118959783
21	1.894853	0.261102	6.005339	3.175	2.543959	500	0.315528	0.137795406	0.082236842	0.17064071
22	0.947696	0.105833	2.527364	3.175	1.249372	500	0.374974	0.111674381	0.033333333	0.097328064
23	0.907142	0.125	1.875	3.175	1.081099	500	0.483809	0.137795406	0.039370079	0.091741679
24	1.633008	0.125	2.875014	1.52	1.947873	500	0.568	0.076546	0.082237	0.197933967
25	1.361104	0.152	3.848014	3.175	1.822124	500	0.353716	0.111674	0.047874	0.159394475
26	0.907143	0.152	2.848002	3.175	1.179821	500	0.318519	0.167559	0.047874	0.095317257
27	0.907143	0.125	4.875015	3.175	1.343126	500	0.18608	0.137795	0.03937	0.12543269
28	0.907141	0.2	4.79999	3.175	1.225837	500	0.188988	0.220473	0.062992126	0.091932134
29	0.907142	0.125	2.874997	1.52	1.217896	800	0.315528	0.137795406	0.082236842	0.147385989
30	0.947696	0.105833	2.527364	3.175	1.249372	800	0.374974	0.111674381	0.033333333	0.077936307
31	0.907142	0.125	1.875	3.175	1.081099	800	0.483809	0.137795406	0.039370079	0.073180926
32	1.633008	0.125	2.875014	1.52	1.947873	800	0.568	0.076546	0.082237	0.171042657
33	1.361104	0.152	3.848014	3.175	1.822124	800	0.353716	0.111674	0.047874	0.135580035
34	0.907143	0.125	4.875015	3.175	1.343126	800	0.18608	0.137795	0.03937	0.10021425
35	0.907143	0.152	2.848002	3.175	1.179821	800	0.318519	0.167559	0.047874	0.075759757
36	0.907143	0.125	4.875015	3.175	1.343126	800	0.18608	0.137795	0.03937	0.10021425
37	0.907141	0.2	4.79999	3.175	1.225837	800	0.188988	0.220473	0.062992126	0.073711483
38	0.907142	0.125	2.874997	1.52	1.217896	1000	0.315528	0.137795406	0.082236842	0.138526385
39	0.947696	0.105833	2.527364	3.175	1.249372	1000	0.374974	0.111674381	0.033333333	0.070755287
40	0.907142	0.125	1.875	3.175	1.081099	1000	0.483809	0.137795406	0.039370079	0.066262241
41	1.633008	0.125	2.875014	1.52	1.947873	1000	0.568	0.076546	0.082237	0.160776
42	0.907143	0.125	4.875015	3.175	1.343126	1000	0.18608	0.137795	0.03937	0.091296
43	0.907143	0.152	2.848002	3.175	1.179821	1000	0.318519	0.167559	0.047874	0.068407
44	0.907143	0.125	4.875015	3.175	1.343126	1000	0.18608	0.137795	0.03937	0.091296
45	0.907141	0.2	4.79999	3.175	1.225837	1000	0.188988	0.220473	0.062992126	0.066905946

Table A1.2 Simulation of Colburn Factor (*j*) Data of Water

Sl. No	s	t	h	l	Dh	Re	s/h	t/s	t/l	j
1	0.907142	0.125	2.874996831	1.52	1.217895516	100	0.315528	0.137795406	0.082236842	0.024118445
2	0.907142	0.125	1.875000258	3.175	1.081099372	100	0.483809	0.137795406	0.039370079	0.013809211
3	1.633008126	0.12500024	2.875014306	1.52	1.947872954	100	0.568	0.076546	0.082237	0.028604426
4	1.361104457	0.12499975	4.875015963	3.175	1.961710255	100	0.2792	0.091837	0.03937	0.021706061
5	1.361104196	0.15199995	3.848014215	3.175	1.82212378	100	0.353716	0.111674	0.047874	0.020979529
6	0.907142857	0.12499975	4.875015354	3.175	1.343125589	100	0.18608	0.137795	0.03937	0.011662414
7	0.907142857	0.15199995	2.848002339	3.175	1.179821136	100	0.318519	0.167559	0.047874	0.011582902
8	0.907142857	0.12499975	4.875015354	3.175	1.343125589	100	0.18608	0.137795	0.03937	0.011662414
9	1.103087558	0.15199995	2.280006279	3.175	1.314620788	100	0.483809	0.137795	0.047874	0.011582902
10	0.907140557	0.2	4.799990247	3.175	1.225837382	100	0.188988	0.220473	0.062992126	0.012304257
11	0.907142	0.125	2.874996831	1.52	1.217895516	300	0.315528	0.137795406	0.082236842	0.017869645
12	0.947695724	0.105833333	2.527363827	3.175	1.249371756	300	0.374974	0.111674381	0.033333333	0.011738786
13	0.907142	0.125	1.875000258	3.175	1.081099372	300	0.483809	0.137795406	0.039370079	0.009283897
14	1.633008126	0.12500024	2.875014306	1.52	1.947872954	300	0.568	0.076546	0.082237	0.018942069
15	1.361104457	0.12499975	4.875015963	3.175	1.961710255	300	0.2792	0.091837	0.03937	0.013967926
16	1.361104196	0.15199995	3.848014215	3.175	1.82212378	300	0.353716	0.111674	0.047874	0.013472073
17	0.907142857	0.12499975	4.875015354	3.175	1.343125589	300	0.18608	0.137795	0.03937	0.0079782
18	0.907142857	0.15199995	2.848002339	3.175	1.179821136	300	0.318519	0.167559	0.047874	0.007943397
19	0.907142857	0.12499975	4.875015354	3.175	1.343125589	300	0.18608	0.137795	0.03937	0.0079782
20	0.907140557	0.2	4.799990247	3.175	1.225837382	300	0.188988	0.220473	0.062992126	0.009221673
21	0.947695724	0.105833333	2.527363827	3.175	1.249371756	500	0.374974	0.111674381	0.033333333	0.00991019
22	0.907142	0.125	1.875000258	3.175	1.081099372	500	0.483809	0.137795406	0.039370079	0.007973978

23	1.633008126	0.12500024	2.875014306	1.52	1.947872954	500	0.568	0.076546	0.082237	0.017039927
24	1.361104457	0.12499975	4.875015963	3.175	1.961710255	500	0.2792	0.091837	0.03937	0.011720001
25	1.361104196	0.15199995	3.848014215	3.175	1.82212378	500	0.353716	0.111674	0.047874	0.011373899
26	0.907142857	0.15199995	2.848002339	3.175	1.179821136	500	0.318519	0.167559	0.047874	0.006832526
27	0.907142857	0.12499975	4.875015354	3.175	1.343125589	500	0.18608	0.137795	0.03937	0.006830279
28	0.907140557	0.2	4.799990247	3.175	1.225837382	500	0.188988	0.220473	0.062992126	0.008031199
29	0.947695724	0.105833333	2.527363827	3.175	1.249371756	800	0.374974	0.111674381	0.033333333	0.008692838
30	0.907142	0.125	1.875000258	3.175	1.081099372	800	0.483809	0.137795406	0.039370079	0.00715631
31	1.633008126	0.12500024	2.875014306	1.52	1.947872954	800	0.568	0.076546	0.082237	0.016149233
32	1.361104457	0.12499975	4.875015963	3.175	1.961710255	800	0.2792	0.091837	0.03937	0.010318766
33	1.361104196	0.15199995	3.848014215	3.175	1.82212378	800	0.353716	0.111674	0.047874	0.010167726
34	0.907142857	0.12499975	4.875015354	3.175	1.343125589	800	0.18608	0.137795	0.03937	0.006041321
35	0.907142857	0.15199995	2.848002339	3.175	1.179821136	800	0.318519	0.167559	0.047874	0.00610868
36	0.907142857	0.12499975	4.875015354	3.175	1.343125589	800	0.18608	0.137795	0.03937	0.006041321
37	0.907140557	0.2	4.799990247	3.175	1.225837382	800	0.188988	0.220473	0.062992126	0.006945847
38	0.947695724	0.105833333	2.527363827	3.175	1.249371756	1000	0.374974	0.111674381	0.033333333	0.00813431
39	0.907142	0.125	1.875000258	3.175	1.081099372	1000	0.483809	0.137795406	0.039370079	0.006885696
40	1.633008126	0.12500024	2.875014306	1.52	1.947872954	1000	0.568	0.076546	0.082237	0.015674
41	1.361104457	0.12499975	4.875015963	3.175	1.961710255	1000	0.2792	0.091837	0.03937	0.009796
42	0.907142857	0.12499975	4.875015354	3.175	1.343125589	1000	0.18608	0.137795	0.03937	0.005743
43	0.907142857	0.15199995	2.848002339	3.175	1.179821136	1000	0.318519	0.167559	0.047874	0.005747
44	0.907142857	0.12499975	4.875015354	3.175	1.343125589	1000	0.18608	0.137795	0.03937	0.005743
45	0.907140557	0.2	4.799990247	3.175	1.225837382	1000	0.188988	0.220473	0.062992126	0.006425548

APPENDIX-II

SENSORS CALIBRATION PROCEDURE AND REPORTS

A2.1 PRESSURE SENSORS

Pressures sensors are used in test facility are.

- Absolute pressure sensors
- Differential pressure sensors

A2.1.1 Pressure Transducer

Pressure transducers are calibrated using dead weight method.

A2.1.1.1 Instruments required

- a) Pressure transducer / transmitter (Unit under Test)
- b) Power supply: 24V
- c) Voltage standard: NI Multifunction Calibrator, Make: Yokogawa, Model: CA51, S/N:T1F2002, NAL/PR/HSCTF/ C-55, DRUCK / DPI 605 /DPI 610
- d) Pressure standard: Dead weight Pressure Calibrator

A2.1.1.2 Calibration Procedure

Initially the required level of oil is ensured in the calibrator by visual examination. The pressure transmitter to be calibrated is connected to the calibration port of the calibrator. The transmitter is wired through 24V power supply and a 100 ohm resistor to the Multi Function calibrator / DPI 605/610

The priming handle is attached to the location and rotated anti-clock wise completely, after opening the air vent port, the handle is rotated clockwise fully inside to expel the air bubbles formed inside. The same procedure is repeated one more time. Then finally the handle moved out fully by rotating anti-clock wise and air vent port is closed. By using the computer program provided by the calibrator supplier, the weights required to produce required pressure is calculated. Then these weights are kept on the respective pistons (low pressure and High Pressure) as directed by the computer program. Then the pressurizing handle is rotated clock-wise such that the

pistons move up and the weights float till the provided mark in the indicating bar. After the weights are floating slightly rotate the weights and wait for a while. Then measure the electrical output using multifunction calibrator / DPI 605/DPI 610 and compares it with the standard value. If the error in measurement is within the specified limit of the device, then it is accepted and declared as “calibration passed”. If the error is not within the specified limit of the device, then calibration is repeated once again and the measurement is verified further. The results are shown in Table A2.1.

Table A2.1 Calibration Report of Pressure Transducer / Transmitter

Unit Under Test (UUT)		Calibrator Information	
Document No: PR/CLOCTER/VCRS/PRT/01		Dead weight Pressure Calibrator	
Make: Measurement Specialties		S/N: 2031811	
Model No: M5156		Cal Ref: NAL/PR/HSCTF/C-56	
S/N: 030108D262, Cal date: 9 MAR 2015			
Date of Next Calibration: 8 MAR 2016			
Calibration Data			
Standard Reading (barg)	Sensor O/P (mA)	Actual Reading (barg)	Error %FS
0.00	4.292	0.007	0.02
5.00	6.263	4.943	-0.13
10.00	8.296	10.033	0.09
15.00	10.275	14.989	-0.02
20.00	12.287	20.027	0.07
25.00	14.286	25.032	0.09
30.00	16.28	30.025	0.07
35.00	18.242	34.938	-0.15
40.00	20.256	39.981	-0.04

A2.1.2 Differential pressure transducer

A2.1.2.1 Instruments required

- a) Pressure transducer / transmitter (Unit under Test)
- b) Power supply: 24V DC
- c) Voltage standard: DRUCK / DPI 605 /DPI 610
- d) Pressure standard: DRUCK / DPI 605 /DPI 610

A2.1.2.2 Calibration Procedure:

Energize with 24V DC power supply and connect transmitter's pressure port to the calibrator and ensure leak proof tightness. After closing Calibrators went port, required value of pressure is applied to the transmitter using its hand priming pump.

The current generated by the transmitter for the applied pressure is read by the DPI 605/610 along with the calibrators known value. The standard value and the measured values are compared for error.

If the error in measurement is within the specified limit of the device, then it is accepted and declared as "calibration passed". If the error is not within the specified limit of the device, then calibration is repeated once again and the measurement is verified further. A typical calibration result is shown in Table A2.2.

Table A2.2: Calibration Report of Differential Pressure Transducer

Unit Under Test (UUT)		Calibrator Information	
Document No: PR/CLOCTER/VCRS/DPRT/01		DRUCK / DPI 605 PRESSURE CALIBRATOR	
Make: SENSOCON		S/N: 60505988	
Model No: 251-01		Cal Ref: GTRE Calibration Certificate no.: NAL/CAL/TM/DEC/2013/242(A) dated 24th Dec 2013	
S/N: Q01404, Cal date: 18 DEC 2015		CAL Due: 24th DEC 2015	
Date of Next Calibration: 17 DEC 2016			
Calibration Data			
Standard Reading (psi)	Sensor O/P (mA)	Actual Reading (psi)	Error %FS
0.0000	3.783	-0.022	-0.43
1.0047	7.02	1.001	-0.07
2.0125	10.258	2.025	0.24
3.0288	13.519	3.055	0.52
4.0384	16.682	4.055	0.32
5.0039	19.556	4.963	-0.82

A2.2 FLOW METER: Two types of flow meters are used in test facility.

- Coriolis mass flow meter
- Turbine flow meter

A2.2.1 Coriolis mass flow meter

A2.2.1.1 Instruments required

- a. Mass flow meter (Unit under Test)
- b. Power supply: 230V

- c. Reference Mass flow Meter: Micro motion, Model No: R050, S/N: 712795
- d. Equipments used: Pump, Pressure transmitter to ensure safe pressure limits at the headers, control valves to adjust the flow, on /off valves.
- e. Medium of calibration: kerosene

A2.2.1.2 Calibration Procedure

Start the kerosene pump and then switch on the on-off valve and set the kerosene flow by adjusting the flow control valve. Then close the on-off valve and make the Instruments reading zero. After that open the on-off valve and allow the flow for a predetermined time. Then note down the readings of Reference and UUT meter readings. Then the reading in the flow meters can be compared for errors. Repeat the same procedure for different flow rate till the maximum range of the meter. If the error in measurement is within the specified limit of the device, then it is accepted and declared as “calibration passed”. If the error is not within the specified limit of the device, then calibration is repeated once again and the measurement is verified further. If the same error persists, it is declared as “calibration failed” and discarded from measurements at VCRS. A typical calibration result is shown in Table A2.3.

Table A2.3: Calibration report of Coriolis Mass flow meter

Unit Under Test (UUT)		Calibrator Information	
Document No: PR/CLOCTER/VCRS/MF/03		Make: MICROMOTION	
Make: MICROMOTION		Model No: RO50	
Model No: F100S		S/N: 712795	
S/N: 14075013, Cal date: 16 March 2015		Cal Ref: FCRI/OFL/C/2012/021	
Date of Next Calibration: 15 March 2018		Calibrated at FCRI, Palakkad	
Calibration Data			
UUT Meter Reading (kg/min)	Time (min)	Reference Reading (kg/min)	Error %rd
4.75	10.00	4.75	-0.04
10.20	10.00	10.21	-0.05
15.55	10.00	15.54	0.06
20.05	8.00	20.04	0.05
26.23	10.00	26.24	-0.04
31.24	10.00	31.25	-0.03
40.22	8.00	40.23	-0.02

50.60	5.00	50.61	-0.02
60.80	5.00	60.81	-0.02

A2.2.2 Turbine flow meter

A2.2.2.1 Calibration Procedure

The flow meter under test is installed in the metering run of approximate size.

Dynamic start-stop method is used in the calibration. Water is allowed collect in the tank which is placed on a weighing scale. The pulses generated by the meter as well as time taken for a fixed quantity of liquid is recorded.

A2.2.2.2 Calculations

Calibration factor (Pulses/Litre) $K = \text{Total pulses/volume collected}$

Average calibration factor $= \frac{K_{\max} + K_{\min}}{2}$

Linearity band $= \frac{K_{\max} - K_{\min}}{\text{Average calibration factor}} * 100$

Flow rate (LPM) $= \frac{\text{Volume collected}}{\text{Time in sec}} * 60$

A2.2.2.3 Sample Calculations

Volume of water collected = 20 lt

Total pulse recorded = 22272

Calibration factor = 1113.60 pulses/lt

Flow rate = 67.57 LPM




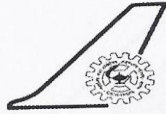
 NABL CERTIFICATE Nos. : C-0314, C-0537, C-0538 As per ISO 17025 : 2005	CALIBRATION REPORT	DIMENSIONS																																
	Report No. : C1415/2260/T01 Date of Issue : 26.11.2014 Page : 1 of 1	# 128, 19th Cross, 8th Main, CHBS Layout Vijayanagar, Near BDA Complex B E N G A L U R U - 5 6 0 0 4 0 ; Phone : 080 - 2314 3921, 2314 3914 E-mail : frontoffice@dimensions-callab.com URL : www.dimensions-callab.com																																
1.0 Name and address of the customer : M/s. NATIONAL AEROSPACE LABORATORIES, NWTC , Belur, Bangalore - 560 037.																																		
2.0 Customer Reference : Received thru Delta Systems dated 13.11.2014																																		
3.0 Date of receipt and condition : 13.11.2014 :: Satisfactory																																		
4.0 Description of the instrument : Temperature Sensor Make : Delta Systems Model : -- Range : -50 to 100°C Calibrated Range: -20 to 100°C Sl No : 14111201 ID. No. : -- Accuracy : Class A Type : PT100																																		
5.0 Date /s & Place of Calibration : 13.11.2014 :: Inhouse																																		
5.1 Due for Calibration : 12.11.2015																																		
6.0 Master Used for Calibration : 1. CHUBE-4 Thermometer Readout (A83732) 2. SPRT (DMN-INS-TM-04)																																		
7.0 Master's Traceability & Validity : 1. Traceable to ETDC(Bg)/C-45943 & 30.12.2014 2. Traceable to ARAI/CAL/1301/1927 & 06.02.2015																																		
8.0 Calibration Procedure No. : DMN-CPT-003																																		
9.0 Environmental Conditions : Temp: 25±2.5°C Humidity: 35 to 65% RH																																		
10.0 Measurement Uncertainty is reported at 95% confidence level with k = 2.																																		
RESULTS OF CALIBRATION																																		
<table border="1"> <thead> <tr> <th>Sl No.</th> <th>STD Reading in °C</th> <th>DUC Reading in °C</th> <th>Error Claimed ± in °C</th> <th>Deviation Observed in °C</th> <th>Measurement Uncertainty (±) in °C</th> </tr> </thead> <tbody> <tr> <td>1</td> <td>-19.48</td> <td>-19.45</td> <td rowspan="5" style="text-align: center;">0.35</td> <td>0.03</td> <td>0.2</td> </tr> <tr> <td>2</td> <td>0.72</td> <td>0.82</td> <td>0.10</td> <td>0.2</td> </tr> <tr> <td>3</td> <td>24.93</td> <td>24.96</td> <td>0.03</td> <td>0.2</td> </tr> <tr> <td>4</td> <td>49.87</td> <td>49.88</td> <td>0.01</td> <td>0.2</td> </tr> <tr> <td>5</td> <td>99.99</td> <td>99.95</td> <td>-0.04</td> <td>0.2</td> </tr> </tbody> </table>	Sl No.	STD Reading in °C	DUC Reading in °C	Error Claimed ± in °C	Deviation Observed in °C	Measurement Uncertainty (±) in °C	1	-19.48	-19.45	0.35	0.03	0.2	2	0.72	0.82	0.10	0.2	3	24.93	24.96	0.03	0.2	4	49.87	49.88	0.01	0.2	5	99.99	99.95	-0.04	0.2		
Sl No.	STD Reading in °C	DUC Reading in °C	Error Claimed ± in °C	Deviation Observed in °C	Measurement Uncertainty (±) in °C																													
1	-19.48	-19.45	0.35	0.03	0.2																													
2	0.72	0.82		0.10	0.2																													
3	24.93	24.96		0.03	0.2																													
4	49.87	49.88		0.01	0.2																													
5	99.99	99.95		-0.04	0.2																													
Remarks : Calibration points are selected as per the customer's request. All readings are within the limits as per the Manufacturer's specification.																																		
Prepared By: 		Authorised By:  M.R. Magesh Kumar Technical Manager.																																

Fig A2.2 : Calibration report RTD sensors

A2.3.2 Thermocouples

Drywell calibrator is used for calibration of Thermocouples as given the Fig A2.3. Sample Calibration report of thermocouples is shown in Fig. A2. 4.

Calibration Standards Aerospace Electronics & Systems Division National Aerospace Laboratories (Tel: 080-2508 6575, 6570)	
<i>TEMP/ALD/CS/37</i>	<i>Page 1 of 6</i>

<i>Calibration Report</i>

Calibration of K-Type Thermocouple

Work request from	Head Propulsion		
Date	09/08/2012		

Item Description: K-Type Thermocouple

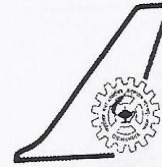
Serial No. : K-115,K-114, K-117,K-089,K-113,K-157,K-059, K-092,K-060, K-156,K-153,K-155,K-132,K-154,K-128			
Range	-40°C to 100 °C	Tolerance	Not Provided
Date of Calibration	29-08-2012	Calibration Due	29-08-2013
Environmental Conditions	RT: 20 +/-2 °C		

Standard Instruments Used:

<i>Nomenclature</i>	<i>Make/Model</i>	<i>Cal. at</i>	<i>Cal. Validity</i>
Dry Well Calibrator	Hart Scientific/9107	ETDC	30-07-2013
Thermometer Readout	Hart Scientific/1529	ETDC	09-04-2013
PRT	Hart Scientific/5626	ETDC	15-11-2012

Fig A2.3 : Caibration standard of Thermocouples

Calibration Standards
Aerospace Electronics & Systems Division
National Aerospace Laboratories
(Tel: 080-2508 6575, 6570)



Page 2 of 6

TEMP/ALD/CS/37

Calibration Report

Calibration Results

Sl.No	Set Temp (°C)	Ref Temp (°C)	K-115 (°C)	Error	K-114 (°C)	Error	K-117 (°C)	Error
1	-40	-39.641	-36.95	2.691	-36.96	2.681	-37.00	2.641
2	-30	-29.448	-27.37	2.078	-27.40	2.048	-27.41	2.038
3	-20	-19.409	-17.89	1.519	-17.95	1.459	-17.96	1.449
4	-10	-9.420	-8.39	1.030	-8.39	1.030	-8.38	1.040
5	0	0.419	0.88	0.461	0.85	0.431	1.17	0.751
6	10	10.182	10.45	0.268	10.43	0.248	10.72	0.538
7	20	20.031	19.92	-0.111	19.93	-0.101	20.23	0.199
8	30	29.987	29.67	-0.317	29.72	-0.267	29.95	-0.037
9	40	40.224	39.52	-0.704	39.49	-0.734	39.81	-0.414
10	50	50.010	49.31	-0.700	49.28	-0.730	49.59	-0.420

Fig A2.4 : Calibration report of Thermocouples

APPENDIX – III

Detailed Procedure to Calculate Two Phase h_r and ΔP_f

A3.1 Procedure to calculate refrigerant saturated heat transfer coefficient (h_r) and two phase frictional pressure drop (ΔP_f)

The Step by step procedure to determine saturated heat transfer coefficient (h_r) and two phase frictional pressure drop (ΔP_f) are explained below:

Step 1: Geometry data of refrigerant and Water side

Refrigerant : Free flow area (A_{f_r}), Heat Transfer area (A_{h_r})

Water : Free flow area (A_{f_w}), Heat Transfer area (A_{h_w})

Step 2: Experimental measured data:

Refrigerant : mass flow rate (m_r), Inlet Pressure (P_{rin}), Outlet Pressure (P_{rou}), Differential Pressure (ΔP_r), Inlet Temperature (T_{rin}), Outlet Temperature (T_{rou})

Water : mass flow rate (m_w), Inlet Pressure (P_{win}), Outlet Pressure (P_{wou}), Differential Pressure (ΔP_w), Inlet Temperature (T_{win}), Outlet Temperature (T_{wou}), Specific Heat (C_{p_w})

Step 3: From observed inlet pressure, refrigerant inlet saturation temperature is calculated from Eq.1 below which is obtained after fitting third order polynomial In the 2001 ASHRAE Fundamentals Handbook (SI) data of Refrigerant R134a.

$$T_{cali} = -0.168 * P_{rin}^2 + 7.11 * P_{rin} - 14.81 \quad (1)$$

Step 4: From the observed inlet pressure, the refrigerant inlet vapour enthalpy is calculated from Eq.2, which is obtained after fitting third order polynomial in the 2001 ASHRAE Fundamentals Handbook (SI) data of Refrigerant R134a.

$$h_g = 0.007 * P_{rin}^3 - 0.324 * P_{rin}^2 + 5.88 * P_{rin} + 385.3 \quad (2)$$

Step 5: From the observed outlet pressure, the refrigerant outlet saturation temperature is calculated from Eq.3, which is obtained after fitting third order polynomial in the 2001 ASHRAE Fundamentals Handbook (SI) data of Refrigerant R134a.

$$T_{\text{calout}} = -0.168 * P_{\text{rout}}^2 + 7.11 * P_{\text{rout}} - 14.81 \quad (3)$$

Step 6: From the observed outlet pressure, the refrigerant outlet liquid enthalpy is calculated from Eq.4, which is obtained after fitting third order polynomial in the 2001 ASHRAE Fundamentals Handbook (SI) data of Refrigerant R134a.

$$h_f = -0.208 * P_{\text{rout}}^2 + (9.744 * P_{\text{rout}}) + 178.9 \quad (4)$$

Step 7: Calculate the heat load of refrigerant (kW) from Eq . 5 as,

$$Q_r = \dot{m}_r(h_g - h_f) \quad (5)$$

Step 8: From observed inlet and outlet temperature, bulk mean temperature (T_b) is calculated from Eq. 6

$$T_b = \frac{T_{\text{win}} + T_{\text{wout}}}{2} \quad (6)$$

Step9: Specific heat at bulk mean temperature of water is calculated from Eq .7 below, which is obtained after fitting a second order polynomial in the NIST data for the water.

$$C_{pw} = 1.08 \times 10^{-5} \times T_b^2 - 6.66 \times 10^{-3} \times T_b + 5.21 \quad (7)$$

Step10: Heat gained by water while flowing through heat exchanger is estimated from energy Eq. 8

$$\dot{Q}_w = \dot{m}_w C_{pw} (T_{\text{wout}} - T_{\text{win}}) \quad (8)$$

Step11: The fluid temperature in the test section varies logarithmically along the flow length. The variation of temperature of fluid with constant refrigerant temperature is as shown in Figure 1.1. So the overall Log Mean temperature Difference (LMTD) of Water and Refrigerant is from Eq. 9 as,

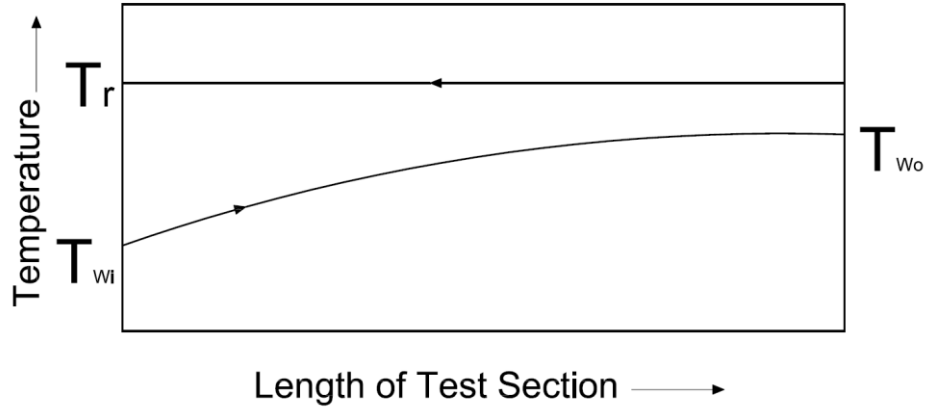


Figure 1: Temperature variation along the core length

$$\text{LMTD} = \frac{(T_{rin} - T_{win}) - (T_{rout} - T_{wout})}{\ln \frac{T_{rin} - T_{win}}{T_{rout} - T_{wout}}} \quad (9)$$

Step12: The overall Heat Transfer Coefficient of Water and Refrigerant ($\text{W/m}^2\text{K}$) is calculated from eq.10 as:

$$U = \frac{Q_w * 1000}{A_{hr} * \text{LMTD}} \quad (10)$$

Step13: Viscosity at bulk mean temperature of water is calculated from Eq.11, which is obtained after fitting a third order polynomial in the NIST data for the water.

$$\mu_w = -2.54 \times 10^{-9} * T_b^3 + 2.65 \times 10^{-6} * T_b^2 - 9.27 \times 10^{-4} * T_b + 1.09 \times 10^{-1} \quad (11)$$

Step14: The mass flux of water (G_w) is calculated from Eq.12 as:

$$G_w = \frac{m_w}{60 * A_{fw}} \quad (12)$$

Step15: Reynolds number of water (Re_w) is calculated from Eq.13 as:

$$Re_w = \frac{G_w D_{hw}}{\mu_w} \quad (13)$$

Step16: Water side heat transfer coefficient is calculated from Eq. 14 which is obtained after performing the CFD analysis of fin with flow geometry conditions

$$h_w = 0.049 * \lambda_w / D_{hw} * Re_w^{0.69} * Pr_w^{1/3} \quad (14)$$

Step 17: The heat transfer coefficient of Refrigerant is calculated from Eq. 15 as:

$$\frac{1}{U} = \frac{1}{\eta_{or}h_r} + \frac{t}{\lambda(A_p/A_r)} + \frac{1}{\eta_w h_w (A_w/A_r)} \quad (15)$$

Step 18: Longo (2010) is presented the correlation for Mean Density of Refrigerant in eq.16 as:

$$\rho_m = \left[\frac{X_m}{\rho_g} + (1 - X_m)/\rho_l \right]^{-1} \quad (16)$$

Step 19: The mass flux of Refrigerant (G_r) is calculated from Eq. 17 as:

$$G_r = \frac{m_r}{A_{fr}} \quad (17)$$

Step 20: The pressure drop due to momentum is calculated from Eq. 18 as:

$$\Delta P_a = G_r^2 (v_g - v_l) |\Delta X| \quad (18)$$

Step 21: The pressure drop due to Gravity is calculated from Eq. 19 as:

$$\Delta P_g = g \rho_m L \quad (19)$$

Step 22: The pressure drop due to manifold is calculated from Eq.20 as:

$$\Delta P_c = \frac{1.5 G_r^2}{2 \rho_m} \quad (20)$$

Step 23: The core frictional pressure Drop is calculated from below eq.21 as:

$$\Delta p_f = \Delta p_t - \Delta p_c + \Delta p_a + \Delta P_g \quad (21)$$

Step24: Finally display the Heat Transfer Coefficient of Refrigerant and Core frictional Drop (ΔP_f)

A3.2 Sample Calculations:

The sample calculations to determine two phase condensation heat transfer coefficient and two phase frictional pressure drop for R134a using serrated fins are presented below:

A3.2.1 Geometric data of fins (TC2):

Parameter	Unit	Value	
		DM Water side	Refrigerant side
Type		Serrated (Lanced & Offset)	
Material		Aluminium	
Fin frequency	FPI	28	

Fin height	mm	5	5
Fin thickness	mm	0.127	
Serration length	mm	3.175	3.175
No of layers		2	1
Total heat transfer area	m ²	0.4616	0.2286
Hydraulic diameter	mm	1.3450	1.3450

A3.2.2 Calculation of refrigerant heat transfer coefficient using LMTD method:

1. Refrigerant mass flow rate (m_r) : 0.019330001 kg/s
2. Condenser Inlet Pressure (P_{rin}) : 11.14000027 bar (abs)
3. Calculated temperature (T_{calin}) using eq.1

$$T_{calin} = -0.168 * 11.14^2 + 7.11 * 11.14 - 14.81$$

$$T_{calin} = 43.5466681 \text{ } ^\circ\text{C}$$

4. Condenser Inlet Temperature (T_{rin}) = 43.51604334 $^\circ\text{C}$
5. Temperature difference = $T_{rin} - T_{calin}$ = -0.030624 $^\circ\text{C}$
6. Vapor Enthalpy is calculated using eq.2:

$$h_g = 0.007 * 11.14^3 - 0.324 * 11.14^2 + 5.88 * 11.14 + 385.3$$

$$= 420.2722167 \text{ kJ/kg}$$

7. Condenser outlet Pressure (P_{rout}) = 11.0924 bar (abs)
8. Calculated outlet temperature (T_{calout}) using eq.3

$$T_{calout} = -0.168 * 11.0924^2 + 7.11 * 11.0924 - 14.81 = 43.3860 \text{ } ^\circ\text{C}$$

9. Liquid Enthalpy is calculated using eq.4:

$$h_f = -0.208 * 11.0924^2 + 9.744 * 11.0924 + 178.9 = 261.3917 \text{ kJ/kg}$$

10. Water Inlet Temperature (T_{win}) = 29.9199996 $^\circ\text{C}$
11. Water Outlet Temperature (T_{wout}) = 33.500458 $^\circ\text{C}$
12. Water flow rate (m_w) = 12.2299 kg/min

13. Bulk mean water fluid temperature (T_b) is calculated using eq.6:

$$T_b = \frac{(T_{wout} + T_{win})}{2} = 31.710228 \text{ } ^\circ\text{C}$$

14. Specific heat of water (C_{pw}) calculated using eq.7:

$$C_{pw} = 1.08 \times 10^{-5} \times 304.85^2 - 6.66 \times 10^{-3} \times 304.85 + 5.21 = 4.183 \text{ kJ/kg.K}$$

15. Water Heat load is calculated using eq.8:

$$\dot{Q}_w = 12.2299 \times 4.183 \times (33.500458 - 29.9199996)/60 = 3.0528234 \text{ kW}$$

16. Refrigerant Load is calculated using eq.5:

$$Q_r = 0.019330001 * (420.2722167 - 261.3917) = 3.071159 \text{ kW}$$

17. Heat Balance deviation

$$\% = \frac{3.071159 - 3.0528234}{3.071159} = 0.59\%$$

18. Logarithmic Mean Temperature Difference (LMTD)

$$\Delta T_{\ln} = \frac{13.5960 - 7.19365}{\ln \frac{13.5960}{7.19365}} = 10.05748 \text{ } ^\circ\text{C}$$

19. R134a side Primary heat transfer area (A_{rprim}) : 0.0426 m²

20. Secondary Heat Transfer area (A_{rsecd}) : 0.228839 m²

21. Refrigerant heat transfer area (A_{hr})

$$A_{hr} = A_{rprim} + A_{rsecd} * \eta_{oer} = 0.230048 \text{ m}^2$$

22. Water side primary heat transfer area (A_{wprim}) = 0.08520 m²

23. Water side secondary heat transfer area (A_{wsecd}) = 0.4577 m²

24. Water heat transfer area (A_{hw})

$$A_{hw} = A_{wprim} + A_{wsecd} * \eta_{oew} = 0.460096 \text{ m}^2$$

25. Overall heat transfer coefficient 'U'

$$U = \frac{3.0528234 * 1000}{0.230048 * 10.05748} = 1361.640297 \text{ W/m}^2\text{K}$$

26. Water free flow area (A_{fw}): 0.001190182 m²

27. Mass flux of water

$$G_w = \frac{12.2299}{60 * 0.001190182} = 171.2623159 \text{ kg/m}^2\text{s}$$

28. Viscosity of water at bulk mean temperature (μ_w) is calculated using eq.11 as:

$$\mu_w = 0.00073 \text{ Pa. s}$$

29. Water Reynolds Number (Re_w)

$$Re_w = \frac{G_w D_{hw}}{\mu_w} = \frac{156.908777 * 1.345 * 0.001}{0.00073} = 315.5449$$

30. Water Heat Transfer coefficient (h_w)

$$\begin{aligned}h_w &= 0.049 * \lambda_w / D_{dw} * Re_w^{0.69} * Pr_w^{1/3} \\ &= 0.049 * 0.6 / 0.001345 * 315.5449^{0.69} * 6.993^{1/3} \\ &= 2215.489 \text{ W/m}^2\text{K}\end{aligned}$$

31. Fin height = 5 mm

32. $l = \text{fin height}/2 = 2.5 \text{ mm}$

33. Water side fin effectiveness

$$\begin{aligned}\eta_w &= \frac{\tanh(ml)}{ml} \\ m_w &= \sqrt{\frac{2 * 2215.489 * (1 + \frac{0.127}{150})}{202.4 * 0.000127}} = 417.806\end{aligned}$$

$$\eta_w = 0.7485$$

34. Refrigerant fin effectiveness

$$\eta_r = \frac{\tanh(ml)}{ml} = 0.76617$$

35. Overall fin effectiveness water

$$a \text{ of water } (a_w) = 0.84306$$

$$\eta_{oew} = 1 - a_w(1 - \eta_w) = 0.78623$$

36. Overall fin effectiveness refrigerant

$$a \text{ of refrigerant } (a_r) = 0.84306$$

$$\eta_{oer} = 1 - a_r(1 - \eta_r) = 0.80286$$

37. Plate area (A_p) = $0.15 * 0.142 = 0.0213 \text{ m}^2$

38. Heat Transfer coefficient of Refrigerant side is

$$\frac{1}{U} = \frac{1}{\eta_{or} h_r} + \frac{t}{\lambda (A_p / A_r)} + \frac{1}{\eta_w h_w (A_w / A_r)}$$

$$h_r = 3614.605117 \text{ W/m}^2\text{K}$$

39. Refrigerant mass flux

$$G_r = \frac{m_r}{A_{fr}} = 32.487395 \text{ kg/m}^2\text{s}$$

40. Refrigerant Heat flux

$$q_r = \frac{Q_r}{A_{hr}} = 13.78 \text{ kW/m}^2$$

A3.2.3 Refrigerant two phase frictional pressure drop:

1. Total Differential Pressure (Δp_t) = 4.76 kPa (0.69 Psi)
2. Density of gas (ρ_g) = 52.241289 kg/m³
3. Density of liquid (ρ_l) = 1119.3336 kg/m³
4. Mean volume fraction (Δx) = 1
5. The pressure Drop due to momentum is calculated from

$$\Delta P_a = G_r^2 (v_g - v_l) |\Delta x| = 0.01926 \text{ kPa}$$

6. Mean Density

$$\rho_m = \left(\frac{x}{\rho_g} + \frac{1-x}{\rho_l} \right)^{-1} = 52.241289 \text{ kg/m}^3$$

7. Flow length (L) = 0.15 m

8. The pressure drop due to Gravity is calculated from

$$\Delta P_g = g \rho_m L = 0.07687 \text{ kPa}$$

9. The pressure drop due to manifold is calculated from

$$\Delta P_c = \frac{1.5 G_r^2}{2 \rho_m} = 0.01515 \text{ kPa}$$

10. The core frictional pressure Drop is calculated from

$$\Delta p_f = \Delta p_t - \Delta p_c + \Delta p_a + \Delta p_g = 4.84 \text{ kPa}$$

11. Kinetic Energy per Unit Volume

$$KE/V = \frac{G_r^2}{2 * \rho_m} = 10.1015 \text{ J/m}^3$$


```

phom=1/((xm/phov) + ((1-xm)/phol))           " Mean refrigerant density"
Reeq= ((1-xin)+(xin*(phol/phov)^0.5)))       " Equivalent Reynolds number"
Cplr=1.25
mul=0.25
klr=0.02
PrLr = mul*Cplr/klr                          " Liquid refrigerant prandtl number"
h_v =( 0.007*P_13^3)-(0.324*P_13^2)+(5.88*P_13)+385.3 " Refrigerant vapor
                                                    Enthalpy"
h_l = -(0.208*P_14^2)+(9.744*P_14)+178.9     " Refrigerant Liquid Enthalpy"
lr=Qr/Ahr                                     " Refrigerant heat flux"
lw=Qw/Ahw                                     " Water flux"
Qw = mw*cpw*(T_8-T_7)/60                     "Water heat load kW"
Qr= mr*(h_v-h_l)                             "Refrigerant heat load kW"
U = (Qw*1000)/(Ahr*LMTD)                     " Overall heat transfer coefficient "
hw= 0.0498*(0.6/DH)*Rew^0.69*6.99^(1/3)     " Water HTC w/m2K"
hr1 = 1/U
hr2= 0.002/(202.4*(Ap/Ahr))
hr3= 1/(Wfoe*hw*(Ahw/Ahr))
hr4 = (hr1-hr2-hr3)*Rfoe
hr=1/hr4                                     " Refrigerant HTC w/m2K"

"\\\\"*****End of the Program*****\\\\"

```


LIST OF PUBLICATIONS BASED ON THE Ph.D RESEARCH WORK

Journal References:

Ramana Murthy, K.V., Ranganayakulu, C., Ashok Babu, T.P. (2015). "Development of Heat Transfer Coefficient and Friction Factor Correlations for Serrated Fins in Water Medium using CFD." *Int. J. Physical Science and Application.*, 5(3), 238-248.

Ramana Murthy, K.V., Ranganayakulu, C., Ashok Babu, T.P. (2016). "Thermodynamic Analysis of Vapor Compression Refrigeration System For Aircraft With Refrigerant R134a." *Journal of Aerospace Sciences and Technologies.*, 68(1), 47-55.

Ramana Murthy, K.V., Mahesh, B., Ranganayakulu, C., Ashok Babu, T.P. (2016). "Influence of hydraulic diameter on heat transfer and pressure drop during Condensation of R134a refrigerant in a brazed plate fin heat exchangers." *Int. J. Eng. Sci. Innovative Technology .*, 5(7), 21-31.

Ramana Murthy, K.V., Ranganayakulu, C., Ashok Babu, T.P. (2017). "Condensation Heat Transfer and Pressure Drop of R-134a Saturated Vapour inside a Brazed Compact Plate Fin Heat Exchanger with Serrated Fin." *J. Heat Mass Transfer.*, 53(1), 331-341.

Conference proceedings:

Ramana Murthy, K.V., Raghu, J.N., Ranganayakulu, C., Ashok Babu, T.P. (2014). "Generation of Heat Transfer Coefficient and Friction Factor Correlations for Lance & Offset Fins of a Compact Heat Exchanger for water using CFD Analysis." Proceedings of 16th Annual CFD Symposium, Bangalore, pp. 107-111.

Ramana Murthy, K.V., Mahesh, B., Ranganayakulu, C., Ashok Babu, T.P., Vasudeva Rao, V., (2015). "Development of Vapour Compression Refrigeration System Test Rig and Evaluation of Test Data for R134a Condensation in Compact Heat Exchangers With Serrated Fin." Int. Conference on Heat Transfer Fluid Mechanics & Thermodynamics (HEFAT 2015). South Africa, pp. 184-193.

CURRICULUM VITAE



Name : K.V.Ramana Murthy
Date of Birth : 10/04/1971
Department : Mechanical Engineering, NITK, Surathkal.
Degree Registered : Ph.D
Education : B.Tech (Mech.), JNTU College of Engg., Anapatur
M.E (Mech.), IIT-Roorkee
Experience :

Sl.No	Organization	Designation	From Date	To Date
1.	ADA, Bangalore	Scientist 'E'	2004	Till Date
Nature of Work	<ul style="list-style-type: none">• Design and Development of Compact Heat Exchangers required for Environmental Control System and Secondary Power System of Light Combat Aircraft (Tejas Aircraft).• Qualification of heat exchangers as per Aeronautical standards.• Developmental Flight test data analysis• Development of test rigs for component installation checks.• Air flow distribution analysis and implementation• System level participation in defect investigation.			
2.	M/s BHPV Ltd, Visakhapatnam	Engineer	1997	2004
Nature of Work	<ul style="list-style-type: none">• Design and development of brazing furnaces.• Preparation of component drawings.• Developed the Welding Fixtures for Welding of Components to Compact Heat Exchangers of Aluminum Alloy and Stainless Steel materials to minimize the weld distortions.• Development of Brazing Fixtures for brazing of compact heat exchanger cores in the Vacuum Brazing Furnace required for the Aluminum alloy and Stainless steel materials.			

Address

: Residence

308, Sree Sapthagiri Paradise Apartment
KGF Munireddy Layout, Mahadevapura
Bangalore-560 048

Office

Scientist-‘E’
General Systems Directorate
Aeronautical Development Agency (ADA)
P. B. No.1718, Vimanapura Post
Bangalore-560 017

Email

**: katabathuni@gmail.com
katabathuni@jetmail.ada.gov.in**

Phone No

**: 080-32216756 (R), 080-25087152 (O)
9886883474 (Mobile)**